Role of LSR in the regulation of cholesterol homeostasis in the central nervous system

Aseel El Hajj

UNIVERSITÉ DE LORRAINE

ÉCOLE DOCTORALE SIRENA

Laboratoire de recherche URAFPA (Qualivie)

T H È S E

pour obtenir le grade de

DOCTEUR DE L'UNIVERSITÉ DE LORRAINE

Discipline : Sciences agronomiques

Présentée et soutenue par :

Aseel EL HAJJ

le : 18 Décembre 2019

Rôle du LSR dans la régulation de l'homéostasie du cholestérol dans le système nerveux central

Sous la direction de :

M. Thomas CLAUDEPIERRE – Pr., Université de Lorraine

Mme. Marie-Claire LANHERS-MCF, Université de Lorraine

Membres du jury :

M.Lionel BRETILLON	Centre des Sciences du Goût et de l'Alimentation	Rapporteur
Mme Chantal MATHIS	Laboratoire de neurosciences cognitives et adaptatives	Rapporteur
Mme Isabelle DENIS	Unité de Neurobiologie de l'Olfaction-INRA	Examinateur
M. Christophe EGLES	Université de Technologie de Compiègne	Examinateur
M. Cyrille VAILLEND	Institut des Neurosciences Paris-Saclay	Examinateur

Remerciements

J’adresse en premier lieu mes vifs remerciements au docteur Chantal Mathis (directeur de recherche, CNRS) et au docteur Lionel Bretillon (directeur de recherche, INRA) pour m’avoir fait l’honneur d’examiner mon travail en tant que rapporteurs et pour le temps qu’ils y ont consacré. Je tiens également à remercier chaleureusement Docteur Isabelle Denis (Chargée de recherche, INRA), Docteur Cyrille Vaillend (directeur de recherche, CNRS) pour avoir accepté de juger ce travail en tant qu’examinateurs ainsi que Professeur Christophe Égles (Université de Technologie de Compiègne) pour avoir eu la gentillesse de présider mon jury. Un grand merci a ces personnes pour l’intérêt bienveillant qu’ils ont manifesté à l’égard de ce travail.

Mes remerciements vont également à l’ensemble des statutaires de l’équipe Qualivie. Un grand merci tout particulier à mes encadrants, Thomas Claudepierre et Marie-Claire Lanhers. Thomas et Marie-Claire, j’ai beaucoup apprécié ces 4 années de thèse passées sous votre encadrement, au cours desquelles vous m’avez donné votre pleine confiance et une grande liberté quant à la manière de faire avancer ce projet qui m’a été confié. Merci de m’avoir fait découvrir le monde de la recherche et ses subtilités et de m’avoir inculqué le savoir nécessaire pour poursuivre ma carrière. Je tiens tout particulièrement à vous remercier pour votre précieuse implication dans l’élaboration de ce manuscrit et la rédaction des publications scientifiques. Nos discussions et vos conseils auront été très enrichissants. J’espère que nous aurons l’occasion de nous recroiser par la suite.

Je remercie également Frances Yen Potin. Merci pour votre gentillesse et votre compréhension. J'apprécie particulièrement vos conseils et vos commentaires pour la rédaction d'articles et la présentation d'affiches. Je remercie également Thierry Oster pour ses conseils et sa volonté de m'aider. Nous avons parlé et partagé des moments heureux, j'espère que nous nous rencontrerons à l'avenir. Merci Frédéric Desor pour ton aide, en particulier en partageant ta passion pour les études comportementales et les statistiques. Je voudrais remercier ma chère Fathia. Merci beaucoup pour ton aide, support et ton sourire. Je te souhaite la meilleure du monde! Merci Maxime et Daria, pour un partage des moments jolis dans le bureau de cette dernière année, je vous souhaite une bonne continuation de votre thèse. Tu n'es plus au labo Samina, mais tu seras toujours dans mon cœur, merci mon ami pour ta maturité et support.

Je remercie les membres de l’UR AFPA en général, spécifiquement Guido Rychen, Pascale Fontaine, Cyrille, Agnès, Stephane, Claire Collas, et Herve. Merci pour l’équipe technique, Claire Soligot, Marion Huguet, Pamela Hartmeyer, et Frederic Desor. Vous m’avez beaucoup aidé et on a partagé des bons moments. Merci pour l’équipe administrative Catherine Larriere, Nathalie Cadario, et Nathalie Vailleume pour s’occuper de toutes mes commandes et documents essentielles.

Je veux remercier mes collègues et mais (dans un ordre alphabétique pour ne pas faire de jaloux) : Aurore, Aurelia, Daria, Hela, Fathia, François, Maïlie, Martina, Mathieu, Maxime, Nadine, Samina, Sarah, et Sylvain. J'ai été très heureux de vous compter dans mon entourage professionnel et personnel. Je n'oublierai jamais cette ambiance si particulière et unique qu'il me sera sûrement impossible de retrouver ailleurs et toutes ces soirées passées ensemble. Un autre merci particulier à Pamela et Marion pour leur précieuse aide, technique et moral, et surtout pour les bons moments passes.

Merci à mon ami proche, ma colocataire, ma collègue: Aurore. Merci pour etre a ma cote quand j'avais besoin de toi, pour les discussions, les soirees, la danse, la folie. Je ne peux pas te remercier assez, je voudrais qu'on reste comme on est pour toujours. Merci Aurelia, ma belle italienne, pour tout. Tu étais la quand ça aller et ça ne va pas. Tu m'as fait rire quand je n'ai pas pu surire. On a eu des discussions si profonde dans une manière si naturelle. Je te souhaite le meilleur pour la suite, on restera très proche même si on est loin, je suis sûr! Mon pot, Francois, merci pour tout! Tu es genial comme tu es, reste comme ça.

Merci pour la famille Messayke pour être ma deuxième famille sur Nancy. Merci à Julie, la belle voisine. Amal et Sabrine, les jolies Tunisiennes pour nos soirees si folles. Je suis ravie de vous rencontrer. Merci à Hiba, ma grande soeur, pour etre si sage et si comprehensive. Merci à Ziad, mon pote, bon courage dans ta thèse. Merci a au groupe libanais: Dima, Kassem, Hayat, Ayman, Asma, Mohamad K pour tout.

Je tiens à remercier les personnes qui me sont les plus chères. Tout d'abord, ma famille et tout particulièrement mes parents, qui m'auront tout donné pendant ces années et qui auront permis de me construire dans un environnement plus que parfait. Sans vous, je n'aurais pu arriver là où j'en suis aujourd'hui. Cette thèse est aussi la vôtre et l'accomplissement de toutes ces années pendant lesquelles vous m'aurez toujours soutenu dans mes choix et décisions.

شكرا لك أبي على العطاء, التضحية و الحب اللامتناهي. أنت حبي و سندي الأول, كل الأحرف و الكلمات لا ممكن أن تعبر لك عن حبي و أمتناني. أمي حبيبتي, لقد ضحيتي بكل شيء من أجلنا' أنا و أخوتي.أشكرك على كل شيء يا نبع الحنان. أحبك أمي. أشكر أخوتي أحمد, منصور, عبد الله, و ابراهيم على الحب و اللحظات الجميلة. أشكر جدي عبد اللطيف و جدتي قرنفلة, رحمكم الله يا أحبائي, أهديكم عملي أتمنى أن تكونوا في جنات الخلد فخورين بي. أشكر جدتي سميرة على الدعم و الحب و العطاء, كنتي و ما زلتي سبب ثقتي بنفسي.

Merci pour ma fille, le soleil de mon jour, pour sa présence dans ma vie. Je t'adore ma bichette, je fais tout ça pour toi, pour que tu sois fière de ta maman.

Enfin, le plus important pour moi, merci à toi Ahmad, ta confiance, ton soutien, ta patience, pour avoir su trouver les mots justes dans les moments les plus difficiles, et bien entendu pour ton amour…

اللهم لك الحمد والشكر عدد ذرات الكون في السموات والأرض وما بينهما وما وراء ذلك. أحمدك و أشكرك يا خالقي على نعمة العقل و السمع و البصر. سبحانك ربي عدد خلقك و رضا نفسك و زنة عرشك و مداد كلماتك.

Contents

List of abbreviations

ACAT1	cholesterol acyltransferase 1
AD	Alzheimer's disease
Apo	Apolipoprotein
APP	Amyloid Precursor Protein
BBB	Blood-Brain-Barrier
BRB	Blood-Retinal-Barrier
CDT	Clostridium Difficile Transferase
cKO	glia-specific lsr knockout mice
CLU	Clusterin
CNS	Central Nervous System
CoA	coenzyme A

Cre	GlastCreERT2
CSF	cerebrospinal fluid
CYP46A1	cholesterol 24-hydroxylase
CYP51	lanosterol 14 alpha demethylase
DHC	dehydrocholesterol
DHCR	Dehydrocholesterol reductase
DNA	deoxyribonucleic acid
EC	Endothelial cell
EGFP	Enhanced Green Fluorescent Protein
ER	endoplasmic reticulum
FFA	free fatty acids
GFAP	glial fibrillary acidic protein
HD	Huntington's disease

HDL	High Density Lipoproteins
HMG-CoA	3-hydroxy-3-methyl glutaryl coenzymeA
HTT	Huntingtin
Iba-1	Ionized calcium binding adaptor
IL	Interleukin
Ilβ	Interleukin β
KO	Knockout
LBPA	Lysobiphosphatidic Acid
LDLR	Low Density Lipoprotein Receptor
LPL	lipoprotein lipase
LRP	lipoprotein receptor
LSR	lipolysis stimulated lipoprotein receptor
LTP	Long-term potentiation

LXR	Liver X Receptor
NeuN	Neuronal Nuclei
NMDA	N-methyl-D-aspartate
NPC	Niemann-Pick type C
OHC	hydroxycholesterol
PM	Plasma Membrane
PPAR	Peroxisome Proliferator-Activated Receptor
PSD95	post-synaptic density protein-95
PUFA	polyunsaturated fatty acids
RAP	Receptor Associated Protein
RXR	Retinoid X Receptor
S1P	Site-1 protease
S2P	Site-2 protease

SHH	sonic hedgehog
SLOS	Smith-Lemli-Opitz Syndrome
SR-BI	scavenger receptor class B type I
SRE	Sterol Regulatory Element
SREBP	Sterol-regulatory element binding protein
TG	Triglyceride
TNFα	Tumor Necrosis Factor-α
VLDL	very low-density lipoproteins
WT	Wild Type mice

Résumé en Français

Ce projet de thèse a été mené au sein de l'équipe «Qualité de l'alimentation et vieillissement» (Qualivie) du laboratoire «Unité de Recherche Animal et Fonctionnalités des Produits Animaux» (UR AFPA). Qualivie se concentre sur la caractérisation des mécanismes qui affectent la biodisponibilité et les fonctions des lipides alimentaires qui, à leur tour, peuvent contribuer au développement des déficiences métaboliques et cellulaires associées au vieillissement.

En effet, les perturbations de l'homéostasie lipidique sont considérées comme des facteurs de risque de diverses maladies neurodégénératives telles que la maladie d'Alzheimer (MA), qui représentent toutes des préoccupations importantes pour la santé publique dans le monde. Il est donc important de comprendre les mécanismes sous-jacents à la régulation du statut lipidique. Le maintien d'un état lipidique normal est obtenu par une interaction complexe de divers récepteurs de lipoprotéines, enzymes et protéines de transport qui fonctionnent en coopération les uns avec les autres.

Le récepteur de lipoprotéines stimulé par lipolyse (LSR) qui a été caractérisé dans notre laboratoire s'est avéré réguler la distribution des lipides entre les différents tissus. En effet, il participe activement à l'élimination des lipoprotéines riches en triglycérides (TG) de la circulation sanguine pendant la phase postprandiale (Bihain & Yen, 1992; Yen et al., 2008; Stenger et al., 2012). Une diminution de l'expression du LSR est associée à une augmentation de la prise de poids (Stenger et al., 2010) et a été observée dans des modèles de souris obèses avec une masse grasse accrue (Narvekar et al., 2009). De plus, le LSR

nécessite la présence d'acides gras libres pour son activation. Il se lie aux apolipoprotéines (Apo) E et aux lipoprotéines contenant ApoB. Des études antérieures ont tenté de démêler la fonction du LSR en développant des KO (KO) complets. Fait intéressant, l'inactivation complète de *lsr* a provoqué une létalité embryonnaire, avec des hémorragies localisées au cerveau et une réduction de la taille du cerveau et du foie. Cela a été suivi par le développement de souris hétérozygotes lsr +/-. Ces souris ont surveillé les fonctions cognitives modifiées et la distribution du cholestérol dans le cerveau. Ce sont toutes des indications de l'importance vitale du LSR dans la distribution du cholestérol et le développement normal du cerveau.

Compte tenu de l'importance du LSR dans la régulation de l'homéostasie lipidique, nous voulions d'abord étudier le modèle d'expression du LSR dans les cellules neuronales et gliales dans différentes régions du cerveau, pour nous aider à assigner nos cibles. Une fois atteint, nous avons cherché à développer des KO spécifiques aux cellules de LSR pour dévoiler les fonctions LSR.

Cette thèse est présentée de la manière suivante:

Introduction: Ce chapitre représente une revue de la littérature et est divisé en trois sections principales:

- La première section décrit les fonctions et l'importance du cholestérol dans le système nerveux central (SNC).
- La deuxième section décrit l'homéostasie du cholestérol dans le SNC, qui comprend quatre sous-sections décrivant la synthèse, le transport, l'excrétion et la régulation du cholestérol.

- La troisième section décrit le lien entre le métabolisme du cholestérol et différentes maladies neurodégénératives, notamment la maladie de Niemann-Pick de type C (NPC), le syndrome de Smith-Lemli-Opitz (SLOS), la maladie de Huntington (HD) et la MA.
- Enfin, la troisième section explique la découverte des protéines LSR, leur structure et la létalité de l'inactivation complète du LSR. Il explique la fonction du LSR en périphérie, suivi de son importance dans la barrière hémato-encéphalique (BBB) et le SNC.

Chapitre II: Ce chapitre est notre premier article publié (PLOS One). Il décrit la caractérisation de l'ARNm du LSR et de l'expression des protéines dans différentes régions du cerveau qui sont importantes pour l'apprentissage et la mémoire, et la caractérisation de l'expression du LSR aux niveaux glial et neuronal des cultures cellulaires primaires. Pour comprendre la fonction du LSR, il était essentiel de caractériser d'abord le modèle d'expression du LSR. Il était important d'étudier si l'expression du LSR était omniprésente et similaire, ou variable dans les régions cérébrales étudiées et au fil du temps. Une fois l'expression du LSR déterminée, nous ciblerions les régions du cerveau qui expriment fortement le LSR. Nous avons pris en considération non seulement le LSR total, mais aussi les sous-unités membranaires LSR α et α ', et la sous-unité membranaire non traversante LSR β, car elles ont hypothétiquement des fonctions différentes. Pour caractériser l'ARN LSR et l'expression des protéines dans différentes régions du cerveau, RT-qPCR et western blots ont été effectués, respectivement. Nous avons en outre étudié si l'expression du LSR est spécifique

des neurones ou de la glie en colorant des cultures de cellules neuronales et gliales pures et mixtes préparées à partir de différentes régions du cerveau.

Chapitre III: Ce chapitre décrit la génération de souris knockout lsr spécifiques à glia (cKO), la batterie d'études comportementales effectuées sur cKO par rapport aux souris de type sauvage (WT). Ce chapitre comprend également des résultats préliminaires sur l'effet du knockout lsr spécifique de glia sur l'expression de l'ARNm des enzymes et des transporteurs liés au métabolisme du cholestérol. Après avoir étudié le modèle d'expression de LSR et souligné la forte expression de LSR dans les cellules gliales, nous avons décidé de générer un *lsr* KO spécifique de glia en utilisant le système Cre / lox conditionnel inductible de tamoxifène (TAM). Une batterie de tests comportementaux a été réalisée pour étudier les effets de la suppression gliale du LSR sur l'activité, l'anxiété, la vision, l'olfaction, la sociabilité, la mémoire spatiale à court et à long terme

Chapitre IV: Ce chapitre décrit le phénotype comportemental intéressant de notre deuxième groupe témoin GlastCreERT2 (Cre), où ces souris ont surveillé un trait hyperactif prédominant. Lorsque nous avons effectué la deuxième grande partie de notre étude, la génération, l'induction et le phénotypage comportemental de la suppression spécifique du glia du LSR chez la souris, nous avions initialement prévu d'avoir deux groupes témoins: un groupe témoin négatif WT et un groupe GLASTCreERT2 induit par TAM (Cre). Ce dernier était destiné à évaluer l'effet des injections de TAM sur les phénotypes observés. Étonnamment, le groupe Cre a rapidement montré des signes d'hyperactivité et un comportement anormal dans les tests nécessitant

une attention. Par conséquent, nous avons décidé de limiter la comparaison entre les souris WT et cKO pour le phénotypage comportemental du knock-out spécifique de la glie du LSR chez la souris. Cependant, nous avons analysé plus en détail les souris Cre comme un modèle possible de souris hyperactives. Dans ce chapitre, nous avons rassemblé les données intéressantes et le développement réel du groupe Cre induit par TAM.

Le dernier chapitre résume les principales conclusions de la thèse et présente les conclusions ainsi que les perspectives soutenues par ce travail expérimental.

Le but de ce travail était de déchiffrer le rôle du LSR dans l'homéostasie du cholestérol, qui, comme indiqué précédemment, est crucial pour le bon fonctionnement du cerveau. Comme l'a dit Francis Crick: «Si vous voulez comprendre la fonction, étudier la structure», c'est pourquoi la première partie de notre étude a été d'étudier le modèle d'expression du LSR; les niveaux d'expression de différentes sous-unités LSR dans différentes régions du cerveau et éventuellement cibler les régions exprimant fortement LSR dans d'autres études pour comprendre sa fonction éventuelle. Nous avons d'abord démontré que l'expression LSR dans le SNC est régio-spécifique, chaque zone CNS a son propre profil d'expression pour les différentes chaînes LSR, permettant ainsi une combinaison spécifique de sous-unités formant ce récepteur de lipoprotéines. Certaines régions du SNC présentaient une expression de LSR plus forte au niveau de l'ARNm et / ou des protéines. Nous avons montré que le LSR est exprimé de manière différentielle à travers le cerveau à la fois au niveau de l'ARN et des protéines. Au niveau de l'ARN, les HT, HIP, OB et CB présentent

tous des niveaux élevés d'expression totale de l'ARN lsr. Au niveau des protéines, les immunoblots montrent que les HT, OB et RET expriment les niveaux les plus élevés de LSR lorsqu'ils sont normalisés en β-TUB, ce qui peut refléter un besoin spécifique de ces régions de réguler étroitement le cholestérol pour un bon fonctionnement. Il est connu que le LSR est présent dans les cellules endothéliales aux jonctions serrées, cependant tous les tissus collectés contiennent des vaisseaux sanguins, donc des niveaux élevés de LSR trouvés dans des zones cérébrales spécifiques ne peuvent pas être uniquement dus aux cellules endothéliales, réparties de manière homogène dans tout le SNC, mais reflètent plutôt l'expression de l'expression du LSR dans les cellules du SNC, et donc les neurones ou les cellules gliales. De plus, nous avons démontré que le vieillissement affecte significativement l'expression du LSR. Avec l'âge, l'expression de l'ARN lsr diminue à la fois dans le HT et le HIP; c'est également le cas au niveau des protéines où le LSR est clairement régulé à la baisse dans le HT, et montre une tendance à la régulation à la baisse dans le HIP et l'OB.

De plus, nous avons prouvé une forte expression de la glie du LSR par rapport aux neurones. Nous avons noté que l'expression du LSR était omniprésente dans les cellules gliales, mais plus centrée sur le soma dans les neurones. Nous avons constaté que les cellules gliales sont les principales cellules exprimant le LSR dans le SNC, suggérant ainsi un rôle essentiel de cette lipoprotéine dans le trafic de cholestérol entre les neurones et les cellules gliales. En effet, bien que nous ayons montré cela dans le CB, qui a fourni suffisamment d'ARNm pour comparer les niveaux de lsr dans les cellules gliales et les neurones, l'immunocytomarquage d'autres structures montre clairement un niveau protéique significatif de LSR dans les cellules GFAP positives. Compte

tenu de cela, et sur la base du rôle du LSR en tant que récepteur des lipoprotéines, nous avons émis l'hypothèse que le LSR présent sur les cellules gliales pourrait jouer un rôle dans le dialogue croisé glie-neurone dans le contrôle rétroactif de la synthèse du cholestérol, régulant le cholestérol circulant et maintenant ainsi le bon fonctionnement du cerveau. Ce qui nous amène à la deuxième grande partie de notre étude : la génération et le phénotypage comportemental de souris inductibles spécifiques de glia knockout conditionnel de lsr cKO par rapport à des souris WT. La suppression in vivo spécifique de lsr dans les cellules gliales a induit des perturbations dans le comportement des souris cKO, qui pourraient être dues à la perturbation de l'homéostasie du cholestérol. Dans leur environnement, les souris cKO étaient plus actives pendant la seconde moitié de la période nocturne que WT. Tous les tests comportementaux ont été effectués 1 à 3 heures après le début de la période sombre, donc pendant la période où le WT et le cKO ont des niveaux d'activité similaires. Dans un nouvel environnement, les souris cKO avaient tendance à rester à la périphérie pendant de plus longues périodes par rapport aux souris WT reflétant la thigmotaxie. Néanmoins, ils ont parcouru la même distance à la périphérie, ce qui indique des périodes immobiles plus longues à la périphérie. L'immobilité et la thigmotaxie auraient pu être une forme d'anxiété ou d'apathie de l'État. Les souris cKO ont pu visualiser des objets et identifier des indices visuels, car elles ont exploré le même ensemble d'objets pendant un temps presque égal. En outre, ils ont pu visualiser les indices géométriques dans le labyrinthe de Barnes pour trouver la chambre d'évacuation. Cependant, ils ne pouvaient pas distinguer ou mémoriser entre un ancien et un nouvel objet. Ils ont également effectué un pourcentage d'alternance propre plus faible dans le labyrinthe en Y que les souris WT, ce qui indique un déficit de mémorisation des

armes déjà visitées. Concernant l'olfaction, les souris cKO ont mis deux fois plus de temps à retrouver le cookie enfoui. De plus, ils ont passé moins de temps à renifler de nouvelles odeurs et ne pouvaient pas distinguer les odeurs subtiles. Cela démontre que les performances de la mémoire olfactive sont plus faibles chez les souris cKO. Ils ont pu détecter différentes odeurs asexuées et sexuelles mais n'ont pas pu identifier de différences subtiles. Les cKO étaient moins sociaux que les souris WT, ce qui pourrait être lié à des déficits olfactifs car les rongeurs utilisent principalement ce sens pour identifier et reconnaître les étrangers. Cependant, chez les souris plus âgées, elles ont pu faire la distinction entre les anciens et les nouveaux étrangers. Par conséquent, les souris cKO ont montré un dysfonctionnement olfactif, qui est le premier signe de neurodégénérescence. Au total, ces tests ont suggéré que la mémoire sensorielle et la mémoire spatiale à court terme étaient affectées. Chez les souris cKO, les performances de la mémoire de travail étaient inférieures à celles du WT chez les animaux jeunes et plus âgés, mais bien qu'elles aient diminué dans le WT - reflétant un processus de vieillissement normal - elles semblaient plus stables dans le cKO suggérant une restructuration cognitive ou une neuroplasticité. Dans notre phénotypage comportemental, trois groupes ont été étudiés: 1- souris WT, nos témoins négatifs. 2- Souris Cre, souris témoins témoins induites par l'enzyme Glia spécifique de TAM. 3- Souris cKO, souris induites par TAM induites par glia spécifiques de glia exprimant lsr supprimées. Le phénotype comportemental était assez complexe, où étonnamment les souris Cre surveillaient un trait hyperactif par rapport aux souris WT et cKO. Ce trait hyperactif interdit aux souris Cre d'être un groupe témoin approprié pour les souris cKO dans les tâches d'apprentissage et de mémoire comme dans le test de discrimination d'odeur et le labyrinthe de Barnes. Par conséquent, nous

avons discuté des souris Cre dans un chapitre séparé, où nous avons comparé les souris Cre vs WT et Cre vs cKO. Premièrement, dans l'activité en cage à domicile, les souris Cre ont parcouru de plus longues distances et pendant de plus longues périodes que les souris WT. De plus, ils ont montré un comportement de toilettage et de grattage plus élevé que les souris WT. Cependant, la seule différence entre les souris Cre et cKO était la distance de marche, ce qui indique une hypoactivité cKO par rapport aux souris Cre. Deuxièmement, dans le paradigme d'exploration libre, aucune variation significative entre les souris WT et Cre, mais les souris cKO passaient moins de temps dans la nouvelle zone et avaient tendance à prendre plus de temps pour entrer dans la nouvelle zone pour la première fois. Par conséquent, les souris Cre n'ont contrôlé aucun trait d'anxiété, mais cKO l'a fait par rapport aux souris Cre. Troisièmement, dans le test en champ ouvert, Cre et cKO sont restés pendant un temps similaire à la périphérie, plus longtemps que les souris WT. Cependant, les souris Cre ont parcouru de plus longues distances que les souris cKO. Cela confirme que les souris Cre sont hyperactives et indique que les souris cKO étaient immobiles pendant de plus longues périodes. Quatrièmement, les souris Cre étaient capables de sentir, de détecter les odeurs, mais n'étaient pas capables de discriminer les odeurs subtiles. Les souris Cre étaient les plus rapides à décongeler les aliments et étaient très attirées par les odeurs sexuelles, qui pouvaient être dues en partie à leur hyperactivité. D'un autre côté, les souris cKO ont passé beaucoup plus de temps à trouver des biscuits et ont montré un faible intérêt pour les odeurs non sexuelles et sexuelles. Pourtant, les souris cKO étaient capables de détecter différentes odeurs, mais ne pouvaient pas distinguer les odeurs subtiles, ce qui pourrait être en partie dû au manque d'intérêt et à l'hypoactivité. Cinquièmement, la sociabilité et la mémoire sociale,

les souris cKO étaient moins sociales que les souris WT et Cre et surveillaient les déficits de mémoire sociale. Sixièmement, dans la vision et la mémoire visuelle, les souris Cre et cKO ont exploré des ensembles d'objets pendant une période similaire, ce qui était nettement inférieur à celui des souris WT. De plus, les souris Cre et cKO présentaient une discrimination visuelle et / ou des déficits visuels de mémoire. De plus, Cre et cKO avaient tous deux des déficits de mémoire à court terme. Cependant, cKO a également effectué un nombre d'entrées inférieur à celui des souris Cre, ce qui est un indicateur de néophobie. Enfin, dans le labyrinthe de Barnes, les souris Cre et cKO ont mis plus de temps à lancer leur recherche de la chambre d'évacuation lors du premier jour d'essai 1. Cependant, les souris cKO ont pu apprendre avec des répétitions et n'ont pas surveillé les problèmes de mémoire à long terme. Contrairement aux souris cKO, les souris Cre n'ont pas pu apprendre très probablement en raison de leur caractère d'hyperactivité.

Afin de vérifier la suppression de lsr, en utilisant des échantillons de souris cKO contre des échantillons de WT scarifiés à 3 mois et 13 mois, des RT-qPCR ont été effectués pour étudier le métabolisme lsr et du cholestérol et transporter les niveaux d'expression des ARNm des gènes. À 3 mois, les niveaux d'ARNm lsr étaient stables chez les souris cKO, par rapport aux souris WT, et n'étaient pas régulés à la baisse. L'ARNm de Lsr a même été régulé à la hausse dans le CB (lsr total et lsr β) et l'OB (lsr β). Les tissus ont été prélevés deux semaines après l'induction du TAM, il est possible qu'il y ait eu une expression compensatoire du LSR dans les neurones (Morrison & Münzberg 2012). Que le phénotype comportemental observé soit dû à la suppression du LSR dans la glie, à la surexpression du LSR dans les neurones ou à une combinaison des deux est

une question à laquelle il reste à répondre. Concernant les autres gènes étudiés ; abca1, hmgcr, srebp1 et cyp46a1, seul hmgcr a été régulé à la hausse dans le CB, où le lsr total a également été régulé à la hausse. À 13 mois, une régulation à la baisse des trois sous-unités de lsr a été signalée dans le HIP, une tendance à une régulation à la baisse en OB, qui était significative pour lsr β. De même, une régulation à la baisse de abca1 et srebp1 a été observée dans HIP. L'ARNm de Lsr dans cKO CB n'était pas régulé à la baisse par rapport au WT, mais même régulé à la hausse pour lsr α '. En même temps, abca1 et srebp1 avaient tendance à être régulés à la hausse dans CB de souris cKO.

General Introduction

This thesis project was conducted in the “Qualité de l'alimentation et vieillissement” (Qualivie) team of the “Unité de Recherche Animal & Fonctionnalités des Produits Animaux” (UR AFPA) laboratory. Qualivie focuses on characterizing the mechanisms that affect the bioavailability and the functions of dietary lipids which, in turn, may contribute to the development of metabolic and cellular impairments associated with aging.

Indeed, the disturbances in lipid homeostasis are considered as risk factors for various neurodegenerative diseases such as Alzheimer’s disease (AD), all of which represent important concerns for public health worldwide. It is therefore important to understand the mechanisms underlying the regulation of lipid status. The maintenance of normal lipid status is achieved by an intricate interplay of various lipoprotein receptors, enzymes and transport proteins that work in cooperation with one another.

The lipolysis stimulated lipoprotein receptor (LSR) that was characterized in our laboratory has been shown to regulate the distribution of lipids amongst different tissues. Indeed, it actively participates in the clearance of triglyceride (TG)-rich lipoproteins from the blood circulation during the postprandial phase (Bihain & Yen, 1992; Yen et al., 2008; Stenger et al., 2012). Reduced expression of LSR is associated with increased weight gain (Stenger et al., 2010) and has been observed in obese mouse models with increased fat mass (Narvekar et al., 2009). Furthermore, LSR requires the presence of free fatty acids for its activation. It binds to apolipoprotein (Apo) E and ApoB containing lipoproteins. Previous studies tried to unravel LSR’s function by developing complete *lsr* knockouts (KO). Interestingly, complete *lsr* inactivation caused embryonic lethality, with brain localized hemorrhages and reduced brain and liver size. This was followed by developing heterozygous *lsr* +/- mice. Those mice monitored altered cognitive functions and cholesterol distribution in brain. These are all indications of the vital importance LSR plays in cholesterol distribution and normal brain development.

In view of the importance of LSR in the regulation of lipid homeostasis, we wanted to

first study the pattern of LSR expression in both neuronal and glial cells in different brain regions, to aid us assign our targets. Once achieved, we aimed to develop cell-specific KOs of LSR to unveil LSR functions.

This thesis is presented in the following manner:

Introduction: This chapter represents a review of the literature and is divided into three major sections:

- The first section describes cholesterol functions and importance in the central nervous system (CNS).

- The second section describes cholesterol homeostasis in the CNS, which includes four subsections describing cholesterol synthesis, transport, excretion, and regulation.

- The third section describes the link of cholesterol metabolism to different neurodegenerative diseases including Niemann-Pick type C (NPC) disease, Smith-Lemli-Opitz syndrome (SLOS), Huntington's disease (HD), and AD.

- Finally, the third section explains the discovery of LSR proteins, it's structure, and the lethality of complete *lsr* inactivation. It explains the function of LSR in periphery, followed on LSR's importance in blood-brain-barrier (BBB) and CNS.

Chapter II: This chapter is our first published article (PLOS One). It describes the characterization of LSR mRNA and protein expression in different regions of the brain that are important for learning and memory, and the characterization of LSR expression at the glial and neuronal levels from primary cell cultures.

Chapter III: This chapter describes the generation of glia-specific *lsr* knockout mice (*cKO*), the battery of behavioral studies performed on *cKO* in comparison to wild type (*WT)* mice. This chapter also includes preliminary results on effect of glia-specific *lsr* knockout on mRNA expression of cholesterol metabolism-related enzymes and

transporters.

Chapter IV: This chapter describes the interesting behavioral phenotype of our second control group *GlastCreER^{T2}* (Cre), where those mice monitored a predominant hyperactive trait.

The last chapter summarizes the principle findings of the thesis and presents the conclusions as well as the perspectives supported by this experimental work.

Review of Literature

1. Cholesterol's functions and importance in CNS

The brain consists of three major forms of lipids: glycerophospholipids, sphingolipids, and cholesterol (Korade & Kenworthy 2008). Approximately, 20-25 % of the body's cholesterol are found in the brain (Björkhem Ingemar & Meaney Steve 2004). Cholesterol's concentration in most body tissues is 2 mg/g, however, it reaches 20-25 mg/g in the CNS. Cholesterol (Figure 1.1A), is indeed an essential structural component for cellular membrane and myelin, where 80 % of cholesterol in the brain are found in myelin sheath (Figure 1.1B) (Björkhem Ingemar & Meaney Steve 2004). In addition, cholesterol is a vital component for steroid hormones synthesis, synapses and dendrites formation (Mauch *et al.* 2001; Goritz *et al.* 2005; Fester *et al.* 2009), and axonal guidance (de Chaves *et al.* 1997). For neuronal functions, cholesterol is an essential component for neurotransmission, where cholesterol-kinesin interactions allow the transmission of synaptic vesicles along axonal microtubules (Claudepierre & Pfrieger 2003) (Figure 1.1B). It is also important for exocytotic complexes organization in active presynaptic membranes in lipid rafts, for neurotransmitters receptors clustering in postsynaptic membranes, for extra synaptic receptors pool recruitment, and presynaptic and postsynaptic cell-cell adhesion (Figure 1.1B) (Claudepierre & Pfrieger 2003). Therefore, a deficiency or excess of cholesterol in brain impairs neuronal activity by perturbing synaptic vesicle transmission and exocytosis, thus leading to dendritic spine and synapse degeneration (Frank *et al.* 2008; Linetti *et al.* 2010; Liu *et al.* 2010). Defects in cholesterol trafficking lead to structural and functional CNS diseases such as Niemann-Pick type C (NPC) disease (Madra & Sturley 2010), Smith-Lemli-Opitz syndrome (SLOS) (Nowaczyk & Irons 2012) and are

suspected to be involved in many other neurodegenerative pathologies including HD (Block *et al.* 2010), and AD (Di Paolo & Kim 2011).

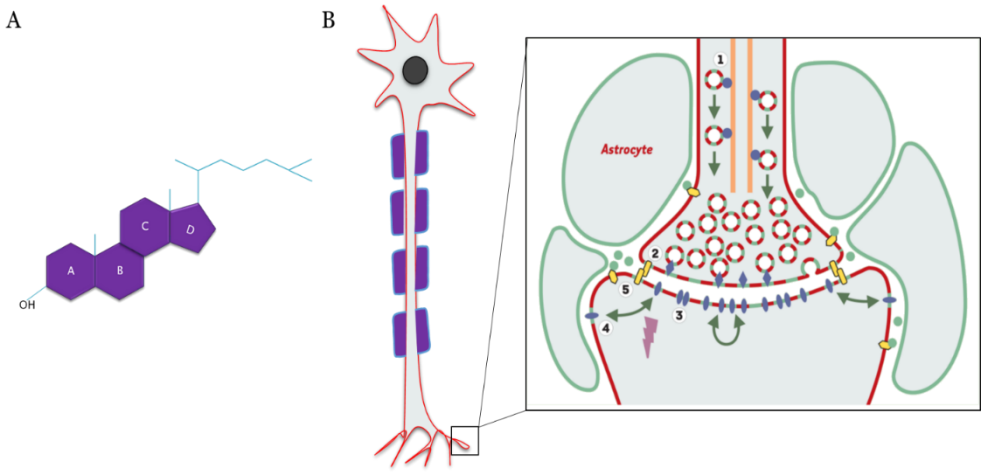

Figure 1.1: Cholesterol's localization and functions. A. Structural representation of cholesterol. B. Cholesterol localization in myelin sheath (axons insulation), and in lipid rafts in various regions of the cell; 1- in synaptic vesicles (axonal transport via cholesterol-kinesin interactions), 2- presynaptic membranes (exocytotic machinery organization), 3-post synaptic membrane (neurotransmitters receptors aggregation), 4-extrasynaptic domains (receptors mobilization), 5- pre and post synaptic cell-cell adhesion. Figure adapted from (Claudepierre & Pfrieger 2003a).

2. Cholesterol homeostasis in the CNS

2.1. Synthesis

Due to its hydrophobic nature, cholesterol is transported within the body in large complexes of lipids and proteins, called lipoproteins. Intact peripheral lipoproteins of the blood stream cannot by-pass the blood brain barrier (BBB), because they are large, highly charged, hydrophilic molecules. Therefore, most of cholesterol is synthesized locally in the brain (Jeske & Dietschy 1980). However, a small fraction can be taken up from the circulation as soluble 27-hydroxycholesterol (27-OHC). Production of 27-OHC in the brain is very low, and most of the 27-OHC in the brain and cerebrospinal fluid (CSF) are of extracerebral origin (Björkhem 2006a). A small fraction of peripheral cholesterol can also come from the activity of the scavenger receptor class B type I receptor (SR-BI) (Goti *et al.* 2001; Karasinska *et al.* 2009a). Cholesterol is therefore synthesized locally by *de novo* synthesis in CNS to satisfy the brain's needs (Jeske & Dietschy 1980). This was discovered when peripherally administered labeled cholesterol wasn't detected in CNS of rats (Jeske & Dietschy 1980; Morell & Jurevics 1996). Similarly, after liver transplantation in humans, ApoE phenotyping revealed

that serum ApoE of the recipient converted to that of the donor unlike that in the CSF which was conserved demonstrating a local synthesis of ApoE-lipoproteins (Linton *et al.* 1991). *De novo* cholesterol synthesis is a complex and resource intense process that occurs in the endoplasmic reticulum (ER) (DeGrella & Simoni 1982). It starts with the conversion of acetyl-CoA (acetyl coenzyme A) to HMG-CoA (3-hydroxy-3-methyl glutaryl coenzyme A) by HMG-CoA synthase. Then HMG-CoA is converted to mevalonate by HMG-CoA reductase. A series of enzymatic reactions occur converting mevalonate into squalene, lanosterol, and 7-dehydrocholesterol (7-DHC) to give then the final product cholesterol via 7-dehydrocholesterol reductase (7-DHCR) (Berg e*t al.* 2002). HMG-CoA to mevalonate is considered the rate-limiting and irreversible step in cholesterol synthesis (Figure 1.2), HMG-CoA reductase enzyme is inhibited by statins; cholesterol lowering drugs (Berg *et al.* 2002).

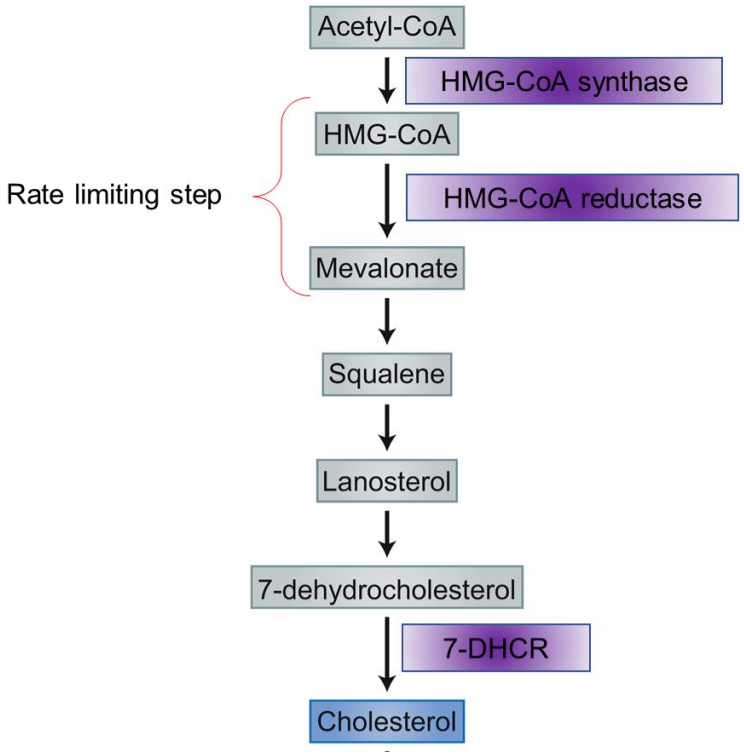

Figure 1.2: Cholesterol biosynthesis. Cholesterol is synthesized from acetyl-CoA. A key intermediate in the pathway, mevalonate, is produced from HMG-CoA by the rate-limiting enzyme of the pathway, HMG-CoA reductase. In the final step of the pathway, 7-dehydrocholesterol (7-DHC) is converted to cholesterol by the enzyme 7-dehydrocholesterol reductase (7-DHCR).

During embryonic stage and early development, most of the growth and myelination is occurring. Thus, the net cholesterol flux and accumulation increase rapidly when neurons are being encircled with myelin by oligodendrocytes. At this stage, neurons are capable to synthesize cholesterol at sufficient levels (Saito *et al.* 1987; Suzuki *et al.* 2007). Cholesterol synthesis ablation in neural stem cells during embryonic development leads to reduced brain size, newly generated neurons and perinatal lethality (Saito *et al.* 2009). After myelination completes, cholesterol synthesis is downregulated in neurons. Due to downregulation of 24-dehydrocholesterol reductase (24-DHCR) and lanosterol 14 alpha demethylase (CYP51) in neurons, lanosterol is difficulty converted to cholesterol. Unlike astrocytes, adult neurons have a lower capacity to compensate for a cholesterol deficit by *de novo* synthesis and mostly rely on surrounding astrocytes which are perfectly capable to synthesize cholesterol that satisfy theirs's and neuron's needs (Figure 1.3) (Quan *et al.* 2003). Conditional ablation of cholesterol synthesis in adult mice neurons leads to significant transfer and uptake of glia-derived cholesterol by neurons (Fünfschilling *et al.* 2012). As adult neurons

mostly rely on glial sources of cholesterol, the mice lacking cellular cholesterol synthesis specifically in adult neurons are phenotypically indistinguishable from controls. Furthermore, no obvious signs of neurodegeneration or inflammation were observed (Fünfschilling *et al.* 2007). Cholesterol-producing glial cells implies mechanisms of release, intercellular transport and uptake via specific receptors. Indeed levels of LDL-R related lipoprotein receptor 1 (LRP1) remains constant in this mouse model indicating that adult neurons express sufficient lipoprotein receptors to import cholesterol as ApoE-containing lipoprotein particles (Fünfschilling *et al.* 2007). All the evidences advocate that some adult neurons do not achieve autonomous cholesterol synthesis, which is very likely to rely on glia cells, especially, astrocytes, as those glia cells express apolipoproteins such as ApoE and maintain high rate of cholesterol synthesis throughout life (Claudepierre & Pfrieger 2003a).

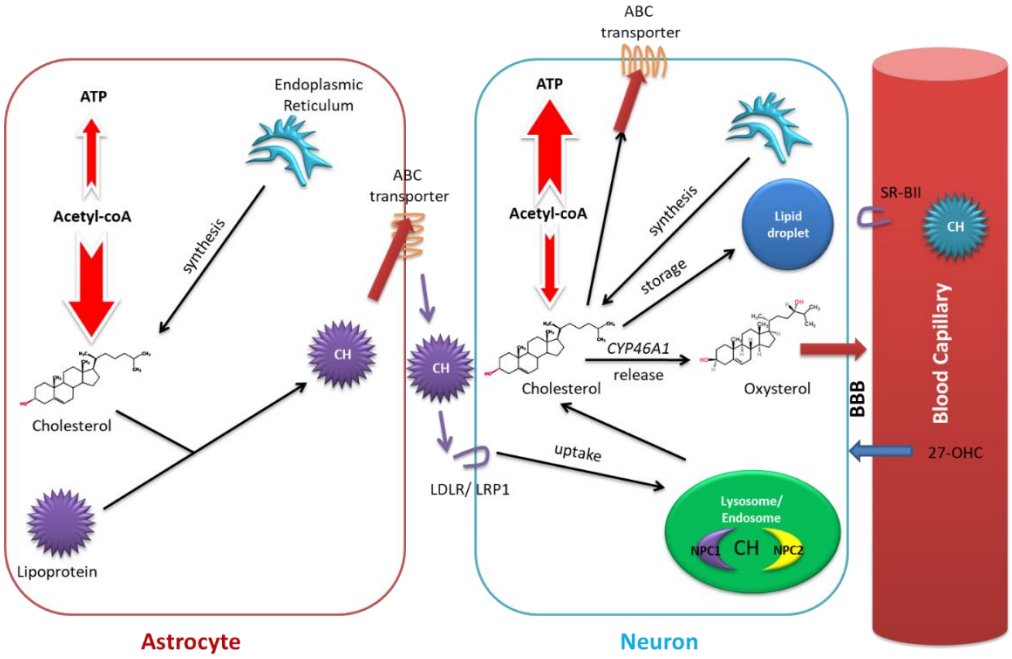

Figure 1.3: Cholesterol transport from astrocytes to neurons. In adult brain, cholesterol synthesis nearly ceases in neurons, and neurons rely on astrocytes (neighboring cells) to get their needs. Astrocytes synthesize enough cholesterol to satisfy the brain's needs. Cholesterol is synthesized in the ER, then it is loaded onto ApoE containing lipoproteins. Those lipoproteins are released from astrocytes near neuronal synapses, where they are internalized via receptor mediated endocytosis. Esterified cholesterol is then hydrolyzed in lysosomes, and free cholesterol is released out of lysosomes via NPC1 and NPC2. Excess cholesterol is excreted via esterification by acyl-coenzyme A: cholesterol acyltransferase 1 (ACAT1) and storage in lipid droplets, hydroxylation to 24-hydroxycholesterol, via cholesterol 24-hydroxylase (CYP46A1), which can readily by-pass the BBB, or loading onto lipoprotein and excretion via ATP binding cassette A1 (ABCA1).

2.2. Transport

In cholesterol producing cells, newly synthesized cholesterol are transported from ER to the plasma membrane (PM) in a rapid ATP-dependent manner (DeGrella & Simoni 1982). During the transport to PM, the Golgi apparatus is partially involved in the process (Heino *et al.* 2000). The transport of cholesterol to the different subcellular compartments occurs using a combination of vesicle-mediated inter-organelle transport and protein-mediated monomeric transfer through the aqueous cytosol (Kaplan & Simoni 1985; Zhang & Liu 2015). Since cholesterol is minimally hydrophilic, only trace amounts of free cholesterol are detected in cytoplasm and most of the cholesterol exists in a protein binding complex form, such as ApoE-binding cholesterol particles in the CNS (Zhang & Liu 2015). The newly synthesized cholesterol is loaded into ApoE containing high density lipoproteins (HDL)-like lipoproteins, which are then exported from astrocytes to neurons, where they bind via ApoE to lipoprotein receptors, and are internalized via receptor mediated endocytosis into neurons (Figure 1.3). There are several lipoprotein receptors that have been identified on neuronal surface including low density lipoprotein receptor (LDLR), (LRP1) (Herz 2009), and the most recently identified lipolysis stimulated lipoprotein receptor (LSR) (Stenger *et al.* 2012). After internalization, the ApoE-cholesterol particles are processed to free cholesterol in lysosomes (Figure 1.3) (Fagan & Holtzman 2000; Ikonen 2008) and then transported to membranes. The cholesterol transport between cells influences and is influenced by the fluidity of cell membranes and the distribution of microdomains such as lipid rafts. Rafts have a special lipid and protein composition, they are especially enriched in glycosphingolipids and sphingomyelin on the exofacial leaflet and glycerolipids (e.g., phosphatidylserine and phosphatidylethanolamine) on the cytofacial leaflet., whereas cholesterol is enriched in both leaflets (Figure 1.4). In lipid rafts, proteins are anchored to membranes by saturated acyl chains, where they are relatively depleted of most transmembrane proteins. Lipid rafts have been implicated in numerous cellular processes, including signal transduction, and protein and lipid sorting (Xu *et al.* 2001). LRP1, was found to be associated to lipid rafts (Wu & Gonias 2005). In addition, when the membrane fluidity increases, the intermolecular packing of phospholipid fatty acyl chains decreases, altering the raft composition (Ollila *et al.*

2007), including LRP1, thus influencing the cholesterol transport.

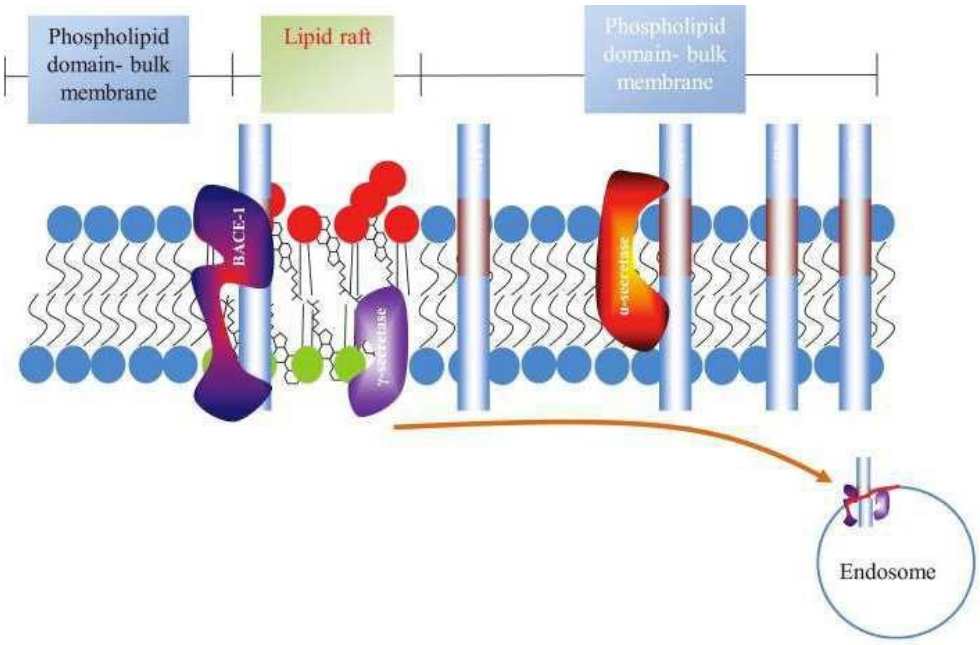

Figure 1.4: Lipid rafts structure. The lipid raft is shown as part of the plasma membrane. The phospholipid domain (light blue) is separate from the lipid raft. The latter is enriched in glycosphingolipids and sphingomyelin (red) on the exofacial leaflet and glycerolipids (e.g., phosphatidylserine and phosphatidylethanolamine; green) on the cytofacial leaflet. Cholesterol (black cyclic structure) is enriched in both leaflets. The acyl chains in lipid rafts are more able to pack together. Amyloid precursor protein APP (Aβ region in maroon) is localized in raft and non-raft fractions but predominates outside rafts. The α-secretase is not raft-associated, while the β- and γ-secretases predominate in rafts. The cell surface is shown for clarity, although β-cleavage predominantly occurs in endosomes. Figure from (Hicks et al. 2012).

2.2.1. Lipoproteins formation and efflux in the CNS

Lipoproteins in CNS are HDL-like particles that resemble that of the plasma (Figure 1.5). Plasma HDL contains primarily all of ApoAI, ApoAII, ApoE, ApoAIV, and ApoCs (Davidsson *et al.* 2010), whereas CNS HDL-like particles contain majorily ApoE and ApoAI, and ApoJ, ApoD, ApoAII and ApoAIV at a lower extent (Borghini *et al.* 1995; Koch *et al.* 2001). However, ApoAI mRNA, but not protein, has been detected in the brain (Roheim *et al.* 1979a; Pitas *et al.* 1987a). This is due to the fact that, unlike ApoE which is synthesized in the CNS, ApoAI is mainly transferred from the plasma to the CNS via the BBB in the choroid plexus (Roheim *et al.* 1979a; Pitas *et al.* 1987a; Linton *et al.* 1991). Another main discrepancy between CNS and peripheral HDL is linked to their respective targets: plasma HDL collect cholesterol from tissues and transports it to liver, while the HDL-like in CNS distributes cholesterol to neurons through interactions with lipoprotein receptors via ApoE (Figure 1.5) (Mahley 2016). Despite

that, for lipoprotein formation and metabolism, enzymes, transporters, and receptors in the CNS are like the ones found in the periphery.

2.2.1.1. Apolipoproteins in the CNS

Apolipoproteins are essential components of lipoproteins as the lipid composition, lipoprotein solubility and receptor affinity depend on their repartition at the surface.

2.2.1.1.1. ApoE

The major apolipoprotein in the CNS is ApoE (34 kDa). The brain is the second most ApoE producing site in the body, where the liver contributes to 75 % of the production (Elshourbagy *et al.* 1985; Linton *et al.* 1991). There is a dynamic exchange of ApoE among brain cells, as ApoE is the major transport protein for cholesterol and other lipids, where ApoE-mediated cholesterol exchange occurs between glial and neuronal cells in CNS (Zhang & Liu 2015). Astrocytes and also specialized radial glia cells (Bergmann glia of the cerebellum, and Müller cells of the retina), possess the highest concentrations of ApoE (Boyles *et al.* 1985) followed by oligodendrocytes, microglia, and ependymal layer cells (Mahley *et al.* 2006). Neurons may also express ApoE under certain conditions, such as excitotoxic injury (Buttini *et al.* 2010). To map ApoE expression in the CNS, Xu *et al.* (2006) have generated "EGFP *apoe* mice" by inserting enhanced green fluorescent protein (EGFP) controlled by the endogenous promoter into one *apoe* allele where the other *apoe* allele maintains normal cellular physiology. Although hippocampal neurons did not express EGFP under normal conditions, kainic acid treatment, which induces excitotoxic injury, actuated intense expression of EGFP in injured neurons. This demonstrates that neurons express ApoE in response to excitotoxic injury (Xu *et al.* 2006).

When nerve injury happens in CNS, the synthesis of ApoE by glial cells increased up to 150-fold (Ignatius *et al.* 1986). In support of this idea, in *apoe*−/− mice there is impaired clearance of degenerating nerves (Fagan *et al.* 1998). *Apoe* −/− mice also have learning deficits (Fullerton *et al.* 1998) and develop neurofibrillary tangles, which are primary markers of AD (Bi *et al.* 2001). In addition, ApoE deficiency in neurons increases the susceptibility of the mice to ischemic injury (Sheng *et al.* 1999), as well as ER stress after ischemia/reperfusion (Osada *et al.* 2009). *In vitro*, cultured *apoe*

knockout astrocytes secreted lipoproteins with low phospholipids and free cholesterol levels (Fagan *et al.* 1999). However, in some *in vivo* studies, *apoe* knockout mice revealed normal cholesterol contents and turnover in the brain (Lomnitski *et al.* 1999; Han *et al.* 2003; Jansen *et al.* 2009). On the other hand, other studies showed reduced cholesterol levels (Levi *et al.* 2005). This suggests that alternative apolipoproteins can, at least partially, substitute for ApoE.

Under normal physiological conditions, conditional deletion of *apoe*, specifically from neurons in *apoe* knock out mice, decreased cortical and hippocampal ApoE protein levels by 20 % (Knoferle *et al.* 2014). This is consistent with the observation that the remaining ApoE was about 20 % of the total ApoE protein levels when ApoE was deleted in astrocytes (Knoferle *et al.* 2014). Thus, neurons likely synthesize and secrete fifth of total ApoE in CNS.

Neurons contain a splicing variant of *apoE* mRNA not found in astrocytes or hepatocytes. Under normal conditions, in wildtype and *apoe* knock in mice, cortical and hippocampal neurons retain intron-3 in *apoe* mRNA and produce low levels of mature *apoe* mRNA ready to be translated to ApoE protein (Xu *et al.* 2008). Mice that were intraperitoneally injected with kainic acid to induce neurodegeneration exhibit a markedly decrease in *apoe* mRNA with intron-3 levels in injured hippocampal neurons, while mature *apoe* mRNA (lacking the intron) and ApoE protein were increased (Xu *et al.* 2006, 2008). The neuron-specific regulation of *apoe* expression demonstrates the critical role of ApoE production, presumably for redistribution of cholesterol for cellular repair and maintenance and possibly as a DNA binding protein and transcriptional regulator of multiple genes (Theendakara *et al.* 2016).

Upon the addition of conditioned culture medium from astrocytic cell lines or from astrocytes isolated from *apoe*-/- mice to cultured neurons, the mRNA and protein expression levels of ApoE in the neurons was markedly increased by 3-4-fold and 4-10-fold respectively. This suggests that neuronal ApoE production is regulated at least in part by an astrocyte-secreted factor or factors through the extracellular signal–regulated kinase pathway (Harris *et al.* 2004). Stress- and injury-induced upregulation of neuronal ApoE production could be partly mediated by astrocyte activation (astrocytosis) after acute injury, including traumatic brain injury, oxidative stress, and

amyloid-β (Aβ) accumulation. The *apoe* gene is a polymorphic gene, with three common alleles, termed E2, E3, and E4. Harboring the E2 allele is protective against onset, while the E3 allele is neutral in this regard. In contrast carrying the E4 allele increases the risk of developing AD 4–10 fold (Eisenstein 2011). ApoE4 has been suggested to affect both β-amyloid and neurofibrillary tangle pathology in AD (Rohn 2013). ApoE4 is a major cholesterol transporter in the brain and cholesterol rich membrane domains that increase β-amyloid production by affecting β and γ-secretase complex (Ye *et al.* 2005).

2.2.1.1.2.ApoAI

ApoAI is a 27-kDa protein, which is one of the most abundant apolipoproteins in the CSF, and ApoAI protein -but not mRNA- has been detected in brain tissues (Roheim *et al.* 1979b; Pitas *et al.* 1987b; Linton *et al.* 1991). Thus, ApoAI is present in the CSF but is not produced within the CNS. In support of this, primary cultures of astrocytes have been found to secrete ApoE, ApoJ and ApoD, but not ApoAI (DeMattos *et al.* 2001). ApoAI in CNS is believed to be plasma derived, crossing the BBB at the choroid plexus, yet the exact mechanism stays unidentified (Roheim *et al.* 1979; Pitas *et al.* 1987). In a recent study, recombinant fluorescently tagged human ApoAI was intravenously injected into mice where it localized to the choroid plexus and rapidly accumulated in the brain (Stukas *et al.* 2014). *In vitro*, human ApoAI was specifically bound, internalized, and transported across confluent monolayers of primary human choroid plexus epithelial cells and brain microvascular endothelial cells (Stukas *et al.* 2014). Although the choroid plexus contains numerous specific transporters, identity of ApoAI transporter is still unknown (Stukas et al. 2014). Last but not least, ApoAI can be synthesized by the endothelial cells of the porcine BBB suggesting an *in situ* synthesis at the BBB (Möckel *et al.* 1994).

Many function(s) of brain ApoAI are still to be discovered and deciphered. It is known that ApoAI plays a major role in peripheral cholesterol transport and it seems probable that ApoAI plays an analogous function in the CNS (Mahley *et al.* 1984). In support of this, ApoAI is an important lecithin-cholesterol acyltranferase (LCAT) activator, and as LCAT is expressed in the brain (Smith *et al.* 1990), this provides a potential mechanism for CNS cholesterol transport.

2.2.1.1.3.ApoJ (clusterin)

ApoJ which is also known as clusterin (CLU), exists as multiple protein isoforms including the 80 kDa glycosylated mature/secreted form of CLU (mCLU), composed of two chains α- and β-, and smaller non-modified nuclear and intracellular forms of CLU (nCLU and icCLU, respectively). These isoforms, which are expressed at the highest levels in the brain, are suggested to play distinct roles in various disease processes such as those involving inflammation and apoptosis (Woody & Zhao 2016). Fagan *et al.* reported that ApoJ containing lipoproteins in the CNS are small, lipid-poor particles that are secreted from astrocytes (Fagan *et al.* 1999b). In the CSF, ApoJ and ApoE are present on distinct lipoprotein particles (Fagan *et al.* 1999b). It is produced majorly by astrocytes, but also in pyramidal neurons of the hippocampus and Purkinje neurons in the cerebellum (Pasinetti *et al.* 1994). ApoJ functions as a lipid-transport protein, with the ability to induce cholesterol efflux, and as a molecular chaperone in the cellular stress response (Gelissen *et al.* 1998; Wyatt *et al.* 2009). ApoJ appears to function in a similar manner to ApoE in lipid metabolism and transport in the CNS, although much less is known about ApoJ. The nCLU and icCLU isoforms increase particularly during cellular stress (Rizzi & Bettuzzi 2010). ApoJ is dramatically upregulated during cellular stress, this upregulation helps protect against oxidative stress and neuroinflammation (Huang *et al.* 2016). Although the knockout of *apoj* -/- alone showed no significant change in the CNS development and morphology (Charnay *et al.* 2008), yet a deficiency of ApoJ intensified the severity of ischemic injury in the brain (Imhof *et al.* 2006) and the susceptibility to axotomy-induced death in motor neurons (Wicher & Aldskogius 2005). Thus, ApoJ plays a neuroprotective role in the CNS. On the other hand, the absence of ApoJ reduced neuronal death after hypoxic-ischemic injury *in vivo* and *in vitro*. Therefore, clusterin may contribute to neurotoxicity (Han *et al.* 2001; Xie *et al.* 2005).

2.2.1.1.4.ApoD

ApoD is a 29-kDa glycoprotein that belongs to the lipocalin family, thus has little homology with other apolipoproteins involved in lipid transport and cannot support the synthesis of nascent lipoprotein particles on its own. It is produced in the brain and is associated with CSF HDL. ApoD is produced by astrocytes and oligodendrocytes

(Rassart *et al.* 2000; Eichinger *et al.* 2007). ApoD expression is low in human neonates and increases in expression throughout life resulting in six- to eight-fold higher levels at the mRNA and protein levels in adults (Kim *et al.* 2009b). Early studies suggested that ApoD binds lipids, including cholesterol, arachidonic acid and a variety of steroids such as pregnenolone, dihydrotestosterone, testosterone, dehydroepiandrosterone and estradiol (Elliott *et al.* 2010). ApoD expression is increased in the dorsolateral prefrontal cortex during normal aging (Kim *et al.* 2009b). The dorsolateral prefrontal cortex is a region that plays a critical role in attention and working memory and is implicated in psychiatric disorders, such as schizophrenia, autism and depression (Lewis & Gonzalez-Burgos 2006; Koenigs & Grafman 2009). ApoD shows neurotrophic and synaptogenic effects in root ganglion neurons *in vitro*. ApoD increased neurite outgrowth and upregulated the expression of presynaptic molecules, including synaptophysin and synaptotagmin, as well as post-synaptic density protein-95 (PSD95). In addition to the neurotrophic effects of ApoD, increased expression of LDLR and ApoER2 was reported (Kosacka *et al.* 2009).

2.2.1.2. ABC transporters

Astrocytes majorly secrete nascent discoidal HDL particles that are further lipidated by ABC transporters (Figure 1.5), those lipoproteins primarily contain phospholipids, unesterified cholesterol, ApoE and ApoJ (Ladu *et al.* 2000). Glia-derived lipoproteins contain low levels of esterified cholesterol and desmosterol, which is a precursor of cholesterol, indicating that it might be converted later on after uptake in neurons (Levi *et al.* 2005). ABC transporters are ATP-binding cassette proteins that requires ATP hydrolysis for secretion and lipidation of ApoE containing lipoproteins (Tachikawa *et al.* 2005; Kim *et al.* 2008). As stated previously, ApoE containing lipoproteins are synthesized by astrocytes but not neurons. Two mechanisms have been proposed for the formation of ApoE containing HDLs by glial cells: 1) Direct secretion of lipidated ApoE; 2) Secretion of nascent ApoE lipoproteins that are extracellularly lipidated upon

efflux of cellular lipids (Chen *et al.* 2013a).

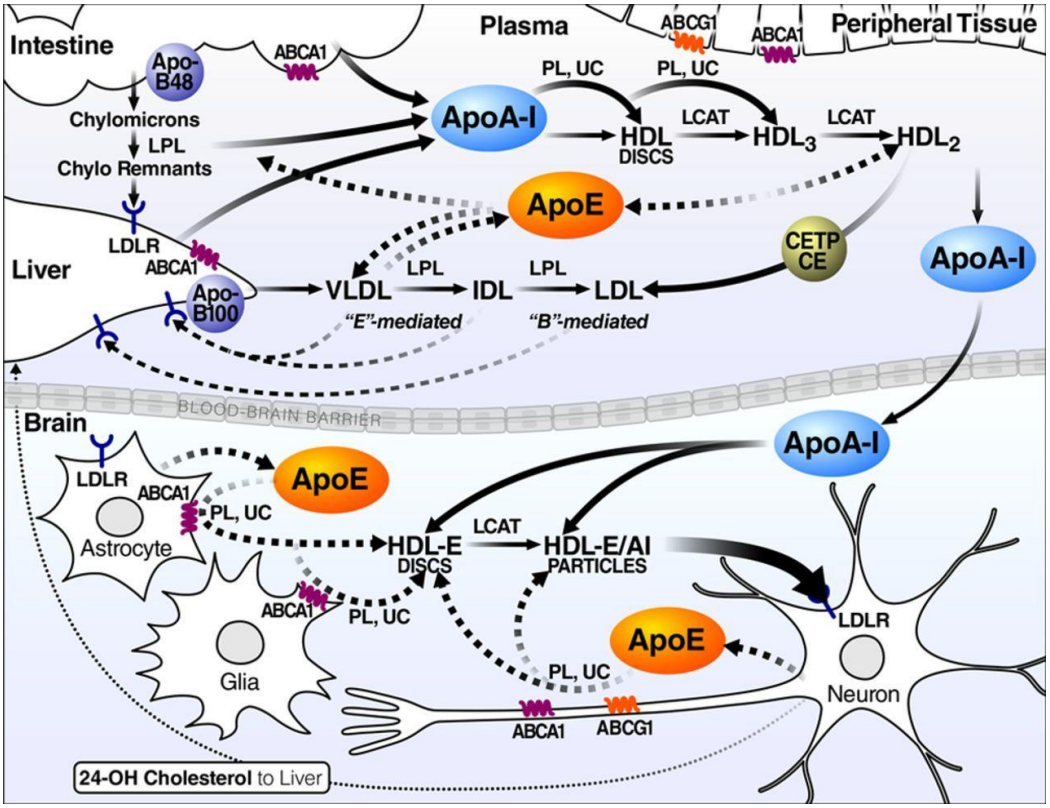

Figure 1.5: Lipoprotein metabolism in periphery and CNS. The upper peripheral portion illustrates the major pathways of plasma lipoprotein metabolism involving chylomicrons synthesized by the intestine and very low-density lipoproteins (VLDL) synthesized by the liver. The origin of high-density lipoproteins (HDL) and apoAI and the role of HDL in the redistribution of lipids from cells with excess cholesterol and to the liver for excretion (reverse cholesterol transport) are illustrated. In the BBB presence, a minimal exchange of peripheral and central lipoproteins occurs. However, small discoidal HDL-like particles can traverse. Most lipoprotein particles originate from astrocytes in the brain, yet many constituents of lipoprotein particles can be synthesized and processed differently in neurons. Astrocytes can secrete lipoprotein particles into the cerebrospinal fluid (CSF) or reabsorb the smaller particles for remodeling and reloading of lipids. Lipoprotein receptors and lipoprotein lipase (LPL) located on the surface of astrocytes and neurons appear to play a regulatory role in lipoprotein metabolism in the CNS, effects that are brain region-specific. Further abbreviations: ABCG1 indicates ATP-binding cassette transporter G1; apo is apolipoprotein; CE, cholesteryl ester; CETP, cholesteryl ester transfer protein; Chylo, chylomicron; E, apoE; LCAT, lecithin–cholesterol acyltransferase; LDLR, LDL receptor family members; LPL, lipoprotein lipase; PL, phospholipid; and UC, unesterified cholesterol. Figure taken from (Mahley 2016).

All of ABCA1, ABCG1, and ABCG4 transporters are highly expressed in both neurons and glia (Figure 1.6) (Tachikawa *et al.* 2005; Kim *et al.* 2007; Wang *et al.* 2008a; Sun 2014). ApoE is secreted by astrocytes as a lipid free or lipid poor lipoprotein (Elshourbagy *et al.* 1985), the initial acquisition of cholesterol by ApoE requires the action of ABC transporter ABCA1, which is expressed on astrocytes, microglia and neurons (Wahrle *et al.* 2004a). ABCG1, which is expressed in multiple tissues including the liver, retina and brain, may also play a role in transferring lipids to ApoE, as it matures into a lipidated lipoprotein particle (Kennedy *et al.* 2005), and there is evidence that ABCG1 can regulate brain lipid homeostasis (Wahrle *et al.* 2004). Thus, the nature of the extracellular acceptor for lipid efflux appears to be different for ABCA1 and ABCG1: lipid efflux mediated by ABCA1 prefers lipid-poor acceptors (nascent lipoproteins), whereas ABCG1 prefers lipidated acceptors such as HDLs.

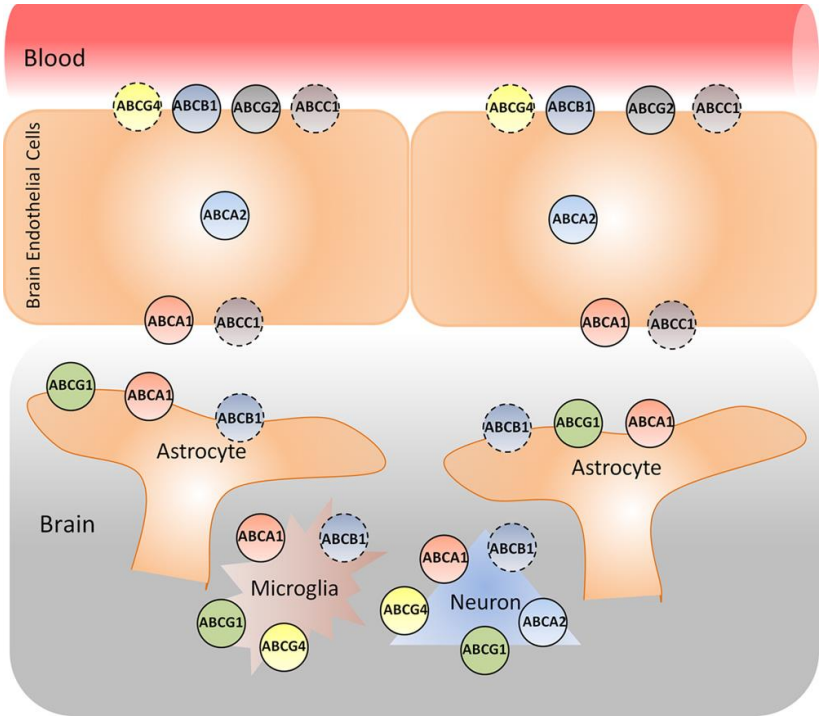

Figure 1.6: ABC transporters in the CNS. Expression of ABC transporters in the brain. Dotted circles indicate transporter localization that requires confirmation due to limited information or conflict in reporting. Figure taken from (Abuznait & Kaddoumi 2012)

In the CNS, the main pathway by which apolipoproteins induce cholesterol efflux is through ABCA1. By modulating ABCA1 levels and activity, it has been shown that ABCA1 is involved in cholesterol efflux from astrocytes but not from neurons (Chen *et al.* 2013a). Experiments with *abca1* -/- mice demonstrated significant reduction of cholesterol and ApoE levels in the CSF (Hirsch-Reinshagen *et al.* 2004; Wahrle *et al.*

2004b) It has been reported that neuron and glia-specific ABCA1 deficiency decreased levels of cholesterol and ApoE in the brain, and caused increase of the HDL receptor SR-BI in brain capillaries thus promoting the uptake of esterified cholesterol from plasma HDL into the brain (Karasinska *et al.* 2009b). The brain specific knockout of *abca1*−/− also demonstrated alteration in motor activity and a reduction of excitatory synapses and synaptic vesicles (Karasinska et al., 2009). These experiments with *abca1* knockout mice showed that ABCA1 is a crucial molecule for the formation of ApoE-containing lipoproteins in the CNS and thus, a key regulator for cholesterol metabolism. Other ABC transporters that are expressed in the brain are ABCG1 and ABCG4. ABCG1 is expressed in multiple tissues while ABCG4 is specifically expressed in the CNS (Bojanic *et al.* 2010a). ABCG1 is involved in cholesterol efflux to apolipoproteins and lipoproteins from astrocytes but not from neurons, while ABCG4, whose expression is much higher in neurons than astrocytes, is involved in cholesterol efflux from neurons but not astrocytes (Chen *et al.* 2013a). Individual deficiency of ABCG1 or ABCG4 in mice showed essentially normal brain sterol levels, where the absence of one transport protein compensated the absence of the other, but *abcg1* −/− *abcg4*−/− mice demonstrated altered expression of cholesterol synthesis related genes, cholesterol accumulation in the brain, and significant increases of some sterol intermediates-desmosterol, lathosterol, lanosterol and oxysterols, in the brain (Wang *et al.* 2008a; Bojanic *et al.* 2010a; Sun 2014). There is a defect in cholesterol efflux from astrocytes to HDL only when both ABCG transporters were eliminated. On the other hand, *abcg4 -/-* mice, but not *abcg1 -/-* mice, demonstrated a defect in associative fear memory (Bojanic *et al.* 2010b). Thus, these studies indicate that ABCG1 and ABCG4 share some functions for sterol efflux, but ABCG4 might more closely relate to brain function. Loss of both ABCG1 and ABCG4 results in accumulation of oxysterols in the retina and/or brain, in altered expression of liver X receptor (LXR) and sterol-regulatory element binding protein-2 (SREBP-2) target genes (Bojanic *et al.* 2010b). Furthermore, overexpression of either ABCG1 or ABCG4 increased the processing of SREBP-2 to the transcriptionally active protein, thus accounting for the observed increase in the expression of SREBP-2 target genes and cholesterol synthesis (Tarr & Edwards 2008).

2.2.2. Lipoprotein receptors in the CNS

There are several receptors of the LDLR family present in the CNS, like LDLR itself,

LRP1, very low density lipoprotein receptor (VLDLR), and ApoE receptor 2 (ApoER2), which are expressed in neurons, astrocytes, microglia, and oligodendrocytes (Brown *et al.* 1997; D'Arcangelo *et al.* 1999; Hayashi *et al.* 2007; Herz 2009).

2.2.2.1. LDLR

The LDLR expression was downregulated following cholesterol-containing lipoproteins accumulation and upregulated following cholesterol deprivation in neuronal and glial cells (Fan *et al.* 2001). In addition, LDLR prefers lipid-bound ApoE over non-lipid bound ApoE (Ruiz *et al.* 2005). Astrocytes secrete lipid bound ApoE particles which are then internalized via LDLR in order to deliver cholesterol to neurons. ApoE containing lipoprotein particles secreted by astrocytes have higher affinity for LDLR over LRP1 (Fagan *et al.* 1996). In *ldlr -/-*, there is a 50 % increase in ApoE particles in the CSF when compared to wild type mice (Fryer *et al.* 2005). In this study, *ldlr -/-* ApoE3 and *ldlr -/-* ApoE4 mice show a strong increase of ApoE levels in extracellular fluid when compared to ApoE3 and ApoE4 mice expressing LDLR. On the contrary, when LDLR is overexpressed there is a 50-90 % decrease in ApoE levels (Kim *et al.* 2009a). Those results showed the importance of LDLR in ApoE containing lipoproteins internalization. Other than its role in ApoE internalization, LDLR plays a role in sustaining cognitive function, since in *ldlr*−/− mice show learning and short- and long- term memory problems associated with a reduction of hippocampal presynaptic boutons, regardless of diet type (Mulder *et al.* 2004; de Oliveira *et al.* 2011). Otherwise, *ldlr -/-* mice show no motor or sensory problems, but increased locomotor activity (Elder *et al.* 2008).

2.2.2.2. LRP1

LRP1 expression has been detected in neuronal cell bodies and proximal processes including the hippocampus and the cerebellum (Pitas *et al.* 1987a; Herz & Chen 2006), as well as in the pericytes (Tooyama *et al.* 1995). LRP1 is also found in astrocytic foot processes and microglia in hippocampus, cortex and cerebellum and along capillary membranes in a discontinuous manner, reflecting a role in the selective permeability at the level of the BBB. Complete *lrp* knockout is embryonic lethal with severe malformations in the CNS (Herz *et al.* 1992). LRP1 deficient mice show increased ApoE levels in the brain due to altered ApoE catabolism. This demonstrates the clear

importance of LRP in CNS development, which clearly shows a critical role of this receptor in CNS development. Indeed, LRP1 has been implicated in phagocytosis of cell debris, and the transport and elimination of the β-amyloid peptide (Fujiyoshi *et al.* 2011; Chung *et al.* 2016). In addition, LRP1 has been shown to have the highest endocytotic rates of ApoE containing lipoproteins (Li *et al.* 2001). Similarly, in an *in vitro* study on an immortalized hypothalamic cell line, LRP1 demonstrates the highest binding capacity to CSF isolated HDL over other lipoprotein receptors like LDLR (Fagan *et al.* 1996). Conditional deletion of *lrp1* gene from neurons in mouse brain significantly decreases ApoE, cholesterol, and sulfatide levels (Liu *et al.* 2010). Nevertheless, glial cell-derived ApoE containing lipoprotein-mediated activation of axonal growth to promote neuron communication is not solely LRP1 dependent and depends on ABCG1 and LDLR (Fryer *et al.* 2005). Thus, other alternative or complementary pathways/transporters may exist that contribute towards the maintenance of adequate lipid status and intercellular lipid exchange in the brain.
Neuronal LRP1 deficient mice present not only metabolic disturbances but also cognitive and neurodegenerative disorders. Indeed, these mice acquire significant alterations in neuronal function during aging. The density of dendritic spines as well as the expression of presynaptic markers (synaptophysin) and postsynaptic markers (PSD95) are decreased. Expressions of glial fibrillary acidic protein (GFAP) and Ionized calcium binding adaptor (Iba-1) molecules are increased in hippocampus, as well as different markers of microglial activation such as Interleukin β (Ilβ), Tumor Necrosis Factor-α (TNFα) and Interleukin 6 (IL-6) (Liu *et al.* 2017). In addition to these inflammatory processes, apoptotic processes and neurodegeneration are present, demonstrated respectively by the activation of caspases 3 and 6 and a decrease in Neuronal Nuclei (NeuN) labeling (Chung *et al.* 2016). At the behavioral level, these LRP1 deficient mice are hyperactive, and exhibit troubles in motor coordination and memory. These behavioral disorders are related to severe long term potentiation deficiency (Liu *et al.* 2010).

2.2.2.3. VLDLR and ApoER2 receptors

The VLDLR and ApoER2 are other family members of LDLR family that are primarily expressed on neuronal surface. In addition to their role in lipoproteins internalization, VLDLR and ApoER2 are involved in reelin signaling, which is crucial for neuronal migration and cell positioning during brain development, synaptic plasticity, dendritic

spines formation, long-term potentiation and neuronal survival. The knockout of those receptors perturbs neuronal and synaptic functions (D'Arcangelo *et al.* 1999; Beffert *et al.* 2006; Niu *et al.* 2008). Apolipoprotein E receptor 2 (ApoEr2) is a postsynaptic protein involved in long-term potentiation (LTP), learning, and memory. ApoER2 form a multiprotein complex with post-synaptic density protein 95 (PSD95) and N-methyl-D-aspartate (NMDA), and play a role in synaptic transmission (Beffert et al. 2005; Hoe et al. 2006). *In vitro* studies on neuronal cell cultures demonstrated that PSD95 increased ApoER2 surface levels, and synaptic and dendritic spines density (Dumanis *et al.* 2011). *Apoer2 -/-* mice display decreased dendritic spines and synaptic density (Dumanis *et al.* 2011). Also, *apoer2 -/-* mice exhibit problems in contextual fear conditioning, where mice spent longer periods of time freezing, and in long term potentiation (Weeber *et al.* 2002).

VLDLR is a multi-ligand ApoE receptor, which plays a role in neuronal migration and involved in brain development through reelin signaling. There is a 50 % sequence homology of VLDLR to ApoER2 (Reddy *et al.* 2011). VLDLR is highly expressed in cortex and cerebellum, where neurons and astrocytes express different splicing variants of VLDLR, potentially resulting in differential lipid uptake between neurons and astrocytes (Sakai *et al.* 2009). *Vldlr*/apoer2 double knockout mice display inversion of cortical layers and cerebellar dysmorphology (Trommsdorff *et al.* 1999*). Vldlr* knockout mice also display contextual fear conditioning deficits and a moderate defects in long term potentiation (Weeber *et al.* 2002). However cholesterol and polyunsaturated fatty acids (PUFA) level remain normal (Rahman *et al.* 2010). This suggests that observed deficits in *vldlr* –/– and *apoE2* –/– mice, like disruption of neuronal migration, cell positioning, and cell plasticity, are more related to the reelin-dependent pathway, where ApoER2 and VLDLR interact with NMDA (Weeber *et al.* 2002; Beffert *et al.* 2005) and PSD-95 (Beffert *et al.* 2005) in the brain.

2.2.2.4. SR-BI

SR-BI, a multi-ligand receptor that promotes the bidirectional flux of cholesterol between lipoproteins and cellular membranes. In the brain, SR-BI is present on the membrane of brain capillary endothelial cells, where it is reported to mediate the selective uptake of cholesterol from plasma HDL and LDL (Rigotti *et al.* 1997). SR-BI can also allow the uptake of vitamin E (Goti *et al.* 2001) that may play an important

role in preventing oxidative stress and protecting brain cells against neurodegeneration (Balazs *et al.* 2004; Thanopoulou *et al.* 2010). SR-BI is therefore one of the few mean permitting cholesterol trafficking between the brain and periphery

2.2.3. Cholesterol utilization in neurons

2.2.3.1. ApoE-cholesterol particles endocytosis

Neurons uptake ApoE-cholesterol particles by receptor-mediated endocytosis. ApoE binds to lipoprotein receptors, those receptors are linked to clathirin molecules intracellularly (Figure 1.7). As endocytosis begins, a clathirin pit forms and eventually engulfs the particle, forming a coated vesicle. Endocytosis is dependent on several factors: the cholesterol/phosphoinoside content in the inner leaflet of the PM, the proteins involved in endocytosis and the forces exerted by the cytoskeleton. The fission of the vesicle and the PM is induced by dynamin 2 protein. After fission, clathirin molecules (triskelions) dissociate from the vesicles, thus uncoating them (El-Sayed & Harashima 2013).

2.2.3.2. Vesicles recycling

The vesicles can be directly recycled to the PM without entering the late endosome/lysosome compartments. The lipid recycling pathway, concerns non-esterified cholesterol and sphingomyelin molecules derived from membranes endocytosed at the same time as lipoprotein particles (Hornick *et al.* 1997; Hao & Maxfield 2000). The slightly slower protein recycling pathway involves lipoprotein receptors, clathrin proteins, ApoE protein, etc. (Hao & Maxfield 2000). If they are not recycled, they enter Rab5 and EEA1 (Early Endosome Antigen) expressing early endosomes (Simonsen *et al.* 1998). A drop in pH driven by proton pumps due to ATP hydrolysis, will cause the dissociation of lipoprotein receptors from the vesicles. Those lipoprotein receptors are then recycled and transported again to the PM, leaving the ApoE-cholesterol particles in an endosome. The endosome then fuses with a lysosome, forming a secondary lysosome, where hydrolytic lysosomal enzymes degrade

lipoproteins to its components; cholesterol, amino acids, and fatty acids (Figure 1.7).

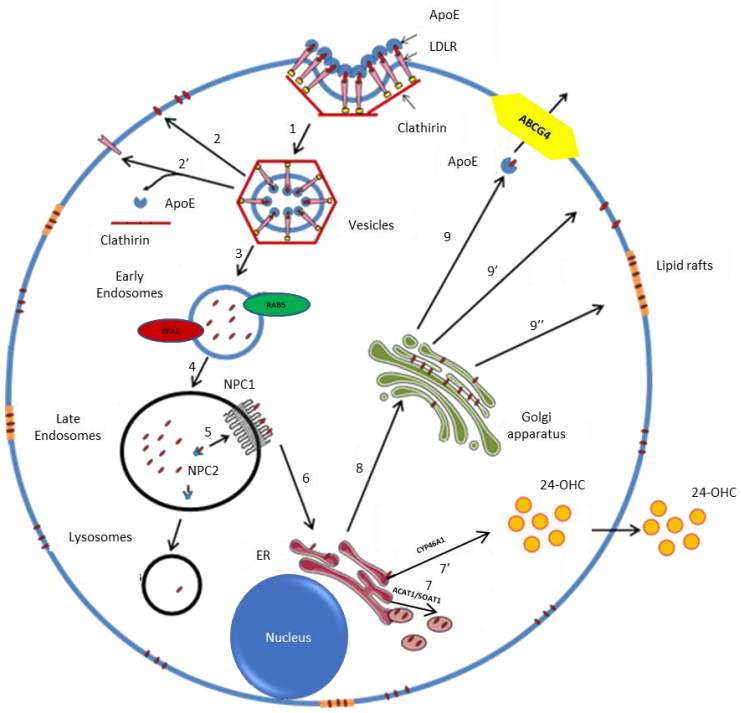

Figure 1.7. Cholesterol-containing lipoproteins internalization and utilization in the cell. 1-Internalization of ApoE-cholesterol lipoparticles after binding to lipoprotein receptors via clathirin vesicles. 2 and 2'- Recycling lipids (2) and proteins (2') 3 and 4- Engagement in the endosomal / lysosomal compartment. 5- Export of cholesterol from late endosomes via NPC1 and NPC2 before the lysosome. 6- Export of cholesterol to the endoplasmic reticulum (ER). 7- Storage in the form of cholesterol esters. 7'-conversion to 24 hydroxycholesterol which can readily bypass. 8- Transfer to the golgi apparatus. 9-Efflux out of the cell (ABCA1 / ApoE). 9' and 9''- Transfer to the lipid membrane or rafts. Symbols: ApoE: apolipoprotein E, LDLR: low-density lipoprotein receptor, RAB5: Ras-related protein 5, EEA1: Early endosome antigen 1, NPC 1, 2: Niemman Pick type C proteins 1 and 2, ER: endoplasmic reticulum, CYP46A1: cholesterol 24-hydroxylase enzyme, 24-OHC: 24-hydroxycholesterol, ACAT1/SOAT1: Acyl-coenzyme A: cholesterol acyltransferase/Sterol O-acyltransferase, ABCA1: ATP-binding cassette A1. Figure adapted from (Djelti 2013)

2.2.3.3. Early endosomes / late endosomes / lysosomes

Early endosomes fuse to form late endosomes followed by lysosomes. Lysosomes consist of a low-cholesterol environment (Liscum & Munn 1999), suggesting that most of the cholesterol is exported out of the late endosomes before forming the lysosomes. Niemann Pick 1 (NPC1) and Niemann Pick 2 (NPC2) proteins are crucial for exporting cholesterol out of the endosomal compartment. Deficiency of NPC1 protein or NPC2 protein leads to non-esterified cholesterol accumulation in late endosomes leading to a fatal autosomal recessive disease associated with lipid overload called Niemann Pick type C disease (Sleat *et al.* 2004). The study of mice whose *npc1* and / or *npc2* gene are suppressed, suggests that NPC1 and NPC2 proteins participate in different steps of the same pathway and that one does not compensate for the other (Sleat *et al.* 2004). NPC2

is a small, soluble protein that functions *in vitro* as a cholesterol transfer protein. This transfer is favored by an acidic pH and the presence of lysobiphosphatidic acid (LBPA) (Cheruku *et al.* 2006). In contrast, the NPC1 protein is a large glycoprotein with 13 transmembrane loops of which five constitute the sterol binding domain (Figure 1.8) similar to that of the SCAP (SREBP Cleavage Activating Protein) protein (Davies & Ioannou 2000). The mechanism for exporting cholesterol from late endosomes is not yet fully understood. One of the possible hypothesis is that the NPC2 protein would transfer cholesterol directly from the membranes (mobilized by LBPA) or after hydrolysis of the esters to the NPC1 protein, which would induce its export out of the late endosome (Figure 1.8) (Cheruku *et al.* 2006). From late endosomes, cholesterol will be distributed in different intracellular compartments: the ER and the golgi apparatus, and the PM (especially in lipid rafts).

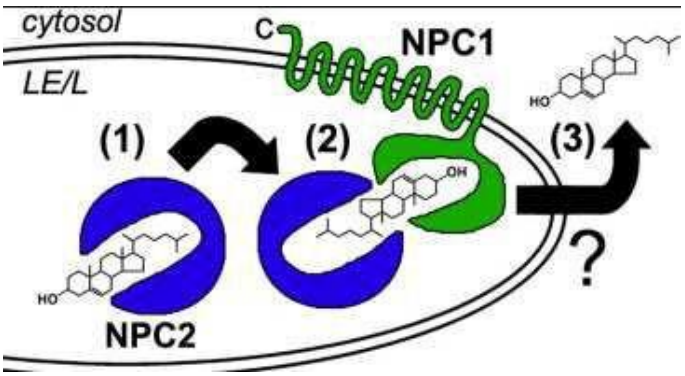

Figure 1.8. Intracellular transport of cholesterol. (1) NPC2 protein is a small soluble protein that functions as a cholesterol-transfer protein to NPC1. (2) NPC1 is a large transmembrane protein that will then export cholesterol out of late endosome (LE) / lysosome (L). Figure taken from (Peake & Vance 2010)

2.2.3.4. Storage at the level of the ER

One-third of late endosome cholesterol is directly transferred to the ER (Schroeder *et al.* 2001). However, since the ER is a cholesterol-poor organelle (0.5 % to 1 % of the cellular cholesterol content) (Lange *et al.* 1999), excess cholesterol in the ER is stored in intracytoplasmic lipid droplets as cholesterol esters (Figure 1.7). This conversion is catalyzed by ACAT, of which two isoforms have been described. The distribution of ACAT1 is ubiquitous whereas ACAT2 is exclusively expressed in the liver and intestine (Joyce *et al.* 2000). These cholesterol esters are less toxic than free cholesterol (Tabas 2002). Esterification could therefore play a protective role in regulating excess cholesterol.

2.2.3.5. Distribution in the Golgi apparatus and at the membrane/lipid rafts

Two-thirds of the cholesterol exported from late endosomes are transferred to the Golgi apparatus and then to the PM (Liscum & Munn 1999). The PM accounts for 60 to 80 % of cellular cholesterol (Liscum & Munn 1999). It consists of a lipid bilayer. The exoplasmic (outer) leaflet contains mainly sphingomyelin and phosphatidylcholine while the cytoplasmic leaflet is enriched in phosphatidylserine and phosphatidylethanolamine. Cholesterol, present in both layers, contributes to the stabilization of the membrane (Ikonen 2008). Maintaining the phospholipid/cholesterol ratio in the membrane is important for cell function. By binding to other lipids, cholesterol increases the membrane's rigidity and decreases its fluidity and permeability. The bulk structure of biological membranes consists of a bilayer of amphipathic lipids. According to the fluid mosaic model proposed by Singer and Nicholson (1972), the glycerophospholipid bilayer is a two-dimensional fluid construct that allows the lateral movement of membrane components. In PM, there are small (100 nm) dynamic microdomains enriched in cholesterol called lipid rafts (Sonnino & Prinetti 2013). Historically, these structures have been defined by their low density (in sucrose gradient) and their insolubility in X100 tritium (detergents) at 4 °C. These properties gave them the name of DRM (Detergent Resistant Membrane). In addition, they are protein poor domains (Sonnino & Prinetti 2013). The lipid rafts, formed of flotillin 1 dimers, are dispersed along the PM. They constitute signaling platforms initiated by neurotrophic factors, neurotransmitter receptors (NMDA, AMPA, glutamate, etc.). Lipid rafts also play an essential role in AD by promoting the production of Aβ peptides.

2.3. Excretion

When the cholesterol synthesis rate exceeds cellular needs, cholesterol's net excretion occurs. This overload of cholesterol often happens in neurons, since they rely mainly on astrocytes which produce cholesterol in excess to satisfy functional needs of adult neurons. Neurons may handle excess of cholesterol by different ways. 1° Cholesterol undergoes hydroxylation to 24-hydoxycholesterol by cholesterol 24-hydroxylase (CYP46A1), which is located in the smooth ER, and then can readily pass the blood

brain barrier BBB to enter the plasma, where it is picked up by plasma lipoproteins, transported to bile acids, and excreted (Meaney *et al.* 2002; Russell *et al.* 2009). 2° It can be esterified by ACAT1 in the ER and then stored in lipid droplets (Wüstner *et al.* 2005). 3° Can be loaded onto ApoE lipoproteins and excreted via ABC transporters, namely ABCA1, ABCG1, ABCG4 (Kim *et al.* 2008). ABC transporters pathway is a CYP46A1 independent pathway for cholesterol elimination. Following loading into lipoproteins, cholesterol can be released in cerebrospinal fluid (CSF); (Koch *et al.* 2001). Then these lipoproteins are removed from the brain via LRP1 or SR-BI, where both are expressed in BBB endothelial cells.

2.4. Regulation

The concentrations of cholesterol must be maintained constant to ensure proper brain functioning (Björkhem 2006b). In the brain, the half-life of cholesterol is between 6 months up to 5 years. However, there is always a fraction of the cholesterol's pool being constantly replaced (Andersson *et al.* 1990). The metabolism of cholesterol in the cell is finely regulated by cholesterol concentration in the cell. The conversion of HMG-CoA to mevalonate, catalyzed by HMG-CoA reductase enzyme, is the rate limiting step in cholesterol synthesis. The activity of this enzyme is regulated by complex transcriptional and translational mechanisms.

2.4.1. Transcriptional regulation of cholesterol synthesis

To maintain steady cholesterol concentrations, cells sense cholesterol levels by membrane-bound transcription factors known as sterol regulatory element-binding proteins (SREBPs), which regulate the transcription of genes encoding enzymes of cholesterol and fatty acid biosynthesis as well as lipoprotein receptors (Brown & Goldstein 1986) to either increase cholesterol synthesis and uptake in sterol-depleted cells or decrease cholesterol-synthesizing enzymes when sterols are overloaded in cells (DeBose-Boyd *et al.* 1999; Nohturfft *et al.* 2000).

The SREBP family consists of 3 members: SREBP1a, SREBP1c and SREBP2. The three members have different functions, where SREBP2 regulates cholesterol metabolism, SREBP1c regulates fatty acids synthesis, and SREBP1a regulates both mechanisms. These proteins, with two transmembrane domains, reside as precursors in ER

membrane (Horton *et al.* 2002). They bind via their C-terminus to the SCAP protein which has a cholesterol sensing domain.

In the absence of sterols, the SCAP protein allows the transfer of SREBP from the ER to the Golgi apparatus by COPII vesicles (Figure 1.9). The SREBP protein is then cleaved consecutively by site-1 protease (S1P) and then by site-2 protease (S2P). These two cleavages allow the release of the SREBP transcription factor from the Golgi apparatus. This factor can travel to the nucleus, bind to SRE (Sterol Regulatory Element) DNA sequences and induce, in the presence of coactivators, the transcription of the HMG-CoA reductase gene but also of the LDLR gene (the lipoprotein receptors).

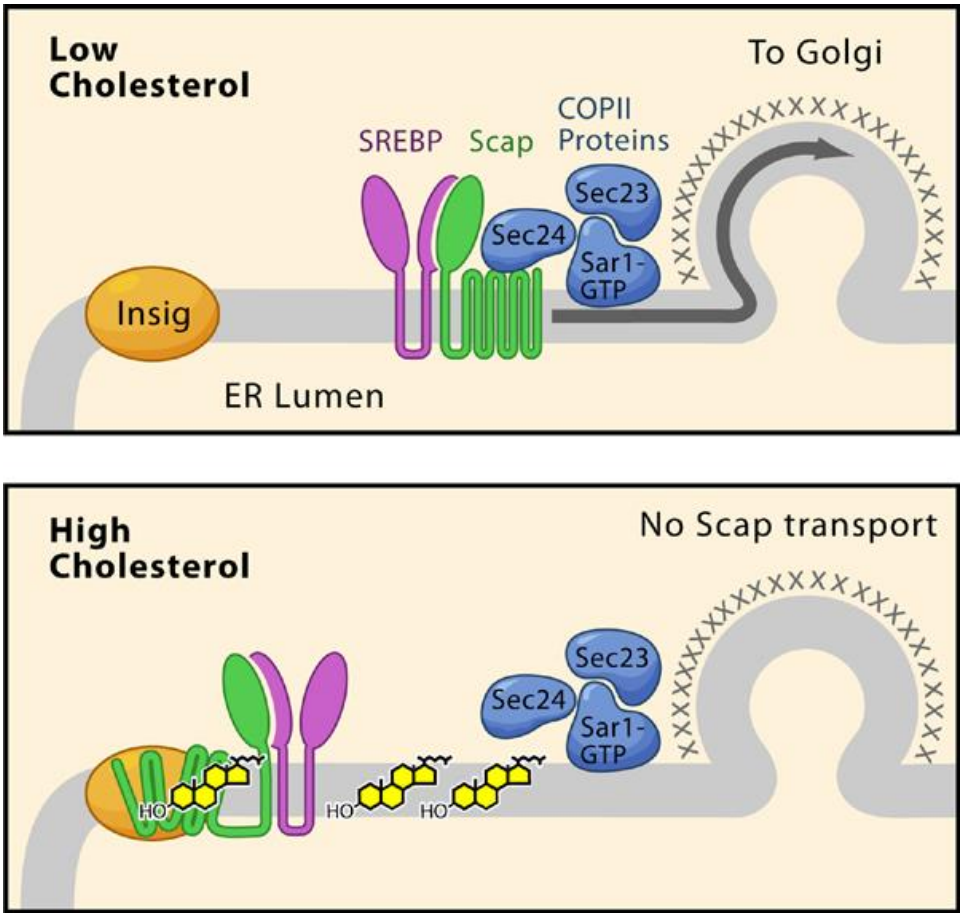

Figure 1.9: Cholesterol-mediated regulation of SREBP2 transport. At low cholesterol concentrations, SREBP2 is mobilized from ER to Golgi apparatus. At high concentrations of cholesterol, SREBP2 binds to Insig via SCAP, this will inhibit the mobilization from ER to the Golgi apparatus. Taken from (Goldstein *et al.* 2006).

In the presence of sterols, the cholesterol binds to the SCAP protein changing its conformation and inducing the binding of the SCAP-SREBP complex with the Insig (Insulin induced gene) protein. This binding prevents the insertion of the complex into the COPII vesicles, its transfer to the Golgi apparatus, the activation of the SREBP

transcription factor, the expression of its target genes (HMG-CoA reductase) and thus the synthesis of cholesterol (Goldstein *et al.* 2006; Espenshade & Hughes 2007).

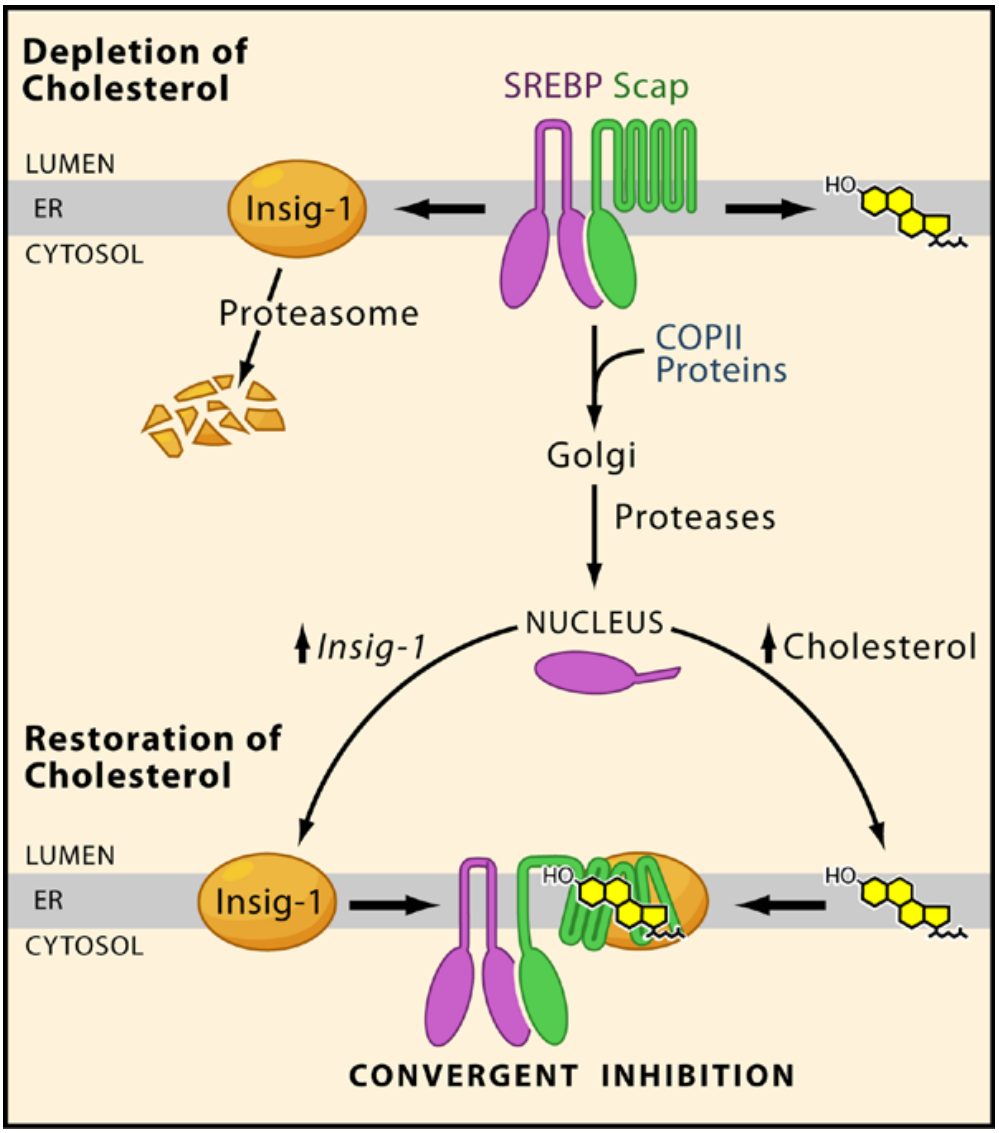

Figure 1.10: Transcriptional regulation of cholesterol synthesis. At low cholesterol concentration levels, Insig protein is ubiquitinylated and proteolyzed by proteasomes by that inhibiting Insig role in downregulation cholesterol synthesis. Figure taken from (Goldstein *et al.* 2006).

The Insig/SCAP/SREBP complexes serve as a reservoir for SREBP. When cells need cholesterol, Insig is not bound to the SCAP/SREBP complex, it is then ubiquitinated and transported to the proteasome to be degraded and thus cannot block cholesterol synthesis (Figure 1.10). The SREBP/SCAP complex can thus migrate towards the Golgi apparatus and at nuclear level. SREBP again becomes sufficient to induce the transcription of the genes involved in the synthesis of cholesterol. In addition, SREBP induces the transcription of the Insig gene, but the protein is rapidly degraded as long

as the cholesterol level is not sufficient to allow interaction with SCAP, which stabilizes Insig and protects it from ubiquitinoylation (Figure 1.10) (Gong *et al.* 2006).

2.4.2. Translational regulation of cholesterol homeostasis

At the same time, degradation of HMG-CoA reductase occurs by another mechanism induced by sterols and isoprenoid derivatives via a pathway dependent on ubiquitination and proteasomes. The enzyme HMG-CoA reductase is an ER protein with 8 helical transmembrane domains. Its N-terminal domain allows the insertion of the protein into the ER. Its transmembrane domains 2 to 6 contain the sterol sensor domain and its C-terminal domain comprises the catalytic activity of the enzyme.

The half-life of the HMG-CoA reductase enzyme is modulated by the absence or presence of cholesterol. In the absence of sterols, the half-life of the HMG-CoA reductase is 12h. It can bind to acetyl CoA to induce cholesterol synthesis. In the presence of an accumulation of sterols and isoprenoid derivatives, the half-life of the HMG-CoA reductase is less than one hour. Its degradation is more strongly induced by lanosterol precursor than by cholesterol (Song *et al.* 2005). The lanosterol accumulation induces the binding of the Insig protein to the YIYF sequence present in the second transmembrane domain of the HMG-CoA reductase protein (Figure 1.11). On the other hand, the Insig protein forms a complex with a group of proteins (Song *et al.* 2005), that allows the ubiquitination of the HMG-CoA reductase protein. Geranylgeraniol compound (isoprenoid derivative) will then bind to the complex and induce extraction of HMG-coA from the complex and its degradation (Figure 1.11) (Sever *et al.* 2003; Song *et al.* 2005).

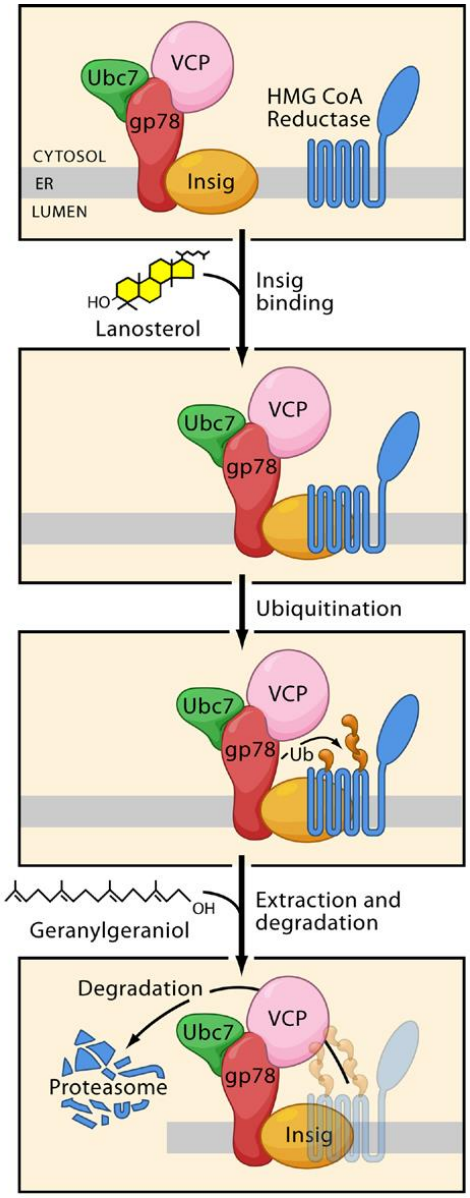

Figure 1.11: Regulation of HMG-coA reductase expression. At high cholesterol concentrations, HMG-CoA reductase is ubiquitinylated and degraded by proteasomes. Figure taken from (Goldstein *et al.* 2006).

2.4.3. Hydroxylation, upload onto lipoproteins, and LXR activation

When cholesterol reaches the maximum required level, 24-hydroxylase catalyzes transformation of cholesterol to 24-hydroxycholesterol (24-OHC), that can be readily eliminated through BBB and protects neurons from the toxic effect of 24-OHC accumulation (Matsuda *et al.* 2013). 24-OHC, besides being a metabolite for elimination of cholesterol, it also serves as an activator of nuclear transcription factors, including liver X receptors (LXRs), which increase the expression of cholesterol

transport genes (Rebeck 2004; Tall 2008) such as ABCA1 in both neuron and glia cell (Fukumoto *et al.* 2002), and apolipoproteins such as ApoE in astrocytes (Liang *et al.* 2011; Pfrieger & Ungerer 2011). LXR activation consequently increases cholesterol efflux from overloaded cells.

LXR receptors are transcriptional regulators of genes involved in many physiological processes. LXR is especially required for the maintenance of cholesterol synthesis rate. Indeed, a depletion of LXR causes an increase in cholesterol synthesis by stimulating in particular the expression and activity of HMG-CoA reductase (Wang *et al.* 2008b). LXR exists under two isoforms, α and β (Apfel *et al.* 1994; Willy *et al.* 1995). LXR α and β can be activated by the same ligands. However, their expression level is different according to the tissue they are expressed in. LXR α is strongly expressed in the liver, adipose tissue, intestine, kidneys and macrophages while LXR β is ubiquitously expressed and is the major isoform found in the CNS (Bełtowski & Semczuk 2010).

LXR receptors function as heterodimers with the retinoid X receptor (RXR) (Claudel *et al.* 2001). RXR is a partner of several nuclear receptors such as PPAR (Peroxisome proliferator-activated receptor) (Chawla *et al.* 2001). The LXR/RXR heterodimers bind to specific sequences of deoxyribonucleic acid (DNA) called LXR response elements (LXRE) in the promoter region of the target genes, resulting in inhibitions or activations of the target genes. LXR receptors can regulate the transcription of target genes in 2 different ways (Figure 1.12).

At low oxysterol concentrations, LXR/RXR heterodimer binds to co-repressors, which will suppress the transcription of the target genes.

At high oxysterol concentrations, oxysterol binds to the LXR / RXR heterodimer, the latter dissociates from the co-repressors, and recruits' coactivators, causing transcription of the target genes (Baranowski 2008).

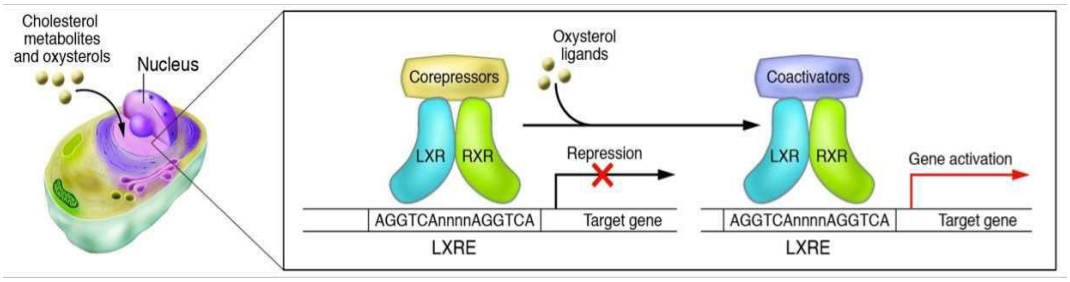

Figure 1.12: Regulation of cholesterol homeostasis via LXR. In the presence of oxysterols, the LXR/RXR heterodimer recruits' coactivators that induces target genes expression. Figure taken from (Zelcer & Tontonoz 2006).

3. Cholesterol and neurodegenerative diseases

3.1. Cholesterol in Niemann-Pick type C (NPC) disease

NPC disease is a relatively rare disease that occurs once in every 150,000 live births. It is an autosomal recessive disease associated with progressive neurodegeneration, hepatosplenomegaly, lung disease, and premature death within the first two decades (Vanier & Millat 2003). It is characterized by massive loss of Purkinje cells in cerebellum, which causes motor function impairment in patients (Sarna *et al.* 2003). Neuronal loss is due to a fatal late endosomal/lysosomal overload of cholesterol in cells, which occurs due to a mutation in either *npc1* (95 % of cases) or *npc2* (5 % of cases) genes. As explained before, NPC1 and NPC2 are responsible for exporting cholesterol out of the endosomal compartment, to the ER and PM. Deficiency of NPC1 or NPC2 proteins leads to non-esterified cholesterol accumulation in late endosomes and blockage of cholesterol transport to ER and PM (Sleat *et al.* 2004). In *npc1* -/- neurons, an increase in cholesterol concentration occurs in cells soma faced with a decrease in cholesterol concentration in distal axons (Karten *et al.* 2002, 2003). This cholesterol deficiency in axons due to NPC1 deficiency alters synaptic vesicle morphology and composition (Karten *et al.* 2006). Furthermore, reduction in the amount of cholesterol in cultured *npc1* $^{-/-}$ neurons attenuates the exocytosis of synaptic vesicles, so that synaptic function is likely to be impaired in NPC disease (Hawes *et al.* 2010). The NPC disorder is accompanied by an elevated accumulation of oxysterols in the brain as a result of oxidative stress (Vance 2012).

Prior to neurological abnormalities and synapses loss, neurodegeneration starts at

nerve terminals where cholesterol levels are heavily reduced, transport of synaptic vesicles to exocytic sites and evoked exocytosis are perturbed (Hawes *et al.* 2010). This is followed by accumulation of defective NPC1 in recycling endosomes (Karten *et al.* 2006). Detection of NPC1 in recycling endosomes of nerve terminals suggests a role for NPC1 in the slow vesicle recycling critical to the maintenance of synaptic vesicles during prolonged synaptic activity (Karten *et al.* 2006). These events are more severe in GABAergic nerve terminals, resulting in an imbalance of inhibitory and excitatory processes (Xu *et al.* 2010). It is tempting to speculate that the alterations affecting the synaptic transmission trigger the abnormalities observed in the Niemann–Pick type C disorder manifested by ataxia, cataplexy, and a loss of reflexes. Following synapses loss, neuronal soma degeneration is the final event in the pathological cascade of the NPC disease.

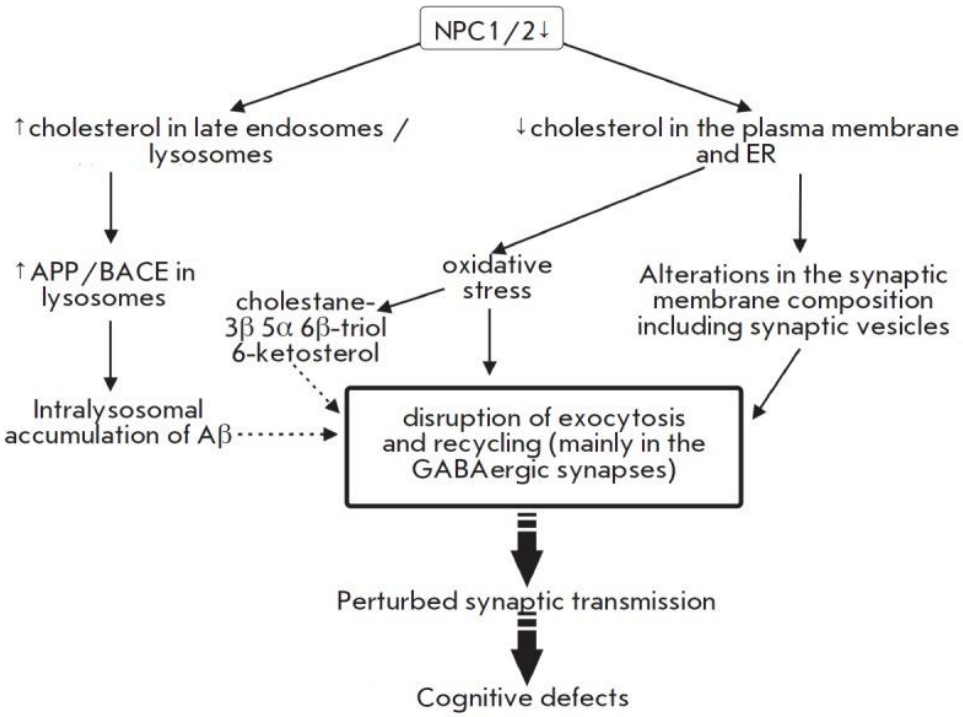

Figure 1.13: Changes in cholesterol metabolism in Niemann Pick disease type C. Figure taken from (Petrov *et al.* 2016).

3.2. Cholesterol in Smith-Lemli-Opitz syndrome (SLOS)

SLOS is an autosomal recessive disease affecting 1 in 20,000 newborns. This disease is due to a deficiency in the gene encoding 7-dehydrocholesterol reductase (*dhcr7*) (Nowaczyk & Irons 2012). The symptoms of SLOS vary greatly in affected individuals

but the pattern of abnormalities that is typical includes growth delay, microcephaly, polydactyly, fused second and third toes, cleft palate, underdeveloped external genitals in males and mental retardation. This disease involves profound brain development abnormalities, intellectual disability, as well as emotional and sleep disorders. There are several forms of the disease that range from mild to severe. 7-DHCR catalyzes the final step in the Kandutsch–Russell cholesterol biosynthetic pathway. A deficiency in 7-DHCR causes the accumulation of 7-dehydrocholesterol (7-DHC) in the brain, peripheral tissues and plasma, and eventually, cholesterol loss (Figure 1.14). In SLOS syndrome, 24-OHC levels drop and 27-OHC levels increase in the plasma (Björkhem *et al.* 2001). Patients with severe cases display plasma cholesterol concentrations that amounts 2 % of the normal range. In the mild form, plasma cholesterol levels may remain unaffected but that cannot stop brain developmental defects, indicating the importance of cholesterol in normal brain functioning (Nowaczyk & Irons 2012). Nevertheless, SLOS symptoms might be due to the accumulation of 7,8-dehydrodesmosterol, the 7-DHCR substrate, and its oxidized derivatives (Korade *et al.* 2010). In addition, the teratogenic effects of SLOS are attributed to a deficiency in sonic hedgehog (SHH)-signaling pathway, since SHH activity requires a covalent linkage of cholesterol to SHH to achieve its key role in organogenesis (Nowaczyk & Irons 2012).

Cholesterol and 7-DHC share physicochemical properties, thus 7-DHC replaces the depleted cholesterol in membranes. These changes leads to increased membrane fluidity, reduced ability to maintain the membrane curvature important for the fusion/fission, and modified lipid rafts composition with abnormal protein interface (Staneva *et al.* 2010).

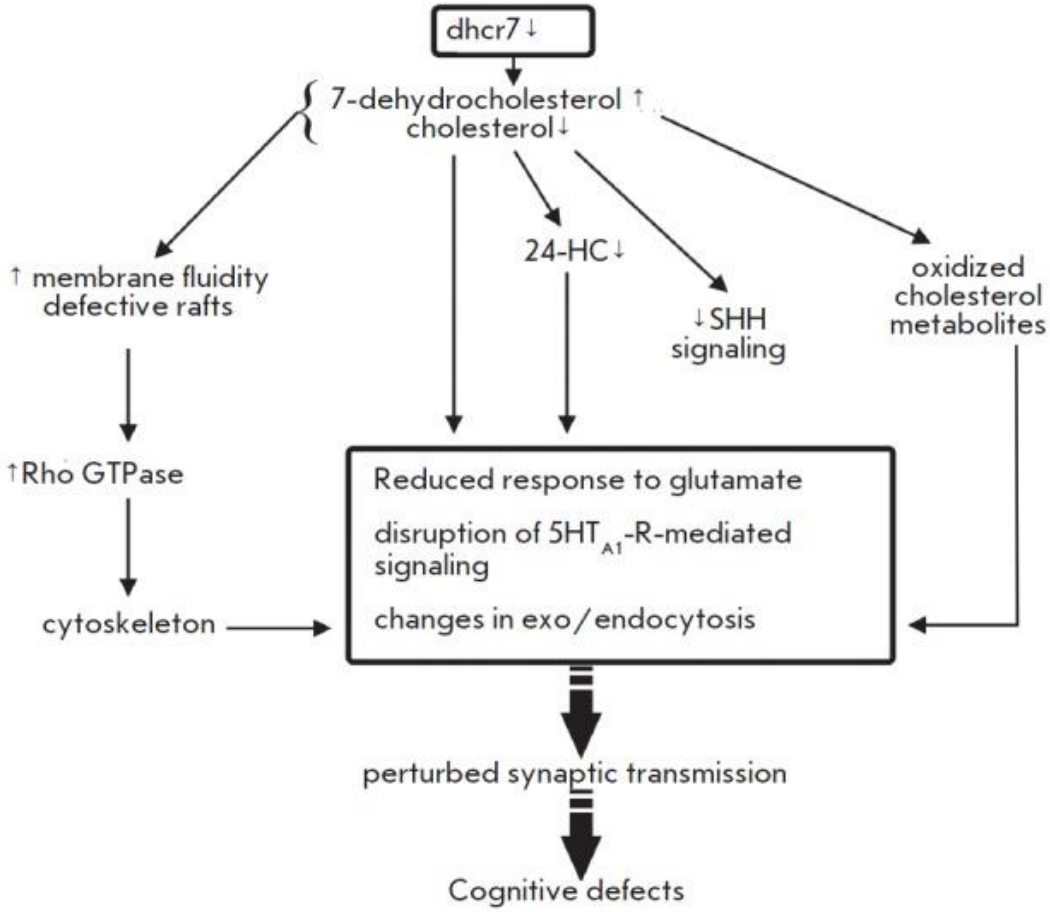

Figure 1.14. Changes in cholesterol metabolism in SLOS disease. 24-HC corresponds to 24-OHC Figure taken from (Petrov *et al.* 2016).

3.3. Cholesterol in Huntington's disease (HD)

An autosomal dominant neurodegenerative disease due to a mutation in huntingtin (HTT) protein. Common symptoms are motor impairment, cognitive decline, psychiatric problems, and progression to death almost 20 years after symptoms onset. Neuropathological characteristics are astrogliosis and striatal and cortical atrophy. Several studies highlight changes in cholesterol homeostasis in Huntington's disease. The precursor content of cholesterol is significantly decreased in the plasma of patients with Huntington's disease (Leoni *et al.* 2011). In addition, a decrease in the expression

of genes involved in cholesterol biosynthesis is demonstrated in the striatum and cortex of patients with Huntington's disease, mouse models or striatal cells overexpressing the mutant HTT protein (Sipione *et al.* 2002; Valenza *et al.* 2005). The biosynthesis of cholesterol is therefore diminished in Huntington's disease.

An increase in cholesterol content is nonetheless observed in patient brain neurons or mouse models of HD. Cholesterol accumulates in plasma membranes, including lipid rafts. This membrane overload contributes to the process of excitotoxicity induced by glutamate receptors (NMDA). Striatal neuron membranes overexpressing the mutated huntingtin protein express a greater amount of NMDA receptors (del Toro *et al.* 2010). The increase in cholesterol could therefore contribute to the neurotoxic processes in Huntington's disease.

3.4. Cholesterol and AD

Alzheimer's disease (AD) is a common progressive neurodegenerative disease. AD patients suffer from memory loss and cognitive decline late in life. An AD brain is characterized by intracellular neurofibrillary tangles of hyperphosphorylated tau, a microtubules-associated protein, and extracellular deposits of Aβ plaques. Loss of neurons and accumulation of Aβ plaques, specifically in the hippocampus, are major events in AD development (Selkoe 2001, 2002). At normal physiological conditions, there is balance between Aβ production and removal from the brain. In AD, either overproduction or impaired clearance of Aβ, or a combination of both, probably play key roles in the pathophysiology. The Aβ peptides are generated by the proteolytic cleavage of the transmembrane protein amyloid precursor protein (APP) by either α- or β-secretase (Figure 1.15). When α-secretase cleave APP, non-amyloidogenic products are generated that do not cause abnormal brain pathology. In contrast, when β-secretase cleaves APP, the C-terminal fragment generated is then further cleaved by γ-secretase, forming Aβ peptides that contain 40 or 42 amino acids, where these peptides are deposited in the pathogenic Aβ plaques (Grimm *et al.* 2012; Lee *et al.* 2012; Tan & Evin 2012).

Relationship between AD and cholesterol metabolism dysregulation is still vague. There are several studies that indicate the cholesterol metabolism dysregulation in the brain contribute to AD pathogenesis (Simonsen *et al.* 1998; Kojro *et al.* 2001), however

it is unclear whether this dysregulation is a cause or a consequence of AD. The Aβ generating enzymes, β- and γ-secretases, that are predominantly localized to lipid rafts in PM (Simonsen *et al.* 1998; Ehehalt *et al.* 2003). Several *in vitro* and *in vivo* studies have demonstrated that cholesterol can regulate Aβ production and deposition. When cellular cholesterol levels decrease, APP cleavage by α-secretase increase, thereby decreasing the processing of APP into the toxic Aβ peptides that accumulate in amyloid plaques (Simonsen *et al.* 1998; Kojro *et al.* 2001). Interestingly, the extracellular N-terminus of APP contains a cholesterol-binding site (Barrett *et al.* 2012), indicating a probable importance of cholesterol in APP cleavage and eventually in proper brain functioning. For example, when the cholesterol content of hippocampal neurons was decreased by statin treatment, synaptic density was reduced and synaptic vesicle release was impaired (Mailman *et al.* 2011). Thus, a deregulation of cholesterol levels, either reduction or accumulation, perturbs the proper functioning of the brain.

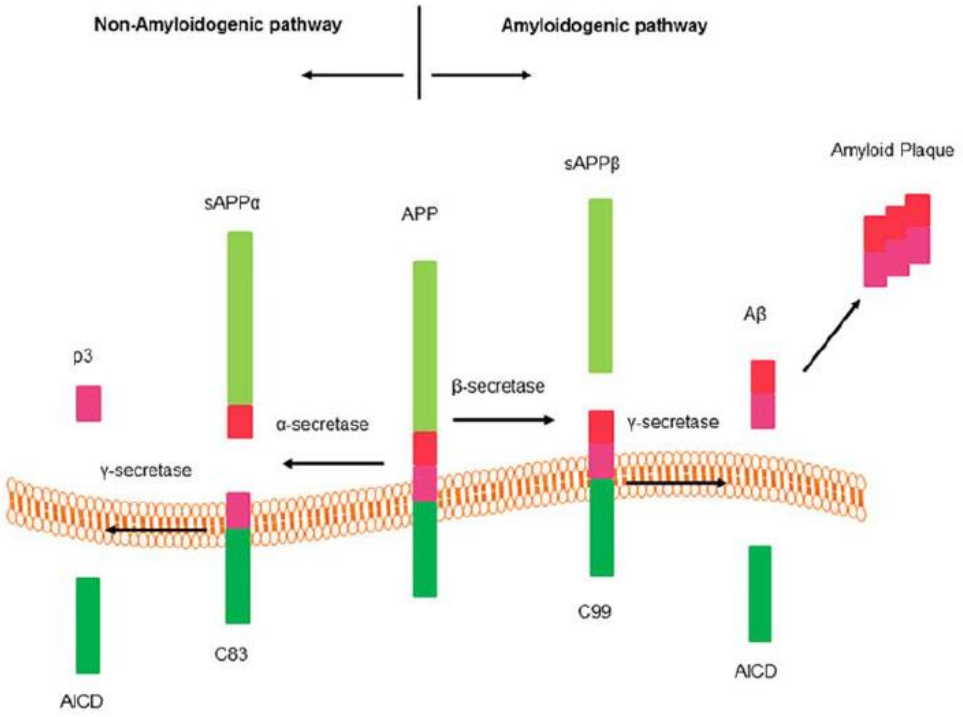

Figure 1.15: Processing of APP. In the non-amyloidogenic pathway of APP processing, APP is proteolytically cleaved within the Aβ region (red box) by α-secretase (α). In the amyloidogenic pathway, APP is cleaved first by β-secretase (β) and subsequently by γ-secretase (γ) to generate the pathological Aβ fragments that accumulate in brains of individuals with AD. Figure taken from (Zhao *et al.* 2016).

Some epidemiological studies suggest that increased levels of plasma cholesterol, particularly during mid-life, are a risk factor for the development of AD (Leoni *et al.* 2010; Umeda *et al.* 2012; Wingo *et al.* 2019). For example, a cholesterol-rich diet in

rabbits increased Aβ production (Sparks *et al.* 1994), but the mechanism by which dietary cholesterol and high levels of plasma cholesterol could contribute to the deposition of Aβ plaques remains unclear, because plasma lipoproteins do not normally cross the BBB (Dietschy & Turley 2001). One suggested explanation for the association between high plasma levels of cholesterol and AD is that the impermeability of the BBB might be compromised in individuals with AD so that cholesterol can be transported into the brain from the plasma (Ujiie *et al.* 2003). However, more recent studies have shown that the levels of plant sterols (the majority of which circulate in plasma) in the brains of individuals with AD are not significantly different from those in non-AD controls, suggesting that the BBB remains intact in AD (Shafaati *et al.* 2011).

In support of the idea that high levels of plasma cholesterol contribute to AD, several studies have suggested that statins, some of which can cross the BBB and are widely used cholesterol-lowering drugs, protect against AD (Shepardson *et al.* 2011). However, randomized double-blind placebo-controlled studies have shown no beneficial effect of statins on the progression of symptoms in individuals with AD despite significantly lowering plasma cholesterol (Sano *et al.* 2011; Shepardson *et al.* 2011). Clearly, additional studies are required to determine whether high plasma cholesterol directly contributes to the onset and progression of AD (Shepardson *et al.* 2011). One possible mechanism underlying the proposed neuroprotection against AD by statins might be attributable to the anti-inflammatory and/or antioxidant properties of the statins, rather than directly to their cholesterol-lowering effect (Vaughan & Gotto 2004). Thus, the idea that statins are beneficial in AD remains controversial.

4. LSR

4.1. Discovery of LSR

In 1992, Bihain and Yen discovered that fibroblasts from patients with familial hypercholesterolemia, in which the LDLR receptor is absent, were still able to internalize a significant amount of LDL only in the presence of oleate. Upon the incubation of fibroblasts (FH) with free fatty acids, such as oleate, an amplification of LDL endocytosis independent of the LDL receptor was detected (Bihain & Yen 1992).

These results suggested the existence of a free fatty acid activated lipoprotein receptor, distinct from the LDLR receptor that was named Lipolysis Stimulated lipoprotein Receptor (LSR). Indeed, once activated by oleate in rat hepatocytes, the receptor undergoes a conformational change revealing the binding sites to ApoB and/or ApoE (Yen *et al.* 1994; Mann *et al.* 1995). The presence of free fatty acids (such as oleate) is required for binding between ApoB or ApoE and LSR and therefore LSR-mediated endocytosis (Yen *et al.* 2008a). The binding to oleate and other free fatty acids is a novel characteristic of LSR.

4.2. LSR structure

The LSR receptor is a heterotrimer composed of 3 different subunits α, α' and β subunits, the two main ones being α and β and have molecular weights of 68 kDa and 56 kDa, respectively in mice. The subunits α and α' form a doublet, which prevents to determine precisely the molecular weight of the subunit α'. LSR α is the complete protein sequence of LSR, which contains a clathrin binding site and a di-leucine lysosomal targeting signal at the N-terminal, a hydrophobic transmembrane domain, a cysteine-rich region and a group of alternatively negatively and positively charged amino acids at the C-terminal which serve as the lipoprotein binding site (Yen *et al.* 1999). While LSR α' has a similar protein sequence to LSR α, the di-leucine lysosomal signal is deleted, but it can still act as a transmembrane protein. However, LSR β protein sequence has lost the transmembrane domain and the cysteine-rich domain responsible for endocytosis and lysosomal targeting, yet it can still bind to free fatty acids and interact with lipoproteins (Yen *et al.* 1999). It is still not fully clear whether

the N-terminal part of the molecule is intra- or extracellular (Yen et al., 1999).

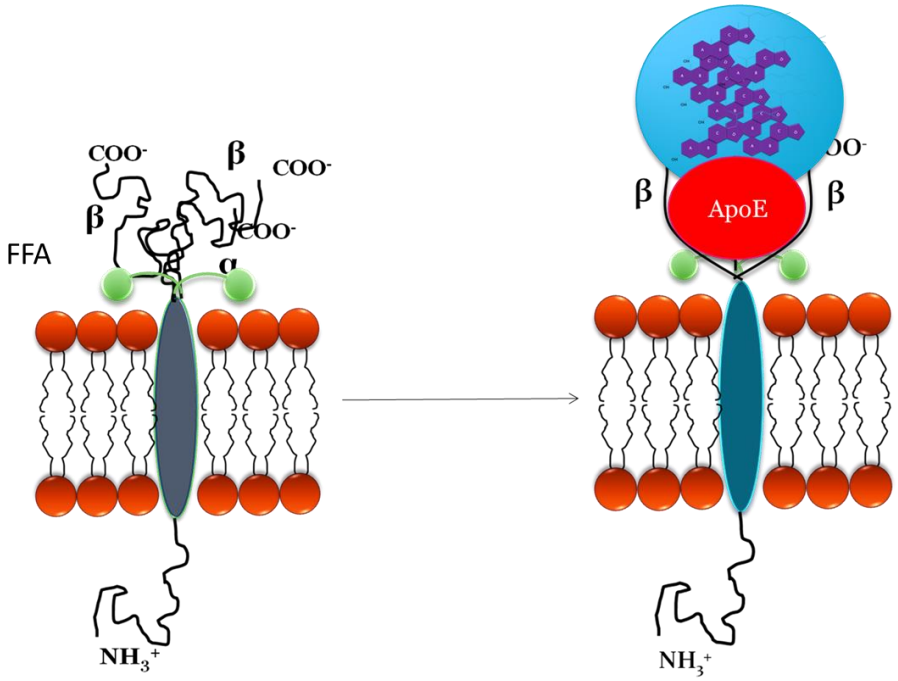

Figure 1.16: Proposed LSR structure. When free fatty acids (FFA) bind to LSR, conformational change of the protein occurs revealing an ApoE binding site.

4.3. Lethality of LSR -/-

LSR receptor mRNA is abundantly expressed in the liver, and less in the lungs, intestine, kidneys, ovaries and testes. It is not detected in the muscles and the heart. In order to be able to study the role of the LSR receptor more precisely and completely, a transgenic mouse model deficient for LSR receptor has been developed. For this purpose, the LSR gene was inactivated in 129/Ola mouse embryonic stem cells by the deletion of a gene segment containing exon 2-5, which were then implanted into mouse embryos. Interestingly, mice homozygous for LSR knockout (LSR -/-) died after 12.5 to 15.3 days of gestation, whereas heterozygous LSR +/- mice were perfectly viable (Mesli *et al.* 2004). There were no obvious abnormalities reported in the organogenesis of the brain other than the BBB permeability (Mesli *et al.* 2004).

4.4. LSR in periphery

LSR ensures rapid clearance of triglyceride (TG)-rich lipoproteins after high fat meal. When LSR +/- mice are placed on a high fat diet, plasma triglyceride and cholesterol accumulation as well as a 50% decrease in TG-rich lipoprotein clearance during the postprandial phase occurred (Yen *et al.* 2008a; Narvekar *et al.* 2009). Lipid deposits

are also present at the aortic level. Unlike wild-type mice, in LSR +/- mice, weight gain is correlated with hyperlipidemia (Yen *et al.* 2008a). In addition, a downregulation of genes involved in lipid transport and metabolism by 80 % in LSR +/- mice under high fat diet (Akbar *et al.* 2016). These results therefore demonstrate that the LSR receptor represents a link between hyperlipidemia, obesity and atherosclerosis. The silencing of the liver-specific LSR receptor by adenovirus-derived small interfering RNAs increases the amount of plasma ApoB and ApoE and causes an increase in postprandial triglycerides (Yen *et al.* 2008a; Narvekar *et al.* 2009). ApoCIII, known to cause hypertriglyceridemia when overexpressed, inhibits LSR activity (Mann *et al.* 1997). The amount of receptors on the hepatocyte surface is negatively correlated with postprandial plasma triglyceride levels, demonstrating the participation of LSR in the clearance of triglyceride-rich lipoproteins in the postprandial phase (Mann *et al.* 1995). Receptor Associated Protein (RAP) inhibits LSR receptor activity by binding to its inactive form (Troussard *et al.* 1995). The activity of this receptor is also inhibited by lactoferrin, a milk protein that inhibits the uptake of chylomicrons in the liver. The binding of lactoferrin to LSR's active form prevents the binding of triglyceride-rich lipoproteins, thus explaining the hyper-triglyceridemic action of plasma lactoferrin (Mann *et al.* 1995; Ahmad *et al.* 2012). In addition, lactoferrin appears to intervene *in vitro* in the clearance of Aβ peptide via the LRP1 receptor by forming complexes with the Aβ peptide (Jaeger and Pietrzik, 2008, Qiu et al., 1999). Figure 1.17 summarizes the functioning of the LSR receptor in the clearance of peripheral lipoproteins rich in triglycerides.

During aging, LSR +/- mice gain weight significantly more than wild type mice and show an increase in plasma leptin content, suggesting a link between the LSR receptor and leptin. Individuals carrying loss-of-function gene form of leptin are morbidly obese. However, when leptin is successfully transported through the BBB, it helps overcoming obesity (Harrison *et al.* 2019). Leptin is a hormone secreted by adipose tissue (adipokine) that regulates food intake and energy expenditure. It induces an anorectic effect and an increase in energy expenditure by binding to its receptors located in the hypothalamus (Okamoto *et al.* 2001).

The administration of physiological doses of leptin to mice by intraperitoneal injections induces an overexpression of the LSR receptor in the liver and improves the

clearance of chylomicrons in postprandial phase (Narvekar *et al.* 2009; Stenger *et al.* 2010) (Figure 1.17). Leptin also has beneficial effects on learning, memory, synaptic transmission, neuroprotection and neurogenesis (Oomura *et al.* 2006; Garza *et al.* 2008). Hippocampal neurons in mice on high fat diet are rendered leptin-resistant, thus leptin-modulated neuronal signal induction and transmission are lost (Mainardi *et al.* 2017). Leptin also inhibits BACE1 expression and Aβ peptide production (Marwarha et al., 2010, 2014, Niedowicz et al., 2013). Several studies indicate a correlation between circulating peripheral levels of leptin and the expression of this hormone as well as its receptor in the brain and AD (Harvey 2010, Paz-Filho et al., 2010).

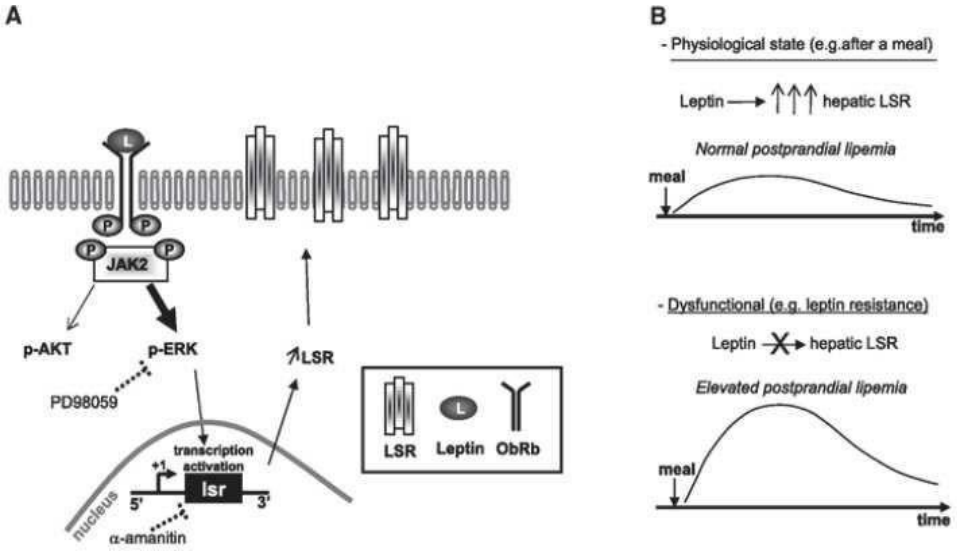

Figure 1.17: Regulation of LSR expression and postprandial lipedema via leptin. Figure taken from (Stenger *et al.* 2010).

4.5. LSR in BBB and CNS

At the BBB, LSR receptor is involved in the maintenance and formation of tight junctions via the recruitment of tricellulin, an important molecular component for the formation of tight junctions. Endothelial cells in the CNS and retina are much less permeable to solutes due to the presence of tight tricellular junctions. Interestingly, Daneman's laboratory identified the presence of *lsr* gene transcript in endothelial cells (ECs) of the BBB (Daneman *et al.* 2010) and their recent publication showed that LSR is a component of paracellular junctions highly enriched in the BBB ECs, but not in ECs in peripheral tissues outside the CNS (Sohet *et al.* 2015). They also demonstrated

that the BBB doesn't seal during embryogenesis in *lsr* knockout mice. Another study reported the high expression of LSR in tricellular junctions, not only in the BBB, but also in retinal ECs that form the inner blood retinal barrier (BRB) (Iwamoto *et al.* 2014). This indicates that LSR plays a critical role in maintaining the blood barrier integrity in all CNS structures and suggests a potential role of LSR in the transport of lipoproteins between the brain parenchyma and the CSF. The LSR receptor belongs to the family of angulins of which ILDR1 and ILDR2 (immunoglobulin-like domain containing receptor 1 and 2) are members. These proteins appear to be involved in diabetes, clearance of peripheral cholesterol, and release of cholecystokinin, an anorectic peptide hormone (Dokmanovic-Chouinard *et al.* 2008; Chandra *et al.* 2013; Watanabe *et al.* 2013). Since the LSR receptor plays a role in the maintenance of tight junctions, the absence of LSR at the embryonic stage of the BBB could explain the lethality observed in LSR-deficient embryos. This involvement in epithelial tissue cohesions is consistent with observations of LSR involvement in a number of cancer processes, such as in stomach (Sugase *et al.* 2018), endometrium (Shimada *et al.* 2016, 2017), bladder (Herbsleb *et al.* 2008) and breast cancers (Reaves *et al.* 2014).

In addition, the LSR receptor has also been described as a host receptor for a toxin produced by the Clostridium difficile bacterium Clostridium Difficile Transferase (CDT), which causes diarrhea and colitis. The LSR receptor allows the endocytosis of another toxin produced by Clostridium spiriform bacteria, which also causes diarrhea in food poisoning (Papatheodorou *et al.* 2011). This shows that the LSR receptor, like other receptors initially described as lipoprotein receptors, can provide multiple ligand binding functions.

4.6. LSR, cognitive functions and aging

LSR is the most recently discovered receptor to be expressed in the CNS (Stenger *et al.* 2012). Complete inactivation of *lsr* is associated with *in utero* lethality at the embryonic stage, most likely due to brain-localized hemorrhages and BBB leakages (Mesli *et al.* 2004; Sohet *et al.* 2015). Since complete inactivation of *lsr* is embryonic lethal, *in vivo* studies conducted on young and aged *lsr* +/- mice suggest that reduced LSR may be associated with cognitive disturbances related to reactivity to novel environments in aged *lsr* +/- mice (Stenger *et al.* 2012). A significant decrease of lipid droplets, which are lipid-rich cellular organelles that regulate the storage and hydrolysis of neutral

lipids, including cholesterol (Martin & Parton 2006), was observed in Purkinje cells of the cerebellum together with an accumulation of filipin-labeled cholesterol in neuronal membranes of the hippocampus in aged *lsr* +/- mice (Stenger *et al.* 2012). Histochemical studies show a neuron-specific strong expression of LSR in hippocampus, Purkinje cells, at ependymal cells surface between brain parenchyma and CSF, and in the capillaries rich region: the choroid plexus (Stenger *et al.* 2012). Interestingly, intracerebroventricular injection of of Aβ42 in male 15-month old LSR+/– mice led to a significant impairment in learning and long-term memory and decreased cortical cholesterol when compared to Aβ42 injected LSR+/+ male mice of same age (Pinçon *et al.* 2015a). Total latency of the Morris test was significantly and negatively correlated with cortical cholesterol content of the LSR+/– mice, but not of controls. The Aβ42 injection itself induced a significant decrease in free cholesterol in the cortex, which was more prominent for the LSR+/– mice, resulting in a significantly lower cholesterol content in the cortex of Aβ42-injected LSR+/– mice as compared to that of Aβ42-injected LSR+/+ mice. Significantly lower cortical PSD95 and SNAP-25 levels were detected in Aβ42-injected LSR+/– mice as compared to Aβ42-injectedLSR+/+ mice. The combined alterations of SNAP-25 and PSD95 expression in the cortex of LSR+/– mice are consistent with the higher sensitivity of LSR+/– to the Aβ42-induced long-term memory deficit. Inaddition,24S-hydroxycholesterol metabolite levels were significantly higher in the cortex of LSR+/– mice. Interestingly, there have been reports of high levels of this marker for cholesterol turnover either in the plasma or cerebrospinal fluid of patients with early AD or early dementia (Papassotiropoulos *et al.* 2002; Popp *et al.* 2012, 2013; Leoni *et al.* 2013). Therefore LSR+/- genotype caused alterations in cholesterol regulation, which rendered mice more susceptible to amyloid stress. On the other hand, immunoblot analysis didn't show any changes of HMG CoA-reductase protein levels between LSR+/+ and LSR+/– mice.

Altogether, the evidence supports a critical role for LSR in cholesterol trafficking in the CNS during the lifespan.

During my first year of PhD, the first experiments carried out allowed us to characterize LSR mRNA and protein expression in different regions of the brain that are important for learning and memory. Following this, we characterized LSR expression at the glial

and neuronal levels from primary cell cultures. Interestingly, both neuronal and glial cells express LSR, however glial cells LSR expression was more predominant. This droves us to develop a conditional glial cell specific LSR knockout followed by behavioral characterization of those mice to further understand the effect of cholesterol deregulation in glial cells on the CNS. The work of this thesis was intended to answer this question.

Chapter II (Article I)

Age-related changes in regiospecific expression of LSR in mice brain

Published in PLOSONE

Short resume:

To understand LSR's function, it was essential to first characterize the pattern of LSR expression. It was important to study whether LSR expression was ubiquitous and similar, or variable across studied brain regions and over time. Once LSR expression determined, we would target brain regions that highly express LSR. We took into consideration not only total LSR, but also the membrane traversing subunits LSR α and α', and the membrane non-traversing subunit LSR β, since they hypothetically have different functions. To characterize LSR RNA and protein expression in different brain regions, RT-qPCR and western blots were performed, respectively. We further studied whether LSR expression is neuron or glia specific by staining pure and mixed neuronal and glial cell cultures prepared from different brain regions.

Age-related changes in regiospecific expression of Lipolysis Stimulated Receptor (LSR) in mice brain

Aseel El Hajj[1], Frances T. Yen[1*], Thierry Oster[1], Catherine Malaplate[1], Lynn Pauron[1], Catherine Corbier[1], Marie-Claire Lanhers[1], Thomas Claudepierre[1*].

[1] Qualivie, UR AFPA laboratory, ENSAIA, University of Lorraine, Vandoeuvre-les-Nancy, Lorraine, France.

* Corresponding authors

E-mails:

Thomas.claudepierre@univ-lorraine.fr (TC)

Frances.yen-potin@univ-lorraine.fr (FYP)

Abstract

Regulation of cholesterol, an essential brain lipid, ensures proper neuronal development and function, as demonstrated by links between perturbations of cholesterol metabolism and neurodegenerative diseases, including Alzheimer's disease. The central nervous system (CNS) acquires cholesterol via *de novo* synthesis, where glial cells provide cholesterol to neurons. Both lipoproteins and lipoprotein receptors are key elements in this intercellular transport, where the latter recognize, bind and endocytose cholesterol containing glia-produced lipoproteins. CNS lipoprotein receptors are like those in the periphery, among which include the ApoB, E binding lipolysis stimulated lipoprotein receptor (LSR). LSR is a multimeric protein that has multiple isoforms including α and α', which are seen as a doublet at 68 kDa, and β at 56 kDa. While complete inactivation of murine *lsr* gene is embryonic lethal, studies on *lsr* +/- mice revealed altered brain cholesterol distribution and cognitive functions. In the present study, LSR profiling in different CNS regions revealed regiospecific expression of LSR at both RNA and protein levels. At the RNA level, the hippocampus, hypothalamus, cerebellum, and olfactory bulb, all showed high levels of total *lsr* compared to whole brain tissues, whereas at the protein level, only the hypothalamus, olfactory bulb, and retina showed the highest levels of total LSR. Immunocytostaining of primary cultures of mature murine neurons and glial cells isolated from different CNS regions showed that LSR is expressed on both neurons and glial cells. However, *lsr* RNA expression in the cerebellum was predominantly higher in glial cells, which was confirmed by the immunocytostaining profile of the cerebellar neurons and glia. Based on this observation, we would propose that LSR present on glial cells might play a key role in the glia-neuron cross talk more specifically in the feedback control of cholesterol synthesis to avoid cholesterol overload in neurons and maintain proper functioning of the brain.

1. Introduction

Cholesterol is essential for neuronal physiology and a tight regulation of cholesterol homeostasis in the central nervous system (CNS) is essential for proper neuronal development and function. Cholesterol is not only an important structural component for cellular

membranes and myelin, it is also a required component for synapse and dendrite formation (Goritz *et al.* 2005; Fester *et al.* 2009), and axonal guidance (de Chaves *et al.* 1997). It ensures functional synaptogenesis and is vital for: synaptic vesicles transmission along axonal microtubules via cholesterol-kinesin interactions, exocytotic complex organization in active presynaptic membranes of lipid rafts, neurotransmitters receptors clustering in postsynaptic membranes, extra-synaptic receptors pool recruitment, and pre- and post-synaptic cell-cell adhesion (Claudepierre & Pfrieger 2003b). Cholesterol is delivered to tissues via lipoprotein particles. However, brain access to cholesterol and other lipids from the peripheral circulation is complicated due to the blood–brain barrier (BBB), which serves as a selective low-permeable multicellular barrier (Quan *et al.* 2003). Cholesterol is therefore supplied by *de novo* synthesis in the brain, which relies on its own network for synthesizing, internalizing and metabolizing these lipids to provide the necessary components for neuronal cell membrane function (Turley *et al.* 1998; Quan *et al.* 2003). Glial cells play a central role towards providing neurons with lipids, particularly cholesterol in the form of lipoproteins. Lipoproteins in the cerebrospinal fluid (CSF) are very different from those of the periphery, and have been characterized as high-density lipoprotein-like (HDL-like) particles containing primarily apolipoprotein (Apo)E and ApoJ (Fagan *et al.* 1999c). Those HDL-like lipoproteins are needed to export cholesterol from astrocytes to neurons, where they bind via ApoE to lipoprotein receptors and are internalized through receptor-mediated endocytosis (Claudepierre & Pfrieger 2003b). A series of lipoprotein receptors expressed in neurons have been identified including the low density lipoprotein receptor (LDL-R) (Herz 2009), low density lipoprotein receptor-related protein 1 (LRP-1) (Herz 2009), and lipolysis stimulated lipoprotein receptor (LSR) (Stenger *et al.* 2012). LSR is the most recently discovered receptor to be expressed in the CNS (Stenger *et al.* 2012). It is a multimeric protein complex that undergoes conformational changes upon binding of free fatty acids, thereby revealing a binding site that recognizes ApoB or ApoE (Bihain & Yen 1998). There are three different isoforms of LSR that have been clearly identified, LSR α and α' that form a doublet at 68 kDa, and β at 56 kDa (Yen *et al.* 1999). LSR α is the complete protein sequence of LSR, which contains a clathrin binding site and a di-leucine lysosomal targeting signal at the N-terminal, a hydrophobic transmembrane domain, a cysteine-rich region and a group of alternatively negatively and positively charged amino acids at the C-terminal which serve as the lipoprotein binding site (Yen

et al. 1999). While LSR α' has a similar protein sequence to LSR α, the di-leucine lysosomal signal is deleted, but it can still act as a transmembrane protein. However, LSR β protein sequence has lost the transmembrane domain and the cysteine-rich domain responsible for endocytosis and lysosomal targeting, yet it can still bind to free fatty acids and interact with lipoproteins (Yen *et al.* 1999). LSR was initially identified as an important receptor mediating hepatic clearance of triglyceride-rich ApoB, E-containing lipoproteins during the post-prandial phase (Yen *et al.* 2008b). *In vivo* studies have shown that this receptor is necessary for maintaining normal peripheral circulation levels of cholesterol and triglycerides, and in contributing to the regulation of lipid distribution amongst the peripheral tissues (Yen *et al.* 2008b; Narvekar *et al.* 2009). Dyslipidemia in absence of hepatic LSR was confirmed by the observation of increased plasma levels of cholesterol and triglycerides following shRNA-mediated knockdown of hepatic LSR expression in mice (Narvekar *et al.* 2009). Complete inactivation of *lsr* is associated with *in utero* lethality at the embryonic stage, most likely due to brain-localized hemorrhages and BBB leakages (Mesli *et al.* 2004; Sohet *et al.* 2015). Since complete inactivation of *lsr* is embryonic lethal, *in vivo* studies conducted on young and aged *lsr* +/- mice suggest that reduced LSR may be associated with cognitive disturbances related to reactivity to novel environments in aged *lsr* +/- mice (Stenger *et al.* 2012). A significant decrease of lipid droplets, which are lipid-rich cellular organelles that regulate the storage and hydrolysis of neutral lipids, including cholesterol (Martin & Parton 2006), was observed in Purkinje cells of the cerebellum (CB) together with an accumulation of filipin-labeled cholesterol in neuronal membranes of the hippocampus (HIP) in aged *lsr* +/- mice (Stenger *et al.* 2012). Histochemical studies show a neuron-specific strong expression of LSR in HIP, Purkinje cells, at ependymal cells surface between brain parenchyma and CSF, and in the capillaries rich region: the choroid plexus (Stenger *et al.* 2012). Interestingly, Daneman's laboratory identified the presence of *lsr* gene transcript in endothelial cells (ECs) of the BBB (Daneman *et al.* 2010) and their recent report showed that LSR is a component of paracellular junctions highly enriched in the BBB ECs, but not in ECs in peripheral tissues outside the CNS (Sohet *et al.* 2015). They demonstrated that the BBB doesn't seal during embryogenesis in *lsr* knockout mice. Another study reported the high expression of LSR in tricellular junctions, not only in the BBB, but also in retinal ECs that form the inner blood retinal barrier (BRB) (Iwamoto *et al.* 2014). This indicates that LSR plays a critical role in maintaining the BBB integrity and suggests a

potential role of LSR in the transport of lipoproteins between the brain parenchyma and the CSF. Altogether, the evidence supports a critical role for LSR in cholesterol trafficking in the CNS during the lifespan. Our objective was to establish a detailed profile of LSR RNA and protein expression in the brain of young and old mice, both on whole brain tissue and in specific CNS areas including the hypothalamus (HT), hippocampus (HIP), olfactory bulb (OB), retina (RET), cortex (CX), and cerebellum (CB). We also compared LSR expression between primary cultures of glial and neuronal cells from different CNS regions. This work revealed differential expression of LSR isoforms in different regions, which would help us, in the future, understand the possible role of LSR in the cholesterol crosstalk between glial cells and neurons.

2. Materials and methods

2.1. Animals

Three month and eighteen-month-old male and female C57Bl/6JRj mice (Janvier Breeding, Le Genest Saint Isle, France) were used for the study (n = 3 for each group). For primary cell cultures, newborn C57Bl/6JRj mice aged 5-7 days were sacrificed (n = 7-10). The C57Bl/6JRj mice were housed in certified animal facilities (N° B54-547-24) on a 12-h light/dark cycle with a mean temperature of 21–22 °C and relative humidity of 50 ± 20 % and provided rodent chow diet (16.4 % protein, 4 % fat, ref 2016, Envigo Teklad, Gannat, France) and water *ad libitum*. Animal care followed French State Council guidelines for the use and handling of animals: all tissues used in the study were collected after sacrifice of animals using isoflurane anesthesia followed by decapitation.

2.2. Immunoblots

Tissues were collected, and different regions of the brain were isolated: HT, HIP, OB, RET, CX, and CB. Whole cell extracts were isolated using RIPA lysis Buffer (10x RIPA buffer, ref 20-188 Millipore, Darmstadt, Germany) supplemented with 10 mM sodium orthovanadate (ref S6508, Sigma Aldrich, Saint-Quentin Fallavier, France), 10 mM phenylmethylsulfonyl fluoride (ref P7626, Sigma Aldrich), and protease inhibitors (ref 11 836 145 001, Roche, Mannheim, Germany). The concentration of the isolated proteins was determined using Pierce BCA Protein Assay Reagent (ref 3225

Thermofisher Scientific, Villebon-sur-Yvette, France). Twenty micrograms of the protein were separated on a 10 % SDS-PAGE and electrophoretically transferred to nitrocellulose membranes (ref 10600003, Sigma Aldrich). Membranes where then incubated with primary polyclonal antibodies against the LSR protein; LSR Sigma (1:100, rabbit, ref HPA007270-100UL, Sigma Aldrich), and against the control protein β-Tubulin (β-TUB) using a mouse monoclonal antibody (1:1000, mouse, ref T5201, Sigma Aldrich). LSR was detected with HRP-conjugated sheep anti-rabbit IgG antibody used at 1:2000 (ref 7074, Cell signaling technologies, Leiden, Netherlands), whereas β-TUB was detected with HRP-conjugated sheep anti-mouse IgG antibody used at 1:2000, (ref 7076, Cell signaling technologies) and visualized with the Luminata Crescendo Western HRP substrate (ref WBLUR0500, Millipore, Molsheim, France), according to manufacturer's instructions.

2.3. RNA extraction and RT-qPCR

Freshly collected tissues were conserved in RNAlater (ref 76104, Qiagen, Les Ulis, France) as per manufacturer's instructions and stored at -80 °C until use. Different regions of the brain were isolated separately including HT, HIP, OB, RET, CX, and CB. Total RNA was extracted using TRI reagent (ref T9424, Sigma Aldrich), according to the manufacturer's instructions. RNA quantity and purity were estimated by a Nanodrop ND-1000 spectrophotometer (Thermo Scientific; Villebon-sur-Yvette, France), and the samples with a 260/280 nm ratio ≥ 1.7 were used for subsequent analyses. RNA quality was verified by bleach agarose gel electrophoresis (Aranda *et al.* 2012). RNA samples showing intact 28S and 18S ribosomal subunits were considered suitable for further cDNA synthesis. Reverse transcription was performed using 1 µg of RNA in a final volume of 20 mL including 0.5 mL of random primers (3 mg/mL; Invitrogen, Carlsbad, CA, USA), 1 µL of 10 mM dNTP mix, in RNase-free water (ref 10977049, Invitrogen, Cergy Pontoise, France). After denaturation of RNA samples at 65 °C for 5 min, 4 µL of buffer (5x), 2 µL of 0.1 mM DTT, 1 µL of Superscript II reverse transcriptase (ref 18064022, Invitrogen), and 1 µL of RNase OUT (ref 10777019, Invitrogen) were added. Samples were homogenized and were transcribed in an Applied Biosystems 2720 thermal cycler according to the following conditions: 25 °C for 10 min, 42 °C for 50 min, and 70 °C for 15 min. The cDNA from individual animals was used as a template for the PCR array using the applied biosystem kit (ref A25742, Thermofischer scientific) with the following final concentrations in a 25 µL final

volume: 1 × Master Mix, 100 nM forward and reverse primers, 0.4 ng/µL cDNA. The mix was placed in a 7500 Fast Real-Time PCR system (Applied Biosystems; Foster City, CA, USA). The thermal cycling conditions were: initial 5 min denaturation at 95 °C, followed by 42 cycles of 15 s at 95 °C, 1 min at 60 °C, and a final dissociation step. The primer specificity was determined based on the presence of a single peak in the melting curve. We followed four target mRNA sequences: total *lsr*, *lsr* α, *lsr* α', and *lsr* β, whose expression levels were compared to those of three reference sequences: hypoxanthine guanine phosphoribosyl transferase (*Hprt*) (Yen *et al.* 2008b), phosphoglycerate kinase 1 (*Pgk1*) (Boda *et al.* 2009), and transferrin receptor protein 1 (*Tfrc1*) (Boda *et al.* 2009) (Table 2.S1). *Lsr* primer sequences were selected using the Primer-BLAST Genbank based on *lsr* gene sequence (NM_017405). Quantitation was performed by the $2^{-\Delta\Delta Ct}$ method (Livak & Schmittgen 2001). The obtained results were tested for statistical significance ($p<0.05$) using the Relative Expression Software Tool 2009 (REST Version 2.0.13). The fold changes of mRNA samples of young animals were compared to whole brain levels, and old 18-month-old animals were compared to 3-month-old ones.

2.4. Mixed cell culture

Different brain structures (HT, HIP, OB, RET, CX, and CB) were collected from mice (n = 7-10 mice) of 5-7 days of age immediately after sacrifice. Tissues were collected in D-PBS and were cut into small pieces of 1 mm^3. Afterwards, tissues were digested using papain digestion solution, which contains 20 U/mL papain (ref LS003126, Worthington Biochemical Corporation, Lakewood, NJ, USA) and 200 U/mL DNase (ref D4527, Sigma Aldrich), for 1 hour at 37 °C with constant rotation. This was followed by mechanical dissociation of the pellet for 3 times using a 0.02 % BSA solution (ref A4161, Sigma Aldrich) containing 333 U/mL DNase (ref D4527, Sigma Aldrich). This is followed by cell counting using a hemocytometer and centrifugation at 1000 rpm for 10 minutes. Cells are resuspended in a glia culture medium at 1000 cells/µL and are plated at 200,000 cells/glass slide. The culture medium is a DMEM medium (ref 41965-039, Gibco Life technologies,) supplemented with 10 % fetal bovine serum (ref 16000-044, FBS-Invitrogen/Gibco), 2 mM glutamine (Sigma, G7513), 1 mM sodium pyruvate (ref 11360-039, Invitrogen/Gibco), 100 U/mL penicillin and 100 µg/mL streptomycin (Pen/Strep solution, ref 151 40-122, Invitrogen/Gibco). Cells were incubated at 37 °C with 5 % CO_2 for 8 days and medium was changed every 3 days.

2.5. Immunoisolation and culture of CNS neurons from postnatal mice

Neurons were isolated from HT, HIP, RET, OB and CB of freshly sacrified postnatal C57Bl/6J mice (n = 7-10) of 5-7 days of age with an immunopanning technique, according to a previously published protocol (Steinmetz *et al.* 2006).Mice were sacrificed by decapitation according to institutional guidelines. Different tissues were collected in D-PBS and were cut into small pieces of 1 mm^3. Afterwards, tissues were digested using papain digestion solution, which contains 33 U/mL papain (ref LS003126, Worthington Biochemical Corporation, Lakewood, NJ, USA) and 200 U/mL DNase (ref D4527, Sigma Aldrich), for 1 hour at 37 °C with constant rotation. The tissues were the sequentially triturated in a 0.02 % bovine serum-albumin (BSA, ref A4161, Sigma Aldrich) containing 333 U/mL DNase (ref D4527, Sigma Aldrich). Cells were filtered using a wet nylon mesh (Nitex 20 μm, Tetko/Sefar Filtration, Rüschlikon, Switzerland) with 0.02 % BSA, then spun down (1000 *rpm* for 10 min) and resuspended with 15 mL 0.02 % BSA (ref A4161, Sigma Aldrich). For immunopanning, one (HT, HIP, CB, OB, and CX) or two (Retinal ganglion cells-RGCs) subtraction plates (150 mm diameter Petri-dishes; Falcon; BD Biosciences/VWR, Fontenay sous Bois, France) and one selection plate (100 mm diameter Petri-dish) were incubated for >12 h at 4 °C with 10 μg/mL secondary antibody in 50 mM Tris-HCl (pH 9.5). For subtraction: goat anti-rabbit IgG (ref 111-005-003, Jackson Immunoresearch Laboratories, Marseille, France); for selection: HT, HIP, CB, OB, CX, goat anti-rat IgG (ref 112-005-003, Dianova, West Grove, PA, USA); for RGCs, goat anti-mouse IgM (ref 111-005-020, Jackson Immunoresearch Laboratories). After washing for three times with PBS, selection plates were covered with 0.2 % BSA (ref A4161, Sigma Aldrich) and incubated for at least 2 h at room temperature (HT, HIP, OB, CX, CB) with 0.2 µg/ mL of rat anti-L1CAM IgG (ref MAB5275, Millipore, Darmstadt, Germany) or (RET) 0.2 µg/mL of mouse IgM anti-Thy1.2 (ref MCA01, Serotec, Cergy Saint-Christophe, France) and then washed with D-PBS. The filtered cell suspension was incubated on subtraction plates for 40 min. The supernatant was filtered and incubated on the selection plate (45-60 min). Non-adherent cells were thoroughly washed off and bound cells were released by washing several times with 30 % fetal bovine serum (ref 16000-044, Gibco/Invitrogen, Cergy Pontoise, France). After determination of cell counts using a hemocytometer and centrifugation at 1000 rpm for 10 minutes. Cells are resuspended in a fully saturated culture medium (FSM) at

1000 cells/µL and are plated at 2.10^4 cells/well, in 12-well plates, containing 8 mm in diameter coverslips previously coated successively with poly-orthinine (ref P0421, Sigma), and kept in a humidified chamber at 37 °C containing 5 % CO_2 for 8 days *in vitro* (D-VIII). The FSM contained Neurobasal medium (ref 21103049, Gibco/Invitrogen) supplemented with (all from Sigma, except where indicated) 1 mM pyruvate (ref 11360-039, Invitrogen/Gibco), 2 mM glutamine (ref G7513), 60 µg/mL *N*-acetyl-l-cysteine (ref A9165), 16 µg/mL putrescine (ref P5780), 40 ng/mL sodium selenite (ref S5261), 100 µg/mL BSA (ref A4161), 100 µg/mL streptomycin and 100 U/mL penicillin (ref 15140-122, Invitrogen/Gibco), 40 ng/mL triiodothyronine (ref T6397), 100 µg/mL holotransferrin (ref T4132), 10 µM forskolin (ref F6886), 5 µg/mL insulin (ref I6634), 62 ng/mL progesterone (ref P8783) and 1:50 B27 (ref 17504-036, Gibco/Invitrogen). This medium is referred to as minimally supplemented medium (MSM). To support neuronal survival, this medium was further supplemented with 25 ng/mL brain-derived neurotrophic factor (BDNF; ref 450-02, PeproTech, London, UK), and 10 ng/mL ciliary neurotrophic factor (CNTF; ref 450-50, PeproTech). This medium is referred to as fully supplemented medium (FSM).

2.6. Immunocytochemistry

After fixation with 2 % paraformaldehyde (PAF; ref 158217, Sigma) followed by 4 % PAF for 20 min each, cells were permeabilized and blocked using a 0.2 % Triton (ref T8787, Sigma Aldrich) and 30 % Cas-Block (ref 008120, Invitrogen) solution prepared in 1X D-PBS (ref 141900094, Gibco) for about 1 hour at room temperature. This is followed by incubating cells, for 2 hours at room temperature, with the primary antibody mix which is either a rabbit anti LSR X-25 (1:100, ref sc-133765, Santa-Cruz, CA, USA) and mouse GFAP (1:500, ref MAB360, Chemicon, CA, USA) or mouse AQP4 (ref sc-32739, Santa-Cruz) or LSR X-25 (1:100, ref sc-133765, Santa-Cruz) and mouse β-TUB III (ref 201202, Biolegend, San Diego, USA) prepared in the permeabilization and blocking solution mentioned above. This is followed by incubating cells with a secondary antibody solution, for 1 hour at room temperature, which contains Alexa 488-anti mouse (1:500, ref A11001) and Alexa594-anti rabbit (1:500, ref A21428) conjugated secondary antibodies, those antibodies were acquired from Molecular Probes (Invitrogen, Cergy Pontoise, France). After the nuclei were marked using DAPI (1:1000, ref D9542, Sigma) for 10 min at room temperature. Finally, the slides were mounted on glass slides using Fluoromount-G (ref 1798425, Electron Microscopy

Sciences, Hatfield, PA, USA), and left at room temperature overnight, protected from light. Slides were then examined Fluoview FV10i (Olympus, Center Valley, PA, USA).

2.7. Statistical analysis

For immunoblots: the area of bands was calculated using Image J, then the ratio LSR/β-TUB was calculated for each lane, followed by calculation of the mean and standard error. Statistical significance was calculated using t-test ± SEM.

For RT-qPCRs : The statistical data in the boxplot were obtained using REST software tool, where (+) represents the mean value, the middle line represents the median, the lower (Q1) and upper (Q3) lines in the bar represent the 25 % and 75 % quartile, respectively. While the upper and lower lines represent the observations outside the 9-91 percentile range, data falling outside of Q1 and Q3 range are plotted as outliers of the data.

3. Results

3.1. Lsr RNA profiling in mice brain

3.1.1. Variation of lsr mRNA levels in different CNS areas

Expression levels of *lsr* mRNA were estimated after performing RT-qPCR on total RNA fractions extracted from different brain regions. In young 3-month-old males, we observed a more than 4-fold increase in total *lsr* expression in both the HT ($P = 0.007$) and HIP ($P = 0.007$), while in the OB ($P = 0.007$) and CB ($P = 0.03$) it was a 2-2.7 fold increase relative to that measured in whole brain tissues of male mice of the same age (Figure 2.1A). When comparing different splicing variants of *lsr, lsr* β mRNA expression was significantly higher than that of the whole brain in all of the above mentioned regions (Figure 2.1B); there was more than 7-fold expression in the HT ($P = 0.007$), HIP ($P = 0.003$), OB ($P = 0.007$), and CX ($P = 0.017$), whereas it was 2-3 fold increase in RET ($P = 0.01$), and CB ($P = 0.026$). Concerning *lsr α*, there was a 2-3-fold increase in both the HT ($P = 0.006$), and HIP ($P = 0.006$). Last but not least, there was a 2-fold increase of *lsr α'* in CB ($P = 0.013$), a 3.5-4.5-fold increase in both the HT ($P = 0.013$) and HIP ($P = 0.009$), and a 15-fold increase in the OB ($P = 0.013$).

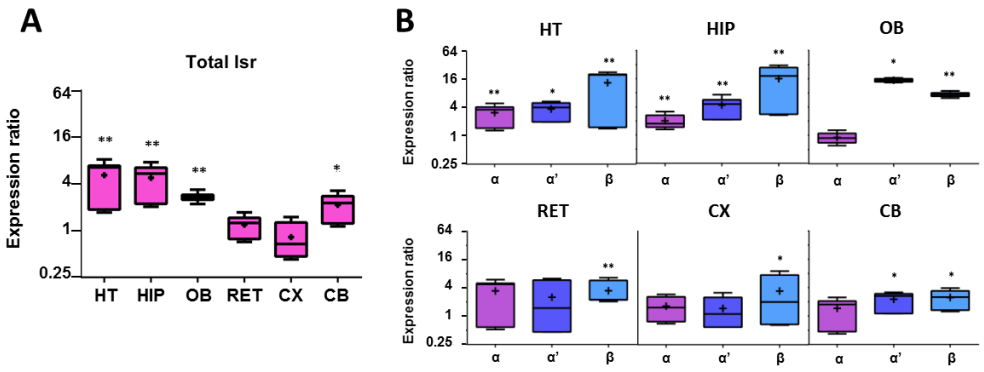

Figure 2.1. Boxplot of RT-qPCR data of *lsr* mRNA expression in different brain regions of 3-month-old male C57Bl/6JRj mice (n = 3) with respect to whole brain homogenates (n = 3). (A) Box plot of total *lsr* expression in various regions including hypothalamus (HT), hippocampus (HIP), olfactory bulb (OB), retina (RET), cortex (CX), and cerebellum (CB). (B) Expression ratio of different *lsr* isoforms α, α', and β, respectively. Statistical significance is represented as: * $P \leq 0.05$, ** $P \leq 0.01$, *** $P \leq 0.001$.

3.1.2. Age-related changes in lsr expression

To determine if *lsr* expression was modified with age, RT-qPCR analysis was also performed on brain regions from older 18-month old mice, and results were expressed compared to 3-month old males (Figure 2.2). There was a significant decrease in total *lsr* mRNA expression in both HT (P = 0.032) and HIP (P= 0.039) to 0.1-0.2-fold compared to 3-month-old mice (Figure 2.2A), while *lsr* RNA expression remained relatively unchanged in the other structures. When considering the different variants (Figure 2.2B), *lsr* α' mRNA expression was significantly reduced in the HT (0.269-fold, P = 0.032) and HIP (0.27-fold, P = 0.0001).-Similarly, *lsr* β showed a tendency to decrease with age in both HT (0.073-fold, P = 0.14) and HIP (0.138-fold, P = 0.094), but this was not statistically significant (Figure 2.2B). Although total *lsr* mRNA levels in the OB tended to increase in the older mice (1.469-fold, P = 0.07, Figure 2.2A), *lsr* α levels were slightly increased (1.251-fold, P = 0.288), yet *lsr* α' (0.115-fold, P = 0.03), and *lsr* β (0.273-fold, P = 0.03) levels decreased significantly (Figure 2.2B).

RT-qPCR analysis of total *lsr* from brain regions of young female mice revealed no statistically significant differences with that of male mice in RET, CB or HIP. Yet, total *lsr* mRNA was 4-fold higher (P = 0.03) in the CX region, but 4.5-fold lower (P = 0.03) in HT region of young female as compared to young male mice, while total *lsr* mRNA was 4.5-fold lower in females compared to young male mice (Figure 2.S1). Older 18-month old female mice showed no significant variation in total *lsr* expression when compared to 18-month old male mice except in HIP and HT, where there was a 4-fold (P = 0.01) and 2.47-fold (P = 0.03) increase, respectively (Figure 2.S2).

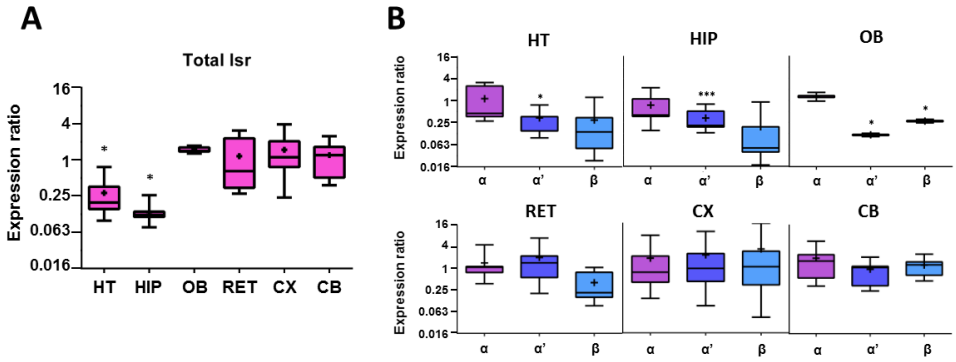

Figure 2.2 Boxplot of RT-qPCR data of *lsr* mRNA expression in different brain regions of 18-month-old male with respect to 3-month-old male C57Bl/6JRj mice. (A) Boxplot of total *lsr* expression in various regions including HT, HIP, OB, RET, CX, and CB. (B) Expression ratio of different *lsr* isoforms α, α', and β, respectively. Statistical significance is represented as: * $P \leq 0.05$, ** $P \leq 0.01$, *** $P \leq 0.001$.

3.2. LSR differential expression in different brain regions and the retina

In order to assess LSR protein levels, immunoblots using anti-LSR antibody (LSR Sigma) to detect LSR were performed on protein extracts from different regions of the brains of 18-month old mice, including the HT, HIP, OB, RET, CX, and CB. Interestingly, when comparing LSR expression, there was a differential expression of the LSR subunits α/α' (68 kDa), and β (56 kDa) in the various CNS areas. LSR Sigma (Figure 2.S4) detected the major two bands corresponding to the α/α' isoforms, seen as a doublet at 68 kDa, while the β isoform was identified as the lower band migrating at 56 kDa. Interestingly, the different isoforms of LSR (α, α', and β) were not equally expressed throughout the CNS. To examine this, the differences in the relative amounts of the three LSR isoforms (Figure 2.3, immunoblots and table) or total LSR protein normalized to β-TUB (Figure 2.3, bar graphs) were compared in brain regions from old

versus young male mice. For example, the β-chain represents only 10 % of total LSR in the HIP (Figure 2.3B), and more than 50 % in the CX (Figure 2.3E).

When normalized to β-TUB, by calculating the ratio of total LSR/ β-TUB, total LSR expression in young males seems to be the highest in the OB (1.22 ± 0.24, Figure 2.3C), RET (0.908 ± 0.24, Figure 2.3D), and HT (0.907 ± 0.097, Figure 2.3A). Yet, the CX (0.658 ± 0.176, Figure 2.3E), HIP (0.581 ± 0.209; Figure 2.3B), and CB (0.488 ± 0.037; Figure 2.3F) express less LSR than the other mentioned regions when compared to their respective β-TUB expression. With aging, no major changes in LSR expression was observed, except in HT and OB were LSR expression was lower by 36.25 % (n = 3, *P* = 0.027, Figure 2.3A) and 30.31 % (n = 3, *P* = 0.05, Figure 2.3C), respectively. Yet, there was also a tendency of decreased expression by 80.03 % in HIP (n = 3, *P* = 0.093, Figure 2.3B) of 18-month-old male mice.

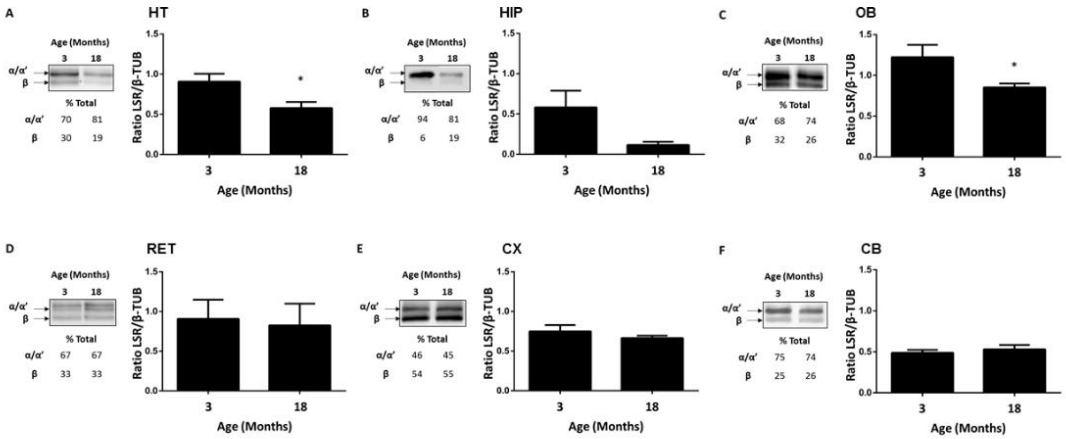

Figure 2.3. Age dependent changes in LSR protein levels in C57Bl/6JRj male mice. A, B, C, D, E, and F correspond to hypothalamus (HT), hippocampus (HIP), olfactory bulb (OB), retina (RET), cortex (CX), and cerebellum (CB), respectively. In each panel there are immunoblots of LSR in different structures, calculated percentages of α/α' and β compared to total LSR, and expression ratio of total LSR with respect to β-TUB from young 3-month old (n = 3), and old 18-month old (n = 3). Statistical significance is represented as : * $P \leq 0.05$, ** $P \leq 0.01$, *** $P \leq 0.001$.

3.1. LSR expression in neurons and glial cells

In view of these results, we performed immunocytostaining of LSR in pure neuronal vs mixed cultures from other CNS regions (Figure 2.4A). LSR was detected in neurons isolated from HIP, HT, OB, and RET (Figure 2.4A). LSR staining was observed primarily around cell soma, but some neurites were also weakly stained**.** On the other

hand, immunocytostaining of glial cells from these same regions revealed colocalization of LSR with the glial cell marker, GFAP, as well as the astrocyte marker AQP4 (Figure 2.4B).

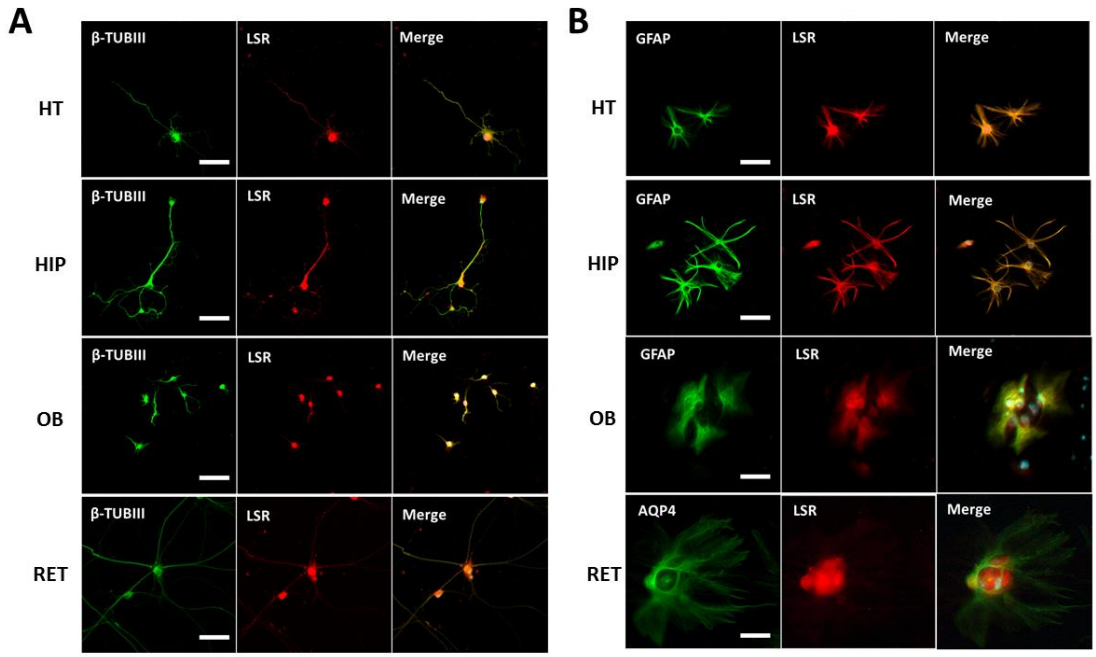

Figure 2.4. Immunocytostaining of neuronal (A) and glial (B) cell cultures of different brain regions. HT, HIP, OB, and RET. β-III tubulin (β-TUB III) was the primary antibody used to stain neurons, GFAP and AQP4 was used to label astrocytes, and LSR Sigma was used to identify LSR protein. Images were taken using Fvi10 confocal microscope at a 40-X magnification, the white bar indicated is a 20 μm scale.

3.2. Glial cells highly express LSR in cerebellum

Immunocytostaining of neuronal CB cultures with β-TUB III, a specific neuronal marker and LSR X-25 revealed LSR expression in CB that was relatively weak and mostly located in the soma (Figure 2.5A). On the other hand, immunocytostaining of glial cell cultures, revealed a strong expression of LSR in this cell type (Figure 2.5B), where GFAP and LSR colocalize. To validate the results,three different CB cell cultures of neurons and glia were performed, where sufficient amount of cells were obtained, followed by RNA extraction and RT-qPCR (Figure 2.5B). Results confirmed higher *lsr* expression in glia (0.959-fold, $P = 0.35$), as compared to that in neurons (0.02-fold, $P = 0.0001$), when normalized to cerebellar mixed cell cultures. LSR isoforms were differentially expressed in glia, where *lsr α* was upregulated (1.76, $P = 0.017$, Figure 2.5B), whereas both *lsr α'* (0.471, $P = 0.0001$, Figure 2.5B) and β (0.441, $P = 0.019$,

Figure 2.5B) were downregulated relatively to cerebellar mixed cultures.

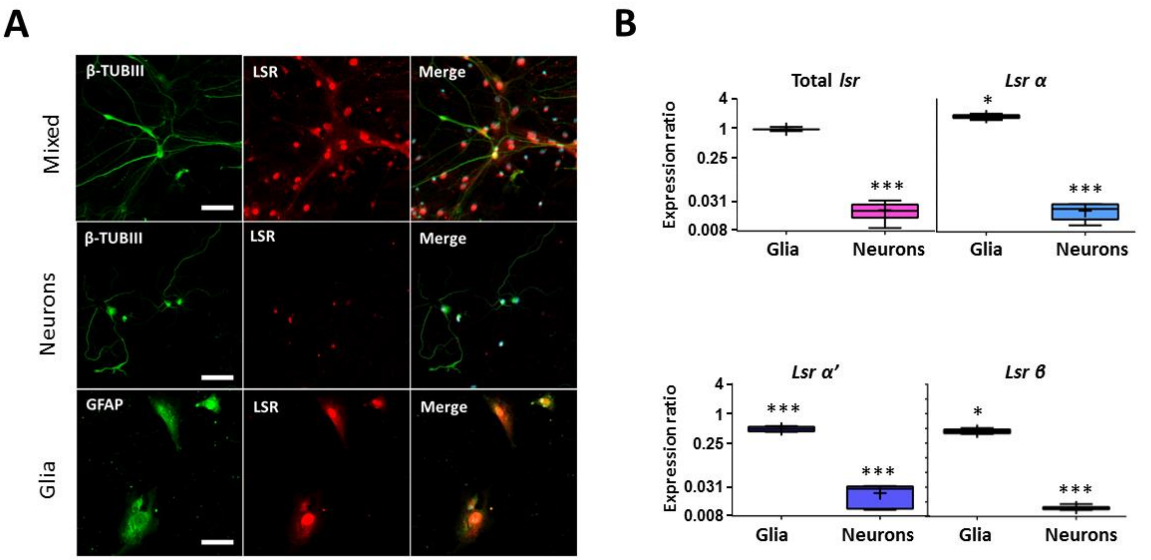

Fig 2.5. LSR is mainly expressed in glial cells in the CB. (A) Immunocytostaining of primary mixed, pure neuronal, and glial cerebellar cell cultures with antibodies to detect β-III tubulin (β-TUB III) for neurons, GFAP for astrocytes, and LSR X-25 for LSR. Images were taken using Fvi10 confocal microscope at a 40-X magnification, the white bar indicated is a 20 µm scale. (B) Boxplot representation of RT-qPCR of total RNA extracted from cerebellar glial and neuronal cell cultures compared to mixed cerebellar cultures, where expression ratio of total *lsr*, α, α', and β are represented, respectively. Statistical significance is represented as: * $P \leq 0.05$, ** $P \leq 0.01$, *** $P \leq 0.001$.

4. Conclusions and discussion

Here we demonstrate that LSR expression in the CNS is regio-specific, each CNS area has its own expression profile for the different LSR chains, thus allowing for specific combination of subunits forming this lipoprotein receptor. Some CNS regions exhibit a stronger LSR expression at the mRNA and/or protein level. Moreover, we demonstrated that aging significantly affects LSR expression, and a strong glia expression of LSR compared to neurons. As previously shown, LSR may play a role in regulation of cholesterol distribution in the CNS (Stenger *et al.* 2012). The presence of the BBB prevents access of circulating peripheral lipoproteins to the CNS. Thus, the brain relies on itself to satisfy neuronal needs of cholesterol (Turley *et al.* 1998; Quan *et al.* 2003). Adult neurons rely on astrocytes to fulfill those needs (Zhang & Liu 2015). In adult astrocytes, the newly synthesized cholesterol is loaded into ApoE-containing lipoproteins. These HDL-like lipoproteins are needed to export cholesterol from

astrocytes, via ABCA1 and ABCG1 transporters, to neurons where they bind to lipoprotein receptors, such as LSR, via ApoE, and are internalized through receptor-mediated endocytosis (Chen *et al.* 2013a). Here we show that LSR is differentially expressed across the brain at both RNA and protein levels. At the RNA level, the HT, HIP, OB, and CB all show high levels of total *lsr* RNA expression. At the protein level, immunoblots show that the HT, OB, and RET express the highest levels of LSR when normalized to β-TUB, which may reflect a specific need of these regions to tightly regulate cholesterol for proper functioning. It is known that LSR is present in the endothelial cells at tight junctions, however all tissues collected contain blood vessels, therefore high levels of LSR found in specific brain areas cannot be only due to endothelial cells, homogeneously distributed throughout the CNS, but rather reflect the expression of LSR expression in CNS cells, and therefore neurons or glial cells. Here we found that glial cells are the main cells expressing LSR in the CNS, thus suggesting an essential role of this lipoprotein in the cholesterol trafficking between neurons and glial cells. Indeed, although we showed this in the CB, which provided sufficient mRNA to compare *lsr* levels in glial and neurons, immunocytostaining of other structures clearly show significant protein level of LSR in GFAP-positive cells. In view of this, and based on LSR's role as lipoprotein receptor, we would hypothesize that the LSR present on glial cells might play a role in the glia-neuron cross talk in feedback control of cholesterol synthesis, regulating circulating cholesterol and thus maintaining proper functioning of the brain. Glial LSR might have a possible role in internalizing excess ApoE containing lipoprotein particles excreted from neurons, thus possibly activating a signaling pathway to suppress the synthesis and/or loading of cholesterol onto lipoproteins in glial cells. After internalization, ApoE-cholesterol particles are processed to free cholesterol in lysosome (Fagan & Holtzman 2000; Ikonen 2008) and then transported to membranes. Excess cholesterol in neurons are either uploaded onto ApoE-containing lipoproteins where they are then exported via ABCG4 to the CSF (Chen *et al.* 2013a), or esterified into cholesterol esters via acyl-coA cholesterol acyltransferases (ACAT1) and then stored in lipid droplets (Liu *et al.* 2009; Bryleva *et al.* 2010), or hydroxylated to 24-hydoxycholesterol (24S-OHC), by cholesterol 24-hydroxylase (CYP46A1), which can readily by-pass the BBB (Meaney *et al.* 2002). An *in vitro* study shows that treatment of activated primary microglial cells with ApoE peptide (EP) caused downregulation of ApoE synthesis in culture (Pocivavsek *et al.* 2009). This demonstrate that proper cholesterol synthesis and/or transport regulation

require a strict mechanism of glial retro-control. If LSR is deficient, such mechanism of control might be disturbed in glia cells and cholesterol synthesis and lipoprotein secretion could be upregulated, leading ultimately to a possible saturation of neurons with cholesterol. Excess of cholesterol might accumulate in lipid droplets and in neuronal membranes, which could in turn disrupt protein and lipid trafficking required for synapse assembly in neurons and cause neurodegeneration (Pennetta & Welte 2018). With age, *lsr* RNA expression decreases in both the HT, and HIP; this is also the case at the protein level where LSR is clearly downregulated in the HT, and shows a tendency of downregulation in the HIP and OB. Whether this decrease of LSR in the CNS might lead to age-related problems in thermoregulation, sex drive, wake/sleep cycle, or hunger which are important functions of the HT (Saper & Lowell 2014), problems in learning and or memory which are functions of the HIP (Leuner & Gould 2010), olfactory deficits which are related to the OB (Lledo *et al.* 2008), motor control problems which are related to the CB (Sullivan 2010) are open questions that are currently under investigation in our laboratory. Inducible glia-specific and neuron-specific conditional knockout of *lsr* are currently under development which would help us to decipher more precisely the role of LSR in the CNS.

Table 2.1. Differential *total lsr* mRNA expression summary. Summary of *total lsr* mRNA expression in different brain regions of young male versus the whole brain, young versus old male brain, young females versus old males, old females versus old males, and old females versus young females. (Y) young, (O) old, (♂) male, (♀) female, (HT) hypothalamus, (HIP) hippocampus, (OB) olfactory bulb, (RET) retina, (CX) cortex, (CB) cerebellum, (↑) upregulation, (↓) downregulation, (=) no change, (/) tendency, (▄) no data.

Target		***VS***	**Reference**		**Region**					
Age	**Sex**	***VS***	**Age**	**Sex**	**HT**	**HIP**	**OB**	**RET**	**CX**	**CB**
Y	♂	***VS***	Y Brain	♂	↑	↑	↑	=	= / ↓	↑
O	♂	***VS***	Y	♂	↓	↓	=	=	=	=
Y	♀	***VS***	Y	♂	↓	=	▄	=	↑	=
O	♀	***VS***	O	♂	↑	↑	▄	=	=	=
O	♀	***VS***	Y	♀	↑	= / ↓	▄	= / ↑	=	↓

Table 2.2. Differential total LSR protein expression in young and old males. Ratio of LSR (target) over β-TUB (reference). If ratio is equal to 1: equal expression, less than 1: lower, larger than 1: higher. (Y) young, (O) old, (♂) male, (HT) hypothalamus, (HIP) hippocampus, (OB) olfactory bulb, (RET) retina, (CX) cortex, (CB) cerebellum.

			Region					
Protein	**Age**	**Sex**	**HT**	**HIP**	**OB**	**RET**	**CX**	**CB**
Ratio LSR/β-TUB	Y	♂	0.91	0.58	1.22	0.91	0.75	0.49
	O	♂	0.57	0.12	0.85	0.83	0.66	0.53

5. Additional data and supporting information

When comparing 3 month old females(n= 3) with respect to males of the same age, total *lsr* stays relatively constant in all mentioned regions except in HT where it is downregulated to 0.22 folds (P = 0.03), and upregulated to 4 folds in CX (P = 0.03). In the HT, all *lsr α, α',* and *β* tended to be downregulated, howeer only *lsr α'* was significantly downregulated to 0.269 folds (P = 0.03). On the other hand, in the CX only *lsr α* was significantly upregulated to 5-folds (P = 0.0001).

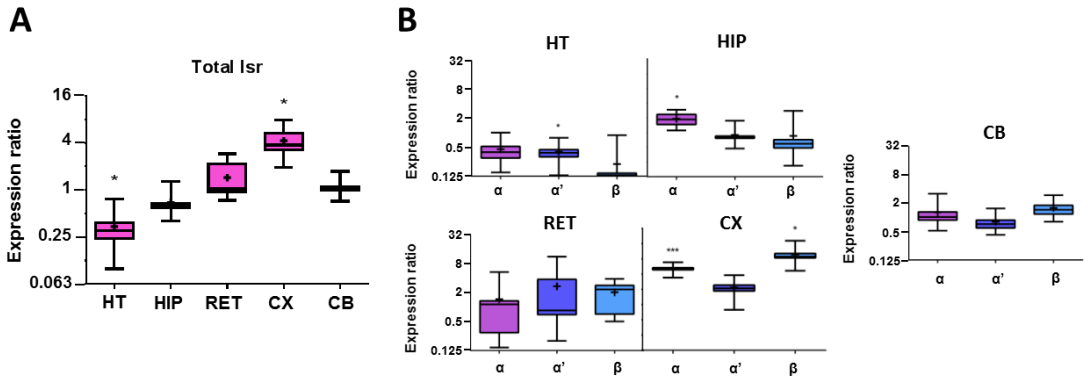

Figure 2.S1 Boxplot of RT-qPCR data of lsr mRNA expression in different brain regions of 3-month-old female C57Bl/6JRj mice (n = 3) with respect to 3-month-old male C57Bl/6JRj mice (n = 3). (A) Box plot of total lsr expression in various regions including hypothalamus (HT), hippocampus (HIP), retina (RET), cortex (CX), and cerebellum (CB). (B) Expression ratio of different lsr isoforms α, α', and β, respectively Statistical significance is represented as: * P ≤ 0.05, ** P ≤ 0.01, *** P ≤ 0.001.

When comparing 18 month old females(n= 3) with respect to males of the same age, total *lsr* stays relatively constant in all mentioned regions except in HT where it is upregulated to 4.09 folds (P = 0.034), and tends to be upregulated to 4 folds in HIP (P = 0.07). In the HT, only *lsr α* is significantly upregulated to 2.25 folds (P = 0.019).

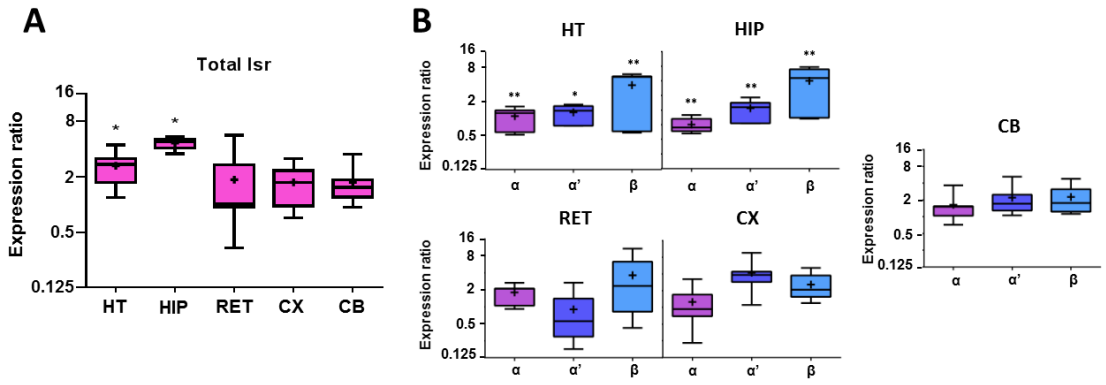

Figure 2.S2 Boxplot of RT-qPCR data of *lsr* mRNA expression in different brain regions of 18-month-old female C57Bl/6JRj mice (n = 3) with respect to 18-month-old male C57Bl/6JRj mice (n = 3). (A) Box plot of total lsr expression in various regions including hypothalamus (HT), hippocampus (HIP), retina (RET), cortex (CX), and cerebellum (CB). (B) Expression ratio of different lsr isoforms α, α', and β, respectively Statistical significance is represented as : * P ≤ 0.05, ** P ≤ 0.01, *** P ≤ 0.001.

When comaring *lsr* RNA expression with age in females, *total lsr* expression increased in HT (1.8 folds, P = 0.032), and RET (1.52 folds, P = 0.04) and decreased in HIP (0.805 folds, P = 0.014) and CB (0.65 folds, P = 0.04).

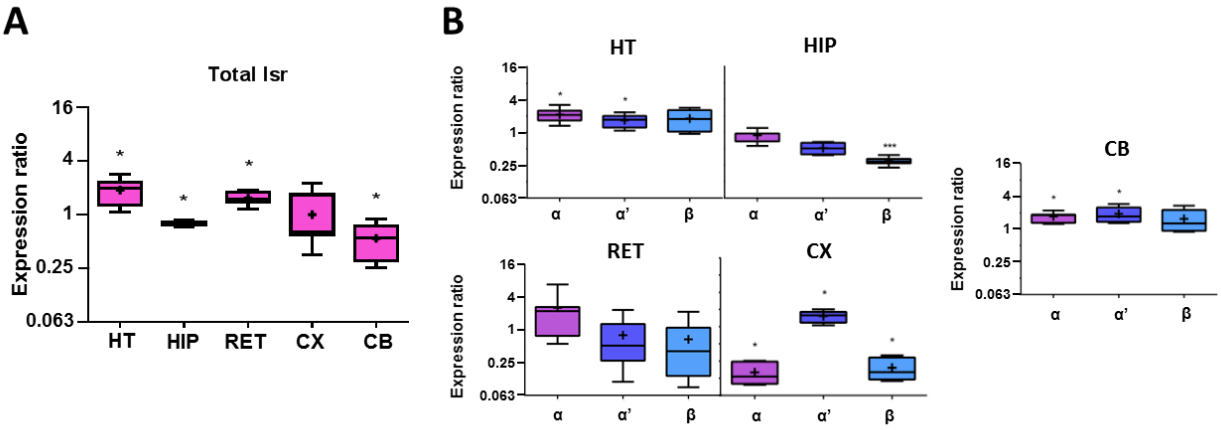

Figure 2.S3 Boxplot of RT-qPCR data of lsr mRNA expression in different brain regions of 18-month-old female C57Bl/6JRj mice (n = 3) with respect to 3-month-old female C57Bl/6JRj mice (n = 3). (A) Box plot of total lsr expression in various regions including hypothalamus (HT), hippocampus (HIP), retina (RET), cortex (CX), and cerebellum (CB). (B) Expression ratio of different lsr isoforms α, α', and β, respectively Statistical significance is represented as : * P ≤ 0.05, ** P ≤ 0.01, *** P ≤ 0.001.

Whole cell protein extracts were collected from different regions of the brain including

the HT, Hip, OB, Ret, CX, and CB. Interestingly, when comparing LSR expression in different regions of the brain, there is a differential expression of the different LSR subunits α (72 KDa), α’ (68 KDa), and β (56 KDa) (Figure 2.S4.). In all cases, both LSR Sigma and LSR X-25 identify the major two bands α and β. But, LSR Sigma's signal is quite stronger than that of LSR X-25. On the other hand, LSR X-25 seems to identify smaller bands of about 51, 36, and 28 kDa. The different isoforms of LSR (α, α', and β) are unequally expressed throughout the CNS and should lead to functional specificity in the considered areas. The small truncated bands might either be degradation of a larger LSR band or different soluble forms of LSR, further experiments must be conducted to draw an appropriate conclusion. We consider sequencing those lower bands to determine their exact identity. The main outcome of this study is that, LSR protein expression profile is quite different among the six regions of the brain we studied. The different isoforms of LSR (α, α', and β) are unequally expressed throughout the CNS and should lead to functional specificity in the considered areas.

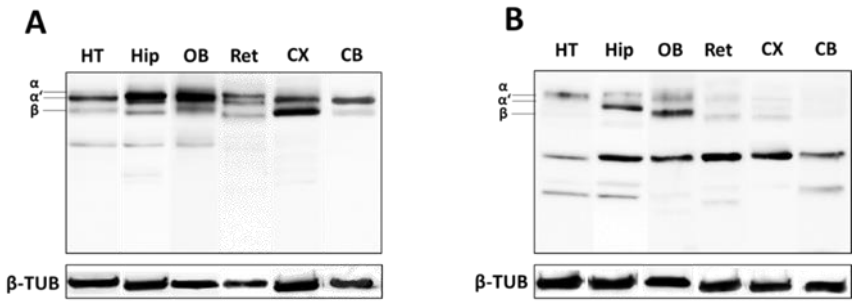

Figure 2.S4. Western blot profiles of LSR protein expression among different regions of the 18-month-old male brain. In both panel (A) and (B), data that correspond to HT, Hip, OB, Ret, CX, and CB are represented, respectively. In (A), the LSR Sigma antibody was used. LSR Sigma marks the major isoforms α and α’ which usually form together a thick band, and β. On the other hand, in panel (B) Santa Cruz LSR X-25 was used, which lightly marks the major isoforms α, α’, and β, but mainly recognizes shorter bands possibly corresponding to novel truncated forms of LSR. The β-TUB expression of each region is shown below that of LSR.

Gene	Primer	Sequence (5'-3')	Length
Hprt F	Forward	TCA-GAC-TGA-AGA-GCT-ACT-GTA-ATG-ATC-A	28
Hprt R	Reverse	AAA-GTT-GAG-AGA-TCA-TCT-CCA-CCA-A	25
Pgk1F	Forward	GAG-CCT-CAC-TGT-CCA-AAC-TA	20
Pgk1R	Reverse	CTT-TAG-CGC-CTC-CCA-AGA-TA	20
Tfrc F	Forward	GTC-TTC-TGT-TGA-AAC-TTG-CCC-A	22
Tfrc R	Reverse	GAA-AGG-TAT-CCC-TCC-AAC-CAC-TC	23
LSR-T F	Forward	AGT-AAT-ACA-CTC-CAC-TGT-CTC-CCC-AG	26
LSR-T R	Reverse	CAG-GAG-AAT-CAC-CAT-CAC-AGG-AA	23
LSR F	Forward	AAG-ATC-TGG-ATG-GGA-ACA-ACG-AG	23
LSRα R	Reverse	CTT-CTG-AGG-TCC-TGC-CAA-GG	20
LSRα' R	Reverse	CAA-AGA-GCC-AAT-CAA-GGA-CAA-TG	23
LSRβ R	Reverse	CCA-GCA-GCA-TAA-ACA-AGG-ACA-AT	23

Table 2.S1. RT-qPCR primers used in the study. Forward and reverse primers of the three reference genes used Hprt, Pgk1, and Tfrc, and target isoforms of lsr, total (T), α, α', and β

Below are additional examples of LSR staining of mixed cell cultures (Figure 2.S5a), primary neuronal (Figure 2.S5b) and glial cultures (Figure 2.S5c and S5d). LSR is expressed in both neurons and glial cells. However, LSR expression in neurons is more soma-centered with a weak expression in axons, while it is more ubiquitous in glial cells.

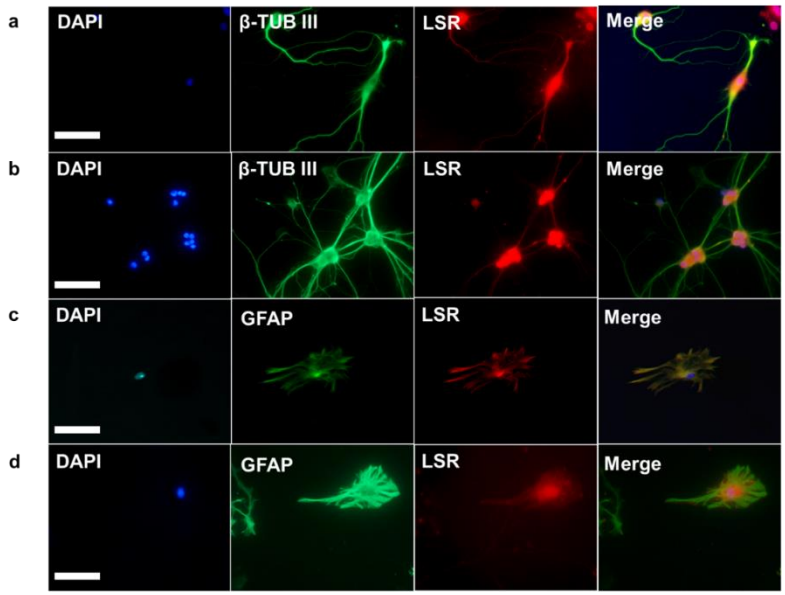

Figure 2.S5. LSR staining of primary neuronal and glial cell cultures. a) Mixed neuronal and glia culture of HT at day 14. b) Pure retinal ganglion cells culture at day 14. c) Glial cell culture in CB at day 14. d) Glial cell culture in hippocampus at day 14. DAPI for staining nuclei, β-TUB III for staining neurons, GFAP for staining glia, LSR X-25 for staining LSR, and merge of blue, green, and red staining respectively. Images were taken using Fvi10 confocal microscope at a 40-X magnification, the white bar indicated is a 20 μm scale.

Glial lipoprotein receptor LSR disruption in mouse nervous system leads to cognitive deficits resembling AD.

To be submitted to *Genes, Brain, and Behavior* journal

Chapter III

Glial lipoprotein receptor LSR disruption in mouse nervous system leads to cognitive deficits resembling AD

To be submitted to Genes, brain, and behavior journal.

Short resume

After studying LSR expression pattern and pointing out the strong LSR expression in glial cells, we decided to generate glia-specific *lsr* KO using tamoxifen (TAM) inducible conditional Cre/lox system. A battery of behavioral tests was done to study the effects of glial LSR suppression on activity, anxiety, vision, olfaction, sociability, spatial short-, and long-term memory.

Resume

As demonstrated by links between perturbations of cholesterol metabolism and neurodegenerative diseases, a precise glia-neuron crosstalk is essential to achieve a tight regulation of cholesterol trafficking within the central nervous system (CNS). Proper cholesterol supply via ApoE lipoproteins is needed for neurons in order to ensures their development and functions. CNS lipoprotein receptors are keystone elements to achieve this control. Here we focus on the ApoB, E lipolysis stimulated lipoprotein receptor (LSR). Previous studies on *lsr* +/- mice revealed altered brain cholesterol distribution and cognitive functions. Interestingly, we recently found a strong LSR expression in glial cells compared to neurons. To decipher the role of this lipoprotein receptor in glia cells, we obtained glia-specific LSR knockout animals (*cKO*) by crossing glia-specific inducible *GLASTCreER*^{T2} (*Cre*) mice with floxed LSR mice (*LSR*$^{loxP/loxP}$). Cre enzyme was activated in adult mice by intraperitoneal tamoxifen (TAM) injections. Behavioral phenotyping of these animals after TAM induction of Cre enzyme revealed a hyperactivity during nocturnal period, a deficit in olfactory function affecting social memory and causing possible apathy, as well as visual memory (despite no effect on vision), and short-term working memory problems. This demonstrated that glial LSR is important for working, spatial and social memory related to sensorial input. Our observations are in lines with studies reporting hyperactivity, apathy, olfactory deficits, and short term visual and working memory problems in AD. Since aging *lsr* +/- mice show increased susceptibility to amyloid stress, we propose that LSR represents a novel pathway to study the link between cholesterol trafficking, and AD.

1. Introduction

Cholesterol transport and homeostasis should be tightly regulated in the CNS to ensure proper development and functioning of the brain throughout life. During normal aging, cholesterol homeostasis is modified. Brain cholesterol levels change in a regio-specific manner, especially in hippocampus (Söderberg *et al.* 1990) and cortex (Svennerholm & Gottfries 1994) leading to a moderate reduction of total cholesterol in the brain. These cholesterol changes could influence the cortical lipid rafts composition modifications observed during aging (Díaz *et al.* 2018) and jeopardize ultimately the synaptic functions and normal aging process of the brain (Ledesma *et al.* 2012). Indeed

many studies have underlined the link between cholesterol perturbation and neurodegenerative disease including AD (Martin *et al.* 2010; Hicks *et al.* 2012). Due to the presence of BBB (Pitas *et al.* 1987a), the brain relies on itself for acquiring cholesterol by *de-novo* synthesis (Jeske & Dietschy 1980). Glial cells provide neurons with cholesterol in the form of lipoproteins, which are primarily apolipoprotein (Apo) E and J containing high density like (HDL-like) lipoproteins (Fagan *et al.* 1999d). Those HDL-like particles are exported from astrocytes via ABCA1 and ABCG1 transporters (Chen *et al.* 2013b) where they then bind to lipoprotein receptors via ApoE and are internalized in targeted cells through receptor-mediated transporters. Lipoproteins and their receptors are key elements to ensure the tight control of cholesterol trafficking. One of the lipoprotein receptors found in the CNS is LSR, lipolysis stimulated lipoprotein receptor. LSR is a multimeric protein complex, which is activated in the presence of free fatty acids, thereby revealing a binding site that recognizes Apo B and E (Bihain & Yen 1998). It was first discovered in the liver (Yen *et al.* 2008b), and most recently in CNS (Stenger *et al.* 2012), where it is supposed to have similar functions as peripheral LSR; maintaining normal levels of cholesterol and triglycerides, and contributing to the regulation of lipid distribution (Yen *et al.* 2008b; Narvekar *et al.* 2009). Dyslipidemia in absence of LSR was confirmed by the observation of increased plasma levels of cholesterol and triglycerides following shRNA-mediated knockdown of hepatic LSR expression (Narvekar *et al.* 2009).

1.1. Scientific question

What are the consequences of *lsr* inactivation?

The consequence of a complete inactivation of *lsr* cannot be studied as it is associated with *in utero* lethality at the embryonic stage, most likely due to brain-localized hemorrhages and a leaky BBB (Mesli *et al.* 2004; Sohet *et al.* 2015). *In vivo* studies conducted on young and aged *lsr* +/- mice suggest that reduced LSR may be associated with cognitive disturbances related to reactivity to novel environments in aged *lsr* +/- mice (Stenger *et al.* 2012). A significant decrease of lipid droplets, which are lipid-rich cellular organelles that regulate the storage and hydrolysis of neutral lipids, including cholesterol (Martin & Parton 2006), was observed in Purkinje cells of the cerebellum together with an accumulation of filipin-labeled cholesterol in neuronal membranes of the hippocampus in aged *lsr* +/- mice (Stenger *et al.* 2012). We have recently identified

the regional expression profile of LSR subunits within the CNS and specific age-induced changes in LSR protein expression mainly in hypothalamus, hippocampus and olfactory bulb (El Hajj *et al.* 2019). Moreover, we established that glial cells exhibit a high level of LSR expression compared to neuronal cells (El Hajj *et al.* 2019).

1.2. Goal of the study

To decipher the role of glial LSR in the cholesterol crosstalk within the CNS, we used a conditional Cre/lox recombination system developed in a glia-specific transgenic mouse line that allow for temporally controlled site-specific recombination (Slezak *et al.* 2007). Their approach depends on cell specific expression of TAM-dependent $CreER^{T2}$ recombinase and on transgenes derived from bacterial artificial chromosomes (BACs). The *Cre* mouse line showed highest Cre-mediated recombination in the glia cells from cerebellum, hippocampus, and olfactory bulb with lower activity in other brain areas and eye. Outside the CNS, Cre activity was observed in both the spleen and skin (Slezak *et al.* 2007). In the present study, we suppressed LSR expression in glial cells at the age of 2 months using the TAM-induced *GlastCreER*^{T2} floxed *lsr* (*cKO*) mouse model, followed by a series of behavioral studies for the assessment of activity, olfaction, vision, sociability, and short- and long-term memory. The behavioral phenotyping revealed a series of traits resembling AD, with a sequence of events mimicking early and later steps of the pathology. Our findings therefore demonstrate that glial LSR disruption is enough to switch from normal to pathological aging of the CNS.

2. Materials and methods

2.1. Animals

Animal studies were conducted in accordance with the European Communities Council Directive (EU 2010/63) for the use and care of laboratory animals. All experimental procedures were carried out in accordance with the ethical committee CELMEA N°066 with an approval number APAFIS #12079-201711081110404. Animals were housed in certified animal facilities (#B54-547-24) on an inverted 12-hour light/dark cycle with a mean temperature of 21–22 ◦C and relative humidity of 50 ± 20 %, and provided a standard chow diet (Envigo Teklad, Gannat, France) and water *ad libitum*. To generate conditional knockout male mice (*cKO*, n = 18), *Cre* mice were crossed with $LSR^{loxP/loxP}$

mice; then outbred males and females carrying both the *Cre* allele and the floxed *lsr* allele were crossed with homozygous LSR$^{loxP/loxP}$ mice to obtain mice homozygous to floxed *lsr and Cre* allele. The Cre mice and the floxed lsr mice were generated and obtained from Institut Clinique de la Souris (ICS, Ilkrich, France). C57BL/6J male mice (*WT*, n = 20) were used as controls (Charles River, Saint Germain Nuelles, France).

2.2. Breeding and generation of experimental groups

For *cKO* generation, we first crossed *Cre* mice (ICS, Ilkrich, France) with floxed lsr mice LSR$^{loxP/loxP}$ mice together to obtain the first generation F1 (Figure 3.1). The F1 generation was about 50 % heterozygous for the lox P allele and hemizygous for the *Cre* transgene (*GLASTCreERT2-LSR*$^{loxP/wt}$). The *GLASTCreERT2-LSR*$^{loxP/wt}$ mice were crossed back to the *LSR*$^{loxP/loxP}$ mice and approximately 25 % of the F2 generation contained *cKO* mice; the experimental mice. Since, we need a sufficient number of mice for statistical robustness (n = 18), those 25 % of F2 were crossed together (avoiding close relatives mating) in order to increase their number (Figure 3.1). Concerning control groups, we chose to maintain two control groups, wild type mice (*WT*- negative controls,n = 20) and *Cre* (n = 18). Both *Cre* and *cKO* were induced with TAM in order to link any behavioral/physiological change to the loss of LSR function (Figure 3.3). To avoid “litter effect” i.e. the tendency for littermates all to respond in the same way to stimuli, unlike animals from different litters, each mouse used for behavioral phenotyping came from a different mother. All 18 *cKO* mice were a result of 18 different

breading pairs.

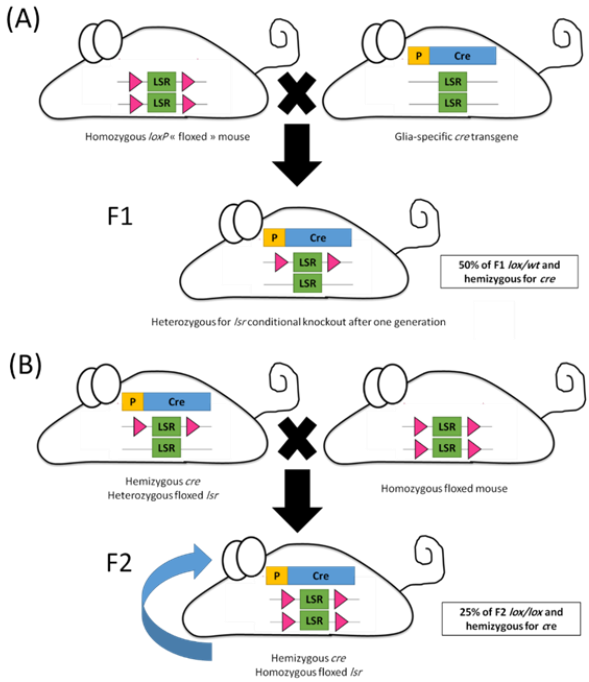

Figure 3.1: Breeding plan. (A) LSR$^{fl/fl}$ crossed with Cre mice line to obtain 50% GLASTCreERT2-LSRloxP/wt in F1. (B) The GLASTCreERT2-LSRloxP/wt mice were crossed against LSRloxP/loxP mice to obtain 25% cKO in F2.

2.3. Genotyping of *Cre* and floxed *lsr* mice

Mouse genomic DNA was isolated from ear biopsies following overnight digestion at 55 °C in Direct PCR lysis buffer (Viagen Biotech, Los Angeles, CA, USA) and 0.2 mg/mL of Proteinase K (Invitrogen, Cergy Pontoise, France) followed by heat inactivation of Proteinase K. For genotyping of *Cre* expression, two sets of primers were used for the same PCR reaction, TK139 and TK140, which gives a 350 base pair (bp) DNA band, specific for the *Cre* allele, and ADV28 and ADV30, a 250 bp band, which correspond to a myogene, that serves to verify the success of the PCR amplification. The PCR reaction temperature were as follows: 95 °C for 2 minutes, 95 °C for 30 seconds, 55 °C for 30 seconds, 72 °C for 30 seconds for 30 cycles, then 72 °C for 10 minutes. In order to detect whether the mice were heterozygous or homozygous for the LSR$^{loxP/loxP}$, the protocol of ICS (# IR00004190 / K4190) was followed, using two sets of primers; set A: Lf/Lr 7987-7989 (check the presence of the distal loxP site) and set B: 11 Ef/Er 7990-7991 (check excision of the selection marker). Basically, when the mice are homozygous

for the floxed allele, a 289 bp and a 362 bp cDNA for set A and B, will be obtained respectively. Whereas for wildtype, 209 and 260 bp cDNA for set A and B, will be obtained respectively. However, for the heterozygous floxed allele it gives 209 and 289 bp of cDNA for set A and 260 and 362 bp of cDNA for set B (Figure 3.2). The PCR reaction temperature were as follows: 95 °C for 4 minutes, 95 °C for 30 seconds, 62 °C for 30 seconds, 72 °C for 1 minute for 34 cycles, then 72 °C for 7 minutes, and 20 °C for 5 minutes.

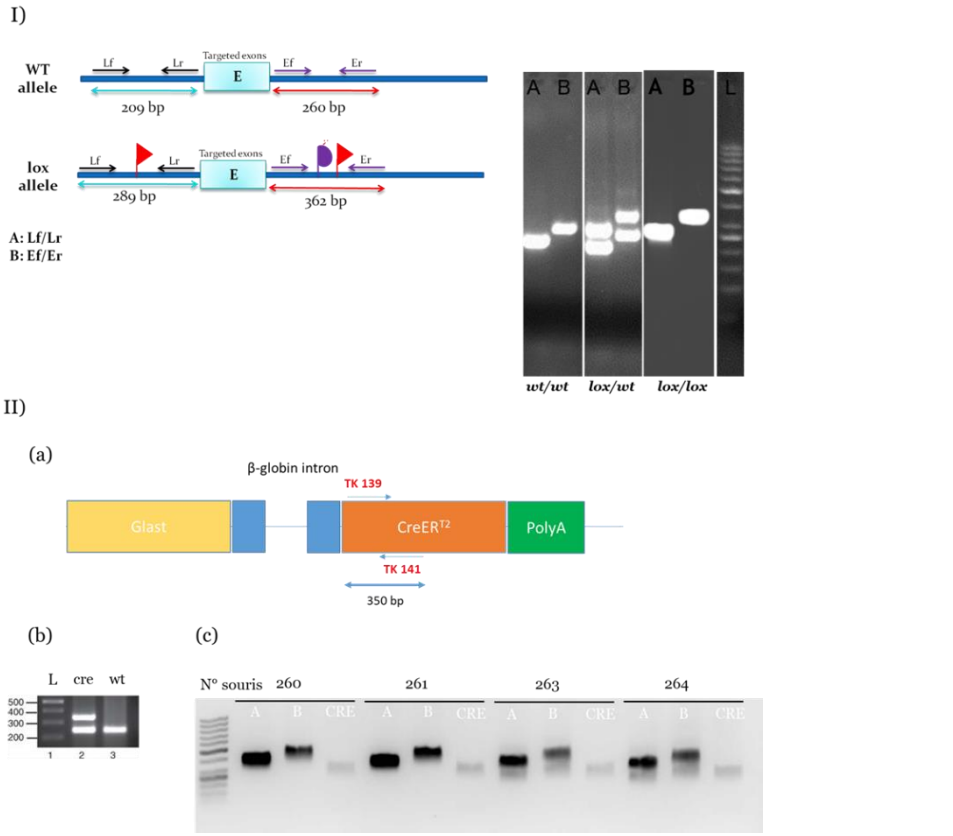

Figure 3.2: I) Genotyping of LSR$^{loxP/loxP}$ mice. I) Genetic representation of LSR $^{wt/wt}$, LSR$^{loxP/loxP}$ on left. Agarose gel of the amplified PCR products of LSR $^{wt/wt}$, LSR $^{loxP/wt}$, and LSR $^{loxP/loxP}$. II) Genotyping of *Cre* mice. (a) Schematic structure of the *Cre* transgene. The Glast promoter, the CreERT2 coding sequence, and the simian virus 40 polyadenylation signal (polyA) are represented by yellow, orange, and green boxes, respectively. The β-globin intron and splice donor- and acceptor sites are depicted by a line and blue boxes, respectively. The position of the PCR primers TK139 and TK141, and the length of the PCR-amplified DNA segment are indicated. (b) Identification of *Cre* transgenic mice by PCR-mediated ear genomic DNA amplification. PCR-amplified DNA segments were run on a 2 % agarose gel. Lanes 2 and 3, amplification products from *Cre* and WT mice, respectively. Lane 1, DNA ladder (L). The size of the DNA segments is given in base pairs. Cre, DNA segment amplified from the *Cre* transgene with the primer pair TK139 and TK141 is about 350 bp. IC (Internal control): DNA segment amplified from an endogenous mouse gene (myogenin) with the primer pair ADV28 and ADV30. c) DNA agarose gel of *CreERT2-LSR*$^{loxP/loxP}$ and *GLASTCreERT2-LSR*$^{loxP/wt}$ amplified PCR products for the *lox* (A and B) and *Cre* gene. Mice 260 and 261 are *cKO* mice and 263 and 264 represent *GLASTCreERT2-LSR*$^{loxP/wt}$ mice.

2.4. Tamoxifen (TAM) induction of GlastCreERT2 enzyme

Tamoxifen (Sigma, St Louis, MO) was dissolved in a 9:1 sunflower oil (Sigma, St Louis, MO) and ethanol (CARLO ERBA Reagents, Val de Reuil Cedex, France) at a concentration of 15 mg/mL at 37 °C and then sterile-filtered and stored up to 7 days at 4 °C in the dark. A 23 G needle tuberculin syringe (Henke Sass Wolf, Tuttlingen, Germany) was used for intraperitoneal injections. At the age of 8 weeks, mice were injected intraperitoneally for 5 consecutive days with 150 µg of TAM per g of body weight. Multiple injections in the same mouse were separated by a 24-hours interval (Slezak et al. 2007).

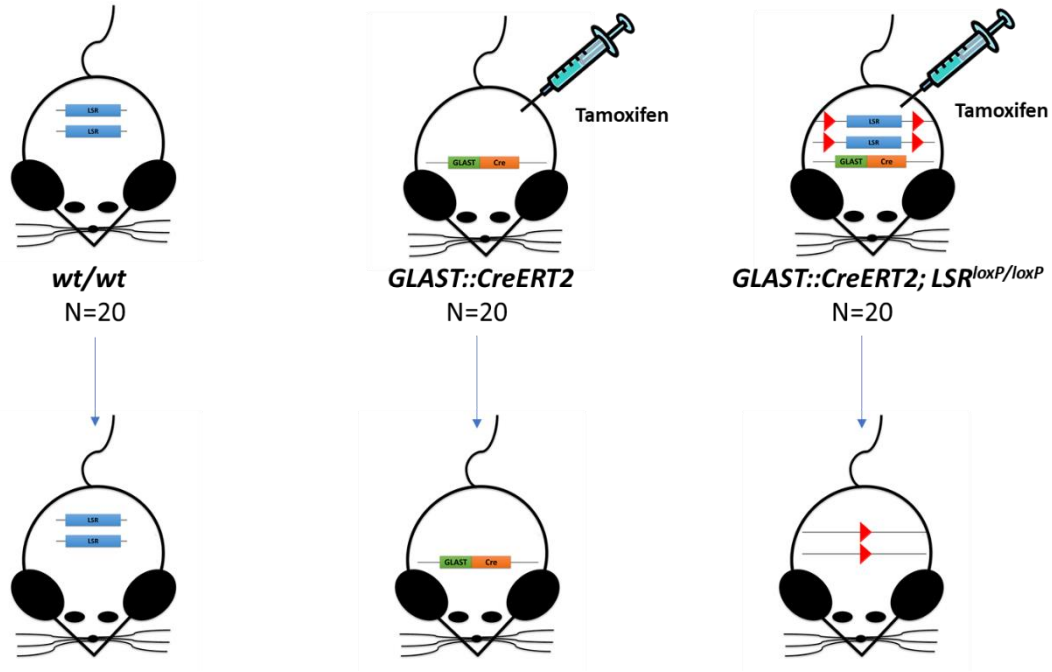

Figure 3.3: Experimental groups used in the study. Wt are control naïve animal with the same genetic background(N=20) *Cre* mice without the floxed construct represent a control group of injected mice in order to monitor the effects of tamoxifen on the behavioral analysis. cKO represent the glia deficient LSR mice obtained after tamoxifen injection. 2 mice in each injected group died after tamoxifen treatment. 18 mice were therefore used for behavioral analysis

2.5. Behavioral tests

Following TAM induction, we waited for two weeks before starting any behavioral studies. Behavioral tests were performed to decipher the possible effects of *lsr* knockout using the same mice in the whole study (Figure 3.4). The open field test (OFT), three-chamber sociability and social novelty test (C3C), object recognition test

(ORT) and the Y-maze test were performed at two different age points. All the mentioned tests were performed 1 hour after the beginning of the dark cycle.

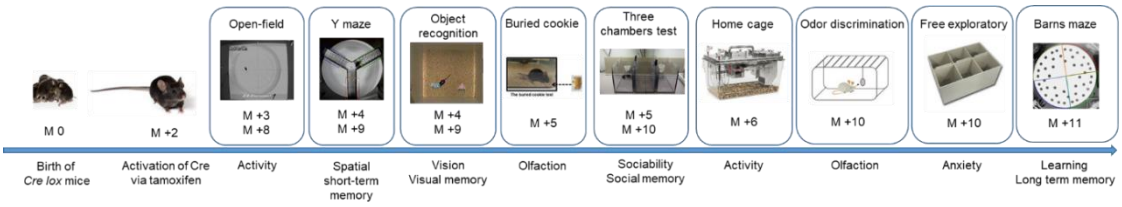

Figure 3.4. Timeline of behavioral tests. After the induction of Cre enzyme at 2 months (M +2), a series of behavioral tests were performed. Each test mentioned in a separate box, with a descriptive photo, the age it was performed (M+n: age in months) with the main aim of the test and the age in which it was performed.

2.5.1. Activity and anxiety

2.5.1.1. Home cage activity

This test was performed at the age of 6-7 months on *cKO* mice (n = 16) and *WT* mice (n = 18). There was a technical issue for data recording on one of the experimental days, thus data for 2 *cKO* and 2 *WT* mice were lost. The general activity, including walking time and fine movements, was measured by monitoring mice, using the Promethion High-Definition Behavioral Phenotyping System (Sable Instruments, Inc, Las Vegas, NV, USA), over a period of 24-hours. The mice were left in their own individual cages (308 L x 115 W x 120 H cm), with food and water *ad libitium*. Instrument setup and data acquisition were done using MetaScreen software version 2.2.18.0, and the raw data obtained were then processed *via* ExpeData version 1.8.4 using an analysis script for data transformation, following Sable's system guidelines. Ambulatory and voluntary activities and animal positions were monitored simultaneously by collecting the calorimetry data using the XYZ beam arrays with a beam spacing of 0.25 cm.

2.5.1.2. Open Field test

This test was performed twice at the age of 3 and 8 months on *cKO* mice (n = 18) and *WT* mice (n = 20). The test apparatus was a large circle-shaped frame, of an 80 cm diameter and 60 cm height, virtually divided into three different zones using the SMART software (Bioseb, Vitrolles, France). An external zone Z1, an intermediate zone

Z2, and a central zone Z3, each of a 20 cm diameter. The apparatus was illuminated with two opposite lamps, where the center (Z3) was illuminated at 120 lux. Each animal was placed individually in same side of Z1 facing the wall and allowed to explore it freely for 5 min. After each trial, the test arena was cleaned carefully with disinfectant (Belhaj *et al*. 2013). The following parameters were recorded: Time spent in each zone, total distance, average velocity, as well as number of entries in each zone were calculated.

2.5.1.3. Free exploratory paradigm

This test was done at the age of 10 months with 15 *cKO* mice and 15 *WT* mice. We followed the same protocol described by Elhabazi (Elhabazi *et al*. 2006)**.** The apparatus was a polyvinyl chloride box (60 L × 42 W × 22 H cm) covered with plexiglass and subdivided into six equal square units interconnected by small holes. The box could be divided into two by means of three temporary partitions. Twenty-four hours before testing, each animal was randomly placed in one half of the apparatus which constitutes the familiar compartment. During this time, the other compartment remains inaccessible to animals by placing partitions. The floor of the familiar compartment was covered with fresh sawdust and the animals had unlimited access to food and water. At the start of test, the animals were exposed to both familiar and novel environments by removing the partitions without being itself removed from the box. Then, the behavior of the animals was recorded under red light for 5 min, using a video

camera on infrared mode (Figure 3.5).

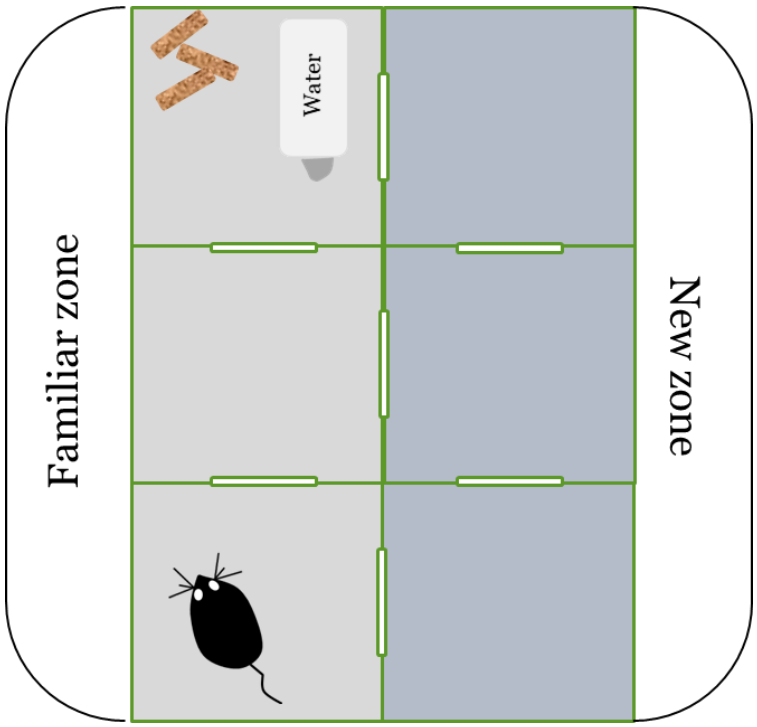

Figure 3.5: Free exploratory paradigm. It consists of 6 compartments, 3 familiar compartments (light grey) where no partitions are placed in between and water and food are ad libitum (familiar zone), and 3 new compartments with no partitions in between (new zone). The partitions between the familiar zone and new zone are closed for 24 hours and are opened only for the 5-minutes test duration.

2.5.2. Olfaction

2.5.2.1. Buried cookie test

This test was performed at the age of 5 months with 18 *cKO* mice and 20 *WT* mice. The protocol was adapted from previous papers (Fleming *et al.* 2008; Yang & Crawley 2009). The test took three days to be accomplished. On the first two days, mice were habituated to the cookie (Honey pops, Kellogg's, Limoges, France), where each mouse was given a cookie per day, and the latency to approach and start eating the cookie was calculated. On day three, the mice were put to fast 6-7-hours before the test time, with free access to water. The test was carried out in the room of the tested mice, in red light, and in their own cages. A barrier was put in the middle of the cage, and the cookie was buried 1 cm under the litter, in the opposite side of the cage. The test was filmed using a video camera in night mode, the barrier was removed and the latency to find and start eating the cookie was measured (Figure 3.6).

Figure 3.6: Buried cookie test. 1) Habituation phase; one honey pop was introduced per day for 2-3 consecutive days before test day.2) On test day, mice fasted for 6-7 hours on food with free access to water. 3) A honey pop was buried 1 cm under litter and latency to find and eat cookie was calculated.

2.5.2.2. Odor discrimination test

It was performed when *cKO* (n = 10) and *WT* (n = 10) were 10 months old. This test consisted of three habituation trials for 1 min to a tea ball with mineral oil (Sigma Aldrich), separated by a 1-minute pause each. Odor memorization can be identified this way. Then the test continue with three 2 minutes habituation to rose oil, separated by 1 minute pause each, in order to measure the ability to perform new vs old odor discrimination, followed by three 2 minutes habituation to female urine, separated by 1 minute pause each, in order to identify specifically sexual odor discrimination. The test then ends with a 2 minutes odor discrimination step to female urine containing 1% lemon oil in order to identify fine odor discrimination abilities. The protocol used was based on previous studies (Fleming *et al.* 2008; Yang & Crawley 2009; Vaz *et al.* 2018).

2.5.3. Memory

2.5.3.1. Vision and memory (Object recognition test)

This test was performed twice, once at 4 months and another at 9 months on *cKO* mice (n = 18) and WT mice (n = 20). It was conducted to assess vision and visual memory (Figure 3.7). The test was carried out in a dimly illuminated room (25 lux), in a squared opaque plastic box (30 L x 30 W x 26 H cm). The test was done 1h after the start of the dark cycle. Two different sets of objects were used, either colorful plastic blocks (Lego, Billund, Denmark) or litter-filled falcons with a red cap. The test was separated into

three steps, a habituation step, a familiarization session, and visual memory and novelty session. At first, subject mice were allowed to habituate to the empty arena and freely investigate. In the second step, mice were left to explore two similar objects, i.e. either two lego blocks or two litter filled falcons, where the objects were placed in two opposite corners of the arena; namely position A and B (session 1, S1). After one hour, in the visual memory session, the old object, either a lego block or a falcon and a new object, either a falcon or a lego block, were placed in the apparatus randomly; either in position A or B (session 2, S2). In S1 and S2, the mouse was considered exploring an object when the head was directed toward and not farther than 5 cm away from the object (Leger *et al.* 2013).

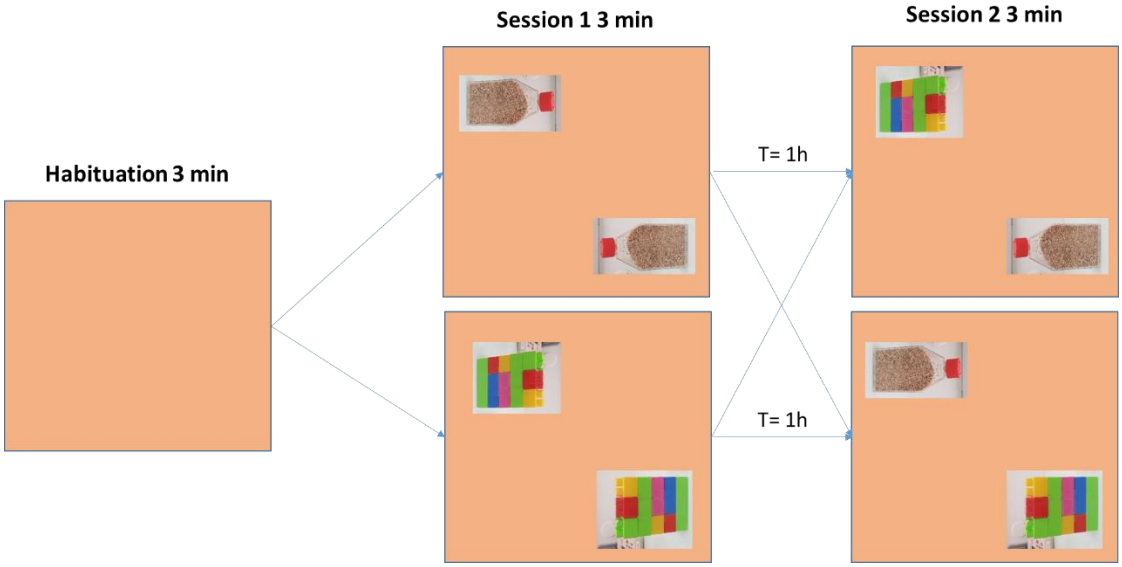

Figure 3.7: Object recognition test. It started by a 3 minutes habituation to the empty apparatus, followed by a 3 minutes familiarization to either two identical falcons or two identical building blocks. After 1 hour, 3 minutes of visual memory session was done, where the old object and new object are placed randomly in the arena.

2.5.3.2. Sociability and memory (Three chamber sociability and social novelty test)

It was done two times, at 5 and 10 months on *cKO* mice (n = 18) and *WT* mice (n = 20). The social approach apparatus was an open-topped box made of acrylic (63 cm L × 42 cm W × 23 cm H) and divided into three chambers with two grey acrylic walls. Dividing walls had retractable doorways allowing access into each chamber. The wire cup used to contain the stranger mice was made of cylindrical chrome bars spaced 1 cm apart (10 cm H; bottom diameter: 10 cm). The test was conducted in a 65-lux

illuminated room. Test mice placed in the central chamber at the beginning of each 5 min phase. During the habituation phase, each of the two side chambers contained an empty inverted wire cup. During the sociability phase (session 1, S1), an unfamiliar mouse (stranger 1) was enclosed in one of the wire cups in a side chamber. The location of the stranger 1 alternated between the two side chambers. During the social novelty phase (session 2, S2), a new unfamiliar mouse (stranger 2) from a different cage than stranger 1 was enclosed in the wire cup that had remained empty during the sociability phase. Exploration of an enclosed mouse or an empty wire cup was defined as when a test mouse oriented toward the cup with the distance between the nose and the cup less than 1 cm (Figure 3.8). The time spent in each chamber and time spent exploring enclosed novel mice or empty cups were recorded from a camera mounted overhead and analyzed afterwards by random order. All stranger mice were male mice of a young age habituated to being enclosed in inverted wire cups in the three-chamber apparatus for 5 minutes daily on two consecutive days prior to the experiment (Lo *et al.* 2016).

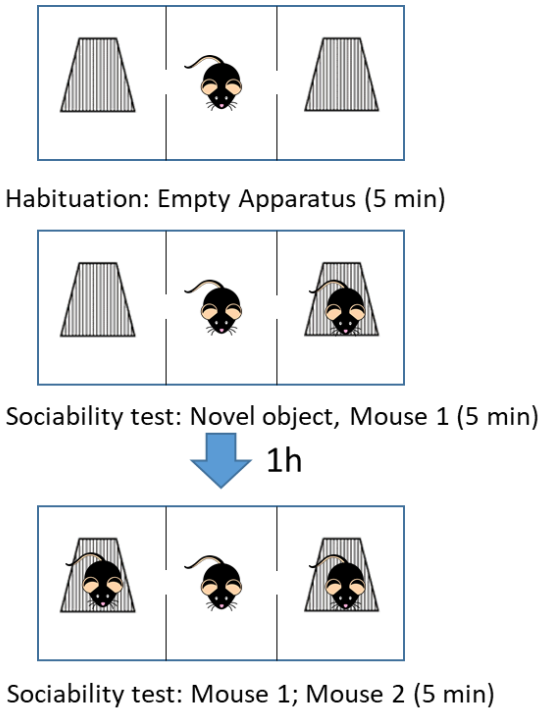

Figure 3.8: Three chamber sociability and social novelty test. Habituation phase: Mice were left to explore freely the three chambers for 5 minutes; empty wired cups were placed in the left and right chambers. In session 1, a stranger mouse 1 was put randomly in one of the cups, test mouse was left to explore freely for 5 minutes. In session 2, 1 hour after session 1, stranger 1 and stranger 2 were placed each in a wired cup, test mouse was left to explore freely for 5 minutes.

2.5.3.3. Spatial short-term memory (Y-maze)

It was performed at 4 and 9 months of age on *cKO* mice (n = 18) and *WT* mice (n = 20). The 3 arms- maze was made of opaque Plexiglas, where each arm was 40-cm long, 16 cm high, and 9 cm wide and positioned at equal angles. Mice were placed at the end of one arm, namely arm A, before starting the experiment countdown. The series of arm entries were recorded visually, and arm entry was validated when the hind paws of the mouse were completely placed in the arm. Spontaneous alternation behavior was monitored during a 5 min interval. Alternation scores were calculated by analyzing overlapping triplet's sets, a sequence of unique visits of the three different arms) reflecting a memorization of the already visited arms. The proper alternation % was calculated as a ratio of proper alternation overlapping triplets over total number of entries multiplied by 100 (Stenger *et al.* 2012).

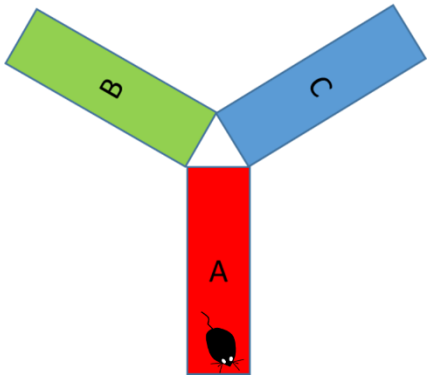

Figure 3.9: Illustration of the Y maze test. It is a three-armed maze, with three arms named A, B, and C. The test always started with the mouse in arm A facing the wall. Proper alternations of entries were recorded and correspond to unique visit of each arm.

2.5.3.4. Learning and long-term memory (Barnes maze)

It was performed when *cKO* mice (n = 15) and *WT* mice (n = 15) were 11 months old. The prototype used here is an upgraded one based on the initial Barnes of 1979 (Barnes 1979). It was a circle-shaped white platform with a 56 cm diameter placed 40 cm from the ground with multiple holes of 5 cm diameter each, virtually divided into four equally portioned zones using the SMART video tracker software. There were distant and proximal visual cues placed on the left, right, up and downwards of the platform, the visual cue "X" was positioned in the zone where the one and only escape chamber was placed. By sprinkling water and using two fans, the platform was made aversive. The test was repeated for 5 uninterrupted days with three consecutive trials per day.

Each trial was put to an end when the mouse found the escape chamber, if not the test stopped at 180 seconds. For the first three days, the mice were placed in the escape chamber for 1 minute before the test started, to increase their motivation for finding the chamber during the test. Each session started in the zone opposing the escape zone. On the fourth day, the test was conducted without the 1-minute session, and on the fifth day, the test sessions were launched in another zone to assess cognitive flexibility. To assess long term memory, two days after the fifth session, a single test session was performed starting in the same launch zone as day 4.

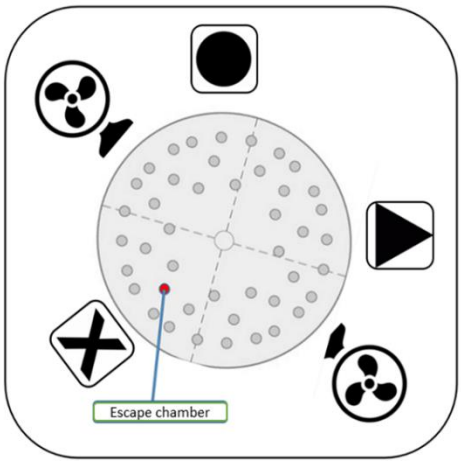

Figure 3.10: Illustration of modified Barnes maze. It was a circle-shaped white platform with a 56 cm diameter placed 40 cm from the ground with multiple holes of 5 cm diameter each, virtually divided into four equally portioned zones using the SMART video tracker software. There were distant and proximal visual cues placed on the left, right, up and downwards of the platform, the visual cue "X" was positioned in the zone where the one and only escape chamber was placed. By sprinkling water and using two fans, the platform was made aversive.

2.6. RNA extraction and RT-qPCR

At the age of 13 months, five *cKO* and five *WT* mice were sacrificed by decapitation after isoflurane anesthesia in order to preserve the integrity of brain structures. Freshly collected tissues were conserved in RNAlater (Qiagen, Les Ulis, France) as per manufacturer's instructions and stored at -80 °C until use. Different regions of the brain were isolated separately including the hippocampus. Total RNA was extracted using TRI reagent (Sigma Aldrich), according to the manufacturer's instructions. RNA quantity and purity were estimated by a Nanodrop ND-1000 spectrophotometer (Thermo Scientific; Villebon-sur-Yvette, France), and the samples with a 260/280 nm ratio ≥ 1.7 were used for subsequent analyses. Reverse transcription was performed using 1 µg of RNA in a final volume of 20 mL including 0.5 mL of random primers (3 mg/mL; Invitrogen, Carlsbad, CA, USA), 1 µL of 10 mM dNTP mix (Invitrogen, Cergy

Pontoise, France), in RNase-free water. After denaturation of RNA samples at 65 °C for 5 min, 4 µL of buffer (5x), 2 µL of 0.1 mM DTT, 1 µL of Superscript II reverse transcriptase (Invitrogen, Cergy Pontoise, France), and 1 µL of RNase OUT (Invitrogen, Cergy Pontoise, France) were added. Samples were homogenized using 23 G needles and transcribed in an Applied Biosystems 2720 thermal cycler according to the following conditions: 25 °C for 10 min, 42 °C for 50 min, and 70 °C for 15 min. The cDNA from individual animals was used as a template for the PCR array using the PowerUP SYBER Green master mix from Applied Biosystems (Foster City, CA, USA) with the following final concentrations in a 25 µL final volume: 1 × Master Mix, 100 nM forward and reverse primers, 0.4 ng/µL cDNA. The mix was placed in a 7500 Fast Real-Time PCR system (Applied Biosystems). The thermal cycling conditions were initial 5 min denaturation at 95 °C, followed by 42 cycles of 15 s at 95 °C, 1 min at 60 °C, and a final dissociation step. The primer specificity was determined based on the presence of a single peak in the melting curve. We followed four target mRNA sequences: total *lsr*, *lsr* α, *lsr* α', and *lsr* β, whose expression levels were compared to those of three reference sequences: hypoxanthine guanine phosphoribosyl transferase (*Hprt*) (Yen *et al.* 2008b), phosphoglycerate kinase 1 (*Pgk1*) (Boda *et al.* 2009), and transferrin receptor protein 1 (*Tfrc1*) (Boda *et al.* 2009) (S1 Table). *Lsr* primer sequences were selected using the Primer-BLAST Genbank based on *lsr* gene sequence (NM_017405). Quantitation was performed by the $2^{-\Delta\Delta Ct}$ method (Livak & Schmittgen 2001). The obtained results were tested for statistical significance ($P < 0.05$) using the Relative Expression Software Tool 2009 (REST Version 2.0.13). The fold changes of mRNA samples of *cKO* animals were compared to *WT* animals.

2.7. Blood glucose test

Mice fasted for 6 hours before the test; water was provided *ad libitum*. Blood samples were collected from the central tail artery using a sterile 25 G needle. No anesthesia was used at the time of blood sampling, to avoid unequal variations between animals and avoid the effects of anesthesia on the blood glucose levels. Mice were fixed by a retainer during blood collection from tail-tip. Blood samples were collected by skilled personnel using the routine technique. The ACCU-CHEK Performa glucometer (Roche Diabetes Care France, Meylan, France) and ACCU-CHEK strips (Roche Diabetes Care France) were used and calibrated for plasma glucose levels.

2.8. Statistical analysis

For behavior: To verify that the data obtained are of a Gaussian distribution, we used the Kolmogorov-Smirnov normality test. After verifying that all the data were of Gaussian distribution, student's *t*-test (two tailed, unpaired) was performed to compare *cKO* and *WT* data with one factor (genotype). Two-way analysis of variance (ANOVA) was performed to analyze data containing two different factors (example genotype x time). The numerical and graphical results are presented as mean ± standard error (SEM). The degree of statistical significance was set at a level of $P < 0.05$, *, $P < 0.01$, **, $P < 0.001$, ***. Statistical calculations were carried out using the Statviews 4.5 statistical package (Abacus Concept, Int.) and the Excel 6.0 (Microsoft, Inc.).

For RT-qPCRs: The statistical data in the boxplot were obtained using REST software tool, where (+) represents the mean value, the middle line represents the median, the lower (Q1) and upper (Q3) lines in the bar represent the 25 % and 75 % quartile, respectively. While the upper and lower lines represent the observations outside the 9-91 percentile range, data falling outside of Q1 and Q3 range are plotted as outliers of the data.

3. Results and conclusions

3.1. *Lsr* downregulation in *cKO* mice

Expression levels of *lsr* mRNA were measured by performing RT-qPCR on total RNA fractions extracted from the hippocampus in 13-month-old male *WT* and *cKO* mice. Total *lsr* was downregulated to 0.385-fold (95 % C.I.: 0.154-0.772, $P = 0.004$) when compared to *WT* mice (Figure 3.11). This was also the case of *lsr α* (0.354-folds, 95 % C.I.: 0.126-0.856, $P = 0.004$), *lsr α'* (0.346-folds, 95 % C.I.: 0.152-0.593, $P = 0.004$), and *lsr β* (0.425-folds, 95 % C.I.: 0.099-1.139, $P = 0.035$). This indicates that *lsr* gene was successfully excised from the GLAST expressing cells; the glial cells in the

hippocampus and was retained after 11 months of TAM injections.

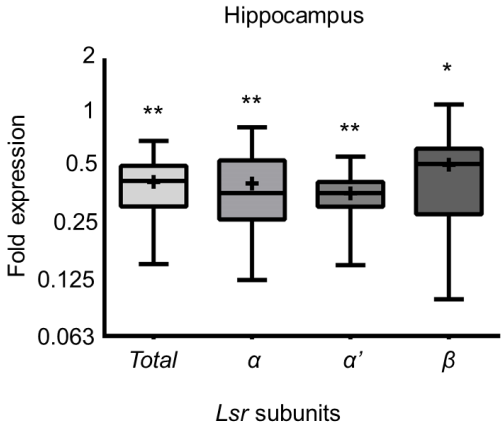

Figure 3.11. Verification of *lsr* gene excision in glial cells using RT-qPCR. Box plot presentation of fold expression of *total lsr* and different *lsr* subunits α, α', and β in 13-month-old *cKO* hippocampus (n = 5) with respect to *WT* hippocampus (n = 5). Statistical significance is represented as: * $P \leq 0.05$, ** $P \leq 0.01$, *** $P \leq 0.001$.

3.2. Activity and anxiety

3.2.1. Home cage activity

In 6-7 months old animals the exploratory activity of *cKO* mice was greater than that of *WT* mice (Two-way ANOVA RM, genotype effect $F_{1,32} = 7.924$, $P = 0.0083$, and a significant interaction between genotype and time $F_{2,64} = 3.456$, $P = 0.0376$, Figure 3.12Aa), where *cKO* mice walked for longer periods of time over the course of 24-h period [t (96) = 3.667, $P = 0.0004$, Figure 3.12A-b]. This was most likely due to increased dark time exploration [t (96) = 2.226, $P = 0.028$, Figure 3.12Ab]. Interestingly, the difference between the distance traveled by *cKO* and *WT* mice was insignificant during the dark cycle (Two-way ANOVA, no genotype effect, Figure 3.S1A). In regard to velocity, *cKO* mice were generally slower than *WT* mice during the dark period (two-way ANOVA, genotype effect: $F_{1,384} = 5.727$, $P = 0.017$, Figure 3.S1B). When fine movements, such as scratching and grooming, were measured, *cKO* mice showed higher levels of such activities than *WT* mice (Two-way ANOVA, genotype effect: $F_{1,759} = 30.65$, $P < 0.0001$, Figure 3.S1C). In conclusion, in their environment, *cKO* mice were more active during the last 4 hours in dark period, exhibiting longer periods of walking time (Figure 3.12Ab). As they move slowly, over the test duration, *cKO* mice travelled the same distance as *WT* mice. Following the Velocity = Distance / Time equation, *cKO* mice moved slower yet for a longer period, thus ending up by

travelling the same distance as *WT* mice. The *cKO* mice didn't exhibit motor coordination or equilibrium problems after careful observation (stumbling/ falling events) thus ruling out the possibility of underlying motor problems.

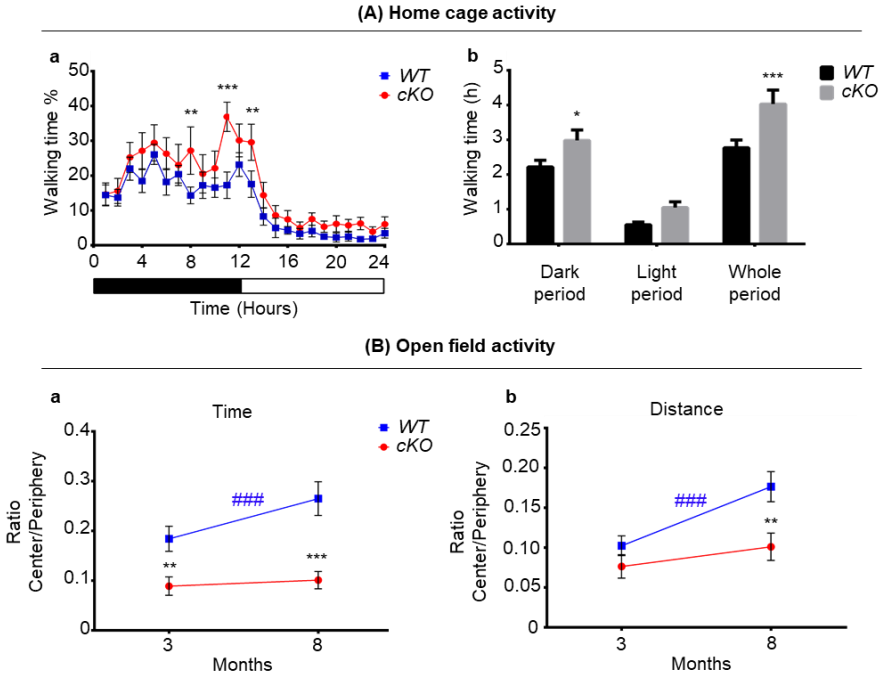

Figure 3.12. Activity assessment in *cKO* mice. (A) Home cage activity. (a). Hourly measurements of walking time % over a 24-hour period. (b). Sum of walking time in hours (h) during dark cycle, light cycle, and whole period. (B) Open field test. (a). Time ratio spent in center over that of periphery. (b). Distance ratio travelled in center over that of periphery. Statistical significance between *WT* vs *cKO* is represented as /* $P \leq 0.05$, ** $P \leq 0.01$, *** $P \leq 0.001$; 3 months vs 8 months is represented as: # $P \leq 0.05$, ## $P \leq 0.01$, ### $P \leq 0.001$.

3.2.2. Open field test

The open field test was conducted when mice were 3 months and 8 months old. At 3 months of age, *WT* mice passed more time in the center (Z3) than *cKO* mice [t (72) = 2.665, $P = 0.0095$, Figure 3.12Ba]. Equally, *cKO* mice travelled a shorter distance in the central zone when compared to *WT* mice [*t*-test with Welch's correction t (31.73) = 2.76, $P = 0.0095$, Figure 3.12Bb]. However, at this age, both *cKO* and *WT* mice passed the same time and travelled the same distance at the periphery Z1 (Figure 3.S2A).

The same *WT* mice at 8 months old tended to pass more time in the center Z3. Thus, the ratio of time spent in the center over the periphery (Z3/Z1) increased [t (36) = 3.117, $P = 0.0036$, Figure 3.12Ba]. However, in *cKO* mice the ratio of time Z3/Z1 was left nearly unchanged [t (36) = 0.4428, $P = 0.66$, Figure 3.12Bb], and the difference

between *cKO* and *WT* mice was thus greater at 8 months of age [t (72) = 4.59, $P < 0.0001$].

The *cKO* mice passed more time in the periphery Z1 than *WT* mice [t (34.66) = 2.086, $P = 0.044$]. However, both *cKO* and *WT* mice travelled the same distance in Z1 (Figure 3.S2). When comparing both genotypes at the two time points of the experiments (3 and 8 months) using two-way ANOVA, a highly significant genotype effect was seen ($F_{1,72} = 26.32$, $P < 0.0001$), and an age effect tendency ($F_{1,72} = 3.388$, $P = 0.069$), but no genotype x age interaction. We conclude that, in a novel environment, *cKO* mice tended to stay at the periphery for longer periods of time when compared to WT mice (thigmotaxis). Nevertheless, they travelled the same distance in the periphery, which would indicate longer immobile periods in this zone. This suggests anxiety or a lower motivation to explore in *cKO* mice that reflects apathy.

3.2.3. Free exploratory paradigm

This test was performed in order to assess trait anxiety. No significant differences between *cKO* and *WT* mice were observed; both groups spent similar times in new environment (Figure 3.S3), indicating an absence of trait anxiety behavior in *cKO* mice reinforcing the hypothesis of apathy in the open field test.

3.3. Olfaction

3.3.1. Buried cookie test

This test was performed at 5-months of age. During the habituation phase of the buried cookie test, there was no significant difference between the *cKO* and *WT* mice in the time it took to take the visible cookie and start eating it (Figure 3.13Aa). However, during the test phase, *cKO* mice took a 2-fold longer period to find the buried cookie (203 ± 26.44 seconds), when compared to *WT* mice [Figure 3.13Ab, 104 ± 20.52 seconds, t (32.95) = 2.958, $P = 0.0057$]. In order to verify that it was not a satiety problem, fasting blood glucose level and body mass were measured. There was no significant difference between control and test groups (data not shown), leading us to conclude that *cKO* mice display olfactory deficits.

3.3.2. Odor discrimination test

This test was perfomed when the mice were 10 months old. To test further this disability, odor discrimination test was performed. There was a significant difference between the two genotypes; *cKO* and *WT* (Two-way ANOVA RM, $F_{1,18}$ = 6.664, *P* = 0.0188). The *cKO* and *WT* mice responded differently to the sequence of different odors introduction at different times, where there was a clear interaction between genotype x time ($F_{9,162}$ = 2.160, *P* = 0.0274). When comparing the exploration time of the third introduction of mineral oil (H3) and the first introduction of rose odor (R1), *WT* mice and *cKO* mice were both able to distinguish the introduction of new rose odor and discriminate mineral and rose oils by spending more time sniffing the new odor source [Figure 3.13B, H3 vs R1, t (162) = 5.364, *P* < 0.0001 for *WT* and t (162) = 2.472, *P* = 0.0145 for *cKO*]. However, during R1, *WT* showed twice the interest in rose odor (38.76 seconds) when compared to *cKO* mice [19.77 seconds, R1, *WT* vs *cKO*, t (180) = 3.125, *P* = 0.0021]. To determine whether mice were habituated to rose oil, R3 vs R1 was calculated. Both *WT* [t (162) = 4.62, *P* < 0.001] and *cKO* [t (162) = 2.19, *P* = 0.03] mice exhibited decrease interest reflecting habituation, thus demonstrating that both mice strains are able to memorize and recognize this specific odor. However, *WT* mice learnt faster (Figure 3.13B). On the other hand, both *cKO* [R3 vs U1, t (162) = 3.54, *P* = 0.0003] and *WT* [R3 vs U1, t (162) = 5.707, *P* < 0.0001] mice were able to discriminate female urine's odor over rose odor. Although, *WT* mice spent 17 seconds more than *cKO* mice exploring the urine odor [t (180) = 2.802, *P* = 0.0056], both were habituated to female's urine odor [*cKO* t (162) = 4.894, *P* < 0.0001, *WT* t (162) = 6.847, *P* < 0.0001]. Interestingly, *cKO* mice [U3 vs U+1 % L, t (162) = 1.348, *P* = 0.1795] couldn't discriminate the odor of 1% lemon added to female urine, unlike *WT* mice [U3 vs U+1 % L, t (162) = 3.005, *P* = 0.0031]. In addition, *WT* mice explored the female urine with 1 % lemon odor 15 seconds longer than *cKO* mice [t (180) = 2.562, *P* = 0.0112]. In conclusion, *cKO* mice were able to smell, and discriminate odors of different notes, but couldn't discriminate subtle odor changes, such as 1 % lemon in urine, and spent less time sniffing new odors, suggesting a lack of interest or motivation.

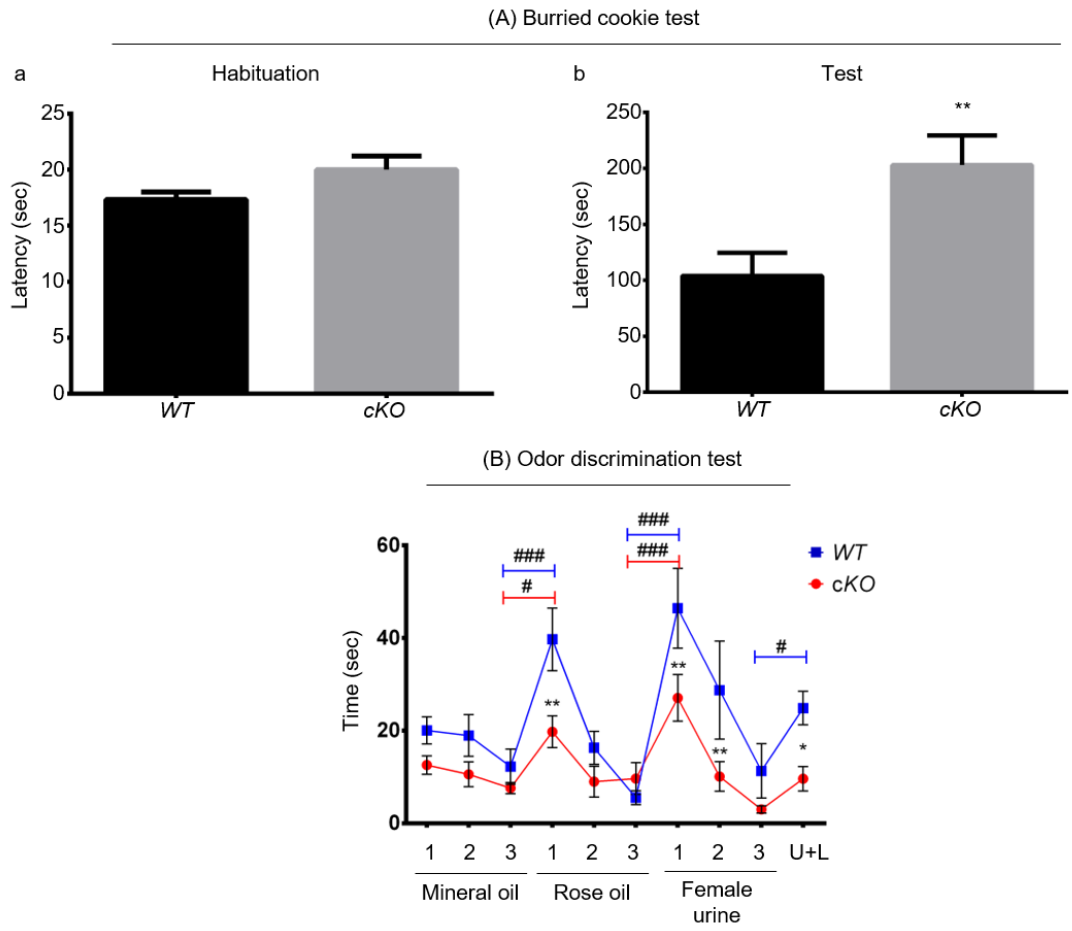

Figure 3.13. Olfactory assessment in *cKO* mice. (A). Buried cookie test. (a) Latency to grab and eat visible cookie in habituation phase (b) Latency to find buried cookie. (B). Odor discrimination test. This test consists of a 5 min habituation step to the tea ball (no odor), then three 2 min habituation sessions to rose oil, followed by three 2 min habituation sessions to female urine. The test then ends with a 2 min odor discrimination step to female urine containing 1% lemon oil (U+L). Statistical significance when comparing a single point between *cKO* vs *WT* is represented as: * $P \leq 0.05$, ** $P \leq 0.01$, *** $P \leq 0.001$. Statistical significance when comparing different sessions for same genotype as # $P \leq 0.05$, ## $P \leq 0.01$, ### $P \leq 0.001$.

3.4. Memory

3.4.1. Object recognition test

During the first session (s1) of the object recognition test, 4 months old *cKO* and *WT* mice spent almost the same time exploring objects A and B, which are sets of similar objects (Figure 3.14a). However, *cKO* mice spent less total exploring time (25.77 seconds N = 18) than *WT* mice (38.08 seconds ± 4.23 N = 20) during the first session [*cKO* vs *WT*, t (36) = 1.955, $P = 0.03$, Figure 3.14b]. There was a clear genotype effect: $F_{1,72} = 7.026$, $P = 0.009$. Nevertheless, the object effect was insignificant for both *cKO*

and *WT* mice, with no genotype x object interaction, indicating that *cKO* mice had no visual problems to localize the object, but showed less interest than *WT* mice in such inanimate stimuli. At both 4 and 9 months, there was a clear genotype effect ($F_{1,34}$ = 7.334, P = 0.01), but no age effect and no genotype x age interaction (Figure 3.14b), suggesting that the behavioral profile observed was age independent.

During the second session (s2), *WT* mice explored the new object two times longer as compared to the old "familiar" object [Old vs new, 8.45 vs 16.77 seconds, t (72) = 3.911, P = 0.0002]. On the other hand, *cKO* mice explored both new and old objects for the same interval of time (Old vs new, 7.75 vs 8.19 seconds, Figure 3.14c). There was a clear genotype effect ($F_{1,72}$ = 9.029, P = 0.0037), novelty effect ($F_{1,72}$ = 8.031, P = 0.006) and a genotype x novelty interaction ($F_{1,72}$ = 6.5, P = 0.0129). This indicate that 4 months old *cKO* mice either were unable to discriminate the new object by its form and color suggesting low visual abilities or were unable to memorize the old object from the new object (Figure 3.14c). In addition, in *cKO* mice (15.94 seconds) the total time spent exploring both objects were lower than in *WT* mice (25.22 seconds, t (36) = 2.514, P = 0.0165, Figure 3.14d), which would suggest apathy behavior in *cKO* mice. At both 4 and 9 months, there was a clear genotype effect ($F_{1,36}$ = 15.97, P < 0.0001) and age effect ($F_{1,36}$ = 7.854, P = 0.0084), but no genotype x age interaction (Figure 3.14d).

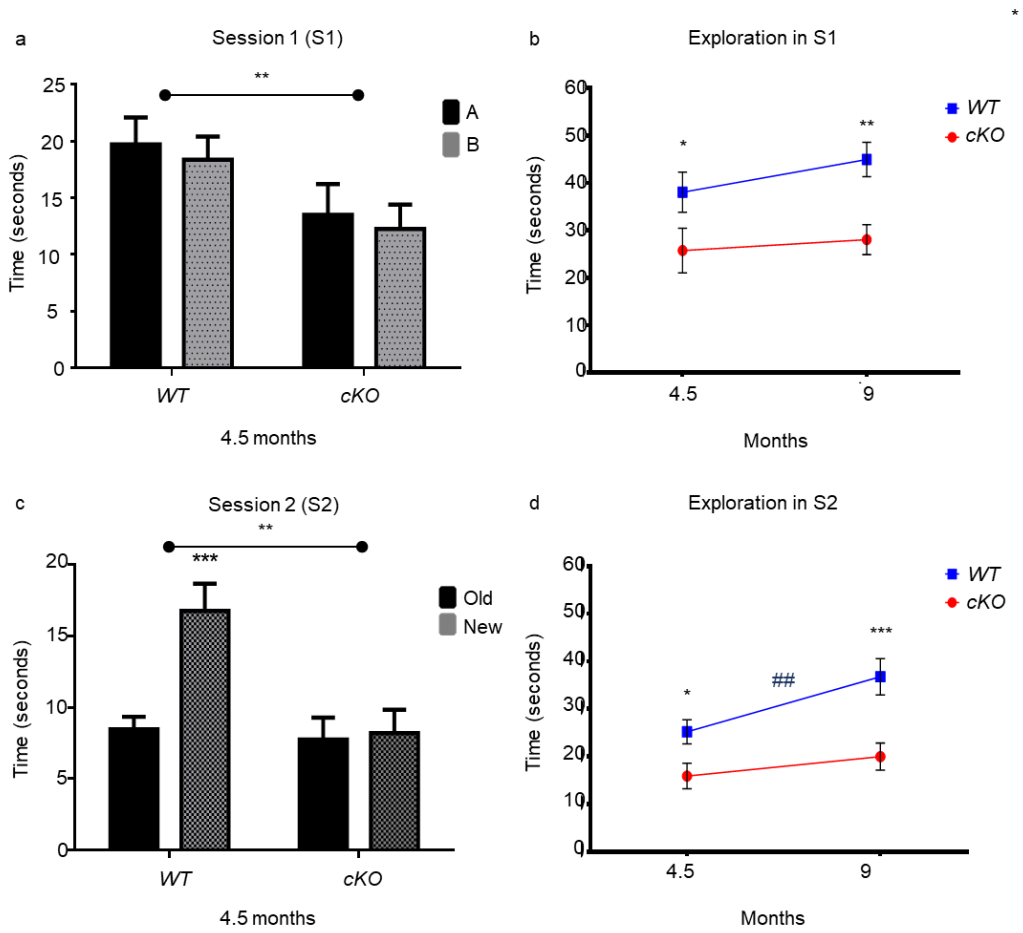

Figure 3.14: Vision and visual memory assessment in *cKO* mice. Object recognition test. (a) Session 1 (S1): Exploration time of the set of same objects in position A and the other at position B (seconds). (b) Total exploration time in S1 in seconds at 4.5 and 9 months of age. (c) Session 2: Exploration time of old object used in S1 and a novel object, which were positioned randomly in apparatus. (d) Total exploration time in S2 in seconds at 4.5 and 9 months of age. Statistical significance is represented as: * $P \leq 0.05$, ** $P \leq 0.01$, *** $P \leq 0.001$.

3.4.2. Three-chamber sociability and social novelty test

Sociability of the two groups was tested at 5 months and at 10 months of age. During the first session (s1) at 5 months of age, both *cKO* [t (72) = 3.97, $P = 0.0002$]. *WT* [t (72) = 10.94, $P < 0.0001$] mice spent more time exploring stranger 1 than the empty cage (Figure 3.15a). However, *cKO* mice spent about half the time (69.66 ± 5.84 seconds) exploring stranger 1 when compared to *WT* mice (118.86 ± 9.8 seconds) [t (72) = 5.661, $P < 0.0001$]. There was a genotype effect ($F_{1,72} = 11.31$, $P = 0.0012$), a subject effect ($F_{1,72} = 108.4$, $P < 0.0001$), and a genotype x subject interaction ($F_{1,72} = 21.56$, $P < 0.0001$). This indicates that *cKO* mice were less social and less motivated to explore stranger 1, when compared to *WT* mice.

During s2 when a second and new individual was introduced, *WT* mice spent then twice the time exploring stranger 2 relative to stranger 1 [t (72) = 4.707, $P < 0.0001$]. On the other hand, *cKO* spent nearly the same time exploring stranger 1 and 2 [t (72) = 1.225, $P = 0.224$, Figure 3.15b]. Statistical analyses revealed a significant genotype effect ($F_{1,72} = 11.74$, $P = 0.001$), novelty effect ($F_{1,72} = 17.05$, $P < 0.0001$), and a genotype x novelty interaction ($F_{1,72} = 5.525$, $P = 0.0215$). This indicates that *cKO* mice are unable to discriminate the old from the new individual impacting their social memory. As odor trace is the main parameter in individual recognition in rodent, the observed phenotype might be due to olfactory deficits, consistent with the poor performances observed with the olfactory tests described above.

This test was repeated at 10 months of age. During S1, there was a genotype effect ($F_{1,72} = 9.835$, $P = 0.0025$), subject effect ($F_{1,72} = 77.32$, $P < 0.0001$), but no longer a genotype x object interaction ($F_{1,72} = 2.443$, $P = 0.122$) as was observed at 5 months of age. Both *cKO* [t (72) = 4.983, $P < 0.0001$] and *WT* [t (72) = 7.524, $P < 0.0001$] mice explored stranger 1 for about 2.71-2.75-fold longer than the empty cup (Figure 3.15c). However, the total time of exploration in *WT* mice was 1.38-fold greater than that of *cKO* mice (Figure 3.15e). *WT* mice exhibit therefore greater interest to congeners than *cKO*, reflecting possible lack in social interest in mutant mice.

During S2, there was a strong genotype effect ($F_{1,72} = 7.652$, $P = 0.007$) and a significant genotype x object interaction ($F_{1,72} = 6.784$, $P = 0.01$). Although both *cKO* and *WT* mice spent more time exploring stranger 2 than stranger 1, *WT* mice explored stranger 2 2.11-fold longer than stranger 1 [t (72) = 6.081, $P < 0.0001$, Figure 3.15d]. On the other hand, *cKO* mice showed only 1.4-fold greater interest in stranger 2 compared to stranger 1 [t (72) = 2.179, $P = 0.032$, Figure 3.15d]. This indicates that although *cKO* mice were able to discriminate and memorize stranger 1, it was to a much less extent as compared to *WT* mice, which could indicate apathy and lack of interest in social interactions.

With age, the total time exploring decreased significantly in *cKO* and *WT* mice in both S1 and S2 (Figures 3.15e and 3.15f). In S1, there was a highly significant time effect ($F_{1,31} = 21.58$, $P < 0.0001$), and a genotype effect ($F_{1,31} = 11.28$, $P = 0.002$), but no genotype x time interaction (Figure 3.15e). During S2, there was a clear time effect ($F_{1,31} = 25.74$,

$P < 0.0001$), and genotype effect ($F_{1,31} = 16.58$, $P = 0.0003$), and a tendency of genotype x time interaction ($F_{1,31} = 3.571$, $P = 0.068$). This indicates a decrease in sociability and willingness to explore with age in both groups.

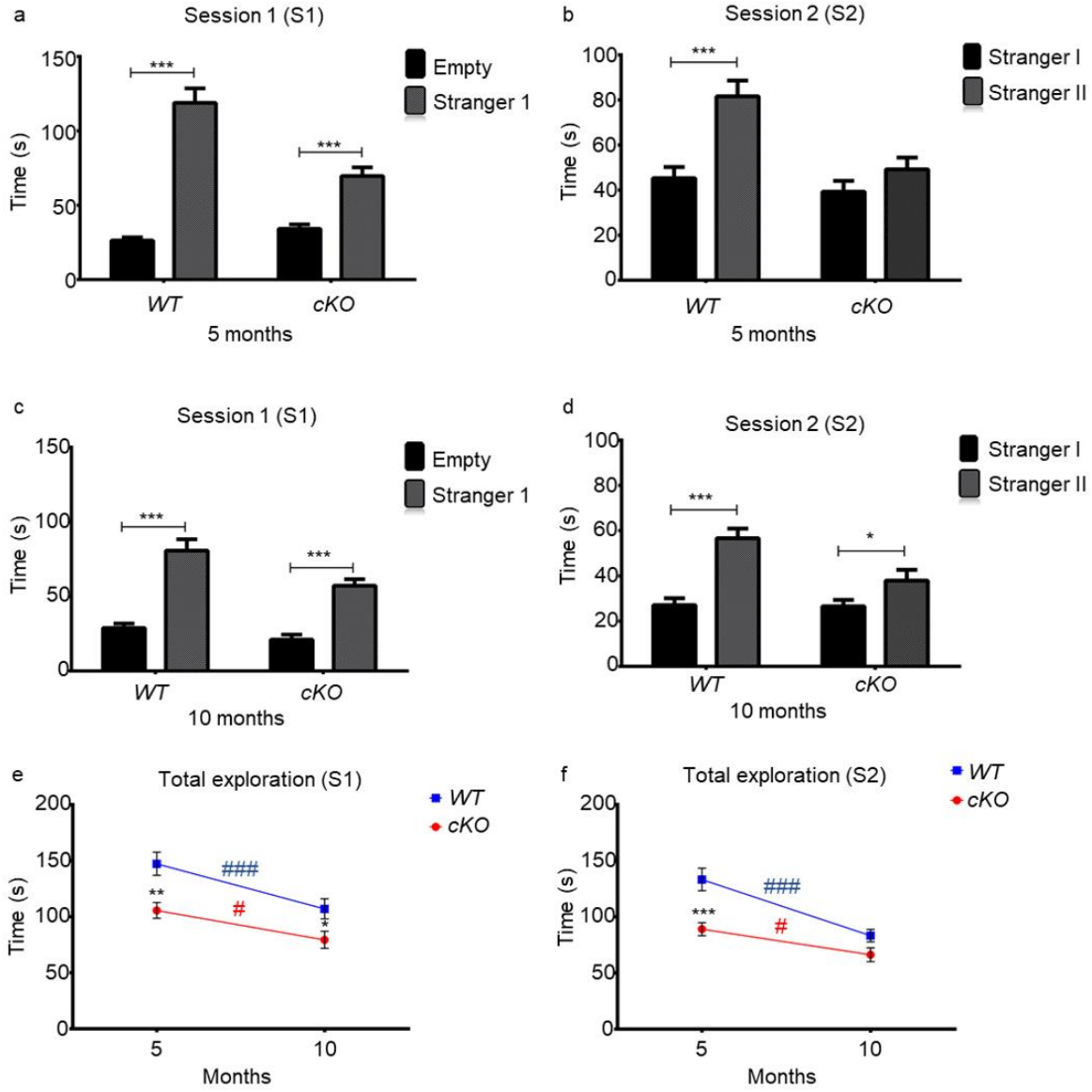

Figure 3.15. Sociability and social novelty assessment in *cKO* mice. (a) and (b) are at 5 months. (a) Session 1 (S1): Exploration time of the stranger 1 vs empty cup (seconds) (b). Session 2: Exploration time of stranger 1 used in S1 and a novel stranger (seconds). (c) and (d) are at 10 months of age, they correspond to S1 and S2, respectively. (e) Total exploration time in S1 in seconds at 5 and 10 months of age. (f) Total exploration time in S2 in seconds at 5 and 10 months of age. Statistical significance between cKO and WT at a certain time point is represented as: * $P \leq 0.05$, ** $P \leq 0.01$, *** $P \leq 0.001$. A statistical significance with time in *cKO* or *WT* mice is represented as: # $P \leq 0.05$, ## $P \leq 0.01$, ### $P \leq 0.001$.

3.4.3. Spatial short-term memory

To study working memory, 4-month old animals were tested for spontaneous

alternations in the Y-maze. The % of proper alternations (±SEM) was 68.14 ± 2.2 % for *WT*, and 55.5 ± 2.47 % for *cKO* mice [t (36) = 3.82, *P* = 0.0005, Figure 3.16a]. At this age, both groups had an equal total number of entries; 19 ± 1 for *WT* and 19 ± 2 for *cKO* mice (Figure 3.16b). Since there were no significant differences in distance and velocity between *cKO* and *WT* mice (Figure 3.S5), these results indicate that *cKO* mice, from a young age, show short term memory problems as they are less performant in recalling explored vs unexplored arms.

At 9 months, an 8.42 % difference in alternations triplets between both groups was observed [t (36) = 2.514, *P* = 0.0165, Figure 3.16a]. In addition, measurement of total number of entries revealed that *cKO* mice tended to enter 10 ± 5 (± SEM) less arms than *WT* mice [t (36) = 2.017, *P* = 0.0512, Figure 3.16b]. Again, there was no significant differences in velocity and distance between both groups (data not shown) and the difference in arm entries might therefore reflect a lack of willingness to explore in *cKO* mice.

With age, % alternation (±SEM) slightly decreased in *WT* mice to 63.17 ± 2 %, whereas it remained fairly constant in *cKO* mice (54.75 ± 2.88 %, Figure 3.16a). Regarding % alternation, there was a clear genotype effect ($F_{1,36}$ = 19.51, *P* < 0.0001), but neither an age effect, nor a genotype x age interaction. This indicates that *cKO* mice show term memory deficits that were not modified with age

However, a higher number of entries with age was observed in both *cKO* and *WT* mice (Age effect: $F_{1,36}$ = 57.23, *P* < 0.0001), where there was a tendency of a genotype effect ($F_{1,36}$ = 3.128, *P* = 0.085), and a genotype x age interaction ($F_{1,36}$ = 4.025, *P* = 0.052). This suggests that both groups may have become more experienced with time due to frequent handling and behavioral testing. *cKO* mice tended however to explore less

arms than *WT* possibly reflecting a lack of motivation due to apathy.

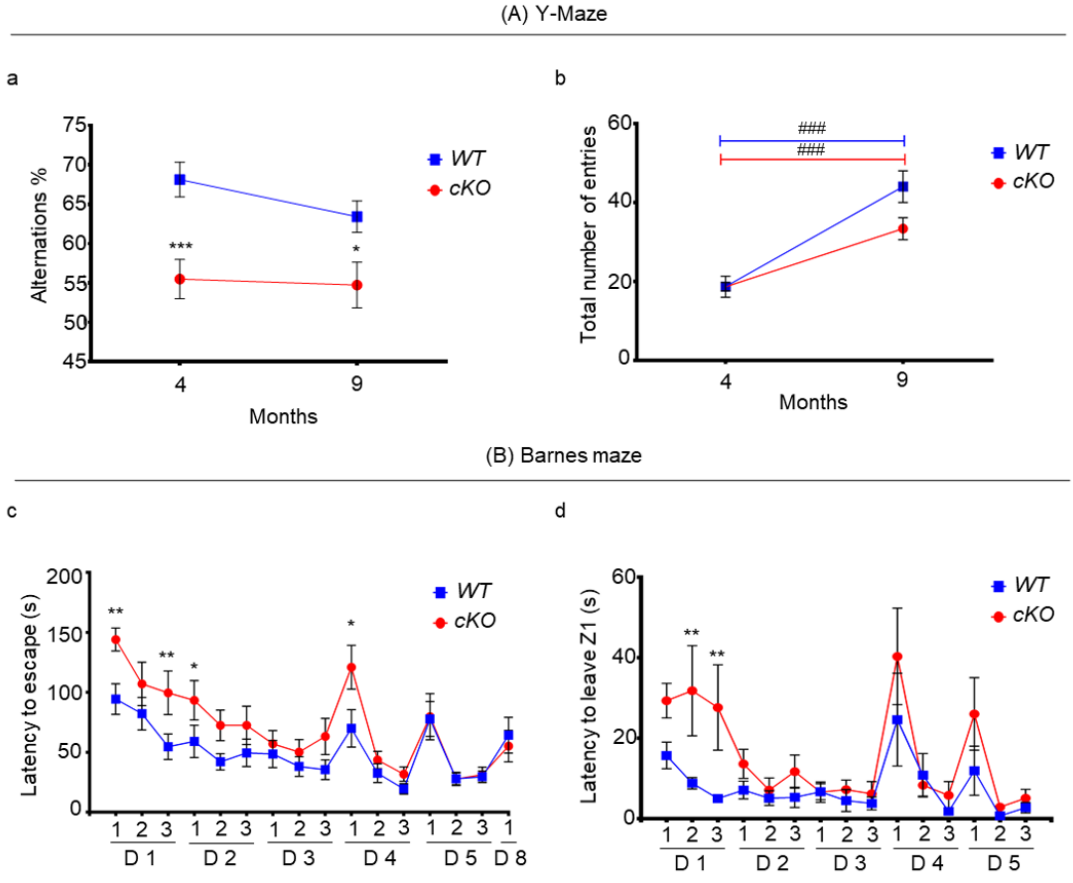

Figure 3.16: Short- and long-term memory assessment in *cKO* mice. (A) Y-maze. (a) Proper alternation % at the age of 4 and 9 months. (b) Total number of entries at the age of 4 and 9 months. (B) Barnes maze. (c) The latency to find the escape chamber, measured 3 times per day for 5 consecutive days, in seconds (s). At day 8, one single test session was performed to assess long-term memory. (d) Latency to leave departure zone (Z1), measured 3 times per day for 5 consecutive days, in seconds (s). Statistical significance between *cKO* and *WT* at a certain time point is represented as: * $P \leq 0.05$, ** $P \leq 0.01$, *** $P \leq 0.001$. A statistical significance with time in *cKO* or *WT* mice is represented as: # $P \leq 0.05$, ## $P \leq 0.01$, ### $P \leq 0.001$.

3.4.4. Learning and long-term memory

To assess learning, 11 months old animals were tested in the Barnes maze 3 times per day for 5 consecutive days. Latency to escape scores gradually decreased over the training period (Figure 3.16c) in both groups of mice. There was a clear time effect ($F_{15,448} = 9.577$, $P < 0.0001$), indicating spatial learning was successfully achieved. However, there was also a genotype effect ($F_{15,448} = 21.81$, $P < 0.0001$). When comparing trial 1 on day 1 with trial 3 on day 5, the time to find the chamber decreased by 112.8 seconds in *cKO* mice [Day 1 trial 1: 144.1 seconds, day 5 trial 3: 31.3 seconds, mean difference: 112.8 seconds, t (448) = 6.499, $P < 0.0001$], and 64.8 seconds in *WT* mice [Day 1 trial 1: 94.4 seconds, day 5 trial 3: 29.6 seconds, mean difference: 64.8

seconds, t (448) = 3.734, *P* = 0.0002], demonstrating ability to learn for both *cKO* and *WT* mice. Despite this, on day 1 and in trial 1 of day 2, *cKO* mice spent significantly more time to find the escape chamber. For example, in trial 1 of day 1 *cKO* mice spent on average 50 seconds more than *WT* mice to find the escape chamber [*WT* vs *cKO*: 94.4 vs 144.1 seconds, mean difference: 49.7 seconds, t (448) = 2.864, *P* = 0.0044]. Interestingly, *cKO* mice in trial 1 on day 1 tended to take 13.6 seconds more than *WT* mice to leave the departure zone Z1 [t (420) = 1.852, *P* = 0.062]. In trial 1 on day 4, where there was no habituation to escape chamber and the subjects were directly placed in Z1 for the first time, *cKO* mice spent on average 121 seconds to find the chamber, whereas *WT* mice spent 69.9 seconds [t (448) = 2.944, *P* = 0.0034]. However, the difference of time to leave Z1 between *cKO* and *WT* mice was not significant. This indicates that *cKO* mice demonstrated neuroplasticity deficits when confronted with novelty, yet they were able to retain information with repetition.

To assess long-term memory, on day 8, after stopping the test for 2 consecutive days, one trial was done. There was no significant difference between *cKO* and *WT* mice, where they spent nearly the same time to find the chamber, suggesting no difference in long-term memory between these 2 groups.

4. Discussion and perspectives

The specific *in vivo* suppression of *lsr* in glial cells induced perturbations in the behavior of *cKO* mice, which might be due to the perturbation of cholesterol homeostasis. In their environment, *cKO* mice were more active in the second part of nocturnal period suggesting a perturbation owhere they walked for longer periods of time, at the beginning and end of the nocturnal period, compared to *WT* (Figure 3.12Aa). Interestingly, it has been previously shown that Alzheimer's disease (AD) mice models were hyperactive during the nocturnal phase (Faure *et al.* 2011; Filali *et al.* 2011; Djelti *et al.* 2015). In a novel environment, *cKO* mice tended to stay at the periphery for longer periods of time when compared to *WT* mice reflecting thigmotaxis. Nevertheless, they travelled the same distance at the periphery, which indicates longer immobile periods at the periphery. The immobility and thigmotaxis might have been a form of anxiety. However, by using the free exploratory paradigm, we validated that they do not display an anxiety behavior and thus would rather exhibit apathy. Interestingly, apathy is considered to be an early marker for neurodegenerative

diseases such as AD, patients with mild cognitive impairment (MCI) exhibiting apathy are at a greater risk of developing AD compared to those with no neuropsychiatric symptoms (Ruthirakuhan *et al.* 2019). The *cKO* mice were able to visualize objects and visual cues, since they explored the same set of objects for a nearly equal time (Figure 3.14a). Also, they were able to visualize the geometric cues in Barnes maze to find the escape chamber (Figure 3.16c). However, they couldn't memorize or discriminate between an old and a new object (Figure 3.14c). They also performed a lower proper alternation % in Y-maze than controls indicating a deficit in the memorization of already visited arms (Figure 3.16a). Altogether those tests suggested that visual and working memory was impacted in our animals. They can navigate and explore their environment as they receive sufficient visual sensorial stimulation and did not suffer from locomotor problems. However, they didn't retain information properly to achieve a specific task with the same efficiency as *WT* animals. Visual and working memory deficits are well documented in AD patients and act as important early AD biomarker (Kawas *et al.* 2003; Jahn 2013; Liang *et al.* 2016). Impaired visual recognition memory is due to entorhinal cortex dysfunctions and predicts Alzheimer's disease in case of MCI (Didic *et al.* 2013) and working memory, that decline through normal aging, is a marker for MCI and evolution to AD (Kirova *et al.* 2015). In our animals, the working memory performance was lower than in *WT* in both young and older animals, but while it declined in *WT* -reflecting a normal aging process- it appeared more stable in *cKO* suggesting cognitive restructuring or neuroplasticity.

Concerning olfaction, *cKO* mice took twice the time to find the buried cookie. In addition, they spent less time sniffing new odors and couldn't discriminate subtle odors. This demonstrate that olfactive memory exists in *cKO* mice even if less efficient. They were able to discriminate neutral vs attractive vs sexual odors. Altogether this suggests that olfaction deficit is likely due to impaired sensorial entries targeting either olfactive epithelium, olfactory bulbs, or olfactory tracks. The *cKO* were less social than *WT* mice, which could be linked to olfactory deficits as rodents are mainly using this sense to identify and recognize strangers. However, they were able to discriminate between the old and new strangers. Therefore, *cKO* mice showed olfactory dysfunction, which is the first sign of neurodegeneration, where olfactory assessment is an important early diagnostic tool for neurological disorders such as Alzheimer disease (Zou *et al.* 2016). A link between olfactory deficit and cholesterol homeostasis

perturbation has been recently highlighted. In Niemann Pick type C disease, a lysosomal storage disorder, cholesterol accumulation leads to microglial activation and inflammatory process, ultimately mediating neuronal death in the olfactory bulb causing the observed olfactory dysfunction (Seo *et al.* 2018). A similar mechanism can be suggested here, where deletion of LSR on glial cells might cause cholesterol accumulation and thus olfactory dysfunction. Inflammatory status in the olfactory tract needs to be analyzed in further studies using specific markers such as sTREM2 (Nordengen *et al.* 2019). The impaired sensorial entries might drive *cKO* to engage less in social interactions than *WT* mice. Similar social withdrawal has been observed in the APPswe/PS1 mice, a model of AD. As *cKO* mice, APPswe/PS1 show less social interactions and avoid unfamiliar stimulus (Filali *et al.* 2011). In most tests, *cKO* mice were apathetic, but also exhibited two very well-documented behaviors found in AD patients (Starkstein *et al.* 2006; Nobis & Husain 2018). Biochemical tests to measure melatonin and cortisol should be performed to decipher the mechanism underlying this nocturnal hyperactivity. At 11 months, *cKO* mice showed low cognitive flexibility and lack of motivation to explore the novel surrounding, which was overcome by repetitive introduction to the aversive environment of Barnes maze. Altogether the cell specific deletion of *lsr* in glia cells lead to a series of behavioral phenotypes that resemble aspects of AD during the time course of the disease.

AD combines cognitive disorders (starting from short term memory loss, spatial memory perturbation to long term memory decay) together with neurophysiological changes (olfactory dysfunction, hippocampal shrinking and amyloid plaque deposition and neurofibrillary tangles accumulation) and neuropsychiatric symptoms (NPS) including apathy, verbal and physical agitation, circadian sleep-wake rhythms perturbation. As the disease progresses, delusions, hallucinations, and aggression become more common, whereas apathy is the most persistent and frequent NPS throughout all the stages of AD (Lyketsos *et al.* 2011). Here we suggest that a glial specific disruption of a lipoprotein receptor would generate AD like symptoms. The mechanism underlying the observed phenotype is still to be deciphered, however it is well known that lipoprotein trafficking and cholesterol homeostasis are linked to AD. ApoE ε4 is a strong risk factor to develop sporadic form of AD (Liu *et al.* 2013). A proposed mechanism suggests that due to poor loading ability of ApoE ε4 lipoproteins, the amyloid beta clearance together with cholesterol trafficking is deficient in patients,

leading to synaptic dysfunction, destruction and neuronal loss, thereby triggering glia cell activation and inflammatory processes (LaDu *et al.* 1994; Bales *et al.* 2000; Rapp *et al.* 2006; Klein *et al.* 2010; Sen *et al.* 2012). We postulate that glial LSR may play a role in feedback control of cholesterol synthesis, limiting circulating cholesterol in brain extracellular fluid, thus maintaining cholesterol homeostasis. In case of glial LSR deficiency, cholesterol regulation is impacted and might lead to subtle cholesterol accumulation in cellular compartment and dysregulation of cholesterol efflux from glia cells. Indeed, glia cells evacuate excess of cholesterol through the BBB by the Cyp46 enzyme that convert cholesterol to 24-hydroxycholesterol. Perturbation of the glia Cyp46A1 has been reported in AD suggesting a link between cholesterol load in the CNS and development of the pathology (Bogdanovic *et al.* 2001). Oxidative processes increases during aging and may target lipid accumulation in the CNS to produce noxious oxysterol with dramatic effects on neuronal survival (Gamba *et al.* 2019). Among them 27-hydroxycholestrol promotes pro-inflammatory molecules release (Testa *et al.* 2014), increases Aβ levels (Prasanthi *et al.* 2009; Gamba *et al.* 2014) and induces synaptic dysfunctions (Merino-Serrais *et al.* 2019). In line with this hypothesis we previously identified that LSR +/- mice exhibit profound oxysterol modifications in the brain (Pinçon *et al.* 2015a).

Further behavioral tests at 18 months of age will be performed in order to detect whether memory-related problems will be aggravated with age, and immunohistochemical tests will be performed in order to study cholesterol distribution, and possible gliosis in *cKO* mice's brain.

Above evidence and observations associate with the fact that aging *lsr* +/- mice show increased susceptibility to amyloid stress (Pinçon *et al.* 2015b) and demonstrates LSR as a pivotal element in glia cells to promote normal aging of the brain. Therefore, we propose that LSR represents a novel pathway to study the link between cholesterol trafficking and neurodegeneration.

5. Supplementary data

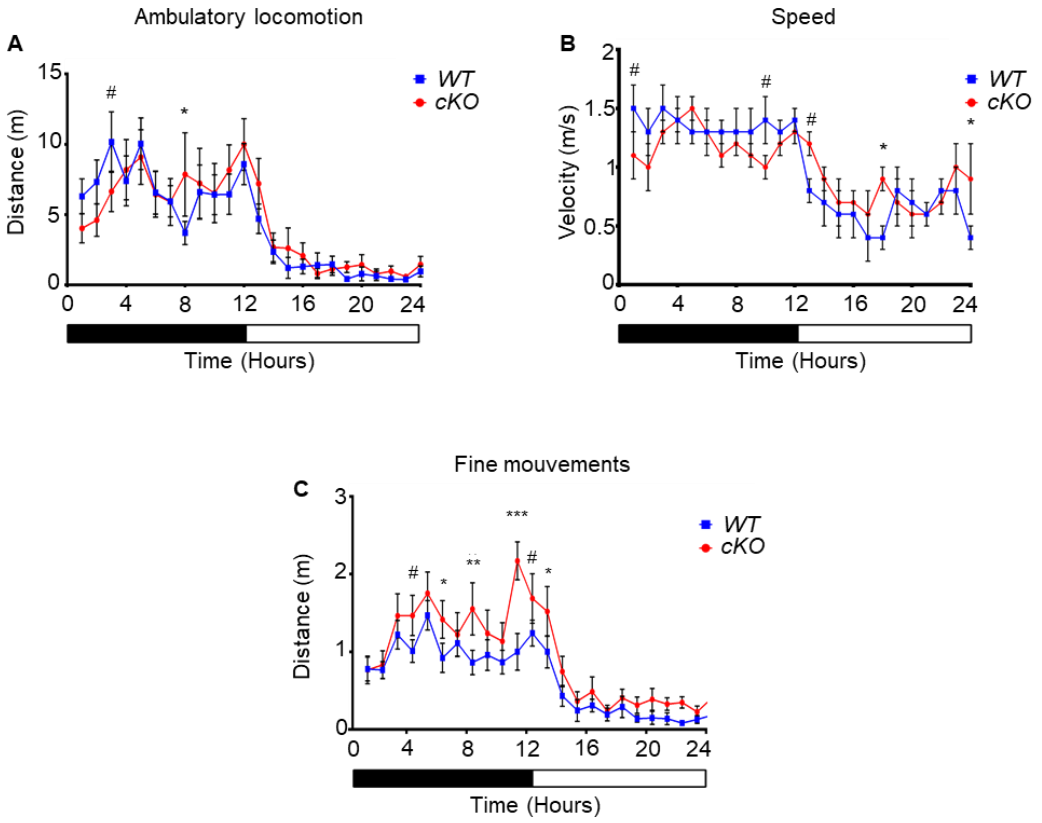

Figure 3.S1: Home cage activity. A) Ambulatory locomotion (m). Horizontal movements over a period of 24 hours. There was no significant difference between WT and cKO mice, except 8 hours in dark cycle, WT VS cKO (3.695 VS 7.856 m) P = 0.02, t (768) = 2.21. Also, there was a tended difference 3 hours after start of darkt cycle, WT VS cKO (10.16 VS 6.646 m) P = 0.06, t (768) = 1.87. B) Velocity (cm/sec) over a period of 24 hours. In dark period, WT mice tended to be faster at t = 1 h (WT VS cKO, 1.5 VS 1.1 cm/sec) P = 0.079, t (768) = 1.75, and t = 10 (WT VS cKO, 1.4 VS 1 cm/sec) P = 0.079, t (768) = 1.75. In light time, cKO mice tended to move faster at t = 13 h (WT VS cKO, 0.8 VS 1.2 cm/sec) P = 0.079, t (768) = 1.75, at t = 18 (WT VS cKO, 0.4 VS 0.9 cm/sec) P = 0.02, t (768) = 2.19, and at t = 24 (WT VS cKO, 0.4 VS 0.9 cm/sec) P = 0.02, t (768) = 2.19. C) Fine movements over 24 hours. Fine movements like scratching and grooming. cKO mice demonstrated higher levels of such activities at t = 4 h (WT VS cKO, 1.01 VS 1.468 m) P = 0.07, t (756) = 1.8, t = 6 h (WT VS cKO, 0.92 VS 1.416 m) P = 0.05, t (756) = 1.94, t = 8 h (WT VS cKO, 0.86 VS 1.55 m) P = 0.007, t (756) = 2.7, t = 11 h (WT VS cKO, 1 VS 2.17 m) P < 0.0001, t (756) = 4.592, t = 12 h (WT VS cKO, 1.24 VS 1.69 m) P = 0.08, t (756) = 1.75, t = 13 (WT VS cKO, 1 VS 1.52 m) P = 0.04, t (756) = 2.04. Statistical significance at a certain time point is represented as: # < 0.10, * P ≤ 0.05, ** P ≤ 0.01, *** P ≤ 0.001.

Supplementary data on open field test (Figure 3.S2). Three months old *WT* mice passed 12.42 % of test time in the center Z3, whereas *cKO* mice of same age passed about half that time (6.39 %) in Z3 [t (36) = 3.5, *P* = 0.001]. However, no significant difference in distance % neither at periphery Z1 nor center Z3 was observed. At 8 months, *WT* mice were more interested to explore where they passed 16.64 % of their time in center Z3, but *cKO* mice passed 7.32 % of the test time in center [t (36) = 4.66, *P* < 0.0001]. At periphery Z1, *cKO* mice passed 78.4 % of their time; 10.53 % more than *WT* mice [t

(36) = 3.07, *P* = 0.004]. In addition, *cKO* tended to move 6.74 % less than *WT* mice in periphery [t (36) = 2.004, *P* = 0.053].

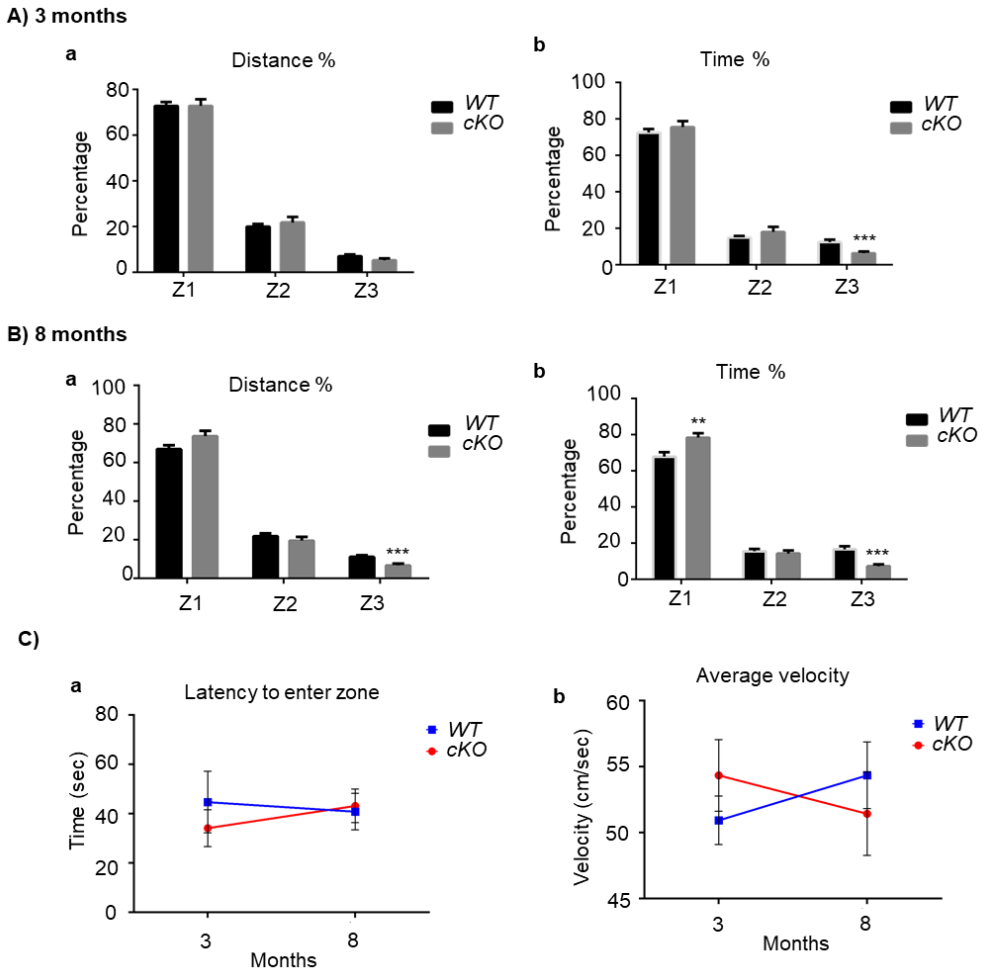

Figure 3.S2: Open field test data. A) Young 3-month-old mice. a) Distance % spent in the different zone: Z1, Z2, and Z3. b) Time % spent in the different zone: periphery (Z1), intermediate (Z2), center (Z3). B) 8 months old mice. a) Time % spent in the different zone: Z1, Z2, and Z3. b) Distance % spent in the different zone: Z1, Z2, and Z3. C) a) Latency to enter central zone (Z3) in seconds in 3 months VS 8 months old *WT* and *cKO*. b) Average velocity in 3 months VS 8 months old *WT* and *cKO*. Data are considered statistically significant when $P \leq 0.05$ where * indicates $P \leq 0.05$, ** indicates $P \leq 0.01$, and *** indicates $P \leq 0.001$.

Supplementary data on free exploratory paradigm (Figure 3.S3). Free exploratory paradigm is a behavioral test used to measure trait anxiety. There were no significant variations between *cKO* and *WT* mice in the different parameters measured in this test. The *cKO* mice took 21.2 ± 3.74 seconds to leave familiar environment for the first time, while *WT* mice took 15.93 ± 3.94 seconds [Figure 3.S3A, t (27.92) = 0.969, *P* = 0.34]. In addition, *cKO* mice spent 176.3 ± 8.79 seconds, which is more than half of test time in new zone (NZ), and *WT* mice spent 190.2 ± 8.51 seconds in NZ (Figure 3.S3B). There was no significant different between both groups [t (27.97) = 1.133, *P* = 0.27]. We also

measured the locomotion within the NZ (Figure 3.S3C), which is the number of movements from one chamber to another in the NZ, no significant variation between *cKO* (50 ± 8) and *WT* (61 ± 9) [t (27.74) = 1.02, *P* = 0.32]. We equally measured locomotion in familiar zone (FZ, Figure 3.S3D), here *WT* (50 ± 9) mice tended to move more within FZ than *cKO* (31 ± 3) mice [t (17.19) = 1.988, *P* = 0.06]. Finally, we measured locomotion from FZ to NZ (Figure 3.S3E), no significant variation between *cKO* (16 ± 3) and *WT* (21 ± 3) [t (27.79) = 1.06, *P* = 0.29]. From the above results, we can confirm that *cKO* do not show a form of trait anxiety.

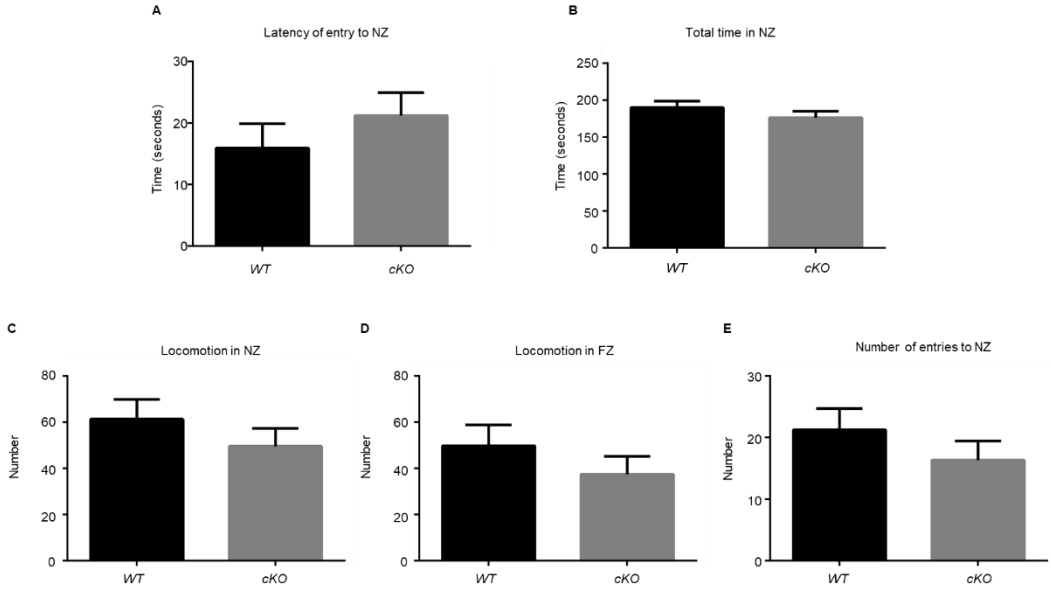

Figure 3.S3: Free exploratory paradigm data comparing *cKO* (n = 15) vs *WT* (n = 15) mice at 10 months. A) Latency to enter new environment (NZ) in seconds (sec). B) Total time in new zone (sec). C) Locomotion in familiar zone (FZ); number of entries in different compartments of familiar zone. D) Locomotion in new zone; number of entries in different compartments of new zone. E) Number of entries from familiar zone to new zone. Data are considered statistically significant when $P \leq 0.05$ where * indicates $P \leq 0.05$, ** indicates $P \leq 0.01$, and *** indicates $P \leq 0.001$.

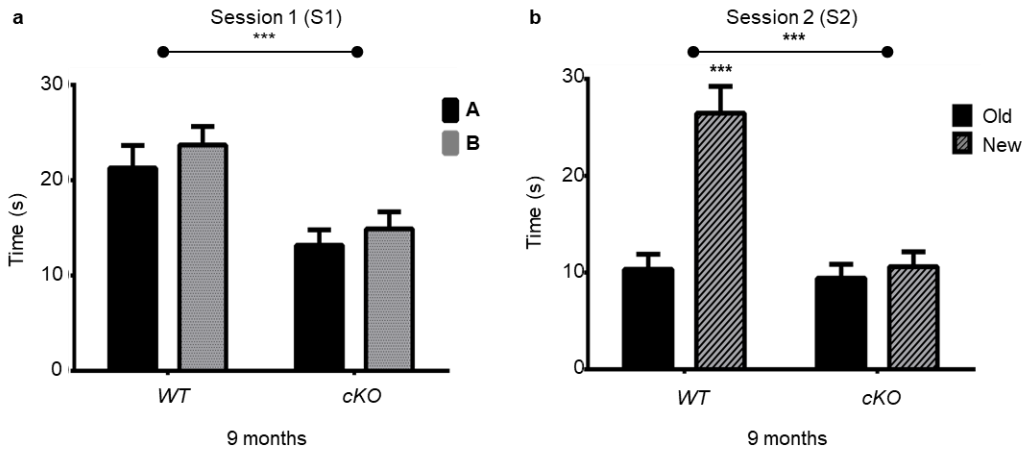

Figure 3.S4: Vision and visual memory assessment in 9 months old *cKO* mice (n = 18) against *WT* (n = 20) . Object recognition test. (a). Session 1 (S1): Exploration time of the set of same objects in position A and the other at position B (seconds). (b). Session 2: Exploration time of old object used in S1 and a novel object, which were positioned randomly in apparatus. Statistical significance is represented as: * P ≤ 0.05, ** P ≤ 0.01, *** P ≤ 0.001.

Supplementary data on object recognition test (Figure 3.S4). During the first session (s1) of the object recognition test, *cKO* mice [A vs B, 13.18 vs 14.89 seconds, t (72) = 0.595, $P = 0.55$] and *WT* mice [A vs B, 21.28 vs 23.71 seconds, t (72) = 0.888, $P = 0.378$] spent almost the same time exploring objects A and B, which are sets of similar objects (Figure 3.S4). There was a clear genotype effect: $F_{1,72} = 18.18$, $P < 0.0001$. Nevertheless, the object effect was insignificant for both *cKO* and *WT* mice, with no genotype x object interaction, indicating that *cKO* mice had no visual problems to localize the object, but showed less interest than *WT* mice in such inanimate stimuli.

During the second session (s2), *WT* mice explored the new object two times longer as compared to the old "familiar" object [Old vs new, 26.46 vs 10.32 seconds, t (72) = 5.988, $P < 0.0001$]. On the other hand, *cKO* mice explored both new and old objects for the same interval of time (Old vs new, 9.412 vs 10.16 seconds, t (72) = 0.4223). There was a clear genotype effect ($F_{1,72} = 18.32$, $P < 0.0001$), novelty effect ($F_{1,72} = 19.6$, $P < 0.0001$) and a genotype x novelty interaction ($F_{1,72} = 14.55$, $P = 0.0003$). This indicate that *cKO* mice either were unable to discriminate the new object by its form and color suggesting low visual abilities or were unable to memorize the old object from the new object (Figure 3.S4).

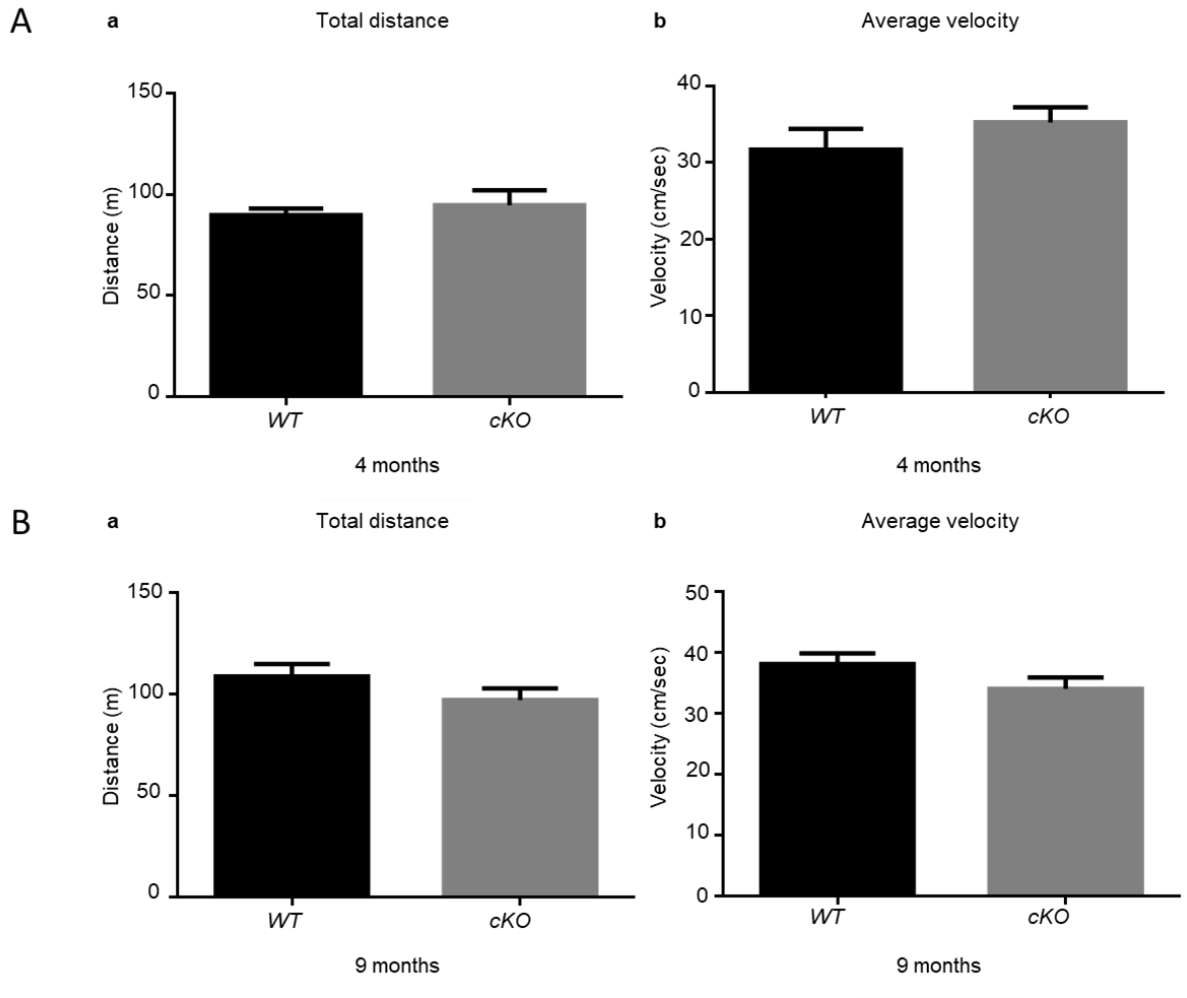

Figure 3.S5: Y maze. A) 4 months old *WT* and *cKO* animals. a) Total distance traveled during the test time in meters. b) Average velocity during test time in cm/sec. B) 9 months old *WT* and *cKO* animals. a) Total distance traveled during the test time in meters. b) Average velocity during test time in cm/sec. No significant difference between both groups was reported.

6. Preliminary results

6.1. *Lsr* excision from hippocampus, cerebellum, and olfactory bulb

Based on previous observations, Cre is highly active in all of hippocampus, cerebellum, and olfactory bulb (Slezak *et al.* 2007). Therefore, we dissected those specific regions and extracted total RNA followed by RT-qPCR. Surprisingly, LSR was not downregulated at 3 months in those structures. T*otal lsr* was upregulated in cerebellum to 1.43 folds (95 % C.I. minimum-maximum: 1.12-1.81 folds, $P = 0.02$). In

addition, *lsr β* was upregulated in both cerebellum (1.4 folds, 95 % C.I. minimum-maximum 1.14-1.85 folds, *P* = 0.0001) and olfactory bulb (2.41 folds, 95 % C.I. minimum-maximum 1.12-5.7 folds, *P* = 0.02). However, no significant differences where find between 3-month-old *cKO* and *WT* mice's hippocampus. As we know from the hypothalamus data that glia-specific knockout of *lsr* was achieved at this age (Figure 3.11) the upregulation in *lsr* expression in those stuctures might have occurred in neuronal and/or surrounding cells as a possible compensatory mechanism affecting especially *lsr β* that was exclusively upregulated in studied regions. Eleven months after TAM induction, when mice were 13-month-old, five *cKO* and five *WT* mice were randomly chosen and sacrificed and cerebral structure isolated. It is important to note that no further TAM injections were performed. At this stage, *total lsr* (0.39 folds, 95 % C.I. minimum-maximum: 0.15-0.72 folds, *P* = 0.004) and all three *lsr* subunits *α* (0.35 folds, 95 % C.I. minimum-maximum: 0.15-0.86 folds, *P* = 0.004), *α'* (0.35 folds, 95 % C.I. minimum-maximum: 0.15-0.54 folds, *P* = 0.004), and *β* (0.43 folds, 95 % C.I. minimum-maximum: 0.10-1.14 folds, *P* = 0.0035) were downregulated to half when compared to *WT* mice. In addition, *lsr β* (0.85 folds, 95 % C.I. minimum-maximum: 0.741-0.959 folds, *P* = 0.008) was downregulated in olfactory bulb. Surprisingly, *lsr α'* was upregulated in cerebellum (1.418 folds, 95 % C.I. minimum-maximum: 0.966-1.818 folds, *P* = 0.028). LSR downregulation was clearer for hippocampus than for olfactory bulb. However, it seems that *lsr* suppression in the cerebellum was either unsuccessful or there is a compensatory mechanism that keeps *lsr* levels normal to upregulated. Specific immunostainings should help to identify the cell types expressing the remaining LSR in the different brain structures and the possible compensatory

mechanism or ongoing reactive gliosis.

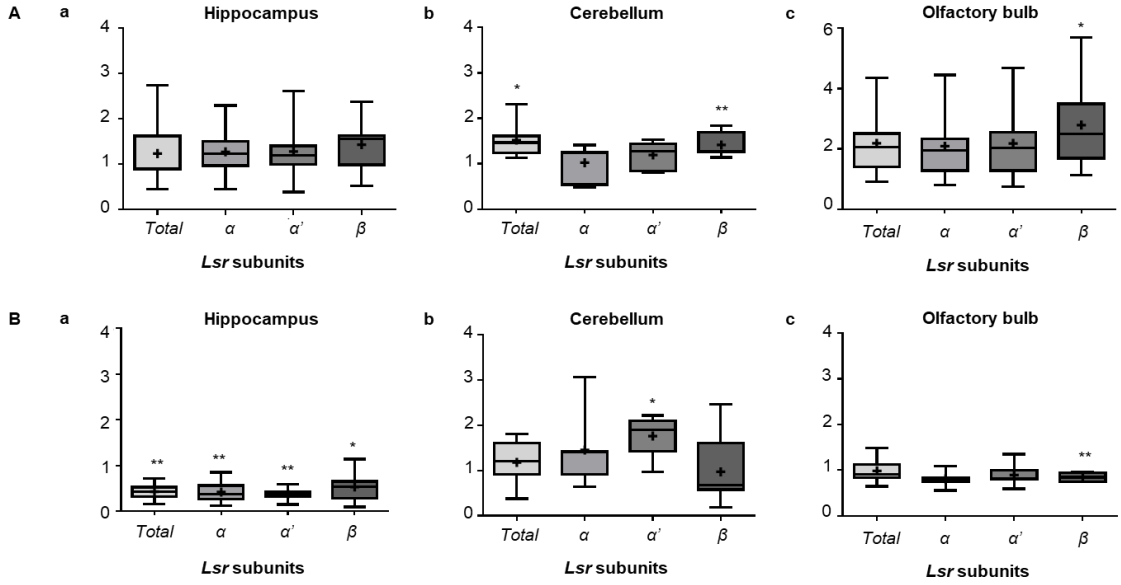

Figure 3.S6: Verification of *lsr* gene excision using RT-qPCR. Box plot presentation of fold expression of *total lsr* and different *lsr* subunits α, α', and β at two different age points at A) 3-month-old and B) 13-month-old mice, where a) is hippocampus, b) cerebellum, and c) olfactory bulb. Five *cKO* mice and five *WT* mice were sacrificed at 3-months of age two weeks after TAM induction and five *cKO* mice and five *WT* mice were sacrificed at 13-months of age. The *cKO* mice (n = 5) data are represented in boxplot with respect to *WT* (n = 5) data. Statistical significance is represented as: * $P \leq 0.05$, ** $P \leq 0.01$, *** $P \leq 0.001$.

Table 1: List of primers and their sequences used for qPCRs.

Oligo name	Chemistry	Mod5'	Sequence	Mod3'	Bases
Cyp46a1_F	DNA Oligos		GGC TAA GAA GTA TGG TCC TGT TGT AAG A		28
Cyp46a1_R	DNA Oligos		GGT GGA CAT CAG GAA CTT CTT GAC T		25
Hmgcr_F	DNA Oligos		CCC CAC ATT CAC TCT TGA CGC TCT		24
Hmgcr_R	DNA Oligos		GCT GGC GGA CGC CTG ACA T		19
SrebpF1_F	DNA Oligos		GGT CCA GCA GGT CCC AGT TGT		21
SrebpF1_R	DNA Oligos		CTG CAG TCT TCA CGG TGG CTC		21
Abca1_F	DNA Oligos		CAA CCC CTG CTT CCG TTA TCC AA		23
Abca1_R	DNA Oligos		GAG AAC AGG CGA GAC ACG ATG GAC		24
Ldlr_F	DNA Oligos		TGG CTA TAC CTA CCC CTC AAG ACA G		25
Ldlr_R	DNA Oligos		GAT CCC GGA AAG AGA CGG AT		20

6.2. Effects of glia-specific *lsr* excision on cholesterol metabolism

In order to better understand the effects of glia-specific LSR deletion, multiple RT-qPCRs were performed, using primers for cholesterol metabolism related enzymes and

transporters, on the same samples taken to verify *lsr* excision (Figure 3.S7). In figure 3.S6, we demonstrated that *total lsr* and *lsr β* expression were upregulated in 3-month-old *cKO* cerebellum (Figure 3.S6Ab). Interestingly, *hmgcr* was also upregulated to 1.475 folds (95 % C.I. minimum-maximum, 1.119-1.867, P = 0.029). In 13-month-old *cKO* cerebellum, upon *lsr α'* was upregulated, *abca1* transporter (1.268 folds, 95 % C.I. minimum-maximum 0.939-1.975, P = 0.08) and *srebp*1 (1.22 folds, 95 % C.I. minimum-maximum 0.899-1.75 folds, P = 0.075) tended to be upregulated. Finally, in 13-month-old hippocampus, where all *lsr* subunits were downregulated by half, both *abca1* (0.649, 95 % C.I. minimum-maximum 0.591-1.021 folds, P = 0.025) and *srebp1* (0.663 folds, 95 % C.I. minimum-maximum 0.400-1.09 folds, P = 0.047) were significantly downregulated when compared to *WT*. The results above show that *lsr* excision from glial cells caused disturbance in normal cholesterol metabolism. It seems that downregulation of *lsr*, caused downregulation of SREBP1, which is a transcriptional regulation factor of genes responsible for *de novo* lipogenesis. In addition, ABCA1 is an ABC cholesterol transporter responsible for cholesterol efflux from producing cells. Therefore, LSR plays a role in modulating cholesterol synthesis and transport through SREBP1 and ABCA1. There are evidence that SREBP1 mediates activation of lipoprotein receptors promotors, like LDL-R promotor, through SRE, insulin, insulin-like growth factor (Streicher *et al.* 1996; Liu *et al.* 2002). Further studies and experiments (studying more cholesterol metabolism related proteins, oxysterol accumulation, LXR pathway) must be performed for better understanding how LSR downregulation causes downregulation of cholesterol metabolism.

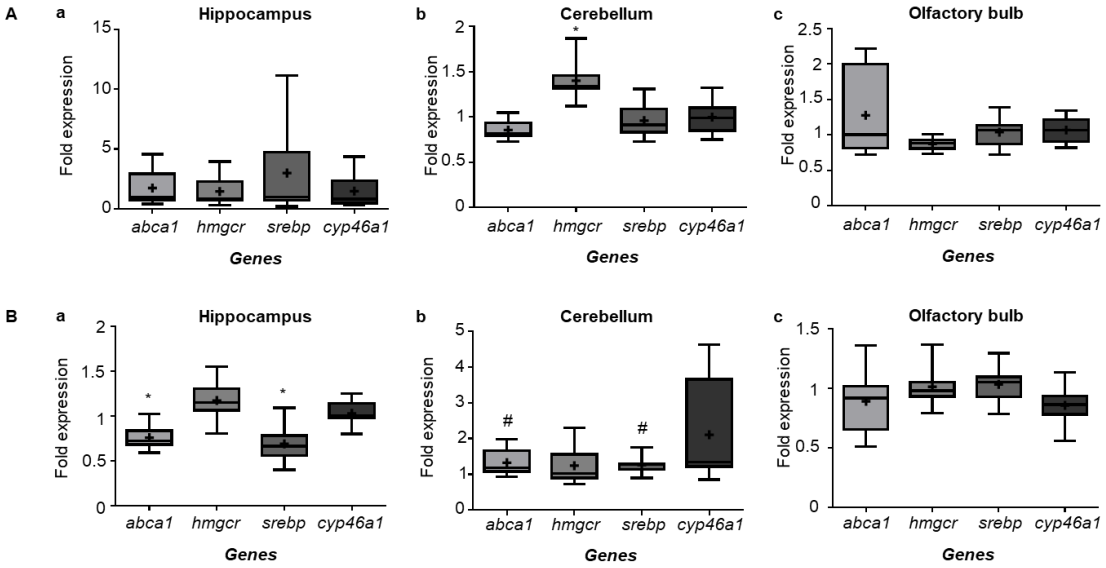

Figure 3.S7: Changes in RNA expression of cholesterol metabolism related enzymes and transporters after glia-specific lsr suppression. All of abca1 (cholesterol transporter onto lipoproteins), hmgcr (rate limiting enzyme in cholesterol synthesis), srebp1 (transcriptional factor responsible for regulating genes for de novo lipogenesis) and cyp46a1 (24-hydroxylase, responsible of generating 24-hydroxycholesterol). Box plot presentation of fold expression of abca1, hmgcr, srebp1, and cyp46a1, respectively, at two different age points at A) 3-month-old and B) 13-month-old mice, where a) is hippocampus, b) cerebellum, and c) olfactory bulb. Five cKO mice and five WT mice were sacrificed at 3-months of age two weeks after TAM induction and five cKO mice and five WT mice were sacrificed at 13-months of age. The cKO mice (n = 5) data are represented in boxplot with respect to WT (n = 5) data. Statistical significance is represented as: # $P < 0.10$, * $P \leq 0.05$, ** $P \leq 0.01$, *** $P \leq 0.001$.

Glial lipoprotein receptor LSR disruption in mouse nervous system leads to cognitive deficits resembling AD.

To be submitted to *Genes, Brain, and Behavior* journal

Chapter **IV**

Cre mice and their hyperactivity trait

Work in progress.

Short resume:

When we performed the second major part of our study, generation, induction, and behavioral phenotyping of glia-specific knockout of LSR in mice, we initially planned to have two control groups: a negative control group *WT*, and a TAM induced *GLASTCreER*^{T2} group (*Cre)*. The latter was set to evaluate the effect of TAM injections on the observed phenotypes. Surprisingly, *Cre* group rapidly showed signs of hyperactivity and abnormal behavior in tests requiring attention. Therefore, we decided to limit the comparison between *WT* and *cKO* mice for the behavioral phenotyping of glia-specific knockout of LSR in mice. However, we further analyzed *Cre* mice as a possible model of hyperactive mice. In this chapter, we gathered the interesting data and the actual development of TAM induced *Cre* group.

1. Introduction

Vectors expressing Cre recombinase have been utilized to turn gene expression on or off. The Cre recombinase is a protein that recognizes and mediates site-specific recombination between loxP site sequences in bacteriophage P1 (Sternberg 1981). Cre-mediated recombination between two loxP sites can result in gene deletion, insertion, translocation, and inversion depending on the location and orientation of the loxP sites. The Cre/loxP recombination system has turned into a useful tool for genetic manipulation in mammalian cells (Sauer & Henderson 1988) and eventually in experimental animals (Tsien *et al.* 1996), especially in the nervous system due to the complex cell types and neural circuits.

The Cre/loxP site-specific recombination system has become a valuable tool for conditional somatic mutation in mice. This method allows one to control gene activity spatially and temporally in order to decipher gene function in almost any tissue of the mouse. The spatial regulation of recombination can be achieved by using cell type-specific promoters that drive expression of Cre in the tissue of interest, like using Glast promoter to drive Cre expression in glial cells. The temporal regulation can be obtained by a small-molecule inducer through fusion of Cre and a ligand-binding domain of steroid receptors. One of the ligand-dependent Cre recombinases is CreER recombinase, which consists of Cre fused to mutated hormone-binding domain of the estrogen receptor. The CreER recombinase is inactive but can be activated by the synthetic estrogen receptor ligand TAM. The more improved versions of the chimeric Cre recombinase have been developed, including $CreER^{T2}$ (Indra *et al.* 1999). By combining tissue-specific expression of a CreER recombinase with its tamoxifen-dependent activity, the Cre-mediated gene regulation can be controlled both spatially and temporally (Li & Snider 2018). Induction of *GLASTCreER^{T2}* mice (*Cre*) with TAM drives glia-specific expression of Cre enzyme (Slezak *et al.* 2007).

In most behavioral studies, the group of interest is usually compared to *WT* littermates, rather than *Cre* controls. Some of these studies showed that their group of interest was hyperactive when compared to *WT* controls (Ade *et al.* 2011; Nelson *et al.* 2012; Bodo *et al.* 2017; Bohuslavova *et al.* 2017). This might result in exaggeration of real variations or even result in false positives. That is why we have chosen to include *Cre* littermates

in our behavioral studies, where the only difference between them and *cKO* mice is the deletion of *lsr* gene. All methods are described in the Chapter III, please note that only data of younger *Cre* mice are presented in this chapter.

2. Results

2.1. Home cage activity:

This test was performed at 6 months of age. When walking distance was measured, a clear genotype effect was observed while comparing the three groups: *WT*, *Cre,* and *cKO* over the 24h-period [F (2,588) = 14.66, $P < 0.0001$]. As we compared the distance traveled by *WT* vs *Cre* mice exclusively in 24-hours, there was a clear genotype effect [F(1,816) = 28.51, $P < 0.0001$] and a significant genotype x time interaction [F (23, 816) = =1.978, $P = 0.0042$]. This was equally significant during dark period [F (1,408) = 20.55, $P < 0.0001$], but non-significant during light period. This indicates that *Cre* mice traveled a longer distance during the dark period and they didn't follow the same activity pattern as *WT* mice (Figure 4.1c). Equally, *Cre* mice walked for longer periods during the dark period [Figure 4.1f, genotype effect: F (1, 408) = 37.51, $P < 0.0001$; genotype x time interaction: F (11, 408) = 1.959, $P = 0.031$]. *Cre* mice walked a total of 2 hours more than *WT* mice during dark period [Figure 4.1b, t (147) = 3.936, $P = 0.0001$]. Altogether, those observations strongly suggest that *Cre* mice might be naturally hyperactive. To further verify that, we calculated fine movements (Figure 4.1d), like grooming and scratching, *Cre* mice monitored higher levels of fine movements than *WT* both in dark [Genotype effect: F(1,408) = 11.03, $P = 0.001$] and light periods [Genotype effect: F (1, 408) = 9.484, $P =0.002$]. However, there was no significant variation in speed between *WT* and *Cre* mice (Figure 4.1e). Those results confirm that *Cre* mice are hyperactive in their own environment.

Cre and *cKO* mice resemble genetically and both were induced with TAM. As we compared distance traveled by *cKO* mice to *Cre* mice, there was a clear genotype effect during dark phase [Figure 4.1a, F (1, 384) = 17.96, $P < 0.0001$] where *Cre* mice traveled a longer distance than *cKO* mice. There was no significant difference during light phase. During dark phase, *cKO* mice traveled 1.18 hours less than *Cre* mice [Figure 4.1b, t (147) = 2.319, $P =0.0218$]. However, there was no significant diference in walking time %, speed, and fine movements. Since *Cre* and *cKO* mice are genetically

closer than *WT* mice and *cKO* mice, we could speculate that deleting LSR rendered mice hypoactive.

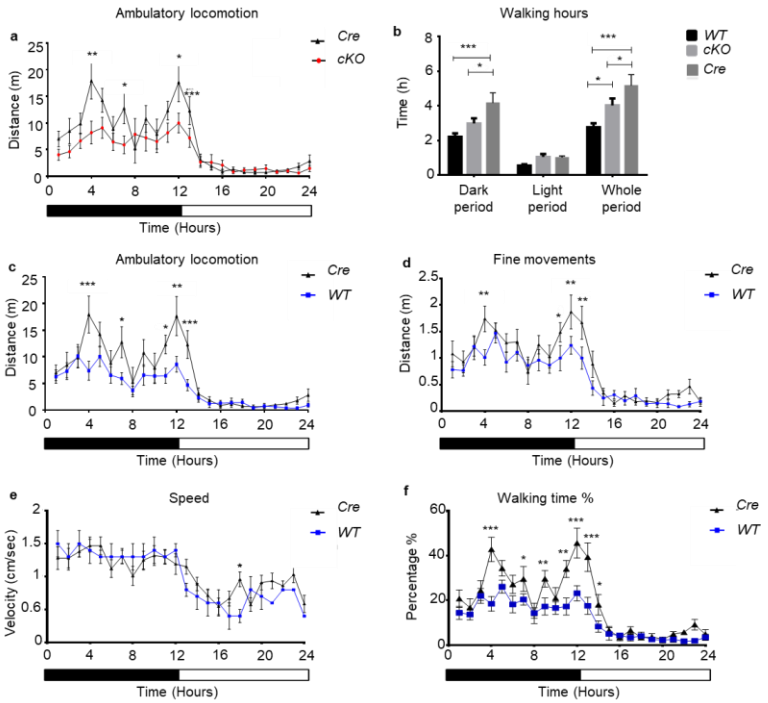

Figure 4.1. Home cage activity of Cre (n = 18) mice. a) Comparison of walking distance traveled between Cre and cKO mice over the 24-hour period. b) Total walking hours traveled by WT, cKO, and Cre, respectively, in dark period, light period, and whole day, respectively. c) Comparison of walking distance traveled between Cre and WT mice over the 24-hour period. d) Fine movements comparison between Cre and WT mice. e) Speed comparison between Cre and WT mice. f) Walking time % comparison between Cre and WT mice.

2.2. Free exploratory paradigm:

This test was performed at 10 months of age to measure trait anxiety. Trait anxiety is a form anxiety where a subject is anxious in their own environment without introducing a stress or novel factor. The *cKO* mice tended to take 10 seconds more than *Cre* mice to enter new zone [Figure 4.2a, t (42) = 1.88, *P* = 0.067]. There was no significant difference in number of entries to new environment between the three groups (Figure 4.2e). In addition, there was no significant difference in number of locomotion in familiar and new zone, yet *Cre* mice tended to move less in familiar zone and new zone when compared to *WT* [Figure 4.2c and 4.2d, t (42) = 1.895, *P* = 0.065]. However, there was a significant difference in time spent in new environment when comparing *Cre* vs *cKO* mice, where *cKO* mice spent 35.07 seconds less than *Cre* mice in new environment [t (42) = 3.082, *P* = 0.0036] and a tendency for *WT* mice to stay 21 seconds less than *Cre* mice in new environment [Figure 4.2b, t(42) = 3.082, *P* = 0.0036]. Thus, *cKO* mice

preferred staying in their own environment when compared to *Cre*. This indicates that the anxiety identified in *cKO* mice might be due to LSR ablation rather than to *Cre* construct.

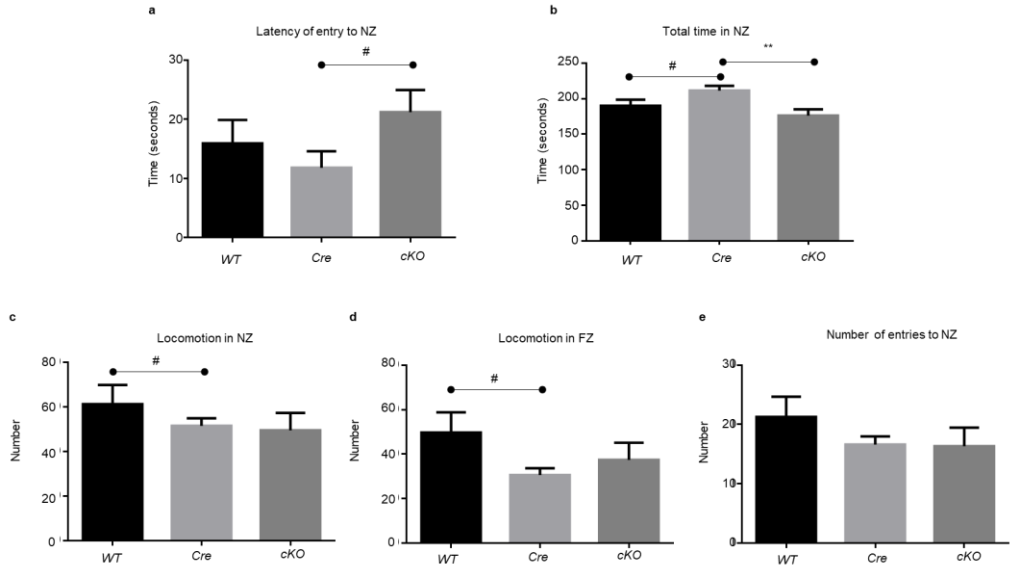

Figure 4.2. Free exploratory paradigm data comparing *cKO* (n = 15) vs *WT* (n = 15) mice vs *Cre* (n = 15). a) Latency to enter new environment in seconds (sec). b) Total time in new zone (sec). c) Locomotion in new zone; number of entries in different compartments of new zone. d) Locomotion in familiar zone; number of entries in different compartments of familiar zone. e) Numbers of entries from familiar zone to new zone. Data are considered statistically significant when $P \leq 0.05$ where # indicates $P < 0.10$, * indicates $P \leq 0.05$, ** indicates $P \leq 0.01$, and *** indicates $P \leq 0.001$.

2.3. Open field test:

This test was performed to measure activity and state anxiety at the age of 3-month-old. State anxiety is a form anxiety where a subject is anxious due to introduction of a stress or novel factor. The *Cre* mice spent 4.13 minutes in peripheral Z1 (test time 5 minutes), which was longer than both *cKO* mice [3.77 minutes, *Cre* vs *cKO,* t(159) = 2.779, $P = 0.006$] and *WT* mice [3.63 minutes, *WT* vs *Cre,* t(159)=4.07, $P < 0.0001$] in Z1 (Figure 4.3a). Both *cKO* and *Cre* mice spent 30-35 seconds less in central Z3 when compared to *WT* mice [*WT* vs *Cre,* t (159) = 2.741, $P = 0.007$; *WT* vs *cKO,* t (159) = 2.444, $P = 0.016$]. There was no significant different in time spent in Z3 between *Cre* and *cKO* (Figure 4.3a). Although *Cre* mice spent more time in Z1 and less time in Z3, the latency to enter Z2 and Z3 was insignificantly different to that of *WT* and *cKO* (Figure 4.3b). This was equally the case of number of entries to each zone (Figure 4.3e). However, *Cre* mice moved more, where they traveled longer distances than *WT* and *cKO* mice (Figure 4.3d, *WT* vs *Cre*, t (56) = 4.186, $P = 0.0001$, *Cre* vs *cKO,* t(56) =

5.089, $P < 0.0001$). Also, they were about 10 cm/sec faster than *WT* mice [t (56) = 2.936, $P = 0.0048$] and tended to be faster than *cKO* mice [Figure 4.3c, t (56) = 1.79, $P = 0.078$]. This indicates that *Cre* mice were hyperactive and monitored state anxiety traits. *cKO* mice were less active than *Cre* and monitored state anxiety traits, which might be a result of either Cre enzyme or LSR suppression.

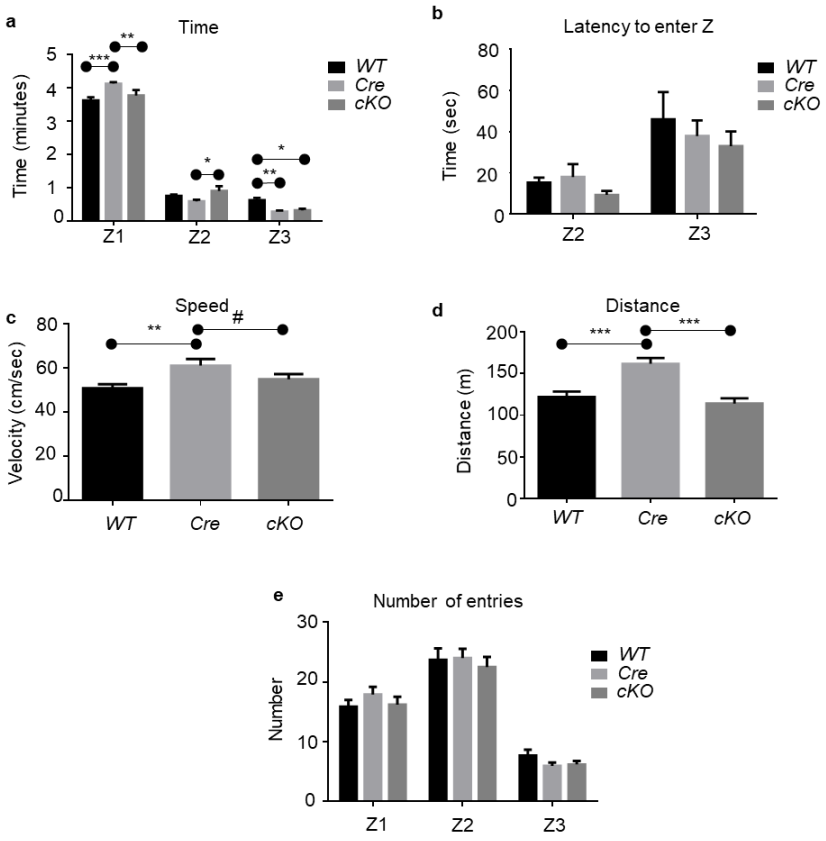

Figure 4.3. Open field test to measure activity and state anxiety. a) Time spent in peripheral zone (Z1), middle zone (Z2), and central zone (Z3). b) Latency to enter Z1, Z2, and Z3. c) Average speed of *WT, Cre,* and *cKO* mice. d) Distance traveled by *WT, Cre,* and *cKO* mice. e) Number of entries to Z1, Z2, and Z3. Data are considered statistically significant when $P \leq 0.05$ where # indicates $P < 0.10$, * indicates $P \leq 0.05$, ** indicates $P \leq 0.01$, and *** indicates $P \leq 0.001$.

2.4. Buried cookie test:

To assess olfaction, the buried cookie test was performed at 5 months of age. During the habituation phase, no significant difference between the three groups was recorded; they nearly took the same time to approach and eat the cookie (Figure 4.4a).

During the test session, *Cre* mice were the most rapid in unburying the cookie and eating (Figure 4.4b), where they took only 32 seconds, whereas *WT* mice took 103.6 seconds [t (53) = 6.039, *P* < 0.0001]. The *cKO* mice were the slowest and took 203 seconds to eat the cookie [t (53) = 6.039]. This indicates that *Cre* mice can smell and were the fastest to find the cookie maybe due to their hyperactive nature.

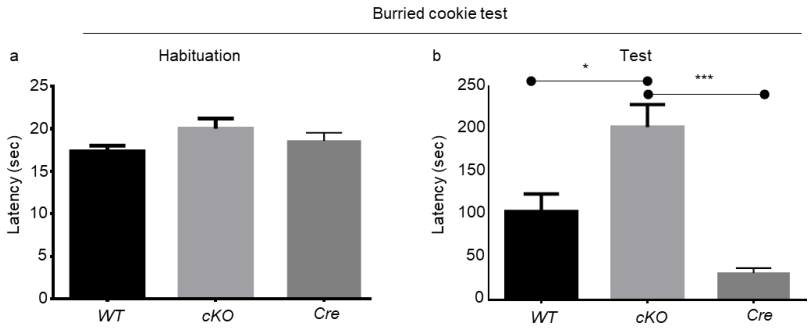

Figure 4.4: Buried cookie test. a) Habituation phase to cookie. b) Buried cookie test comparing time to unbury and eat cookie. Data are considered statistically significant when P ≤ 0.05 where # indicates P < 0.10, * indicates P ≤ 0.05, ** indicates P ≤ 0.01, and *** indicates P ≤ 0.001.

2.5. Odor discrimination test:

Another olfaction assessment test performed at 10 months of age. In general, *Cre* (n = 10) were more active and explored more than both *WT* and *cKO* mice. In the habituation phase, there was no significant difference between *WT* and *Cre*. However, during H2 and H3, *Cre* mice explored the odorless tea ball for 14.34-14.58 seconds more than *cKO* mice [*Cre* vs *cKO*: H2 t (270) = 2.194, *P* = 0.0291, H3 t (270) = 2.231, *P* = 0.027]. During the rose odor phase, there was no significant difference between neither *WT* vs *Cre* nor *Cre* vs *cKO*. When comparing the exploration time of R3 vs R1 for *Cre* mice, it showed a learning tendency for *Cre* mice [R3 vs R1 t (270) = 2.756, *P* = 0.069]. Upon the introduction of a sexual odor, female urine, *Cre* mice showed a very high interest, where they passed 78 seconds (test time = 120 seconds) sniffing the odor [R3 vs U1, t (270) = 9.254, *P* < 0.000]. On the other hand, *WT* mice spent 44.1 seconds [*WT* vs *Cre,* t (270) = 5.181, *P* < 0.0001] and *cKO* spent 27.08 seconds only [*Cre* vs *cKO,* t (270) = 7.786, *P* <0.0001] in U1 phase. *Cre* mice were able to learn, since their interest in female urine decreased with multiple introductions [U3 vs U1, t (270) = 5.367, *P* < 0.0001]. Yet, *Cre* mice were not able to discriminate 1% lemon in female urine [U+1% lemon vs U3, t (270) = 0.694, *P* = 0.488]. In conclusion, *Cre* mice were hyperactive, showed high interest in sexual odors, thus can smell but couldn't

discriminate introduction subtle odors like 1% lemon oil.

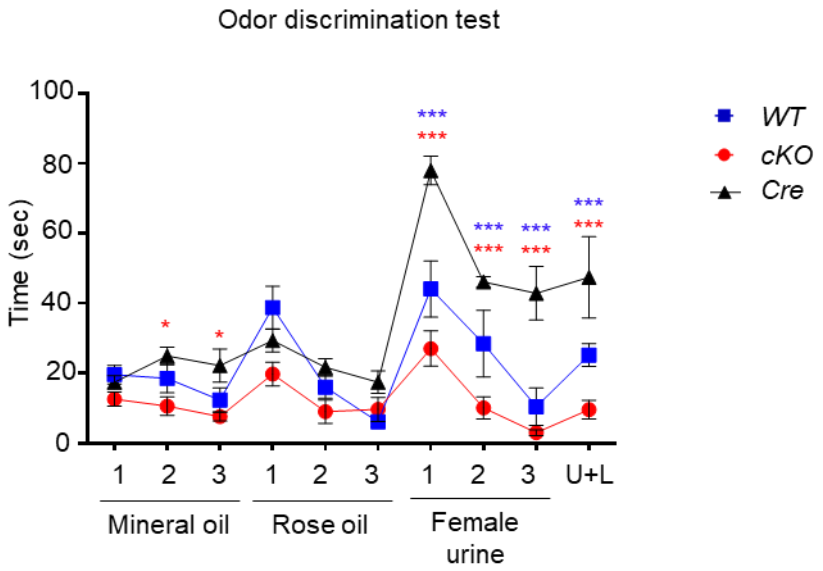

Figure 4.5. Odor discrimination test. This test consists of a 5 min habituation step to the tea ball (no odor), then three 2 min habituation sessions to rose oil, followed by three 2 min habituation sessions to female urine. The test then ends with a 2 min odor discrimination step to female urine containing 1% lemon oil (U+L). Statistical significance when comparing a single point between *Cre* vs *WT* is represented as: * $P \leq 0.05$, ** $P \leq 0.01$, *** $P \leq 0.001$, and *Cre* vs *cKO* is represented as: * $P \leq 0.05$, ** $P \leq 0.01$, *** $P \leq 0.001$

2.6. Object recognition test:

This test was performed on 4 months old *WT* (n = 20), *Cre* (n = 18), and *cKO* (n = 18) mice. During familiarization phase (Figure 4.6a), all three groups explored objects A and B (set of same objects) for an equal amount of time (no object effect). However, there was a clear genotype effect [F (2,106) = 5.851, P = 0.0039]. There was a significant difference in total exploration time between *WT* vs *Cre* with a mean difference (M.D.) of 12.24 seconds [t (36) = 2.385, P = 0.023], and a M.D. 12.32 seconds for *WT* vs *cKO* [t (36) = 1.955, P = 0.058], but no difference between *Cre* and *cKO* was recorded (Figure 4.6b).

In session 2, object recognition and visual memory session, there was a clear genotype effect [F (2,106) = 4.222, P = 0.0172], object effect [F (1, 106) = 6.095, P = 0.0152] and a genotype x object effect [F (2,106) = 3.711, P = 0.0277]. This indicates that different groups explored the old and new object in a different manner. Indeed, this was the case where *WT* mice passed more time close to new object when compared to old object [M.D. 8.32 seconds, t (106) = 3.736, P = 0.0003]. But this was not the case of *Cre* and

cKO mice (Figure 4.6c). When total exploration time was calculated, no significant difference was observed between *Cre* and *WT* mice, neither between *Cre* and *cKO,* yet a significant difference between *WT* and *cKO* [Figure 4.6d, M.D. 9.3 seconds, t (36) = 2.514, P = 0.016]. In conclusion, *Cre* and *cKO* mice monitored visual and/or visual memory problems, since they couldn't discriminate the new from old object. In addition, *Cre* mice showed a variable interest in surrounding objects between session 1 and 2.

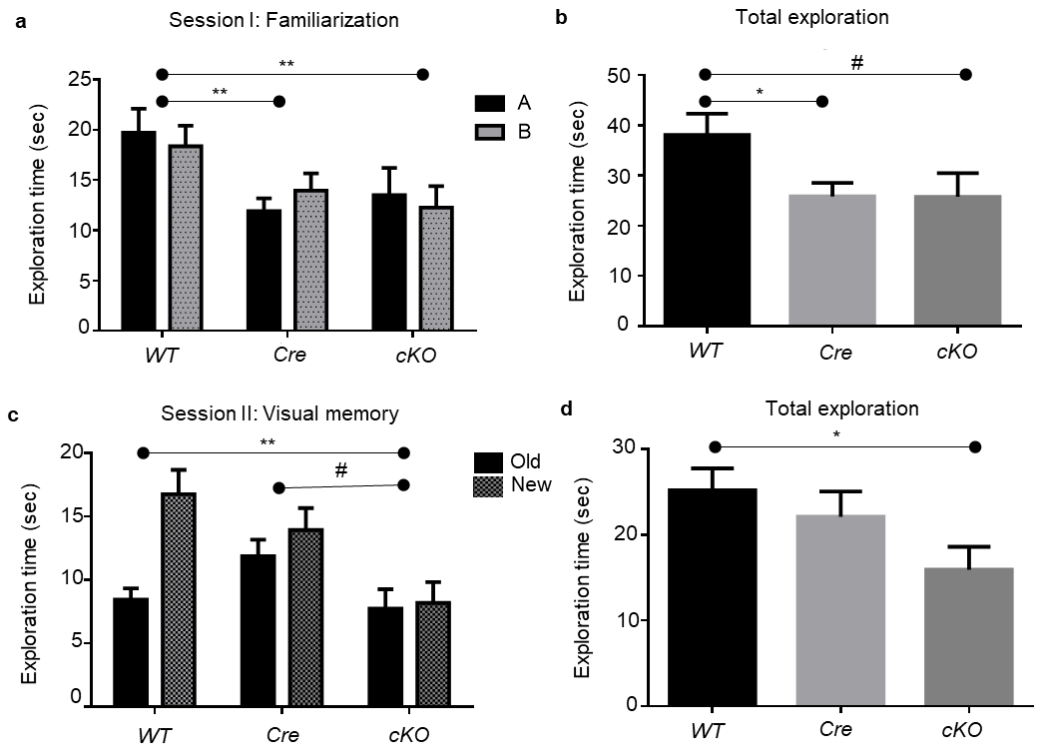

Figure 4.6. Vision and memory assessment using object recognition test. a) Session I: Familiarization phase. b) Total exploration time. c) Session II: Visual memory. d) Total exploration time. Statistical significance is represented as: # for $P < 0.10$, * for $P < 0.05$, ** for $P < 0.01$, *** for $P < 0.001$.

2.7. Three-chambered sociability test:

This test was done to assess sociability, and social memory at the age of 5 months. In session I, sociability test session, there was a clear genotype effect [F (2, 106) = 10.16, $P < 0.0001$], sociability effect [F (1, 106) = 18.11, $P < 0.0001$], and a genotype x sociability interaction [F (2, 106) = 13.37, $P < 0.0001$]. The *WT* mice were the most social with a M.D. of 92.5 seconds between empty cage and cage with stranger I [Figure 4.7a, t (106) = 12.04, $P < 0.0001$], where they passed 80.52 % of their exploration time with stranger I (Figure 4.7c). *Cre* mice explored stranger 1 for 79 seconds [Empty vs

stranger I M.D. 57.7 seconds, t (106) = 7.123, *P* < 0.0001], where they passed 78.5 % of their exploration time with stranger I (Figure 4.7c). The *cKO* mice explored stranger I for 69.43 seconds [Empty vs stranger I M.D. 35.43 seconds, t (106) = 4.375, *P* < 0.0001], where they passed 66.33 % of their exploration time close to stranger I [Figure 4.7c, *WT* vs *cKO,* t (53) = 4.212, *P* < 0.0001; *Cre* vs *cKO,* t (53) = 3.53, *P* = 0.0009]. *Cre* and *cKO* mice had a similar total exploration time, which was 40-45 seconds lower than *WT* mice [*WT* vs *Cre*, t (53) = 4.055, *P* = 0.0002]. This might be due to hyperactive nature for *Cre* and a lower interest towards their surrounding for *cKO*, however *Cre* mice were more social than *cKO*, which might be due to an olfactory deficit in *cKO* mice.

During session II, social novelty and memory test session, there was a genotype effect [F (2, 106) = 12, *P* < 0.0001], novelty effect [F (1,106) = 31.18, *P* < 0.0001] and a genotype x novelty interaction [F (2, 106) = 3.249, *P* = 0.043]. The *WT* mice sniffed stranger II 36.26 seconds more than stranger I [Figure 4.7d, t (106) = 5.096, *P* < 0.0001], where they passed 64.85 % of their exploration time with stranger II (Figure 4.7f). *Cre* mice sniffed stranger II 25.1 seconds more than stranger I [Figure 4.7d, t (106) = 3.347, *P* = 0.0011], where they passed 66.02 % of their exploration time with stranger II (Figure 4.7f). The *cKO* mice explored stranger I and stranger II for a similar amount of time, where they passed 54.55 % of their exploration time close to stranger I [Figure 4.7f, *WT* vs *cKO,* t (53) = 2.469, *P* = 0.017; *Cre* vs *cKO,* t (53) = 2.679, *P* = 0.0098]. *Cre* and *cKO* mice had a similar total exploration time in session II, which was 38-48 seconds lower than *WT* mice [Figure 4.7e, *WT* vs *Cre*, t (53) = 4.268, *P* < 0.0001, *WT* vs *cKO,* t (53) = 3.516, *P* = 0.0009]. A possible cause that *Cre* mice explored the stranger mice less is their hyperactive nature. However, they were able to discriminate and remember stranger I from stranger II, thus no olfactory or social memory problem exists in those mice. On the other hand, *cKO* showed lower interest in their environment, and were less social than control groups, which might be due to

an olfactory and or memory deficit in *cKO* mice wich is therefore clearly link to the deficit in glial LSR.

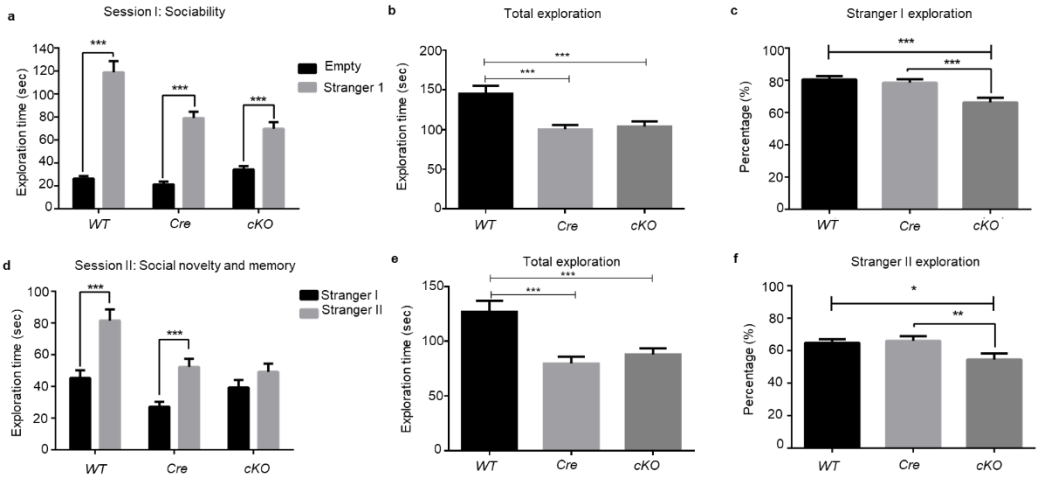

Figure 4.7. Three chambered sociability test. a) Session I: Sociability session. b) Total exploration session I. c) Stranger exploration %. d) Session II: Social novelty and memory. e) Total exploration time in session II. f) Stranger II exploration %. Statistical significance is represented as: # for $P < 0.10$, * for $P < 0.05$, ** for $P < 0.01$, *** for $P < 0.001$.

2.8. Y-maze:

This test was performed to measure spatial; short-term memory in 4 months old male *WT* (n = 20), *Cre* (n = 18), and *cKO* (n = 18). There was no significant difference in proper alternations % between *Cre* and *cKO* mice (Figure 4.8a). However, the difference was highly significant between *WT* and *Cre* mice, where there was a 13.5 % difference [Figure 4.8a, t (53) = 4.192, $P = 0.0001$]. *Cre* mice scored the highest number of entries during the test, with a mean of 27 entries, whereas *WT* and *cKO* mice scored a mean of 19 entries [Figure 4.8b, *WT* vs *Cre* t (53) = 3.081, $P = 0.0033$, *Cre* vs *cKO* t (53) = 3.016, $P = 0.0039$]. Concerning distance, *Cre* mice traveled the longest distance with 18.53 meters M.D. between *Cre* and *WT* mice [Figure 4.8c, t (53) = 2.53, $P = 0.014$], and 13.54 meters mean difference between *Cre* and *cKO* mice [t(53) = 1.801, $P = 0.08$]. In addition, *Cre* mice were faster than *WT* mice with a M.D. of 7.8 cm/sec [t (53) = 2.35, $P = 0.02$], still the difference between *cKO* and *Cre* mice were non-significant (Figure 4.8d). Also, both *Cre* and *cKO* mice took longer time to leave central Z4 to arms B and C when compared to *WT* (Figure 4.8e), but *cKO* mice also took longer time to leave primary arm A to Z4 for the first time [*WT* vs *cKO*: Z4 t (28) = 3.102, $P = 0.004$]. In conclusion, Cre mice are hyperactive which causes lower proper alternations and higher number of entries. On the other hand, *cKO* mice when compared to *Cre*

mice, are hypoactive where they score lower number of entries but a similar proper alternation % as *Cre*. The *cKO* mice tended to travel a shorter distance but at a similar velocity, which indicates longer immobile periods. In addition, *cKO* mice took a longer time to leave arm which indicates neophobia.

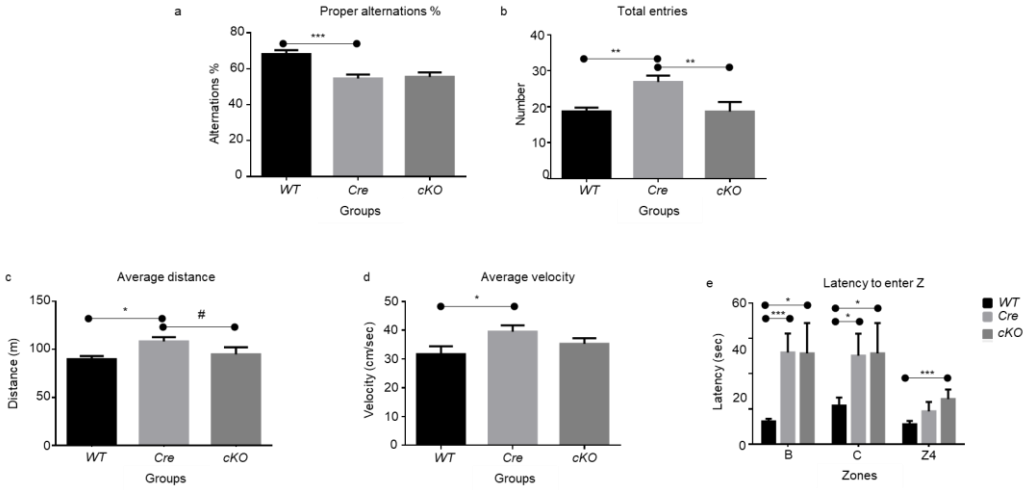

Figure 4.8. Y-maze test for spatial short-term memory assessment. a) Proper alternations percentage. b) Total number of arm entries. c) Average distance traveled. d) Average velocity. e) Latency to enter to a zone for the first time. Statistical significance is represented as: # for $P < 0.10$, * for $P < 0.05$, ** for $P < 0.01$, *** for $P < 0.001$.

2.9. Barnes maze:

This test was used to measure learning ability, cognitive flexibility, and long-term memory. This test was performed on the three test groups *WT* (n=15), *Cre* (n=15), and *cKO* (n=15) at the age of 11 months. In general, there was a significant difference between *Cre* and *WT* mice to find the chamber at most trials, where *Cre* took more time to find the chamber (Figure 4.9a).

To measure spatial learning, we measured the time difference between day 1 trial (D1T1) and D3T3, all three groups *WT*, *Cre* and *cKO* took less time on D3T3, thus were able to learn. On D4, no habituation phase preceded T1, *WT* were able to learn [D4 T1 vs D4 T3, M.D. 50.4 seconds, t (672) = 2.663, $P = 0.0079$], this was equally the case of *cKO* mice [D4 T1 vs D4 T3, M.D. 89.2 seconds, t (672) = 4.71, $P < 0.0001$], but not the case for *Cre* mice.

Equally, when measuring cognitive flexibility, where both *WT* mice [D5 T1 vs D5 T3, M.D. 48.2 seconds, t (672) = 2.547, $P = 0.011$] and *cKO* [D5 T1 vs D5 T3, M.D. 48.4 seconds, t (672) = 2.557, $P = 0.0108$] were able to learn, *Cre* mice couldn't (non-significant M.D. between D5 T1 vs D5 T3).

Concerning long-term memory, both *cKO* and *WT* mice retained memory when compared to *Cre* mice [*WT* vs *Cre*, t (672) = 2.784, $P = 0.0055$; *Cre* vs *cKO*, t (672) = 3.265, $P = 0.0011$]. This indicates that *Cre* mice can learn, but when a parameter changes, like stopping habituation or changing departure position, they block from learning, and may suffer from cognitive rigidity and long-term memory problems. This behavior might be generated due to hyperactivity trait of *Cre* mice.

When measuring distance traveled during test time, there was a significant difference in multiple trials between *WT* and *Cre* mice, but only in one trial between *Cre* and *cKO* mice (day 5 trial 3, t (672) = 3.059, $P = 0.0023$), which might be due to the fact that *Cre* mice are hyperactive and took more time to find the chamber, thus walked longer distances than *WT* mice (Figure 4.9b).

The latency to start walking was also measured (Figure 4.9c), at D1 T1 there was no

significant difference between *Cre* and *cKO* mice, yet there was a tendency between *WT* and *Cre* [M.D. 14.3 seconds, t (630) = 1.796, *P* = 0.073]. At D4 T1, where no habituation phase preceded the test, a significant difference between *Cre* and *cKO* was recorded, where *cKO* mice took 22.9 seconds more than *Cre* mice to start walking [t (630) = 3.023, *P* = 0.0026]. When the departure zone changed D5 T1, both *cKO* and *Cre* mice took more time to start moving when compared to *WT* mice [*WT* vs *Cre*, t (630) = 2.033, *P* = 0.043]. This indicates that *Cre* mice might exhibit an adaptation problem accompanied to their hyperactivity, which is especially exacerbated when the habituation phase is removed on D4. This rigidity associated with their hyperactive behavior leads to longer distance of walking and latency to enter the chamber in D5. *Cre* mice are unable to adapt to the changes to learn and retain the information as *WT* and *cKO* mice (D5-D8 trials).

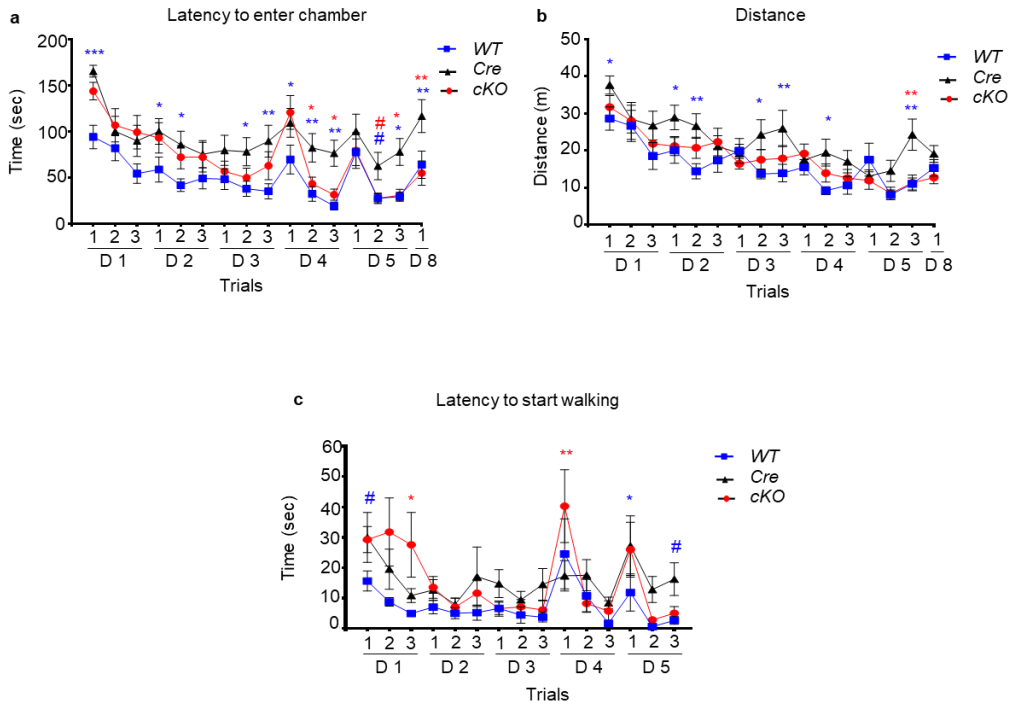

Figure 4.9: Barnes maze test for *Cre* mice vs *WT* vs *cKO* mice. a) Evolution of latency to enter chamber with days. b) Distance traveled in each trial of each day. C) Latency to start walking after test departure. In all panels presented D refers to days, where the test was performed in 5 consecutive days with 3 trials per day and two days after D5 one trial was done. Statistical significance when comparing a single point between *Cre* vs *WT* is represented as: * $P \leq 0.05$, ** $P \leq 0.01$, *** $P \leq 0.001$, and *Cre* vs *cKO* is represented as: * $P \leq 0.05$, ** $P \leq 0.01$, *** $P \leq 0.001$

3. Conclusion and discussion

All performed tests, especially home cage activity where *Cre* mice walked longer distances and groomed and scratched significantly more than *WT* mice, point out the hyperactive trait of *Cre* mice that most likely impacted their performance in all tests.

Cre mice monitor state anxiety behavior but not trait anxiety behavior. In addition, *Cre* mice seem to monitor short-term memory problems, learning and long-term memory problems. The hyperactivity trait of *Cre* mice could alter their performance in all tests. This disruption of information acquisition will inevitably have an impact on the memory performance, in the object recognition since the mice have less explored the objects familiar to the acquisition.

Cre mice were able to smell, they performed well in buried cookie test and showed high interest in female urine odor in odor discrimination test. They performed well in sociability and social novelty test, most probably due to a well-functioning olfactory system. However, they weren't interested in rose odor as in female urine and couldn't discriminate 1% lemon introduction. This is most probably due to their hyperactivity trait.

The main question that remains is whether *WT* or *Cre* is the good control group for behavioral studies. The hyperactivity trait of *Cre* mice blocks it to be a good control group in most tests, since *cKO* mice were hypoactive when compared to *Cre* mice, and more active when compared to *WT* mice on specific tasks (in home cage test at the beginning and end of dark cycle). Although, *Cre* and *cKO* can also show similar behavioral patterns, where they nearly monitored an equal exploration time of objects and subjects, both showed a pause before departure in Barnes maze, both had a low proper alternation %. However, those results observed might not be due to the same reason (hyperactivity and attention errors for *Cre* mice and anxiety for *cKO* mice).

If we compare *cKO* against *Cre* mice, they were hypoactive in most tests. In addition, they showed lack of interest toward their environment and neophobia. They did a lower number of entries in Y-maze, which is a neophobia indicator. Interestingly, similar observations were made when *lsr* +/- performed in Y-maze for the first time (Stenger

et al. 2012). Equally, *cKO* mice were immobile for longer times than *Cre* mice, since they traveled shorter distances at a similar velocity in open field. In Barnes maze, *cKO* mice generally performed better than *Cre* mice. But it is hard to consider *Cre* as a control in Barnes since their hyperactivity trait blocked them from learning and retaining information. There is evidence that hyperactivity can interfere with escape latency, distance and speed (Baeta-Corral & Giménez-Llort 2015). It is possible that *Cre* mice have a visual problem since they performed badly in object recognition test. Further tests that assess vision most be performed to rule out low vision abilities or even blindness since even blind mice can find the escape chamber (Yassine *et al.* 2013).

It's possible that the behavioral profile of *Cre* mice is not specific to that of *GLASTCreER^{T2}* mice but to *CreER^{T2}* mice in general. The behavior of *CreER^{T2}* mice hasn't been thoroughly studied in literature. In previous studies, the group of interest was usually compared to *WT* controls (Ade *et al.* 2011; Nelson *et al.* 2012; Bodo *et al.* 2017; Bohuslavova *et al.* 2017).

The question is:"Can *Cre* mice serve as a model for attention-deficit hyperactivity disorder (ADHD)?". ADHD is a disorder generally characterized of inattention, hyperactivity and impulsivity, and deficits in motivation (Volkow *et al.* 2011). *Cre* mice were hyperactive, impulsive, and lacked motivation and attention. We are studying behavior of uninduced *Cre* and induced *Cre* mice to further understand the origin of such profile.

Under normal circumstances, the prefrontal CX regulates attention, behavior, and emotion. ADHD is characterized by poor impulse control, weak sustained attention, and heightened distractibility, that is why ADHD was linked to deficits in prefrontal CX functioning (Arnsten 2011). In stressed state, there is excessive dopamine and norepinephrine release accompanied which impairs prefrontal CX abilities. Dopamine transporter influences dopamine concentration in synaptic clefts, whereas norepinephrine transporter is responsible for norepinephrine reuptake from synaptic clefts to presynaptic neurons (Wilens 2006). Methylphenidate, a medication for ADHD, blocks the activity of dopamine transporter and norepinephrine transporter leading to increased availability of catecholamines in synaptic cleft, but unlike amphetamine, doesn't induce dopamine release from presynaptic vesicles (Katzman &

Sternat 2014). Excess of Cre recombinase enzyme without target loxP sites might affect dopamine neurotransmission by perturbing the dopamine signals in attentions centers. To confirm this hypothesis, neurotransmitter release measurement and calcium imaging using electrophysiological and biochemical methods should be performed on *Cre* mice with or without methylphenidate pretreatment. We could then monitor if Cre accumulation perturb the dopamine neurotransmission and if *Cre* mice could therefore be a new model of ADHD.

General discussion

1. Summary of results

The aim of this work was to decipher the role of LSR in cholesterol homeostasis, which as stated before is crucial for proper brain functioning. As Francis Crick said: 'If you want to understand function, study structure', that is why the first part of our study was to study LSR expression pattern; the expression levels of different LSR subunits in different brain regions and eventually target the highly LSR expressing regions in further studies to understand its eventual function. We first demonstrated that that LSR expression in the CNS is regio-specific, each CNS area has its own expression profile for the different LSR chains, thus allowing for specific combination of subunits forming this lipoprotein receptor. Some CNS regions exhibited a stronger LSR expression at the mRNA and/or protein level. We showed that LSR is differentially expressed across the brain at both RNA and protein levels. At the RNA level, the HT, HIP, OB, and CB all show high levels of total *lsr* RNA expression. At the protein level, immunoblots show that the HT, OB, and RET express the highest levels of LSR when normalized to β-TUB, which may reflect a specific need of these regions to tightly regulate cholesterol for proper functioning. It is known that LSR is present in the endothelial cells at tight junctions, however all tissues collected contain blood vessels, therefore high levels of LSR found in specific brain areas cannot be only due to endothelial cells, homogeneously distributed throughout the CNS, but rather reflect the expression of LSR expression in CNS cells, and therefore neurons or glial cells. Moreover, we demonstrated that aging significantly affects LSR expression. With age, *lsr* RNA expression decreases in both the HT, and HIP; this is also the case at the protein level where LSR is clearly downregulated in the HT, and shows a tendency of downregulation in the HIP and OB.

Furthermore, we proved a strong glia expression of LSR compared to neurons. We noted that LSR expression was ubiquitous in glial cells, but more soma-centered in neurons. We found that glial cells are the main cells expressing LSR in the CNS, thus suggesting an essential role of this lipoprotein in the cholesterol trafficking between neurons and glial cells. Indeed, although we showed this in the CB, which provided sufficient mRNA to compare *lsr* levels in glial and neurons, immunocytostaining of other structures clearly show significant protein level of LSR in GFAP-positive cells. In view of this, and based on LSR's role as lipoprotein receptor, we hypothesized that the

LSR present on glial cells might play a role in the glia-neuron cross talk in feedback control of cholesterol synthesis, regulating circulating cholesterol and thus maintaining proper functioning of the brain. Which bring us to the second major part of our study: the generation and behavioral phenotyping of inducible glia-specific conditional knockout mice of *lsr cKO* versus *WT* mice. The specific *in vivo* suppression of *lsr* in glial cells induced perturbations in the behavior of *cKO* mice, which might be due to the perturbation of cholesterol homeostasis. In their environment, *cKO* mice were more active during the second half of nocturnal period compared to *WT*. All behavioral tests were performed 1-3 hours after the beginning of dark period, thus within the period where *WT* and *cKO* have similar activity levels. In a novel environment, *cKO* mice tended to stay at the periphery for longer periods of time when compared to *WT* mice reflecting thigmotaxis. Nevertheless, they travelled the same distance at the periphery, which indicates longer immobile periods at the periphery. The immobility and thigmotaxis might have been a form of state anxiety or apathy. The *cKO* mice were able to visualize objects and identify visual cues, since they explored the same set of objects for a nearly equal time. Also, they were able to visualize the geometric cues in Barnes maze to find the escape chamber. However, they couldn't discriminate or memorize between an old and a new object. They also performed a lower proper alternation % in Y-maze than *WT* mice indicating a deficit in the memorization of already visited arms. Concerning olfaction, *cKO* mice took twice the time to find the buried cookie. In addition, they spent less time sniffing new odors and couldn't discriminate subtle odors. This demonstrate that olfactive memory performance is lower in *cKO* mice. They were able to detect different asexual and sexual odors but couldn't identify subtle differences. The *cKO* were less social than *WT* mice, which could be linked to olfactory deficits as rodents are mainly using this sense to identify and recognize strangers. However, in older mice, they were able to discriminate between the old and new strangers. Therefore, *cKO* mice showed olfactory dysfunction, which is the first sign of neurodegeneration Altogether those tests suggested that sensorial memory and spatial short-term memory were affected. In *cKO* mice, the working memory performance was lower than in *WT* in both young and older animals, but while it declined in *WT* -reflecting a normal aging process- it appeared more stable in *cKO* suggesting cognitive restructuring or neuroplasticity.

In our behavioral phenotyping, three groups were studied: 1- *WT* mice, our negative

controls. 2- *Cre* mice, TAM-induced glia-specific Cre enzyme expressing control mice. 3- *cKO* mice, TAM-induced glia-specific Cre-enzyme expressing *lsr* suppressed mice. The behavioral phenotype was quite complex, where surprisingly *Cre* mice monitored a hyperactive trait when compared to both *WT* and *cKO* mice. This hyperactive trait prohibited *Cre* mice from being a suitable control group for *cKO* mice in learning and memory tasks like in odor discrimination test and Barnes maze. Therefore, we discussed *Cre* mice in a separate chapter, where we compared *Cre* vs *WT* and *Cre* vs *cKO* mice. First, in home cage activity, *Cre* mice walked longer distances and for longer periods than *WT* mice. In addition, they showed higher grooming and scratching behavior than *WT* mice. However, the only difference between *Cre* and *cKO* mice was the walking distance, which indicates *cKO* hypoactivity when compared to *Cre* mice. Second, in free exploratory paradigm, no significant variation between *WT* and *Cre* mice, but *cKO* mice spent less time in new zone and tended to take more time to enter new zone for first time. Therefore, *Cre* mice monitored no trait anxiety traits, but *cKO* did when compared to *Cre* mice. Third, in open field test, both *Cre* and *cKO* stayed for a similar time at periphery, longer than *WT* mice. However, *Cre* mice traveled longer distances than *cKO* mice. This confirms that *Cre* mice are hyperactive and indicates that *cKO* mice were immobile for longer periods of time. Fourth, *Cre* mice were able to smell, detect odors, but were unable to discriminate subtle odors. *Cre* mice were the fastest to unbury food and were highly attracted to sexual odors, which might be, in part, due to their hyperactivity. On the other hand, *cKO* mice spent significantly more time to find cookie and showed low interest in non- and sexual odors. Yet, *cKO* mice were able to detect different odors, but couldn't discriminate subtle odors, which might be in part due to lack of interest and hypoactivity. Fifth, sociability and social memory, *cKO* mice were less social than both *WT* and *Cre* mice and monitored social memory deficits. Sixth, in vision and visual memory, *Cre* and *cKO* mice explored object sets for a similar time, which was significantly lower than that of *WT* mice. In addition, both *Cre* and *cKO* mice had visual discrimination and/or visual memory deficits. Also, both *Cre* and *cKO* had short term memory deficits. However, *cKO* also did a lower number of entries than *Cre* mice, which is a neophobia indicator. Finally, in Barnes maze, both *Cre* and *cKO* mice took a longer time to launch their search for the escape chamber on day 1 trial 1. However, *cKO* mice were able to learn with repetitions and didn't monitor long-term memory problems. Unlike *cKO* mice, *Cre* mice were not able to learn most probably due to their hyperactivity trait.

In order to verify *lsr* suppression, using *cKO* mice samples versus *WT* samples scarified at 3-months and 13-months, RT-qPCRs were performed to study *lsr* and cholesterol metabolism and transport genes mRNA expression levels. At 3 months, *lsr* mRNA levels were steady in *cKO* mice, when compared to *WT* mice, and were not downregulated. *Lsr* mRNA was even upregulated in the CB (*total lsr* and *lsr β*) and the OB (*lsr β*). The tissues were collected two weeks after TAM induction, it is possible that there was a compensatory expression of LSR in neurons (Morrison & Münzberg 2012). Whether the behavioral phenotype observed is due to suppression of LSR in glia, overexpression of LSR in neurons, or a combination of both is a question that still needs to be answered. Concerning the other genes studied; *abca1*, *hmgcr*, *srebp1*, and *cyp46a1*, only *hmgcr* was upregulated in the CB, where *total lsr* was also upregulated. At 13-months of age, a downregulation of the three subunits of *lsr* was reported in the HIP, a tendency of downregulation in OB, which was significative for *lsr β*. Equally, a downregulation of *abca1* and *srebp1* was seen in HIP. *Lsr* mRNA in *cKO* CB were not downregulated when compared to *WT*, but even upregulated for lsr α'. At the same time, *abca1* and *srebp1* tended to be upregulated in CB of *cKO* mice.

2. Future perspectives

Further behavioral tests at 18 months of age, including Y-maze, three chambered test, and Barnes maze, will be performed in order to detect whether memory-related problems will be aggravated with age.

Our preliminary studies showed that reduced *lsr* mRNA levels were accompanied with lower *abca1* and *srebp1* mRNA levels. This indicates that glial *lsr* supression might downregulate cholesterol synthesis and transport onto lipoproteins. Further studies targeting different apolipoproteins like ApoE and ApoAI, ABC transporters like ABCG1 and ABCG4, regulators like LXR will clarify the mechanism behind such profile. Upon increase of cholesterol levels, LXR is activated where it increases transcription of ABCA1 and activates SREBP1 which induces fatty acids synthesis (Hagen *et al.* 2010; Ru *et al.* 2013). Thus, the downregulation of *abca1* and *srebp1* mRNA expression here might be due to downregulation of *lxr* due to low cholesterol levels. It is possible that glia-specific knockout of LSR caused a downregulation of cholesterol synthesis. It is therefore critical to measure cholesterol and oxysterol levels in *cKO* brain versus *WT* mice, using GC-MS to confirm downregulation of cholesterol levels. In addition, *cKO*

brain tissue sections at different age are gathered. Filipin and red Nile tissue staining will be performed to verify cholesterol accumulation or reduction in membranes and low or high lipid droplets formation in tissues. Ideally, separation of glial and neuronal cells using fluorescence activated cells sorting (FACS) and studying what happens in vivo specifically in glial cells and or neurons in *cKO* mice would render clearer the observed profile. Hopelessly, FACS is hardly usefull for neuron isolation and pure primary neuronal culture can only be achieved on young animal and not in adults. Alternatively, pure glia cell cultures isolated from different brain areas can be performed and should be informative enough to better monitor the regional changes in *lsr* expression

Furthermore, to study the internalization capacity of LSR, we will sacrifice P7 *cKO* and *WT* mice and prepare primary glial cell culture followed by 4-hydroxy TAM induction. Then fluorescent ApoE lipoproteins will be introduced in culture and internalization will be studied using live cell confocal microscopy. In parallel, after in vitro induction of *lsr* suppression from glial cells, the medium will be collected from *cKO* and *WT* glial cultures to study Apo E expression and lipoprotein release.

There are drawbacks of the conditional Cre-lox system, which include laborious breeding and genotyping to obtain enough outbred *cKO* mice, and variable Cre enzyme activity in different regions of the brain, where LSR suppression is not ubiquitous among all glial cells. An efficient and time-saving tool is using the Adeno associated viral vectors (AAV)-based genetic knockout. This allows temporal and conditional knockout of target mice while targeting a specific region of the brain. Ideally, for glial cells, AAV8 with a GFAP promoter before a *Cre* gene specifically injected in a certain region of floxed *lsr* mice's brain, like HIP, at a certain age will allow a better understanding of LSR function in glial cells. We are also interested in developing a neuron-specific *lsr* gene knockout. Using AAV9 with a Ca^{2+}/calmodulin-dependent protein kinase II (CAM kinase II) promoter before *Cre* gene specifically injected in a certain region of floxed *lsr* mice's brain will allow us to study the effect of temporal and conditional knockout of *lsr* gene in neurons of a specific brain region.

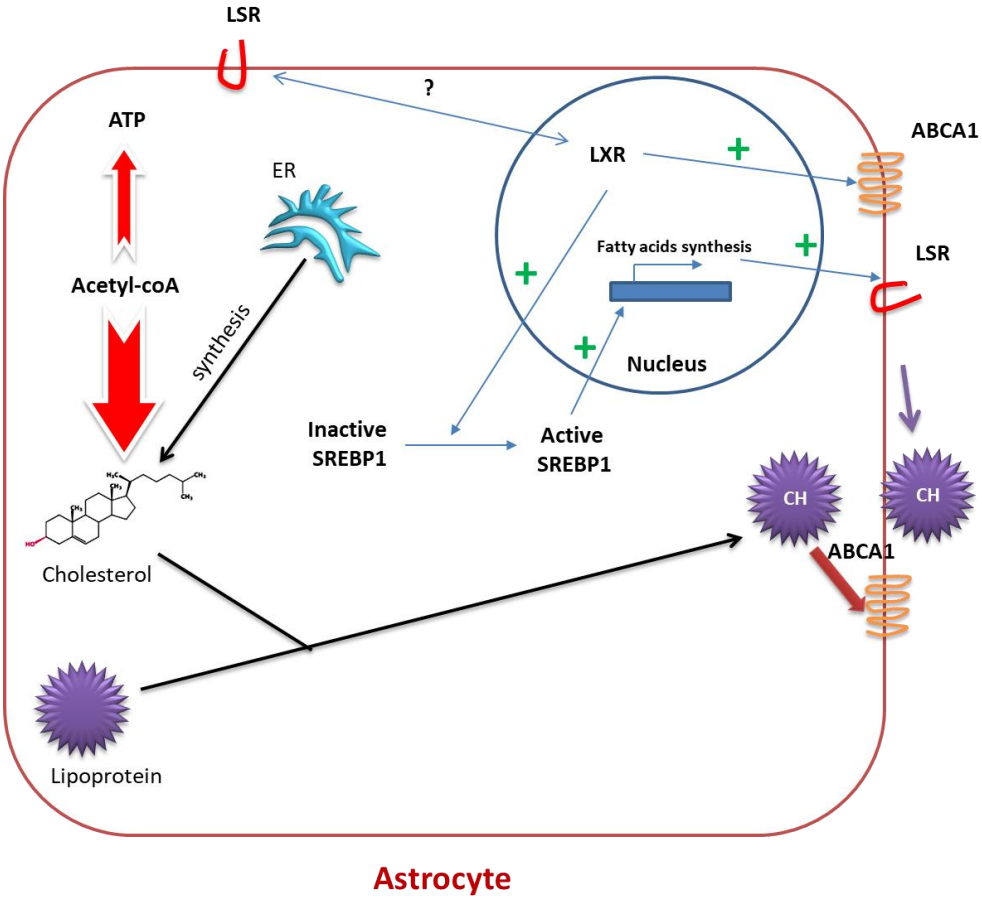

Figure 5.1. Possible function of LSR. LSR possibly activates LXR. LXR activates transcription of lipoprotein transporter ABCA1. In addition, LXR activates SREBP1 activation, active SREBP1 translocate from cytosol to nucleus, where it binds to SRE and induces fatty acids synthesis. LSR is a lipolysis stimulated receptor; it is activated by binding to free fatty acids.

References

Abuznait, A.H. & Kaddoumi, A. (2012) Role of ABC transporters in the pathogenesis of Alzheimer's disease. *ACS Chem Neurosci* **3**, 820–831.

Ade, K.K., Wan, Y., Chen, M., Gloss, B. & Calakos, N. (2011) An Improved BAC Transgenic Fluorescent Reporter Line for Sensitive and Specific Identification of Striatonigral Medium Spiny Neurons. *Front Syst Neurosci* **5**, 32.

Ahmad, N., Girardet, J.-M., Akbar, S., Lanhers, M.-C., Paris, C., Yen, F.T. & Corbier, C. (2012) Lactoferrin and its hydrolysate bind directly to the oleate-activated form of the lipolysis stimulated lipoprotein receptor. *FEBS J* **279**, 4361–4373.

Akbar, S., Pinçon, A., Lanhers, M.-C., Claudepierre, T., Corbier, C., Gregory-Pauron, L., Malaplate-Armand, C., Visvikis, A., Oster, T. & Yen, F.T. (2016) Expression profile of hepatic genes related to lipid homeostasis in LSR heterozygous mice contributes to their increased response to high-fat diet. *Physiological Genomics* **48**, 928–935.

Andersson, M., Elmberger, P.G., Edlund, C., Kristensson, K. & Dallner, G. (1990) Rates of cholesterol, ubiquinone, dolichol and dolichyl-P biosynthesis in rat brain slices. *FEBS Lett* **269**, 15–18.

Apfel, R., Benbrook, D., Lernhardt, E., Ortiz, M.A., Salbert, G. & Pfahl, M. (1994) A novel orphan receptor specific for a subset of thyroid hormone-responsive elements and its interaction with the retinoid/thyroid hormone receptor subfamily. *Mol Cell Biol* **14**, 7025–7035.

Aranda, P.S., LaJoie, D.M. & Jorcyk, C.L. (2012) Bleach gel: a simple agarose gel for analyzing RNA quality. *Electrophoresis* **33**, 366–369.

Arnsten, A.F.T. (2011) Catecholamine Influences on Dorsolateral Prefrontal Cortical Networks. *Biol Psychiatry* **69**, e89–e99.

Baeta-Corral, R. & Giménez-Llort, L. (2015) Persistent hyperactivity and distinctive strategy features in the Morris water maze in 3xTg-AD mice at advanced stages of disease. *Behav Neurosci* **129**, 129–137.

Balazs, Z., Panzenboeck, U., Hammer, A., Sovic, A., Quehenberger, O., Malle, E. & Sattler, W. (2004) Uptake and transport of high-density lipoprotein (HDL) and HDL-associated alpha-tocopherol by an in vitro blood-brain barrier model. *J Neurochem* **89**, 939–950.

Bales, K.R., Du, Y., Holtzman, D., Cordell, B. & Paul, S.M. (2000) Neuroinflammation and Alzheimer's disease: critical roles for cytokine/Abeta-induced glial activation, NF-kappaB, and apolipoprotein E. *Neurobiol Aging* **21**, 427–432; discussion 451-453.

Baranowski, M. (2008) Biological role of liver X receptors. *J Physiol Pharmacol* **59 Suppl 7**, 31–55.

Barnes, C.A. (1979) Memory deficits associated with senescence: a neurophysiological and behavioral study in the rat. *J Comp Physiol Psychol* **93**, 74–104.

Barrett, P.J., Song, Y., Van Horn, W.D., Hustedt, E.J., Schafer, J.M., Hadziselimovic, A., Beel, A.J. & Sanders, C.R. (2012) The amyloid precursor protein has a flexible transmembrane domain and binds cholesterol. *Science* **336**, 1168–1171.

Beffert, U., Durudas, A., Weeber, E.J., Stolt, P.C., Giehl, K.M., Sweatt, J.D., Hammer, R.E. & Herz, J. (2006) Functional dissection of Reelin signaling by site-directed disruption of Disabled-1 adaptor binding to apolipoprotein E receptor 2: distinct roles in development and synaptic plasticity. *J Neurosci* **26**, 2041–2052.

Beffert, U., Weeber, E.J., Durudas, A., Qiu, S., Masiulis, I., Sweatt, J.D., Li, W.-P., Adelmann, G., Frotscher, M., Hammer, R.E. & Herz, J. (2005) Modulation of Synaptic Plasticity and Memory by Reelin Involves Differential Splicing of the Lipoprotein Receptor Apoer2. *Neuron* **47**, 567–579.

Belhaj, N., Desor, F., Gleizes, C., Denis, F.M., Arab-Tehrany, E., Soulimani, R. & Linder, M. (2013) Anxiolytic-like effect of a salmon phospholipopeptidic complex composed of polyunsaturated fatty acids and bioactive peptides. *Mar Drugs* **11**, 4294–4317.

Bełtowski, J. & Semczuk, A. (2010) Liver X receptor (LXR) and the reproductive system--a potential novel target for therapeutic intervention. *Pharmacol Rep* **62**, 15–27.

Berg, J.M., Tymoczko, J.L. & Stryer, L. (2002) The Complex Regulation of Cholesterol Biosynthesis Takes Place at Several Levels. *Biochemistry 5th edition*.

Bi, X., Yong, A.P., Zhou, J., Ribak, C.E. & Lynch, G. (2001) Rapid induction of intraneuronal neurofibrillary tangles in apolipoprotein E-deficient mice. *Proc Natl Acad Sci USA* **98**, 8832–8837.

Bihain, B.E. & Yen, F.T. (1992) Free fatty acids activate a high-affinity saturable pathway for degradation of low-density lipoproteins in fibroblasts from a subject homozygous for familial hypercholesterolemia. *Biochemistry* **31**, 4628–4636.

Bihain, B.E. & Yen, F.T. (1998) The lipolysis stimulated receptor: a gene at last. *Curr Opin Lipidol* **9**, 221–224.

Björkhem, I. (2006a) Crossing the barrier: oxysterols as cholesterol transporters and metabolic modulators in the brain. *J Intern Med* **260**, 493–508.

Björkhem, I. (2006b) Crossing the barrier: oxysterols as cholesterol transporters and metabolic modulators in the brain. *J Intern Med* **260**, 493–508.

Björkhem, I., Starck, L., Andersson, U., Lütjohann, D., von Bahr, S., Pikuleva, I., Babiker, A. & Diczfalusy, U. (2001) Oxysterols in the circulation of patients with the Smith-Lemli-Opitz syndrome: abnormal levels of 24S- and 27-hydroxycholesterol. *J Lipid Res* **42**, 366–371.

Björkhem Ingemar & Meaney Steve. (2004) Brain Cholesterol: Long Secret Life Behind a Barrier. *Arteriosclerosis, Thrombosis, and Vascular Biology* **24**, 806–815.

Block, R.C., Dorsey, E.R., Beck, C.A., Brenna, J.T. & Shoulson, I. (2010) Altered cholesterol and fatty acid metabolism in Huntington disease. *J Clin Lipidol* **4**, 17–23.

Boda, E., Pini, A., Hoxha, E., Parolisi, R. & Tempia, F. (2009) Selection of reference genes for quantitative real-time RT-PCR studies in mouse brain. *J Mol Neurosci* **37**, 238–253.

Bodo, C., Fernandes, C. & Krause, M. (2017) Brain specific Lamellipodin knockout results in hyperactivity and increased anxiety of mice. *Sci Rep* **7**, 5365.

Bogdanovic, N., Bretillon, L., Lund, E.G., Diczfalusy, U., Lannfelt, L., Winblad, B., Russell, D.W. & Björkhem, I. (2001) On the turnover of brain cholesterol in patients with Alzheimer's disease. Abnormal induction of the cholesterol-catabolic enzyme CYP46 in glial cells. *Neurosci Lett* **314**, 45–48.

Bohuslavova, R., Dodd, N., Macova, I., Chumak, T., Horak, M., Syka, J., Fritzsch, B. & Pavlinkova, G. (2017) Pax2-Islet1 Transgenic Mice Are Hyperactive and Have Altered Cerebellar Foliation. *Mol Neurobiol* **54**, 1352–1368.

Bojanic, D.D., Tarr, P.T., Gale, G.D., Smith, D.J., Bok, D., Chen, B., Nusinowitz, S., Lövgren-Sandblom, A., Björkhem, I. & Edwards, P.A. (2010a) Differential expression and function of ABCG1 and ABCG4 during development and aging. *J Lipid Res* **51**, 169–181.

Bojanic, D.D., Tarr, P.T., Gale, G.D., Smith, D.J., Bok, D., Chen, B., Nusinowitz, S., Lövgren-Sandblom, A., Björkhem, I. & Edwards, P.A. (2010b) Differential expression and function of ABCG1 and ABCG4 during development and aging. *J Lipid Res* **51**, 169–181.

Borghini, I., Barja, F., Pometta, D. & James, R.W. (1995) Characterization of subpopulations of lipoprotein particles isolated from human cerebrospinal fluid. *Biochim Biophys Acta* **1255**, 192–200.

Boyles, J.K., Pitas, R.E., Wilson, E., Mahley, R.W. & Taylor, J.M. (1985) Apolipoprotein E associated with astrocytic glia of the central nervous system and with nonmyelinating glia of the peripheral nervous system. *J Clin Invest* **76**, 1501–1513.

Brown, M.S. & Goldstein, J.L. (1986) A receptor-mediated pathway for cholesterol homeostasis. *Science* **232**, 34–47.

Brown, M.S., Herz, J. & Goldstein, J.L. (1997) LDL-receptor structure. Calcium cages, acid baths and recycling receptors. *Nature* **388**, 629–630.

Bryleva, E.Y., Rogers, M.A., Chang, C.C.Y., Buen, F., Harris, B.T., Rousselet, E., Seidah, N.G., Oddo, S., LaFerla, F.M., Spencer, T.A., Hickey, W.F. & Chang, T.-Y. (2010) ACAT1 gene ablation increases 24(S)-hydroxycholesterol content in the brain and ameliorates amyloid pathology in mice with AD. *Proc Natl Acad Sci USA* **107**, 3081–3086.

Buttini, M., Masliah, E., Yu, G.-Q., Palop, J.J., Chang, S., Bernardo, A., Lin, C., Wyss-Coray, T., Huang, Y. & Mucke, L. (2010) Cellular Source of Apolipoprotein E4 Determines Neuronal Susceptibility to Excitotoxic Injury in Transgenic Mice. *Am J Pathol* **177**, 563–569.

Chandra, R., Wang, Y., Shahid, R.A., Vigna, S.R., Freedman, N.J. & Liddle, R.A. (2013) Immunoglobulin-like domain containing receptor 1 mediates fat-stimulated cholecystokinin secretion. *J Clin Invest* **123**, 3343–3352.

Charnay, Y., Imhof, A., Vallet, P.G., Hakkoum, D., Lathuiliere, A., Poku, N., Aronow, B., Kovari, E., Bouras, C. & Giannakopoulos, P. (2008) Clusterin expression during fetal and postnatal CNS development in mouse. *Neuroscience* **155**, 714–724.

de Chaves, E.I., Rusiñol, A.E., Vance, D.E., Campenot, R.B. & Vance, J.E. (1997) Role of lipoproteins in the delivery of lipids to axons during axonal regeneration. *J Biol Chem* **272**, 30766–30773.

Chawla, A., Repa, J.J., Evans, R.M. & Mangelsdorf, D.J. (2001) Nuclear receptors and lipid physiology: opening the X-files. *Science* **294**, 1866–1870.

Chen, J., Zhang, X., Kusumo, H., Costa, L.G. & Guizzetti, M. (2013a) Cholesterol efflux is differentially regulated in neurons and astrocytes: implications for brain cholesterol homeostasis. *Biochim Biophys Acta* **1831**, 263–275.

Chen, J., Zhang, X., Kusumo, H., Costa, L.G. & Guizzetti, M. (2013b) Cholesterol efflux is differentially regulated in neurons and astrocytes: implications for brain cholesterol homeostasis. *Biochim Biophys Acta* **1831**, 263–275.

Cheruku, S.R., Xu, Z., Dutia, R., Lobel, P. & Storch, J. (2006) Mechanism of cholesterol transfer from the Niemann-Pick type C2 protein to model membranes supports a role in lysosomal cholesterol transport. *J Biol Chem* **281**, 31594–31604.

Chung, W.-S., Verghese, P.B., Chakraborty, C., Joung, J., Hyman, B.T., Ulrich, J.D., Holtzman, D.M. & Barres, B.A. (2016) Novel allele-dependent role for APOE in controlling the rate of synapse pruning by astrocytes. *Proc Natl Acad Sci USA* **113**, 10186–10191.

Claudel, T., Leibowitz, M.D., Fiévet, C., Tailleux, A., Wagner, B., Repa, J.J., Torpier, G., Lobaccaro, J.-M., Paterniti, J.R., Mangelsdorf, D.J., Heyman, R.A. & Auwerx, J. (2001) Reduction of atherosclerosis in apolipoprotein E knockout mice by activation of the retinoid X receptor. *Proc Natl Acad Sci U S A* **98**, 2610–2615.

Claudepierre, T. & Pfrieger, F.W. (2003a) [New aspects of cholesterol in the central nervous system]. *Med Sci (Paris)* **19**, 601–605.

Claudepierre, T. & Pfrieger, F.W. (2003b) [New aspects of cholesterol in the central nervous system]. *Med Sci (Paris)* **19**, 601–605.

Daneman, R., Zhou, L., Agalliu, D., Cahoy, J.D., Kaushal, A. & Barres, B.A. (2010) The mouse blood-brain barrier transcriptome: a new resource for understanding the development and function of brain endothelial cells. *PLoS ONE* **5**, e13741.

D'Arcangelo, G., Homayouni, R., Keshvara, L., Rice, D.S., Sheldon, M. & Curran, T. (1999) Reelin is a ligand for lipoprotein receptors. *Neuron* **24**, 471–479.

Davidsson, P., Hulthe, J., Fagerberg, B. & Camejo, G. (2010) Proteomics of apolipoproteins and associated proteins from plasma high-density lipoproteins. *Arterioscler Thromb Vasc Biol* **30**, 156–163.

Davies, J.P. & Ioannou, Y.A. (2000) Topological analysis of Niemann-Pick C1 protein reveals that the membrane orientation of the putative sterol-sensing domain is identical to those of 3-hydroxy-3-methylglutaryl-CoA reductase and sterol regulatory element binding protein cleavage-activating protein. *J Biol Chem* **275**, 24367–24374.

DeBose-Boyd, R.A., Brown, M.S., Li, W.P., Nohturfft, A., Goldstein, J.L. & Espenshade, P.J. (1999) Transport-dependent proteolysis of SREBP: relocation of site-1 protease from Golgi to ER obviates the need for SREBP transport to Golgi. *Cell* **99**, 703–712.

DeGrella, R.F. & Simoni, R.D. (1982) Intracellular transport of cholesterol to the plasma membrane. *J Biol Chem* **257**, 14256–14262.

DeMattos, R.B., Brendza, R.P., Heuser, J.E., Kierson, M., Cirrito, J.R., Fryer, J., Sullivan, P.M., Fagan, A.M., Han, X. & Holtzman, D.M. (2001) Purification and characterization of astrocyte-secreted apolipoprotein E and J-containing lipoproteins from wild-type and human apoE transgenic mice. *Neurochem Int* **39**, 415–425.

Di Paolo, G. & Kim, T.-W. (2011) Linking lipids to Alzheimer's disease: cholesterol and beyond. *Nat Rev Neurosci* **12**, 284–296.

Díaz, M., Fabelo, N., Ferrer, I. & Marín, R. (2018) "Lipid raft aging" in the human frontal cortex during nonpathological aging: gender influences and potential implications in Alzheimer's disease. *Neurobiol Aging* **67**, 42–52.

Didic, M., Felician, O., Barbeau, E.J., Mancini, J., Latger-Florence, C., Tramoni, E. & Ceccaldi, M. (2013) Impaired visual recognition memory predicts Alzheimer's disease in amnestic mild cognitive impairment. *Dement Geriatr Cogn Disord* **35**, 291–299.

Dietschy, J.M. & Turley, S.D. (2001) Cholesterol metabolism in the brain. *Curr Opin Lipidol* **12**, 105–112.

Djelti, F. (2013) *Toxicité neuronale du cholestérol et physiopathologie de la maladie d'Alzheimer : analyse in vivo des conséquences de l'inhibition de la cholestérol-24-hydroxylase*. thesis, Paris 5.

Djelti, F., Braudeau, J., Hudry, E., Dhenain, M., Varin, J., Bièche, I., Marquer, C., Chali, F., Ayciriex, S., Auzeil, N., Alves, S., Langui, D., Potier, M.-C., Laprevote, O., Vidaud, M., Duyckaerts, C., Miles, R., Aubourg, P. & Cartier, N. (2015) CYP46A1 inhibition, brain cholesterol accumulation and neurodegeneration pave the way for Alzheimer's disease. *Brain* **138**, 2383–2398.

Dokmanovic-Chouinard, M., Chung, W.K., Chevre, J.-C., Watson, E., Yonan, J., Wiegand, B., Bromberg, Y., Wakae, N., Wright, C.V., Overton, J., Ghosh, S., Sathe, G.M., Ammala, C.E., Brown, K.K., Ito, R., LeDuc, C., Solomon, K., Fischer, S.G. & Leibel, R.L. (2008) Positional Cloning of "Lisch-like", a Candidate Modifier of Susceptibility to Type 2 Diabetes in Mice. *PLoS Genet* **4**.

Dumanis, S.B., Cha, H.-J., Song, J.M., Trotter, J.H., Spitzer, M., Lee, J.-Y., Weeber, E.J., Turner, R.S., Pak, D.T.S., Rebeck, G.W. & Hoe, H.-S. (2011) ApoE receptor 2 regulates synapse and dendritic spine formation. *PLoS ONE* **6**, e17203.

Ehehalt, R., Keller, P., Haass, C., Thiele, C. & Simons, K. (2003) Amyloidogenic processing of the Alzheimer beta-amyloid precursor protein depends on lipid rafts. *J Cell Biol* **160**, 113–123.

Eichinger, A., Nasreen, A., Kim, H.J. & Skerra, A. (2007) Structural insight into the dual ligand specificity and mode of high density lipoprotein association of apolipoprotein D. *J Biol Chem* **282**, 31068–31075.

Eisenstein, M. (2011) Genetics: finding risk factors. *Nature* **475**, S20-22.

El Hajj, A., Yen, F.T., Oster, T., Malaplate, C., Pauron, L., Corbier, C., Lanhers, M.-C. & Claudepierre, T. (2019) Age-related changes in regiospecific expression of Lipolysis Stimulated Receptor (LSR) in mice brain. *PLOS ONE* **14**, e0218812.

Elder, G.A., Ragnauth, A., Dorr, N., Franciosi, S., Schmeidler, J., Haroutunian, V. & Buxbaum, J.D. (2008) Increased locomotor activity in mice lacking the low-density lipoprotein receptor. *Behav Brain Res* **191**, 256–265.

Elhabazi, K., Dicko, A., Desor, F., Dalal, A., Younos, C. & Soulimani, R. (2006) Preliminary study on immunological and behavioural effects of Thymus broussonetii Boiss., an endemic species in Morocco. *J Ethnopharmacol* **103**, 413–419.

Elliott, D.A., Weickert, C.S. & Garner, B. (2010) Apolipoproteins in the brain: implications for neurological and psychiatric disorders. *Clin Lipidol* **51**, 555–573.

El-Sayed, A. & Harashima, H. (2013) Endocytosis of Gene Delivery Vectors: From Clathrin-dependent to Lipid Raft-mediated Endocytosis. *Molecular Therapy* **21**, 1118–1130.

Elshourbagy, N.A., Boguski, M.S., Liao, W.S., Jefferson, L.S., Gordon, J.I. & Taylor, J.M. (1985) Expression of rat apolipoprotein A-IV and A-I genes: mRNA induction during development and in response to glucocorticoids and insulin. *PNAS* **82**, 8242–8246.

Espenshade, P.J. & Hughes, A.L. (2007) Regulation of sterol synthesis in eukaryotes. *Annu Rev Genet* **41**, 401–427.

Fagan, A.M., Bu, G., Sun, Y., Daugherty, A. & Holtzman, D.M. (1996) Apolipoprotein E-containing high density lipoprotein promotes neurite outgrowth and is a ligand for the low density lipoprotein receptor-related protein. *J Biol Chem* **271**, 30121–30125.

Fagan, A.M. & Holtzman, D.M. (2000) Astrocyte lipoproteins, effects of apoE on neuronal function, and role of apoE in amyloid-beta deposition in vivo. *Microsc Res Tech* **50**, 297–304.

Fagan, A.M., Holtzman, D.M., Munson, G., Mathur, T., Schneider, D., Chang, L.K., Getz, G.S., Reardon, C.A., Lukens, J., Shah, J.A. & LaDu, M.J. (1999) Unique

Lipoproteins Secreted by Primary Astrocytes From Wild Type, apoE (−/−), and Human apoE Transgenic Mice. *J Biol Chem* **274**, 30001–30007.

Fagan, A.M., Murphy, B.A., Patel, S.N., Kilbridge, J.F., Mobley, W.C., Bu, G. & Holtzman, D.M. (1998) Evidence for normal aging of the septo-hippocampal cholinergic system in apoE (-/-) mice but impaired clearance of axonal degeneration products following injury. *Exp Neurol* **151**, 314–325.

Fan, Q.W., Iosbe, I., Asou, H., Yanagisawa, K. & Michikawa, M. (2001) Expression and regulation of apolipoprotein E receptors in the cells of the central nervous system in culture: A review. *J Am Aging Assoc* **24**, 1–10.

Faure, A., Verret, L., Bozon, B., El Tannir El Tayara, N., Ly, M., Kober, F., Dhenain, M., Rampon, C. & Delatour, B. (2011) Impaired neurogenesis, neuronal loss, and brain functional deficits in the APPxPS1-Ki mouse model of Alzheimer's disease. *Neurobiol Aging* **32**, 407–418.

Fester, L., Zhou, L., Bütow, A., Huber, C., von Lossow, R., Prange-Kiel, J., Jarry, H. & Rune, G.M. (2009) Cholesterol-promoted synaptogenesis requires the conversion of cholesterol to estradiol in the hippocampus. *Hippocampus* **19**, 692–705.

Filali, M., Lalonde, R. & Rivest, S. (2011) Anomalies in social behaviors and exploratory activities in an APPswe/PS1 mouse model of Alzheimer's disease. *Physiol Behav* **104**, 880–885.

Fleming, S.M., Tetreault, N.A., Mulligan, C.K., Hutson, C.B., Masliah, E. & Chesselet, M.-F. (2008) Olfactory deficits in mice overexpressing human wildtype alpha-synuclein. *Eur J Neurosci* **28**, 247–256.

Frank, C., Rufini, S., Tancredi, V., Forcina, R., Grossi, D. & D'Arcangelo, G. (2008) Cholesterol depletion inhibits synaptic transmission and synaptic plasticity in rat hippocampus. *Exp Neurol* **212**, 407–414.

Fryer, J.D., Demattos, R.B., McCormick, L.M., O'Dell, M.A., Spinner, M.L., Bales, K.R., Paul, S.M., Sullivan, P.M., Parsadanian, M., Bu, G. & Holtzman, D.M. (2005) The low density lipoprotein receptor regulates the level of central nervous system human and murine apolipoprotein E but does not modify amyloid plaque pathology in PDAPP mice. *J Biol Chem* **280**, 25754–25759.

Fujiyoshi, M., Tachikawa, M., Ohtsuki, S., Ito, S., Uchida, Y., Akanuma, S.-I., Kamiie, J., Hashimoto, T., Hosoya, K.-I., Iwatsubo, T. & Terasaki, T. (2011) Amyloid-β peptide(1-40) elimination from cerebrospinal fluid involves low-density lipoprotein receptor-related protein 1 at the blood-cerebrospinal fluid barrier. *J Neurochem* **118**, 407–415.

Fukumoto, H., Deng, A., Irizarry, M.C., Fitzgerald, M.L. & Rebeck, G.W. (2002) Induction of the cholesterol transporter ABCA1 in central nervous system cells

by liver X receptor agonists increases secreted Abeta levels. *J Biol Chem* **277**, 48508–48513.

Fullerton, S.M., Strittmatter, W.J. & Matthew, W.D. (1998) Peripheral sensory nerve defects in apolipoprotein E knockout mice. *Exp Neurol* **153**, 156–163.

Fünfschilling, U., Jockusch, W.J., Sivakumar, N., Möbius, W., Corthals, K., Li, S., Quintes, S., Kim, Y., Schaap, I.A.T., Rhee, J.-S., Nave, K.-A. & Saher, G. (2012) Critical time window of neuronal cholesterol synthesis during neurite outgrowth. *J Neurosci* **32**, 7632–7645.

Fünfschilling, U., Saher, G., Xiao, L., Möbius, W. & Nave, K.-A. (2007) Survival of adult neurons lacking cholesterol synthesis in vivo. *BMC Neurosci* **8**, 1.

Gamba, P., Guglielmotto, M., Testa, G., Monteleone, D., Zerbinati, C., Gargiulo, S., Biasi, F., Iuliano, L., Giaccone, G., Mauro, A., Poli, G., Tamagno, E. & Leonarduzzi, G. (2014) Up-regulation of β-amyloidogenesis in neuron-like human cells by both 24- and 27-hydroxycholesterol: protective effect of N-acetyl-cysteine. *Aging Cell* **13**, 561–572.

Gamba, P., Staurenghi, E., Testa, G., Giannelli, S., Sottero, B. & Leonarduzzi, G. (2019) A Crosstalk Between Brain Cholesterol Oxidation and Glucose Metabolism in Alzheimer's Disease. *Front Neurosci* **13**.

Garza, J.C., Guo, M., Zhang, W. & Lu, X.-Y. (2008) Leptin increases adult hippocampal neurogenesis in vivo and in vitro. *J Biol Chem* **283**, 18238–18247.

Gelissen, I.C., Hochgrebe, T., Wilson, M.R., Easterbrook-Smith, S.B., Jessup, W., Dean, R.T. & Brown, A.J. (1998) Apolipoprotein J (clusterin) induces cholesterol export from macrophage-foam cells: a potential anti-atherogenic function? *Biochem J* **331**, 231–237.

Goldstein, J.L., DeBose-Boyd, R.A. & Brown, M.S. (2006) Protein sensors for membrane sterols. *Cell* **124**, 35–46.

Gong, Y., Lee, J.N., Lee, P.C.W., Goldstein, J.L., Brown, M.S. & Ye, J. (2006) Sterol-regulated ubiquitination and degradation of Insig-1 creates a convergent mechanism for feedback control of cholesterol synthesis and uptake. *Cell Metab* **3**, 15–24.

Goritz, C., Mauch, D.H. & Pfrieger, F.W. (2005) Multiple mechanisms mediate cholesterol-induced synaptogenesis in a CNS neuron. *Mol Cell Neurosci* **29**, 190–201.

Goti, D., Hrzenjak, A., Levak-Frank, S., Frank, S., van der Westhuyzen, D.R., Malle, E. & Sattler, W. (2001) Scavenger receptor class B, type I is expressed in

porcine brain capillary endothelial cells and contributes to selective uptake of HDL-associated vitamin E. *J Neurochem* **76**, 498–508.

Grimm, M.O.W., Rothhaar, T.L. & Hartmann, T. (2012) The role of APP proteolytic processing in lipid metabolism. *Exp Brain Res* **217**, 365–375.

Hagen, R.M., Rodriguez-Cuenca, S. & Vidal-Puig, A. (2010) An allostatic control of membrane lipid composition by SREBP1. *FEBS Letters*, Gothenburg Special Issue: Molecules of Life **584**, 2689–2698.

Han, B.H., DeMattos, R.B., Dugan, L.L., Kim-Han, J.S., Brendza, R.P., Fryer, J.D., Kierson, M., Cirrito, J., Quick, K., Harmony, J.A., Aronow, B.J. & Holtzman, D.M. (2001) Clusterin contributes to caspase-3-independent brain injury following neonatal hypoxia-ischemia. *Nat Med* **7**, 338–343.

Hao, M. & Maxfield, F.R. (2000) Characterization of rapid membrane internalization and recycling. *J Biol Chem* **275**, 15279–15286.

Harris, F.M., Tesseur, I., Brecht, W.J., Xu, Q., Mullendorff, K., Chang, S., Wyss-Coray, T., Mahley, R.W. & Huang, Y. (2004) Astroglial Regulation of Apolipoprotein E Expression in Neuronal Cells IMPLICATIONS FOR ALZHEIMER'S DISEASE. *J Biol Chem* **279**, 3862–3868.

Harrison, L., Schriever, S.C., Feuchtinger, A., Kyriakou, E., Baumann, P., Pfuhlmann, K., Messias, A.C., Walch, A., Tschöp, M.H. & Pfluger, P.T. (2019) Fluorescent blood–brain barrier tracing shows intact leptin transport in obese mice. *International Journal of Obesity* **43**, 1305.

Hawes, C.M., Wiemer, H., Krueger, S.R. & Karten, B. (2010) Pre-synaptic defects of NPC1-deficient hippocampal neurons are not directly related to plasma membrane cholesterol. *J Neurochem* **114**, 311–322.

Hayashi, H., Campenot, R.B., Vance, D.E. & Vance, J.E. (2007) Apolipoprotein E-containing lipoproteins protect neurons from apoptosis via a signaling pathway involving low-density lipoprotein receptor-related protein-1. *J Neurosci* **27**, 1933–1941.

Heino, S., Lusa, S., Somerharju, P., Ehnholm, C., Olkkonen, V.M. & Ikonen, E. (2000) Dissecting the role of the Golgi complex and lipid rafts in biosynthetic transport of cholesterol to the cell surface. *Proc Natl Acad Sci U S A* **97**, 8375–8380.

Herbsleb, M., Birkenkamp-Demtroder, K., Thykjaer, T., Wiuf, C., Hein, A.-M.K., Orntoft, T.F. & Dyrskjøt, L. (2008) Increased cell motility and invasion upon knockdown of lipolysis stimulated lipoprotein receptor (LSR) in SW780 bladder cancer cells. *BMC Med Genomics* **1**, 31.

Herz, J. (2009) Apolipoprotein E receptors in the nervous system. *Curr Opin Lipidol* **20**, 190–196.

Herz, J. & Chen, Y. (2006) Reelin, lipoprotein receptors and synaptic plasticity. *Nat Rev Neurosci* **7**, 850–859.

Herz, J., Clouthier, D.E. & Hammer, R.E. (1992) LDL receptor-related protein internalizes and degrades uPA-PAI-1 complexes and is essential for embryo implantation. *Cell* **71**, 411–421.

Hicks, D.A., Nalivaeva, N.N. & Turner, A.J. (2012) Lipid Rafts and Alzheimer's Disease: Protein-Lipid Interactions and Perturbation of Signaling. *Front Physiol* **3**.

Hirsch-Reinshagen, V., Zhou, S., Burgess, B.L., Bernier, L., McIsaac, S.A., Chan, J.Y., Tansley, G.H., Cohn, J.S., Hayden, M.R. & Wellington, C.L. (2004) Deficiency of ABCA1 impairs apolipoprotein E metabolism in brain. *J Biol Chem* **279**, 41197–41207.

Hoe, H.-S., Pocivavsek, A., Chakraborty, G., Fu, Z., Vicini, S., Ehlers, M.D. & Rebeck, G.W. (2006) Apolipoprotein E receptor 2 interactions with the N-methyl-D-aspartate receptor. *J Biol Chem* **281**, 3425–3431.

Hornick, C.A., Hui, D.Y. & DeLamatre, J.G. (1997) A role for retrosomes in intracellular cholesterol transport from endosomes to the plasma membrane. *Am J Physiol* **273**, C1075-1081.

Horton, J.D., Goldstein, J.L. & Brown, M.S. (2002) SREBPs: activators of the complete program of cholesterol and fatty acid synthesis in the liver. *J Clin Invest* **109**, 1125–1131.

Huang, Z., Cheng, C., Jiang, L., Yu, Z., Cao, F., Zhong, J., Guo, Z. & Sun, X. (2016) Intraventricular apolipoprotein ApoJ infusion acts protectively in Traumatic Brain Injury. *J Neurochem* **136**, 1017–1025.

Ignatius, M.J., Gebicke-Härter, P.J., Skene, J.H., Schilling, J.W., Weisgraber, K.H., Mahley, R.W. & Shooter, E.M. (1986) Expression of apolipoprotein E during nerve degeneration and regeneration. *Proc Natl Acad Sci USA* **83**, 1125–1129.

Ikonen, E. (2008) Cellular cholesterol trafficking and compartmentalization. *Nat Rev Mol Cell Biol* **9**, 125–138.

Imhof, A., Charnay, Y., Vallet, P.G., Aronow, B., Kovari, E., French, L.E., Bouras, C. & Giannakopoulos, P. (2006) Sustained astrocytic clusterin expression improves remodeling after brain ischemia. *Neurobiol Dis* **22**, 274–283.

Indra, A.K., Warot, X., Brocard, J., Bornert, J.M., Xiao, J.H., Chambon, P. & Metzger, D. (1999) Temporally-controlled site-specific mutagenesis in the basal layer of the epidermis: comparison of the recombinase activity of the tamoxifen-inducible Cre-ER(T) and Cre-ER(T2) recombinases. *Nucleic Acids Res* **27**, 4324–4327.

Iwamoto, N., Higashi, T. & Furuse, M. (2014) Localization of angulin-1/LSR and tricellulin at tricellular contacts of brain and retinal endothelial cells in vivo. *Cell Struct Funct* **39**, 1–8.

Jahn, H. (2013) Memory loss in Alzheimer's disease. *Dialogues Clin Neurosci* **15**, 445–454.

Jeske, D.J. & Dietschy, J.M. (1980) Regulation of rates of cholesterol synthesis in vivo in the liver and carcass of the rat measured using [3H]water. *J Lipid Res* **21**, 364–376.

Joyce, C.W., Shelness, G.S., Davis, M.A., Lee, R.G., Skinner, K., Anderson, R.A. & Rudel, L.L. (2000) ACAT1 and ACAT2 membrane topology segregates a serine residue essential for activity to opposite sides of the endoplasmic reticulum membrane. *Mol Biol Cell* **11**, 3675–3687.

Kaplan, M.R. & Simoni, R.D. (1985) Transport of cholesterol from the endoplasmic reticulum to the plasma membrane. *J Cell Biol* **101**, 446–453.

Karasinska, J.M., Rinninger, F., Lütjohann, D., Ruddle, P., Franciosi, S., Kruit, J.K., Singaraja, R.R., Hirsch-Reinshagen, V., Fan, J., Brunham, L.R., Bissada, N., Ramakrishnan, R., Wellington, C.L., Parks, J.S. & Hayden, M.R. (2009) Specific loss of brain ABCA1 increases brain cholesterol uptake and influences neuronal structure and function. *J Neurosci* **29**, 3579–3589.

Karten, B., Campenot, R.B., Vance, D.E. & Vance, J.E. (2006) The Niemann-Pick C1 protein in recycling endosomes of presynaptic nerve terminals. *J Lipid Res* **47**, 504–514.

Karten, B., Vance, D.E., Campenot, R.B. & Vance, J.E. (2002) Cholesterol accumulates in cell bodies, but is decreased in distal axons, of Niemann-Pick C1-deficient neurons. *J Neurochem* **83**, 1154–1163.

Karten, B., Vance, D.E., Campenot, R.B. & Vance, J.E. (2003) Trafficking of cholesterol from cell bodies to distal axons in Niemann Pick C1-deficient neurons. *J Biol Chem* **278**, 4168–4175.

Katzman, M.A. & Sternat, T. (2014) A Review of OROS Methylphenidate (Concerta®) in the Treatment of Attention-Deficit/Hyperactivity Disorder. *CNS Drugs* **28**, 1005–1033.

Kawas, C.H., Corrada, M.M., Brookmeyer, R., Morrison, A., Resnick, S.M., Zonderman, A.B. & Arenberg, D. (2003) Visual memory predicts Alzheimer's disease more than a decade before diagnosis. *Neurology* **60**, 1089–1093.

Kennedy, M.A., Barrera, G.C., Nakamura, K., Baldán, A., Tarr, P., Fishbein, M.C., Frank, J., Francone, O.L. & Edwards, P.A. (2005) ABCG1 has a critical role in mediating cholesterol efflux to HDL and preventing cellular lipid accumulation. *Cell Metab* **1**, 121–131.

Kim, J., Castellano, J.M., Jiang, H., Basak, J.M., Parsadanian, M., Pham, V., Mason, S.M., Paul, S.M. & Holtzman, D.M. (2009a) Overexpression of low-density lipoprotein receptor in the brain markedly inhibits amyloid deposition and increases extracellular A beta clearance. *Neuron* **64**, 632–644.

Kim, W.S., Rahmanto, A.S., Kamili, A., Rye, K.-A., Guillemin, G.J., Gelissen, I.C., Jessup, W., Hill, A.F. & Garner, B. (2007) Role of ABCG1 and ABCA1 in regulation of neuronal cholesterol efflux to apolipoprotein E discs and suppression of amyloid-beta peptide generation. *J Biol Chem* **282**, 2851–2861.

Kim, W.S., Weickert, C.S. & Garner, B. (2008) Role of ATP-binding cassette transporters in brain lipid transport and neurological disease. *J Neurochem* **104**, 1145–1166.

Kim, W.S., Wong, J., Weickert, C.S., Webster, M.J., Bahn, S. & Garner, B. (2009) Apolipoprotein-D expression is increased during development and maturation of the human prefrontal cortex. *J Neurochem* **109**, 1053–1066.

Kirova, A.-M., Bays, R.B. & Lagalwar, S. (2015) Working Memory and Executive Function Decline across Normal Aging, Mild Cognitive Impairment, and Alzheimer's Disease. *Biomed Res Int* **2015**.

Klein, R.C., Mace, B.E., Moore, S.D. & Sullivan, P.M. (2010) Progressive loss of synaptic integrity in human apolipoprotein E4 targeted replacement mice and attenuation by apolipoprotein E2. *Neuroscience* **171**, 1265–1272.

Knoferle, J., Yoon, S.Y., Walker, D., Leung, L., Gillespie, A.K., Tong, L.M., Bien-Ly, N. & Huang, Y. (2014) Apolipoprotein E4 Produced in GABAergic Interneurons Causes Learning and Memory Deficits in Mice. *J Neurosci* **34**, 14069–14078.

Koch, S., Donarski, N., Goetze, K., Kreckel, M., Stuerenburg, H.J., Buhmann, C. & Beisiegel, U. (2001) Characterization of four lipoprotein classes in human cerebrospinal fluid. *J Lipid Res* **42**, 1143–1151.

Koenigs, M. & Grafman, J. (2009) The functional neuroanatomy of depression: distinct roles for ventromedial and dorsolateral prefrontal cortex. *Behav Brain Res* **201**, 239–243.

Kojro, E., Gimpl, G., Lammich, S., Marz, W. & Fahrenholz, F. (2001) Low cholesterol stimulates the nonamyloidogenic pathway by its effect on the alpha -secretase ADAM 10. *Proc Natl Acad Sci USA* **98**, 5815–5820.

Korade, Z. & Kenworthy, A.K. (2008) Lipid rafts, cholesterol, and the brain. *Neuropharmacology* **55**, 1265–1273.

Korade, Z., Xu, L., Shelton, R. & Porter, N.A. (2010) Biological activities of 7-dehydrocholesterol-derived oxysterols: implications for Smith-Lemli-Opitz syndrome. *J Lipid Res* **51**, 3259–3269.

Kosacka, J., Gericke, M., Nowicki, M., Kacza, J., Borlak, J. & Spanel-Borowski, K. (2009) Apolipoproteins D and E3 exert neurotrophic and synaptogenic effects in dorsal root ganglion cell cultures. *Neuroscience* **162**, 282–291.

LaDu, M.J., Falduto, M.T., Manelli, A.M., Reardon, C.A., Getz, G.S. & Frail, D.E. (1994) Isoform-specific binding of apolipoprotein E to beta-amyloid. *J Biol Chem* **269**, 23403–23406.

Ladu, M.J., Reardon, C., Van Eldik, L., Fagan, A.M., Bu, G., Holtzman, D. & Getz, G.S. (2000) Lipoproteins in the central nervous system. *Ann N Y Acad Sci* **903**, 167–175.

Lange, Y., Ye, J., Rigney, M. & Steck, T.L. (1999) Regulation of endoplasmic reticulum cholesterol by plasma membrane cholesterol. *J Lipid Res* **40**, 2264–2270.

Ledesma, M.D., Martin, M.G. & Dotti, C.G. (2012) Lipid changes in the aged brain: effect on synaptic function and neuronal survival. *Prog Lipid Res* **51**, 23–35.

Lee, C.Y.D., Tse, W., Smith, J.D. & Landreth, G.E. (2012) Apolipoprotein E promotes β-amyloid trafficking and degradation by modulating microglial cholesterol levels. *J Biol Chem* **287**, 2032–2044.

Leger, M., Quiedeville, A., Bouet, V., Haelewyn, B., Boulouard, M., Schumann-Bard, P. & Freret, T. (2013) Object recognition test in mice. *Nature Protocols* **8**, 2531–2537.

Leoni, V., Mariotti, C., Nanetti, L., Salvatore, E., Squitieri, F., Bentivoglio, A.R., Bandettini di Poggio, M., Bandettini Del Poggio, M., Piacentini, S., Monza, D., Valenza, M., Cattaneo, E. & Di Donato, S. (2011) Whole body cholesterol metabolism is impaired in Huntington's disease. *Neurosci Lett* **494**, 245–249.

Leoni, V., Solomon, A. & Kivipelto, M. (2010) Links between ApoE, brain cholesterol metabolism, tau and amyloid beta-peptide in patients with cognitive impairment. *Biochem Soc Trans* **38**, 1021–1025.

Leoni, V., Solomon, A., Lövgren-Sandblom, A., Minthon, L., Blennow, K., Hansson, O., Wahlund, L.-O., Kivipelto, M. & Björkhem, I. (2013) Diagnostic power of 24S-hydroxycholesterol in cerebrospinal fluid: candidate marker of brain health. *J Alzheimers Dis* **36**, 739–747.

Leuner, B. & Gould, E. (2010) Structural Plasticity and Hippocampal Function. *Annu Rev Psychol* **61**, 111-C3.

Levi, O., Lütjohann, D., Devir, A., von Bergmann, K., Hartmann, T. & Michaelson, D.M. (2005) Regulation of hippocampal cholesterol metabolism by apoE and environmental stimulation. *J Neurochem* **95**, 987–997.

Lewis, D.A. & Gonzalez-Burgos, G. (2006) Pathophysiologically based treatment interventions in schizophrenia. *Nat Med* **12**, 1016–1022.

Li, M. & Snider, B.J. (2018) Chapter 1 - Gene Therapy Methods and Their Applications in Neurological Disorders. In Li, M. & Snider, B.J. (eds), *Gene Therapy in Neurological Disorders*, Academic Press, pp. 3–39.

Li, Y., Lu, W., Marzolo, M.P. & Bu, G. (2001) Differential Functions of Members of the Low Density Lipoprotein Receptor Family Suggested by Their Distinct Endocytosis Rates. *J Biol Chem* **276**, 18000–18006.

Liang, W.S., Chen, K., Lee, W., Sidhar, K., Corneveaux, J.J., Allen, A.N., Myers, A., Villa, S., Meechoovet, B., Pruzin, J., Bandy, D., Fleisher, A.S., Langbaum, J.B.S., Huentelman, M.J., Jensen, K., Dunckley, T., Caselli, R.J., Kaib, S. & Reiman, E.M. (2011) Association between GAB2 haplotype and higher glucose metabolism in Alzheimer's disease-affected brain regions in cognitively normal APOEε4 carriers. *Neuroimage* **54**, 1896–1902.

Liang, Y., Pertzov, Y., Nicholas, J.M., Henley, S.M.D., Crutch, S., Woodward, F., Leung, K., Fox, N.C. & Husain, M. (2016) Visual short-term memory binding deficit in familial Alzheimer's disease. *Cortex* **78**, 150–164.

Linetti, A., Fratangeli, A., Taverna, E., Valnegri, P., Francolini, M., Cappello, V., Matteoli, M., Passafaro, M. & Rosa, P. (2010) Cholesterol reduction impairs exocytosis of synaptic vesicles. *J Cell Sci* **123**, 595–605.

Linton, M.F., Gish, R., Hubl, S.T., Bütler, E., Esquivel, C., Bry, W.I., Boyles, J.K., Wardell, M.R. & Young, S.G. (1991) Phenotypes of apolipoprotein B and apolipoprotein E after liver transplantation. *J Clin Invest* **88**, 270–281.

Liscum, L. & Munn, N.J. (1999) Intracellular cholesterol transport. *Biochim Biophys Acta* **1438**, 19–37.

Liu, B., Turley, S.D., Burns, D.K., Miller, A.M., Repa, J.J. & Dietschy, J.M. (2009) Reversal of defective lysosomal transport in NPC disease ameliorates liver

dysfunction and neurodegeneration in the npc1-/- mouse. *Proc Natl Acad Sci USA* **106**, 2377–2382.

Liu, C.-C., Hu, J., Zhao, N., Wang, J., Wang, N., Cirrito, J.R., Kanekiyo, T., Holtzman, D.M. & Bu, G. (2017) Astrocytic LRP1 Mediates Brain Aβ Clearance and Impacts Amyloid Deposition. *J Neurosci* **37**, 4023–4031.

Liu, C.-C., Kanekiyo, T., Xu, H. & Bu, G. (2013) Apolipoprotein E and Alzheimer disease: risk, mechanisms, and therapy. *Nature reviews Neurology* **9**, 106.

Liu, Q., Trotter, J., Zhang, J., Peters, M.M., Cheng, H., Bao, J., Han, X., Weeber, E.J. & Bu, G. (2010) Neuronal LRP1 knockout in adult mice leads to impaired brain lipid metabolism and progressive, age-dependent synapse loss and neurodegeneration. *J Neurosci* **30**, 17068–17078.

Liu, Y., Chen, B.P.-C., Lu, M., Zhu, Y., Stemerman, M.B., Chien, S. & Shyy, J.Y.-J. (2002) Shear stress activation of SREBP1 in endothelial cells is mediated by integrins. *Arterioscler Thromb Vasc Biol* **22**, 76–81.

Livak, K.J. & Schmittgen, T.D. (2001) Analysis of relative gene expression data using real-time quantitative PCR and the 2(-Delta Delta C(T)) Method. *Methods* **25**, 402–408.

Lledo, P.-M., Merkle, F.T. & Alvarez-Buylla, A. (2008) Origin and function of olfactory bulb interneuron diversity. *Trends Neurosci* **31**, 392–400.

Lo, S.-C., Scearce-Levie, K. & Sheng, M. (2016) Characterization of Social Behaviors in caspase-3 deficient mice. *Sci Rep* **6**.

Lyketsos, C.G., Carrillo, M.C., Ryan, J.M., Khachaturian, A.S., Trzepacz, P., Amatniek, J., Cedarbaum, J., Brashear, R. & Miller, D.S. (2011) Neuropsychiatric symptoms in Alzheimer's disease. *Alzheimers Dement* **7**, 532–539.

Madra, M. & Sturley, S.L. (2010) Niemann–Pick type C pathogenesis and treatment: from statins to sugars. *Clin Lipidol* **5**, 387–395.

Mahley, R.W. (2016) Central Nervous System Lipoproteins. *Arterioscler Thromb Vasc Biol* **36**, 1305–1315.

Mahley, R.W., Innerarity, T.L., Rall, S.C. & Weisgraber, K.H. (1984) Plasma lipoproteins: apolipoprotein structure and function. *J Lipid Res* **25**, 1277–1294.

Mahley, R.W., Weisgraber, K.H. & Huang, Y. (2006) Apolipoprotein E4: a causative factor and therapeutic target in neuropathology, including Alzheimer's disease. *Proc Natl Acad Sci USA* **103**, 5644–5651.

Mailman, T., Hariharan, M. & Karten, B. (2011) Inhibition of neuronal cholesterol biosynthesis with lovastatin leads to impaired synaptic vesicle release even in the presence of lipoproteins or geranylgeraniol. *J Neurochem* **119**, 1002–1015.

Mainardi, M., Spinelli, M., Scala, F., Mattera, A., Fusco, S., D'Ascenzo, M. & Grassi, C. (2017) Loss of Leptin-Induced Modulation of Hippocampal Synaptic Trasmission and Signal Transduction in High-Fat Diet-Fed Mice. *Front Cell Neurosci* **11**.

Mann, C.J., Khallou, J., Chevreuil, O., Troussard, A.A., Guermani, L.M., Launay, K., Delplanque, B., Yen, F.T. & Bihain, B.E. (1995) Mechanism of activation and functional significance of the lipolysis-stimulated receptor. Evidence for a role as chylomicron remnant receptor. *Biochemistry* **34**, 10421–10431.

Mann, C.J., Troussard, A.A., Yen, F.T., Hannouche, N., Najib, J., Fruchart, J.C., Lotteau, V., André, P. & Bihain, B.E. (1997) Inhibitory effects of specific apolipoprotein C-III isoforms on the binding of triglyceride-rich lipoproteins to the lipolysis-stimulated receptor. *J Biol Chem* **272**, 31348–31354.

Martin, M., Dotti, C.G. & Ledesma, M.D. (2010) Brain cholesterol in normal and pathological aging. *Biochim Biophys Acta* **1801**, 934–944.

Martin, S. & Parton, R.G. (2006) Lipid droplets: a unified view of a dynamic organelle. *Nat Rev Mol Cell Biol* **7**, 373–378.

Matsuda, A., Nagao, K., Matsuo, M., Kioka, N. & Ueda, K. (2013) 24(S)-hydroxycholesterol is actively eliminated from neuronal cells by ABCA1. *Journal of Neurochemistry* **126**, 93–101.

Mauch, D.H., Nägler, K., Schumacher, S., Göritz, C., Müller, E.C., Otto, A. & Pfrieger, F.W. (2001) CNS synaptogenesis promoted by glia-derived cholesterol. *Science* **294**, 1354–1357.

Meaney, S., Bodin, K., Diczfalusy, U. & Björkhem, I. (2002) On the rate of translocation in vitro and kinetics in vivo of the major oxysterols in human circulation: critical importance of the position of the oxygen function. *J Lipid Res* **43**, 2130–2135.

Merino-Serrais, P., Loera-Valencia, R., Rodriguez-Rodriguez, P., Parrado-Fernandez, C., Ismail, M.A., Maioli, S., Matute, E., Jimenez-Mateos, E.M., Björkhem, I., DeFelipe, J. & Cedazo-Minguez, A. (2019) 27-Hydroxycholesterol Induces Aberrant Morphology and Synaptic Dysfunction in Hippocampal Neurons. *Cereb Cortex* **29**, 429–446.

Mesli, S., Javorschi, S., Bérard, A.M., Landry, M., Priddle, H., Kivlichan, D., Smith, A.J.H., Yen, F.T., Bihain, B.E. & Darmon, M. (2004) Distribution of the lipolysis stimulated receptor in adult and embryonic murine tissues and

lethality of LSR-/- embryos at 12.5 to 14.5 days of gestation. *Eur J Biochem* **271**, 3103–3114.

Möckel, B., Zinke, H., Flach, R., Weiss, B., Weiler-Güttler, H. & Gassen, H.G. (1994) Expression of apolipoprotein A-I in porcine brain endothelium in vitro. *J Neurochem* **62**, 788–798.

Morell, P. & Jurevics, H. (1996) Origin of cholesterol in myelin. *Neurochem Res* **21**, 463–470.

Morrison, C.D. & Münzberg, H. (2012) Capricious Cre: The Devil Is in the Details. *Endocrinology* **153**, 1005–1007.

Mulder, M., Jansen, P.J., Janssen, B.J.A., van de Berg, W.D.J., van der Boom, H., Havekes, L.M., de Kloet, R.E., Ramaekers, F.C.S. & Blokland, A. (2004) Low-density lipoprotein receptor-knockout mice display impaired spatial memory associated with a decreased synaptic density in the hippocampus. *Neurobiol Dis* **16**, 212–219.

Narvekar, P., Berriel Diaz, M., Krones-Herzig, A., Hardeland, U., Strzoda, D., Stöhr, S., Frohme, M. & Herzig, S. (2009) Liver-specific loss of lipolysis-stimulated lipoprotein receptor triggers systemic hyperlipidemia in mice. *Diabetes* **58**, 1040–1049.

Nelson, A.B., Hang, G.B., Grueter, B.A., Pascoli, V., Luscher, C., Malenka, R.C. & Kreitzer, A.C. (2012) A comparison of striatal-dependent behaviors in wild-type and hemizygous Drd1a and Drd2 BAC transgenic mice. *J Neurosci* **32**, 9119–9123.

Niu, S., Yabut, O. & D'Arcangelo, G. (2008) The Reelin Signaling Pathway Promotes Dendritic Spine Development in Hippocampal Neurons. *J Neurosci* **28**, 10339–10348.

Nobis, L. & Husain, M. (2018) Apathy in Alzheimer's disease. *Current Opinion in Behavioral Sciences*, Apathy and Motivation **22**, 7–13.

Nohturfft, A., Yabe, D., Goldstein, J.L., Brown, M.S. & Espenshade, P.J. (2000) Regulated step in cholesterol feedback localized to budding of SCAP from ER membranes. *Cell* **102**, 315–323.

Nordengen, K., Kirsebom, B.-E., Henjum, K., Selnes, P., Gísladóttir, B., Wettergreen, M., Torsetnes, S.B., Grøntvedt, G.R., Waterloo, K.K., Aarsland, D., Nilsson, L.N.G. & Fladby, T. (2019) Glial activation and inflammation along the Alzheimer's disease continuum. *J Neuroinflammation* **16**, 46.

Nowaczyk, M.J.M. & Irons, M.B. (2012) Smith-Lemli-Opitz syndrome: phenotype, natural history, and epidemiology. *Am J Med Genet C Semin Med Genet* **160C**, 250–262.

Okamoto, S., Kimura, K. & Saito, M. (2001) Anorectic effect of leptin is mediated by hypothalamic corticotropin-releasing hormone, but not by urocortin, in rats. *Neurosci Lett* **307**, 179–182.

de Oliveira, J., Hort, M.A., Moreira, E.L.G., Glaser, V., Ribeiro-do-Valle, R.M., Prediger, R.D., Farina, M., Latini, A. & de Bem, A.F. (2011) Positive correlation between elevated plasma cholesterol levels and cognitive impairments in LDL receptor knockout mice: relevance of cortico-cerebral mitochondrial dysfunction and oxidative stress. *Neuroscience* **197**, 99–106.

Ollila, S., Hyvönen, M.T. & Vattulainen, I. (2007) Polyunsaturation in lipid membranes: dynamic properties and lateral pressure profiles. *J Phys Chem B* **111**, 3139–3150.

Oomura, Y., Hori, N., Shiraishi, T., Fukunaga, K., Takeda, H., Tsuji, M., Matsumiya, T., Ishibashi, M., Aou, S., Li, X.L., Kohno, D., Uramura, K., Sougawa, H., Yada, T., Wayner, M.J. & Sasaki, K. (2006) Leptin facilitates learning and memory performance and enhances hippocampal CA1 long-term potentiation and CaMK II phosphorylation in rats. *Peptides* **27**, 2738–2749.

Osada, N., Kosuge, Y., Kihara, T., Ishige, K. & Ito, Y. (2009) Apolipoprotein E-deficient mice are more vulnerable to ER stress after transient forebrain ischemia. *Neurochem Int* **54**, 403–409.

Papassotiropoulos, A., Lütjohann, D., Bagli, M., Locatelli, S., Jessen, F., Buschfort, R., Ptok, U., Björkhem, I., von Bergmann, K. & Heun, R. (2002) 24S-hydroxycholesterol in cerebrospinal fluid is elevated in early stages of dementia. *J Psychiatr Res* **36**, 27–32.

Papatheodorou, P., Carette, J.E., Bell, G.W., Schwan, C., Guttenberg, G., Brummelkamp, T.R. & Aktories, K. (2011) Lipolysis-stimulated lipoprotein receptor (LSR) is the host receptor for the binary toxin Clostridium difficile transferase (CDT). *PNAS* **108**, 16422–16427.

Pasinetti, G.M., Johnson, S.A., Oda, T., Rozovsky, I. & Finch, C.E. (1994) Clusterin (SGP-2): a multifunctional glycoprotein with regional expression in astrocytes and neurons of the adult rat brain. *J Comp Neurol* **339**, 387–400.

Peake, K.B. & Vance, J.E. (2010) Defective cholesterol trafficking in Niemann-Pick C-deficient cells. *FEBS Lett* **584**, 2731–2739.

Pennetta, G. & Welte, M.A. (2018) Emerging Links between Lipid Droplets and Motor Neuron Diseases. *Dev Cell* **45**, 427–432.

Petrov, A.M., Kasimov, M.R. & Zefirov, A.L. (2016) Brain Cholesterol Metabolism and Its Defects: Linkage to Neurodegenerative Diseases and Synaptic Dysfunction. *Acta Naturae* **8**, 58–73.

Pfrieger, F.W. & Ungerer, N. (2011) Cholesterol metabolism in neurons and astrocytes. *Prog Lipid Res* **50**, 357–371.

Pinçon, A., Thomas, M.H., Huguet, M., Allouche, A., Colin, J.C., Georges, A., Derrien, A., Lanhers, M.-C., Malaplate-Armand, C., Oster, T., Corbier, C., Pillot, T., Olivier, J.L. & Yen, F.T. (2015a) Increased susceptibility of dyslipidemic LSR+/- mice to amyloid stress is associated with changes in cortical cholesterol levels. *J Alzheimers Dis* **45**, 195–204.

Pinçon, A., Thomas, M.H., Huguet, M., Allouche, A., Colin, J.C., Georges, A., Derrien, A., Lanhers, M.-C., Malaplate-Armand, C., Oster, T., Corbier, C., Pillot, T., Olivier, J.L. & Yen, F.T. (2015b) Increased susceptibility of dyslipidemic LSR+/- mice to amyloid stress is associated with changes in cortical cholesterol levels. *J Alzheimers Dis* **45**, 195–204.

Pitas, R.E., Boyles, J.K., Lee, S.H., Hui, D. & Weisgraber, K.H. (1987a) Lipoproteins and their receptors in the central nervous system. Characterization of the lipoproteins in cerebrospinal fluid and identification of apolipoprotein B,E(LDL) receptors in the brain. *J Biol Chem* **262**, 14352–14360.

Pitas, R.E., Boyles, J.K., Lee, S.H., Hui, D. & Weisgraber, K.H. (1987b) Lipoproteins and their receptors in the central nervous system. Characterization of the lipoproteins in cerebrospinal fluid and identification of apolipoprotein B,E(LDL) receptors in the brain. *J Biol Chem* **262**, 14352–14360.

Pocivavsek, A., Burns, M.P. & Rebeck, G.W. (2009) Low Density Lipoprotein Receptors Regulate Microglial Inflammation Through C-Jun N-Terminal Kinase. *Glia* **57**, 444–453.

Popp, J., Lewczuk, P., Kölsch, H., Meichsner, S., Maier, W., Kornhuber, J., Jessen, F. & Lütjohann, D. (2012) Cholesterol metabolism is associated with soluble amyloid precursor protein production in Alzheimer's disease. *J Neurochem* **123**, 310–316.

Popp, J., Meichsner, S., Kölsch, H., Lewczuk, P., Maier, W., Kornhuber, J., Jessen, F. & Lütjohann, D. (2013) Cerebral and extracerebral cholesterol metabolism and CSF markers of Alzheimer's disease. *Biochem Pharmacol* **86**, 37–42.

Prasanthi, J.R., Huls, A., Thomasson, S., Thompson, A., Schommer, E. & Ghribi, O. (2009) Differential effects of 24-hydroxycholesterol and 27-hydroxycholesterol on beta-amyloid precursor protein levels and processing in human neuroblastoma SH-SY5Y cells. *Mol Neurodegener* **4**, 1.

Quan, G., Xie, C., Dietschy, J.M. & Turley, S.D. (2003) Ontogenesis and regulation of cholesterol metabolism in the central nervous system of the mouse. *Brain Res Dev Brain Res* **146**, 87–98.

Rahman, T., Taha, A.Y., Song, B.J., Orr, S.K., Liu, Z., Chen, C.T. & Bazinet, R.P. (2010) The very low density lipoprotein receptor is not necessary for maintaining brain polyunsaturated fatty acid concentrations. *Prostaglandins Leukot Essent Fatty Acids* **82**, 141–145.

Rapp, A., Gmeiner, B. & Hüttinger, M. (2006) Implication of apoE isoforms in cholesterol metabolism by primary rat hippocampal neurons and astrocytes. *Biochimie* **88**, 473–483.

Rassart, E., Bedirian, A., Do Carmo, S., Guinard, O., Sirois, J., Terrisse, L. & Milne, R. (2000) Apolipoprotein D. *Biochim Biophys Acta* **1482**, 185–198.

Reaves, D.K., Fagan-Solis, K.D., Dunphy, K., Oliver, S.D., Scott, D.W. & Fleming, J.M. (2014) The Role of Lipolysis Stimulated Lipoprotein Receptor in Breast Cancer and Directing Breast Cancer Cell Behavior. *PLOS ONE* **9**, e91747.

Rebeck, G.W. (2004) Cholesterol efflux as a critical component of Alzheimer's disease pathogenesis. *J Mol Neurosci* **23**, 219–224.

Reddy, S.S., Connor, T.E., Weeber, E.J. & Rebeck, W. (2011) Similarities and differences in structure, expression, and functions of VLDLR and ApoER2. *Mol Neurodegener* **6**, 30.

Rigotti, A., Trigatti, B., Babitt, J., Penman, M., Xu, S. & Krieger, M. (1997) Scavenger receptor BI--a cell surface receptor for high density lipoprotein. *Curr Opin Lipidol* **8**, 181–188.

Rizzi, F. & Bettuzzi, S. (2010) The clusterin paradigm in prostate and breast carcinogenesis. *Endocr Relat Cancer* **17**, R1-17.

Roheim, P.S., Carey, M., Forte, T. & Vega, G.L. (1979a) Apolipoproteins in human cerebrospinal fluid. *Proc Natl Acad Sci USA* **76**, 4646–4649.

Roheim, P.S., Carey, M., Forte, T. & Vega, G.L. (1979b) Apolipoproteins in human cerebrospinal fluid. *Proc Natl Acad Sci USA* **76**, 4646–4649.

Rohn, T.T. (2013) Proteolytic cleavage of apolipoprotein E4 as the keystone for the heightened risk associated with Alzheimer's disease. *Int J Mol Sci* **14**, 14908–14922.

Ru, P., Williams, T.M., Chakravarti, A. & Guo, D. (2013) Tumor Metabolism of Malignant Gliomas. *Cancers* **5**, 1469–1484.

Ruiz, J., Kouiavskaia, D., Migliorini, M., Robinson, S., Saenko, E.L., Gorlatova, N., Li, D., Lawrence, D., Hyman, B.T., Weisgraber, K.H. & Strickland, D.K. (2005) The apoE isoform binding properties of the VLDL receptor reveal marked differences from LRP and the LDL receptor. *J Lipid Res* **46**, 1721–1731.

Russell, D.W., Halford, R.W., Ramirez, D.M.O., Shah, R. & Kotti, T. (2009) Cholesterol 24-hydroxylase: an enzyme of cholesterol turnover in the brain. *Annu Rev Biochem* **78**, 1017–1040.

Ruthirakuhan, M., Herrmann, N., Vieira, D., Gallagher, D. & Lanctôt, K.L. (2019) The Roles of Apathy and Depression in Predicting Alzheimer Disease: A Longitudinal Analysis in Older Adults With Mild Cognitive Impairment. *The American Journal of Geriatric Psychiatry* **27**, 873–882.

Saito, K., Dubreuil, V., Arai, Y., Wilsch-Bräuninger, M., Schwudke, D., Saher, G., Miyata, T., Breier, G., Thiele, C., Shevchenko, A., Nave, K.-A. & Huttner, W.B. (2009) Ablation of cholesterol biosynthesis in neural stem cells increases their VEGF expression and angiogenesis but causes neuron apoptosis. *Proc Natl Acad Sci USA* **106**, 8350–8355.

Saito, M., Benson, E.P., Saito, M. & Rosenberg, A. (1987) Metabolism of cholesterol and triacylglycerol in cultured chick neuronal cells, glial cells, and fibroblasts: Accumulation of esterified cholesterol in serum-free culture. *Journal of Neuroscience Research* **18**, 319–325.

Sakai, K., Tiebel, O., Ljungberg, M.C., Sullivan, M., Lee, H.-J., Terashima, T., Li, R., Kobayashi, K., Lu, H.-C., Chan, L. & Oka, K. (2009) A neuronal VLDLR variant lacking the third complement-type repeat exhibits high capacity binding of apoE containing lipoproteins. *Brain Res* **1276**, 11–21.

Sano, M., Bell, K.L., Galasko, D., Galvin, J.E., Thomas, R.G., van Dyck, C.H. & Aisen, P.S. (2011) A randomized, double-blind, placebo-controlled trial of simvastatin to treat Alzheimer disease. *Neurology* **77**, 556–563.

Saper, C.B. & Lowell, B.B. (2014) The hypothalamus. *Current Biology* **24**, R1111–R1116.

Sarna, J.R., Larouche, M., Marzban, H., Sillitoe, R.V., Rancourt, D.E. & Hawkes, R. (2003) Patterned Purkinje cell degeneration in mouse models of Niemann-Pick type C disease. *J Comp Neurol* **456**, 279–291.

Sauer, B. & Henderson, N. (1988) Site-specific DNA recombination in mammalian cells by the Cre recombinase of bacteriophage P1. *Proc Natl Acad Sci USA* **85**, 5166–5170.

Schroeder, F., Gallegos, A.M., Atshaves, B.P., Storey, S.M., McIntosh, A.L., Petrescu, A.D., Huang, H., Starodub, O., Chao, H., Yang, H., Frolov, A. & Kier, A.B.

(2001) Recent advances in membrane microdomains: rafts, caveolae, and intracellular cholesterol trafficking. *Exp Biol Med (Maywood)* **226**, 873–890.

Selkoe, D.J. (2001) Clearing the brain's amyloid cobwebs. *Neuron* **32**, 177–180.

Selkoe, D.J. (2002) Alzheimer's disease is a synaptic failure. *Science* **298**, 789–791.

Sen, A., Alkon, D.L. & Nelson, T.J. (2012) Apolipoprotein E3 (ApoE3) but not ApoE4 protects against synaptic loss through increased expression of protein kinase C epsilon. *J Biol Chem* **287**, 15947–15958.

Seo, Y., Kim, H.-S. & Kang, K.-S. (2018) Microglial involvement in the development of olfactory dysfunction. *J Vet Sci* **19**, 319–330.

Sever, N., Song, B.-L., Yabe, D., Goldstein, J.L., Brown, M.S. & DeBose-Boyd, R.A. (2003) Insig-dependent ubiquitination and degradation of mammalian 3-hydroxy-3-methylglutaryl-CoA reductase stimulated by sterols and geranylgeraniol. *J Biol Chem* **278**, 52479–52490.

Shafaati, M., Marutle, A., Pettersson, H., Lövgren-Sandblom, A., Olin, M., Pikuleva, I., Winblad, B., Nordberg, A. & Björkhem, I. (2011) Marked accumulation of 27-hydroxycholesterol in the brains of Alzheimer's patients with the Swedish APP 670/671 mutation. *J Lipid Res* **52**, 1004–1010.

Sheng, H., Laskowitz, D.T., Mackensen, G.B., Kudo, M., Pearlstein, R.D. & Warner, D.S. (1999) Apolipoprotein E deficiency worsens outcome from global cerebral ischemia in the mouse. *Stroke* **30**, 1118–1124.

Shepardson, N.E., Shankar, G.M. & Selkoe, D.J. (2011) Cholesterol level and statin use in Alzheimer disease: I. Review of epidemiological and preclinical studies. *Arch Neurol* **68**, 1239–1244.

Shimada, H., Satohisa, S., Kohno, T., Konno, T., Takano, K.-I., Takahashi, S., Hatakeyama, T., Arimoto, C., Saito, T. & Kojima, T. (2017) Downregulation of lipolysis-stimulated lipoprotein receptor promotes cell invasion via claudin-1-mediated matrix metalloproteinases in human endometrial cancer. *Oncol Lett* **14**, 6776–6782.

Shimada, H., Satohisa, S., Kohno, T., Takahashi, S., Hatakeyama, T., Konno, T., Tsujiwaki, M., Saito, T. & Kojima, T. (2016) The roles of tricellular tight junction protein lipolysis-stimulated lipoprotein receptor in malignancy of human endometrial cancer cells. *Oncotarget* **7**, 27735–27752.

Simonsen, A., Lippé, R., Christoforidis, S., Gaullier, J.M., Brech, A., Callaghan, J., Toh, B.H., Murphy, C., Zerial, M. & Stenmark, H. (1998) EEA1 links PI(3)K function to Rab5 regulation of endosome fusion. *Nature* **394**, 494–498.

Sipione, S., Rigamonti, D., Valenza, M., Zuccato, C., Conti, L., Pritchard, J., Kooperberg, C., Olson, J.M. & Cattaneo, E. (2002) Early transcriptional profiles in huntingtin-inducible striatal cells by microarray analyses. *Hum Mol Genet* **11**, 1953–1965.

Sleat, D.E., Wiseman, J.A., El-Banna, M., Price, S.M., Verot, L., Shen, M.M., Tint, G.S., Vanier, M.T., Walkley, S.U. & Lobel, P. (2004) Genetic evidence for nonredundant functional cooperativity between NPC1 and NPC2 in lipid transport. *Proc Natl Acad Sci USA* **101**, 5886–5891.

Slezak, M., Göritz, C., Niemiec, A., Frisén, J., Chambon, P., Metzger, D. & Pfrieger, F.W. (2007) Transgenic mice for conditional gene manipulation in astroglial cells. *Glia* **55**, 1565–1576.

Smith, K.M., Lawn, R.M. & Wilcox, J.N. (1990) Cellular localization of apolipoprotein D and lecithin:cholesterol acyltransferase mRNA in rhesus monkey tissues by in situ hybridization. *J Lipid Res* **31**, 995–1004.

Söderberg, M., Edlund, C., Kristensson, K. & Dallner, G. (1990) Lipid compositions of different regions of the human brain during aging. *J Neurochem* **54**, 415–423.

Sohet, F., Lin, C., Munji, R.N., Lee, S.Y., Ruderisch, N., Soung, A., Arnold, T.D., Derugin, N., Vexler, Z.S., Yen, F.T. & Daneman, R. (2015) LSR/angulin-1 is a tricellular tight junction protein involved in blood-brain barrier formation. *J Cell Biol* **208**, 703–711.

Song, B.-L., Javitt, N.B. & DeBose-Boyd, R.A. (2005) Insig-mediated degradation of HMG CoA reductase stimulated by lanosterol, an intermediate in the synthesis of cholesterol. *Cell Metab* **1**, 179–189.

Sonnino, S. & Prinetti, A. (2013) Membrane domains and the “lipid raft” concept. *Curr Med Chem* **20**, 4–21.

Sparks, D.L., Scheff, S.W., Hunsaker, J.C., Liu, H., Landers, T. & Gross, D.R. (1994) Induction of Alzheimer-like beta-amyloid immunoreactivity in the brains of rabbits with dietary cholesterol. *Exp Neurol* **126**, 88–94.

Staneva, G., Chachaty, C., Wolf, C. & Quinn, P.J. (2010) Comparison of the liquid-ordered bilayer phases containing cholesterol or 7-dehydrocholesterol in modeling Smith-Lemli-Opitz syndrome. *J Lipid Res* **51**, 1810–1822.

Starkstein, S.E., Jorge, R., Mizrahi, R. & Robinson, R.G. (2006) A prospective longitudinal study of apathy in Alzheimer’s disease. *J Neurol Neurosurg Psychiatry* **77**, 8–11.

Steinmetz, C.C., Buard, I., Claudepierre, T., Nägler, K. & Pfrieger, F.W. (2006) Regional variations in the glial influence on synapse development in the mouse CNS. *J Physiol (Lond)* **577**, 249–261.

Stenger, C., Hanse, M., Pratte, D., Mbala, M.-L., Akbar, S., Koziel, V., Escanyé, M.-C., Kriem, B., Malaplate-Armand, C., Olivier, J.-L., Oster, T., Pillot, T. & Yen, F.T. (2010) Up-regulation of hepatic lipolysis stimulated lipoprotein receptor by leptin: a potential lever for controlling lipid clearance during the postprandial phase. *FASEB J* **24**, 4218–4228.

Stenger, C., Pinçon, A., Hanse, M., Royer, L., Comte, A., Koziel, V., Olivier, J.-L., Pillot, T. & Yen, F.T. (2012) Brain region-specific immunolocalization of the lipolysis-stimulated lipoprotein receptor (LSR) and altered cholesterol distribution in aged LSR+/- mice. *J Neurochem* **123**, 467–476.

Sternberg, N. (1981) Bacteriophage P1 site-specific recombination: III. Strand exchange during recombination at lox sites. *Journal of Molecular Biology* **150**, 603–608.

Streicher, R., Kotzka, J., Müller-Wieland, D., Siemeister, G., Munck, M., Avci, H. & Krone, W. (1996) SREBP-1 mediates activation of the low density lipoprotein receptor promoter by insulin and insulin-like growth factor-I. *J Biol Chem* **271**, 7128–7133.

Stukas, S., Robert, J., Lee, M., Kulic, I., Carr, M., Tourigny, K., Fan, J., Namjoshi, D., Lemke, K., DeValle, N., Chan, J., Wilson, T., Wilkinson, A., Chapanian, R., Kizhakkedathu, J.N., Cirrito, J.R., Oda, M.N. & Wellington, C.L. (2014) Intravenously injected human apolipoprotein A-I rapidly enters the central nervous system via the choroid plexus. *J Am Heart Assoc* **3**, e001156.

Sugase, T., Takahashi, T., Serada, S., Fujimoto, M., Ohkawara, T., Hiramatsu, K., Koh, M., Saito, Y., Tanaka, K., Miyazaki, Y., Makino, T., Kurokawa, Y., Yamasaki, M., Nakajima, K., Hanazaki, K., Mori, M., Doki, Y. & Naka, T. (2018) Lipolysis-stimulated lipoprotein receptor overexpression is a novel predictor of poor clinical prognosis and a potential therapeutic target in gastric cancer. *Oncotarget* **9**, 32917–32928.

Sullivan, E.V. (2010) Cognitive Functions of the Cerebellum. *Neuropsychol Rev* **20**, 227–228.

Sun. (2014) The role of transporters ABCG1/4 and ABCA1 in brain cholesterol metabolism [WWW Document]. *ResearchGate*. URL https://www.researchgate.net/publication/281875468_The_role_of_transporters_ABCG14_and_ABCA1_in_brain_cholesterol_metabolism

Suzuki, S., Kiyosue, K., Hazama, S., Ogura, A., Kashihara, M., Hara, T., Koshimizu, H. & Kojima, M. (2007) Brain-Derived Neurotrophic Factor Regulates Cholesterol Metabolism for Synapse Development. *J Neurosci* **27**, 6417–6427.

Svennerholm, L. & Gottfries, C.G. (1994) Membrane lipids, selectively diminished in Alzheimer brains, suggest synapse loss as a primary event in early-onset form (type I) and demyelination in late-onset form (type II). *J Neurochem* **62**, 1039–1047.

Tabas, I. (2002) Consequences of cellular cholesterol accumulation: basic concepts and physiological implications. *J Clin Invest* **110**, 905–911.

Tachikawa, M., Watanabe, M., Hori, S., Fukaya, M., Ohtsuki, S., Asashima, T. & Terasaki, T. (2005) Distinct spatio-temporal expression of ABCA and ABCG transporters in the developing and adult mouse brain. *J Neurochem* **95**, 294–304.

Tall, A.R. (2008) Cholesterol efflux pathways and other potential mechanisms involved in the athero-protective effect of high density lipoproteins. *J Intern Med* **263**, 256–273.

Tan, J. & Evin, G. (2012) B-site APP-cleaving enzyme 1 trafficking and Alzheimer's disease pathogenesis. *J Neurochem* **120**, 869–880.

Tarr, P.T. & Edwards, P.A. (2008) ABCG1 and ABCG4 are coexpressed in neurons and astrocytes of the CNS and regulate cholesterol homeostasis through SREBP-2. *J Lipid Res* **49**, 169–182.

Testa, G., Gamba, P., Badilli, U., Gargiulo, S., Maina, M., Guina, T., Calfapietra, S., Biasi, F., Cavalli, R., Poli, G. & Leonarduzzi, G. (2014) Loading into nanoparticles improves quercetin's efficacy in preventing neuroinflammation induced by oxysterols. *PLoS ONE* **9**, e96795.

Thanopoulou, K., Fragkouli, A., Stylianopoulou, F. & Georgopoulos, S. (2010) Scavenger receptor class B type I (SR-BI) regulates perivascular macrophages and modifies amyloid pathology in an Alzheimer mouse model. *Proc Natl Acad Sci USA* **107**, 20816–20821.

Theendakara, V., Peters-Libeu, C.A., Spilman, P., Poksay, K.S., Bredesen, D.E. & Rao, R.V. (2016) Direct Transcriptional Effects of Apolipoprotein E. *J Neurosci* **36**, 685–700.

Tooyama, I., Kawamata, T., Akiyama, H., Kimura, H., Moestrup, S.K., Gliemann, J., Matsuo, A. & McGeer, P.L. (1995) Subcellular localization of the low density lipoprotein receptor-related protein (alpha 2-macroglobulin receptor) in human brain. *Brain Res* **691**, 235–238.

del Toro, D., Xifró, X., Pol, A., Humbert, S., Saudou, F., Canals, J.M. & Alberch, J. (2010) Altered cholesterol homeostasis contributes to enhanced excitotoxicity in Huntington's disease. *J Neurochem* **115**, 153–167.

Trommsdorff, M., Gotthardt, M., Hiesberger, T., Shelton, J., Stockinger, W., Nimpf, J., Hammer, R.E., Richardson, J.A. & Herz, J. (1999) Reeler/Disabled-like disruption of neuronal migration in knockout mice lacking the VLDL receptor and ApoE receptor 2. *Cell* **97**, 689–701.

Troussard, A.A., Khallou, J., Mann, C.J., André, P., Strickland, D.K., Bihain, B.E. & Yen, F.T. (1995) Inhibitory effect on the lipolysis-stimulated receptor of the 39-kDa receptor-associated protein. *J Biol Chem* **270**, 17068–17071.

Tsien, J.Z., Chen, D.F., Gerber, D., Tom, C., Mercer, E.H., Anderson, D.J., Mayford, M., Kandel, E.R. & Tonegawa, S. (1996) Subregion- and cell type-restricted gene knockout in mouse brain. *Cell* **87**, 1317–1326.

Turley, S.D., Burns, D.K. & Dietschy, J.M. (1998) Preferential utilization of newly synthesized cholesterol for brain growth in neonatal lambs. *Am J Physiol* **274**, E1099-1105.

Ujiie, M., Dickstein, D.L., Carlow, D.A. & Jefferies, W.A. (2003) Blood-brain barrier permeability precedes senile plaque formation in an Alzheimer disease model. *Microcirculation* **10**, 463–470.

Umeda, T., Tomiyama, T., Kitajima, E., Idomoto, T., Nomura, S., Lambert, M.P., Klein, W.L. & Mori, H. (2012) Hypercholesterolemia accelerates intraneuronal accumulation of Aβ oligomers resulting in memory impairment in Alzheimer's disease model mice. *Life Sci* **91**, 1169–1176.

Valenza, M., Rigamonti, D., Goffredo, D., Zuccato, C., Fenu, S., Jamot, L., Strand, A., Tarditi, A., Woodman, B., Racchi, M., Mariotti, C., Di Donato, S., Corsini, A., Bates, G., Pruss, R., Olson, J.M., Sipione, S., Tartari, M. & Cattaneo, E. (2005) Dysfunction of the cholesterol biosynthetic pathway in Huntington's disease. *J Neurosci* **25**, 9932–9939.

Vance, J.E. (2012) Dysregulation of cholesterol balance in the brain: contribution to neurodegenerative diseases. *Dis Model Mech* **5**, 746–755.

Vanier, M.T. & Millat, G. (2003) Niemann-Pick disease type C. *Clin Genet* **64**, 269–281.

Vaughan, C.J. & Gotto, A.M. (2004) Update on statins: 2003. *Circulation* **110**, 886–892.

Vaz, R.P., Cardoso, A., Serrão, P., Pereira, P.A. & Madeira, M.D. (2018) Chronic stress leads to long-lasting deficits in olfactory-guided behaviors, and to neuroplastic changes in the nucleus of the lateral olfactory tract. *Horm Behav* **98**, 130–144.

Volkow, N.D., Wang, G.-J., Newcorn, J.H., Kollins, S.H., Wigal, T.L., Telang, F., Fowler, J.S., Goldstein, R.Z., Klein, N., Logan, J., Wong, C. & Swanson, J.M.

(2011) Motivation Deficit in ADHD is Associated with Dysfunction of the Dopamine Reward Pathway. *Mol Psychiatry* **16**, 1147–1154.

Wahrle, S.E., Jiang, H., Parsadanian, M., Legleiter, J., Han, X., Fryer, J.D., Kowalewski, T. & Holtzman, D.M. (2004a) ABCA1 is required for normal central nervous system ApoE levels and for lipidation of astrocyte-secreted apoE. *J Biol Chem* **279**, 40987–40993.

Wahrle, S.E., Jiang, H., Parsadanian, M., Legleiter, J., Han, X., Fryer, J.D., Kowalewski, T. & Holtzman, D.M. (2004b) ABCA1 is required for normal central nervous system ApoE levels and for lipidation of astrocyte-secreted apoE. *J Biol Chem* **279**, 40987–40993.

Wang, N., Yvan-Charvet, L., Lütjohann, D., Mulder, M., Vanmierlo, T., Kim, T.-W. & Tall, A.R. (2008a) ATP-binding cassette transporters G1 and G4 mediate cholesterol and desmosterol efflux to HDL and regulate sterol accumulation in the brain. *FASEB J* **22**, 1073–1082.

Wang, N., Yvan-Charvet, L., Lütjohann, D., Mulder, M., Vanmierlo, T., Kim, T.-W. & Tall, A.R. (2008b) ATP-binding cassette transporters G1 and G4 mediate cholesterol and desmosterol efflux to HDL and regulate sterol accumulation in the brain. *FASEB J* **22**, 1073–1082.

Watanabe, K., Watson, E., Cremona, M.L., Millings, E.J., Lefkowitch, J.H., Fischer, S.G., LeDuc, C.A. & Leibel, R.L. (2013) ILDR2: An Endoplasmic Reticulum Resident Molecule Mediating Hepatic Lipid Homeostasis. *PLoS One* **8**.

Weeber, E.J., Beffert, U., Jones, C., Christian, J.M., Forster, E., Sweatt, J.D. & Herz, J. (2002) Reelin and ApoE receptors cooperate to enhance hippocampal synaptic plasticity and learning. *J Biol Chem* **277**, 39944–39952.

Wicher, G.K. & Aldskogius, H. (2005) Adult motor neurons show increased susceptibility to axotomy-induced death in mice lacking clusterin. *Eur J Neurosci* **21**, 2024–2028.

Wilens, T.E. (2006) Mechanism of Action of Agents Used in Attention-Deficit/Hyperactivity Disorder. *J Clin Psychiatry* **67**, 32–37.

Willy, P.J., Umesono, K., Ong, E.S., Evans, R.M., Heyman, R.A. & Mangelsdorf, D.J. (1995) LXR, a nuclear receptor that defines a distinct retinoid response pathway. *Genes Dev* **9**, 1033–1045.

Wingo, T.S., Cutler, D.J., Wingo, A.P., Le, N.-A., Rabinovici, G.D., Miller, B.L., Lah, J.J. & Levey, A.I. (2019) Association of Early-Onset Alzheimer Disease With Elevated Low-density Lipoprotein Cholesterol Levels and Rare Genetic Coding Variants of APOB. *JAMA Neurol*.

Woody, S.K. & Zhao, L. (2016) Clusterin (APOJ) in Alzheimer's Disease: An Old Molecule with a New Role.

Wu, L. & Gonias, S.L. (2005) The low-density lipoprotein receptor-related protein-1 associates transiently with lipid rafts. *J Cell Biochem* **96**, 1021–1033.

Wüstner, D., Mondal, M., Tabas, I. & Maxfield, F.R. (2005) Direct observation of rapid internalization and intracellular transport of sterol by macrophage foam cells. *Traffic* **6**, 396–412.

Wyatt, A.R., Yerbury, J.J. & Wilson, M.R. (2009) Structural characterization of clusterin-chaperone client protein complexes. *J Biol Chem* **284**, 21920–21927.

Xie, Z., Harris-White, M.E., Wals, P.A., Frautschy, S.A., Finch, C.E. & Morgan, T.E. (2005) Apolipoprotein J (clusterin) activates rodent microglia in vivo and in vitro. *J Neurochem* **93**, 1038–1046.

Xu, F., Vitek, M.P., Colton, C.A., Previti, M.L., Gharkholonarehe, N., Davis, J. & Van Nostrand, W.E. (2008) Human apolipoprotein E redistributes fibrillar amyloid deposition in Tg-SwDI mice. *J Neurosci* **28**, 5312–5320.

Xu, Q., Bernardo, A., Walker, D., Kanegawa, T., Mahley, R.W. & Huang, Y. (2006) Profile and regulation of apolipoprotein E (ApoE) expression in the CNS in mice with targeting of green fluorescent protein gene to the ApoE locus. *J Neurosci* **26**, 4985–4994.

Xu, S., Zhou, S., Xia, D., Xia, J., Chen, G., Duan, S. & Luo, J. (2010) Defects of synaptic vesicle turnover at excitatory and inhibitory synapses in Niemann-Pick C1-deficient neurons. *Neuroscience* **167**, 608–620.

Xu, X., Bittman, R., Duportail, G., Heissler, D., Vilcheze, C. & London, E. (2001) Effect of the structure of natural sterols and sphingolipids on the formation of ordered sphingolipid/sterol domains (rafts). Comparison of cholesterol to plant, fungal, and disease-associated sterols and comparison of sphingomyelin, cerebrosides, and ceramide. *J Biol Chem* **276**, 33540–33546.

Yang, M. & Crawley, J.N. (2009) Simple behavioral assessment of mouse olfaction. *Curr Protoc Neurosci* **Chapter 8**, Unit 8.24.

Yassine, N., Lazaris, A., Dorner-Ciossek, C., Després, O., Meyer, L., Maitre, M., Mensah-Nyagan, A.G., Cassel, J.-C. & Mathis, C. (2013) Detecting spatial memory deficits beyond blindness in tg2576 Alzheimer mice. *Neurobiol Aging* **34**, 716–730.

Ye, S., Huang, Y., Müllendorff, K., Dong, L., Giedt, G., Meng, E.C., Cohen, F.E., Kuntz, I.D., Weisgraber, K.H. & Mahley, R.W. (2005) Apolipoprotein (apo) E4 enhances amyloid beta peptide production in cultured neuronal cells: apoE

structure as a potential therapeutic target. *Proc Natl Acad Sci USA* **102**, 18700–18705.

Yen, F.T., Mann, C.J., Guermani, L.M., Hannouche, N.F., Hubert, N., Hornick, C.A., Bordeau, V.N., Agnani, G. & Bihain, B.E. (1994) Identification of a lipolysis-stimulated receptor that is distinct from the LDL receptor and the LDL receptor-related protein. *Biochemistry* **33**, 1172–1180.

Yen, F.T., Masson, M., Clossais-Besnard, N., André, P., Grosset, J.M., Bougueleret, L., Dumas, J.B., Guerassimenko, O. & Bihain, B.E. (1999) Molecular cloning of a lipolysis-stimulated remnant receptor expressed in the liver. *J Biol Chem* **274**, 13390–13398.

Yen, F.T., Roitel, O., Bonnard, L., Notet, V., Pratte, D., Stenger, C., Magueur, E. & Bihain, B.E. (2008a) Lipolysis stimulated lipoprotein receptor: a novel molecular link between hyperlipidemia, weight gain, and atherosclerosis in mice. *J Biol Chem* **283**, 25650–25659.

Yen, F.T., Roitel, O., Bonnard, L., Notet, V., Pratte, D., Stenger, C., Magueur, E. & Bihain, B.E. (2008b) Lipolysis stimulated lipoprotein receptor: a novel molecular link between hyperlipidemia, weight gain, and atherosclerosis in mice. *J Biol Chem* **283**, 25650–25659.

Zelcer, N. & Tontonoz, P. (2006) Liver X receptors as integrators of metabolic and inflammatory signaling. *J Clin Invest* **116**, 607–614.

Zhang, J. & Liu, Q. (2015) Cholesterol metabolism and homeostasis in the brain. *Protein Cell* **6**, 254–264.

Zhao, J., Deng, Y., Jiang, Z. & Qing, H. (2016) G Protein-Coupled Receptors (GPCRs) in Alzheimer's Disease: A Focus on BACE1 Related GPCRs. *Front Aging Neurosci* **8**, 58.

Zou, Y., Lu, D., Liu, L., Zhang, H. & Zhou, Y. (2016) Olfactory dysfunction in Alzheimer's disease. *Neuropsychiatr Dis Treat* **12**, 869–875.

Résumé : Le cholestérol est un lipide crucial dans le système nerveux central (SNC) et sa régulation stricte assure un développement et une fonction neuronaux appropriés. Le cholestérol est synthétisé dans le SNC par les cellules gliales qui produisent et sécrètent le cholestérol pour répondre aux besoins neuronaux. Les lipoprotéines et leurs récepteurs sont des éléments clés de ce transport intercellulaire : où ces derniers reconnaissent, lient et endocytent les lipoprotéines contenant du cholestérol. Le récepteur de lipoprotéine stimulé par lipolyse (LSR) est le récepteur le plus récemment découvert dans le SNC. C'est un complexe protéique multimère qui subit des changements conformationnels lors de la liaison des acides gras libres, révélant ainsi un site de liaison qui reconnaît les apolipoprotéines B et E. L'inactivation complète du gène LSR est létale au niveau embryonnaire, probablement due à une fuite de la barrière hématoencéphalique. De plus, des études sur des souris LSR +/- ont révélé une modification de la distribution du cholestérol et des fonctions cognitives. Notre premier objectif était de réaliser le profilage LSR au niveau des tissus et des cellules. Nos résultats ont révélé une expression différentielle des sous-unités de LSR. Les études in vitro sur des cultures de cellules primaires ont démontré que le LSR était fortement exprimé dans différentes régions du SNC, à la fois dans les cellules gliales et neuronales. Notre hypothèse est qu'une forte expression du LSR dans les cellules gliales pourrait jouer un rôle dans le contrôle de la synthèse du cholestérol, en limitant le cholestérol en circulation dans le liquide extracellulaire du cerveau. Pour vérifier cette hypothèse, nous avons développé un système inductible Cre-lox ciblant spécifiquement les cellules gliales. Le phénotypage comportemental démontre un déficit de la fonction olfactive ayant un impact sur la mémoire sociale de ces animaux. Bien qu'aucun problème de vision n'ait été détecté, le test de reconnaissance d'objet a démontré que la mémoire visuelle était affectée. En outre, les tests sur le labyrinthe en Y et celui de Barns semblent affecter la mémoire à court et à long terme. Nos résultats suggèrent que l'inactivation spécifique de LSR dans les cellules gliales altère la mémoire des animaux, affectant la mémoire spatiale et sociale. Fait intéressant et similaire à AD, le signe précoce était lié au déficit en olfaction. En utilisant une stratégie combinant phénotypage comportemental, immunomarquage et analyse biochimique de marqueurs spécifiques de la plasticité synaptique, ce modèle pourrait également être utilisé pour déterminer le rôle du LSR dans la cognition cérébrale et le trafic de cholestérol dans le SNC, et pourrait fournir les moyens de valider le LSR en tant que cible thérapeutique potentielle pour le traitement des dommages causés par le stockage des lipides et le développement de maladies neurodégénératives dans le cerveau vieillissant.

Mots clés : LSR, cerveau, glie, neurones, maladies neurodégénératives, cholestérol, comportement

Abstract: Cholesterol is a crucial lipid in the central nervous system (CNS) and its strict regulation ensures proper neuronal development and function. Cholesterol is synthesized in the CNS by glial cells which produce and secrete cholesterol to meet neuronal needs. Lipoproteins and their receptors are key elements of this intercellular transport: where the latter recognize, bind and endocytose lipoproteins containing cholesterol. The lipolysis stimulated lipoprotein receptor (LSR) is the most recently discovered receptor in the CNS. It is a multimeric protein complex that undergoes conformational changes during the binding of free fatty acids, thus revealing a binding site which recognizes apolipoproteins B and E. Complete inactivation of the LSR gene is lethal at embryonic level, probably due to a leaky blood brain barrier. In addition, studies in LSR +/- mice have revealed a change in the distribution of cholesterol and cognitive functions. Our first goal was to perform LSR profiling at the tissue and cell level. Our results revealed a differential expression of the LSR subunits. In vitro studies in primary cell cultures have shown that LSR is highly expressed in different regions of the CNS, both in glial and neuronal cells. Our hypothesis was that a strong expression of LSR in glial cells could play a role in controlling the synthesis of cholesterol, by limiting the cholesterol circulating in the extracellular fluid of the brain. To verify this hypothesis, we have developed an inducible Cre-lox system specifically targeting glial cells. Behavioral phenotyping demonstrated a deficit in olfactory function which has an impact on the social memory of these animals. Although no visual problems were detected, the object recognition test showed that the visual memory was affected. Additionally, Y and Barnes mazes tests revealed an impacted short- and long-term memory. Our results suggest that specific inactivation of LSR in glial cells impairs animal memory, affecting spatial and social memory. Interestingly and similarly to AD, the early signs monitored olfactory deficits. Using a strategy combining behavioral phenotyping, immunostaining and biochemical analysis of specific markers of synaptic plasticity, this model could also be used to determine the role of LSR in brain cognition and cholesterol trafficking in the CNS, and could provide the means to validate LSR as a potential therapeutic target for the treatment of damage caused by lipid storage and the development of neurodegenerative diseases in the aging brain.

Keyword: LSR, brain, glia, neurons, neurodegenerative diseases, cholesterol, behavior